

**ULTRASONIC DISPERSAL OF BUCKMINSTER FULLERENE [C₆₀] LEADS
TO THE FORMATION OF
[8-HYDROXY]FULLERENOL: SYNTHESIS AND APPLICATION**

SADIA AFREEN, BSc.

**THESIS SUBMITTED TO THE UNIVERSITY OF NOTTINGHAM
FOR THE DEGREE OF DOCTOR OF PHILOSOPHY**

SEPTEMBER 2017

**DEPARTMENT OF CHEMICAL & ENVIRONMENTAL ENGINEERING
THE UNIVERSITY OF NOTTINGHAM MALAYSIA CAMPUS**

DECLARATION

The author declares here no conflicts of interest and this thesis is an original work produced by the author during (2014-2017) the study of the course of Doctor of Philosophy in the Department of Chemical and Environmental Engineering at the University of Nottingham Malaysia Campus (UNMC).

ABSTRACT

This thesis is focused on investigating the possibility of synthesizing polyhydroxylated fullerene/fullerenol from the ultrasonic dispersal of Buckminster fullerene (C_{60}). Interestingly, ultrasonic dispersion of fullerene may result into potential fullerenol moieties, the prospect of which has long been overlooked to date and unnoted by others, hence it lacks quantitative analysis in explaining the possibility. On this context, based on some of the established facts, this thesis is going to evidence the possibility that when pristine fullerene is dispersed in an aqueous medium by ultrasonication, the acoustic cavitation resulting from sonication orchestrates the hydroxylation of fullerene to fullerenol moieties instead of hydration of fullerene molecules in the aqueous medium. This thesis deals with the above-raised possibility with a series of analytical studies and quantitative analysis which ultimately has proven that potential fullerenol moieties could be synthesized by the technique of ultrasonication, and this thesis is first to report that the most possible molecular structure of the potential fullerenol to be synthesized is $C_{60}(OH)_8 \cdot 2H_2O$ with a yield up to 4.0%.

The formation of fullerenol and the possible molecular structure of the synthesized fullerenol was confirmed by FTIR analysis and TGA. A clear broad peak at 3395 cm^{-1} of -OH group coupled with other supporting bond stretching of C=C, C-O-H and C-O at 1625 , 1427 and 1057 cm^{-1} respectively confirmed the formation of hydroxylated C_{60} . The molecular weight calculation based on the percentage of C (82.6 %) and O (17.2%) obtained from FESEM analysis as well as the percentage of C (80.52 wt%) and H (0.96%) obtained from CHN elemental analysis, has proven that the fullerene was hydroxylated with eight -OH groups. TGA result showed 5.58 wt% degradation of the synthesized fullerenol from room temperature up to $100\text{ }^\circ\text{C}$ which could be attributed to two molecules of water associated to the synthesized fullerenol moiety. Upon quantification, based on the data obtained from FTIR, FESEM, elemental analysis and TGA, the most possible structure of the synthesized fullerenol was found to be $C_{60}(OH)_8 \cdot 2H_2O$. The synthesized $C_{60}(OH)_8 \cdot 2H_2O$ was found to be soluble both in water and DMSO at a concentration of $\sim 0.33\text{ mg/mL}$. In addition, AFM image as well as DLS analysis of the $C_{60}(OH)_8 \cdot 2H_2O$ solution in DMSO showed that the particle size of

$C_{60}(OH)_8.2H_2O$ synthesized by the ultrasound-assisted technique was within a range of 135-155 nm.

The next part of this thesis will be focusing on the potential application of the synthesized fullereneol, $[C_{60}(OH)_8.2H_2O]$, in preparing a folic acid-based electrochemical biosensor for the detection of a cancer biomarker folate receptor alpha. Fullereneols containing a different number of hydroxy groups derived via other organic synthesis techniques have previously been used in detecting cancer biomarker. Based on that scope, in this thesis it was investigated whether fullereneol, $[C_{60}(OH)_8.2H_2O]$, synthesized by the proposed method of ultrasonication can perform as a suitable nano-mediator in fabricating a biosensor for the detection of a cancer biomarker folate receptor alpha, which will provide some guidelines for others working in the similar area or related fields of science. Current studies, presented in this thesis show that a biosensor prepared by a simple combination of folic acid and the synthesized $C_{60}(OH)_8.2H_2O$ can detect folate receptor alpha up to 1 nM at a sensitivity of 3 $\mu A/nM.cm^2$, where the stability and the reproducibility of the biosensor were 93% and 86% respectively.

Moreover, developing an electrochemical biosensor using a different combination of analytes, ligands, electrodes and electrolytes always comes with new challenges and this thesis also reports on the research investigations into those most important facts and factors to be associated with designing a folate receptor biosensor in presence of the synthesized fullereneol and folic acid as well as has attempted to provide some useful insights on how to deal with the issues that one might come across while designing and developing a biosensor to target folate receptor alpha with a combination of folic acid and fullereneol. On this ground, there are always some rooms for future studies and at the end of this thesis a potential idea of a 'facile bioconjugation' between folic acid and reference fullereneols $[C_{60}(OH)_{10}.5H_2O, C_{60}(OH)_{36}.8H_2O, C_{60}(OH)_{44}.8H_2O]$ has been proposed in providing some directions toward overcoming the existing issues related to developing folic acid-fullereneol based electrochemical biosensor for the detection of folate receptor alpha.

DEDICATION

This thesis is dedicated firstly to my family, then to my country and the rest of the world

ACKNOWLEDGEMENT

“Acknowledgements are evidence that investments in equipments and people have led to important outcomes”- unknown source.

I came across the above-said quote while I was offered a fellowship in 2016 at Flinders University to conduct part of the research works related to my PhD project. The notebook I received there to log in my experimental data it was printed on that. While I was searching around for some advanced technical and peer supports with a curiosity to investigating the future scopes of my current works through conducting some preliminary experimentation on a potential idea, I came across Prof Joe Shaper from Flinders University, Australia in a conference held in the USA, 2016. Prof Joe Shaper paid attention to my research works and provided me the fellowship so I could do some additional studies pertinent to the future scopes of my current research. Prof Joe’s painstaking academic and technical supports to my endeavor helped me to conduct some experiments over there to understand the next potential levels of my current research, the outcome of the experiments is being presented in the ‘future scopes’ part of this thesis (Chapter 6).

Also in the pursual to meet the objectives of my research project, while I was wondering for some expert’s suggestion on ‘fullerene chemistry’ to make sure that my research was traveling on a right pathway to accomplish the first goal of my project, Prof Ken Kokubo from Osaka University, Japan provided fullerenol samples for comparative study as well as technical supports in characterizing the materials thus eventually became an active collaborator of the project and conducted his valuable suggestion all the time.

For the technical and intellectual supports in my project, other than my main supervisor Prof Sivakumar Manickam and co-supervisor Dr Kasturi Muthoosamy, who in fact guided me to becoming a persuasive researcher, I would like to express my gratitude to the aforementioned peers as well for their contribution to my research.

The main source of funding for the research was received from the grant ‘Fundamental Research Grant Scheme’ (grant code: FRGS/1/2013/SG05/UNIM/01/1). For other technical supports I would also like to acknowledge here Prof. Anandan Shanmugam from The University of Nottingham, Malaysia and Dr. Huang Nay Ming, Xiamen University, Malaysia. In this long pursuit, I cannot leave my note here without mentioning about the contribution and cooperation that I received from all the lab technicians as well as fellows from all the corners of the University of Nottingham. The list is too big to fit here, so my sincere appreciation goes to all of them together.

Last and probably the least mentioned are my parents and family, whom I consider the very first contributors to my research as their latent supports and long patience always put me ahead to my endeavor.

Finally, referring to the quote mentioned here in the beginning, I would like to thank ‘myself’ too for holding my intention to continue the research journey. This acknowledgment evidence that people whom I acknowledged here, their supports and investments for me finally resulted in today’s outcome- this thesis.

ACHIEVEMENTS

List of Publications:

1. Afreen, S., Muthoosamy, K., Manickam, S., & Hashim, U. (2015). Functionalized fullerene (C_{60}) as a potential nanomediator in the fabrication of highly sensitive biosensors. *Biosensors and Bioelectronics*, 63, 354-364.
2. Afreen, S., Kokubo, K., Muthoosamy, K., & Manickam, S. (2017). Hydration or hydroxylation: direct synthesis of fullerenol from pristine fullerene [C_{60}] via acoustic cavitation in the presence of hydrogen peroxide. *RSC Advances*, 7(51), 31930-31939.

List of Conference Presentations:

1. Sadia Afreen, Kasturi Muthoosamy, Ken Kokubo, Sivakumar Manickam, A comparative study on the Π - Π conjugation between hydroxylated fullerenes [$C_{60}(OH)_{10}$, $C_{60}(OH)_{44}$] and folic acid, The World Conference on Carbon, 10-15 July 2016, State College, Pennsylvania, USA.
2. Sadia Afreen, Kasturi Muthoosamy, Ken Kokubo, Sivakumar Manickam, Quantification of hydroxyl groups on C_{60} molecular cage generated by acoustic cavitation in aqueous media in presence of hydrogen peroxide, 2nd Asia Oceania Sonochemical Society Conference (AOSS-2), 25-28 July 2015, Kuala Lumpur, Malaysia.
3. Sadia Afreen, Kasturi Muthoosamy, Sivakumar Manickam, Prospects of fullerene (C_{60}) in amplifying the sensitivity of new generation non-invasive diabetes biosensors based on VOC detection technique, 13th Continuing Professional Development (CPD) Series, 69-70. Diabetes Asia 2014 Conference, 16-19 October 2014, Sunway, Malaysia.

Prospective Manuscripts in Progress:

1. Sadia Afreen, Kasturi Muthoosamy and Sivakumar Manickam, Sono-Nano Chemistry: A new era of functionalizing carbon nanomaterials with –OH and the industrial aspects of synthesis. (Abstract submitted in November 2017, to be considered for the AOSS-3 special issue 2018 of Ultrasonics Sonochemistry).
2. A comparative study on the electrochemical behavior of folic acid dispersion vs. folic acid solution for the detection of FR α (prospective title, in the process of submission)
3. Pi-Pi interaction between folic acid and fulleranol: possibilities and challenges toward a facile technique of bioconjugation (prospective title, in the process of submission)

Table of Contents

	Page
List of Scheme & Figures	xv
List of Tables	xxii
List of Equations	xxiv
List of Symbols	xxvi
List of Abbreviations	xxvii
Chapter 1 Introduction: Research Statement & Thesis Outline	
1.1 Research Statement	1
1.1.1 Motivation of the current research	1
1.1.2 Research problems and questions	2
1.1.3 Objectives of the research	5
1.1.4 Outcomes of the research	5
1.2 Outline of the Thesis	6
1.3 Guide to the Next Chapter	6
References	8
Chapter 2 Literature Review	
Graphical Abstract	9
Abstract	10
2.1 Outline of the Background Studies	11
2.2 Functionalized C ₆₀ and its Application in Biosensing	11
2.2.1 Role of C ₆₀ in biosensor	14
2.2.2 Application of functionalized C ₆₀ in glucose biosensor	17
2.2.3 Application of functionalized C ₆₀ in urea biosensor	23
2.2.4 Application of functionalized C ₆₀ in immunosensors	26
2.2.5 Application of functionalized C ₆₀ in the analysis of drugs	31
2.2.6 Application of functionalized C ₆₀ in the detection of	34

	cancer cells	
2.2.7	Functionalized C ₆₀ based biosensor: over ten years of its development	35
2.2.8	Prospects of the functionalized C ₆₀ based biosensors	38
2.3	Ultrasonication: A Potential Technique of Functionalization	40
2.3.1	Acoustic cavitation	40
2.3.2	Application of ultrasonication in functionalizing nanoparticles	46
2.3.3	C ₆₀ to fulleranol via ultrasonic cavitation: a longstanding overlooked idea and its prospects	48
2.4	Key Points of the Review and Direction to the Next Chapter	52
	References	53
Chapter 3	Hydration or Hydroxylation: direct synthesis of fulleranol from pristine fullerene [C ₆₀] via acoustic cavitation in presence of hydrogen peroxide	
	Graphical Abstract	67
	Abstract	68
3.1	Introduction	69
3.2	Experimental	72
3.2.1	Materials & equipments for the synthesis	72
3.2.2	Methods of characterization	73
3.3	Methodology	73
3.3.1	Synthesis of C ₆₀ (OH) _n . mH ₂ O	73
3.3.2	Separation and purification of C ₆₀ (OH) _n . mH ₂ O	75
3.4	Results and Discussion	75

3.4.1	Identification of –OH groups	75
3.4.2	Estimation of the number of –OH groups and the structure of fullerenol	77
3.4.3	Particle size measurements	81
3.4.4	Color and solubility	84
3.4.5	Reaction pathways	85
3.5	Prospects of the Current Finding	87
3.6	Overview of the Current Chapter and Direction to the Next Chapter	88
	References	90
Chapter 4	A comparative study on the electrochemical behavior of folic acid dispersion vs. folic acid solution by cyclic voltammetry	
	Graphical Abstract	98
	Abstract	99
4.1	Introduction	100
4.2	Experimental	105
4.2.1	Materials & Equipments	105
4.2.2	Methodology	106
4.2.2.1	Selection of electrodes	106
4.2.2.2	Cleaning and pretreatment of electrode	107
4.2.2.3	Selection of electrolyte solution	112
4.2.2.4	Selection of potential window	113
4.2.2.5	Preparation of FA dispersion (FA _{H2O}) and FA solution (FA _{PBS})	114
4.2.2.6	Preparation of a standard redox couple [Fe(CN) ₆ ^{3-/4-}]	115

4.2.2.7	Modifying GCE with FA	115
4.3	Results and Discussion	116
4.3.1	Activity of the cleaned bare GCE	116
4.3.2	Calculating the active surface area of GCE	118
4.3.3	Effect of N ₂ purging	119
4.3.4	Electrochemical behavior of FA: dispersion (FA _{H2O}) vs. solution (FA _{PBS})	120
4.3.4.1	Effect of concentration	120
4.3.4.2	Effect of scan rate (v): comparative study	122
4.3.5	Reaction mechanism	132
4.4	Summary of the Current Chapter and Direction to the Next chapter	137
	References	139
Chapter 5	Synthesized fulleranol [C ₆₀ (OH) ₈ .2H ₂ O]-mediated-folic acid-based biosensor for the detection of folate receptor alpha (FR α)	
	Graphical Abstract	144
	Abstract	145
5.1	Introduction	146
5.1.1	FR α as a potential cancer biomarker	146
5.1.2	Correlation between FR α and folate/FA in cancer etiology	146
5.1.3	Application of synthesized fulleranol [C ₆₀ (OH) ₈ .2H ₂ O] in the detection of FR α	148
5.2	Experimental	150
5.2.1	Materials & Equipments	150
5.2.2	Methodology	152

5.2.2.1	Preparation of the modified electrode GCE/FA _{PBS} /C ₆₀ (OH) ₈ .2H ₂ O	152
5.2.2.2	Preparation of folate receptor alpha (FR α) solution	152
5.2.2.3	Preparation of human serum (HS) solution	153
5.2.2.4	Preparation of bovine serum albumin (BSA) solution	154
5.3	Results & Discussion	154
5.3.1	Inter-day voltammetric response of GCE/FA _{PBS}	154
5.3.2	Control measurement	157
5.3.3	Effect of scan rate on the GCE/FA _{PBS} /C ₆₀ (OH) ₈ .2H ₂ O	159
5.3.4	Detection of FR α	162
5.3.5	Detection of FR α : Stability	165
5.3.6	Detection of FR α : Reproducibility	166
5.3.7	Detection of FR α : limit of detection (LOD) & selectivity	167
5.4	Overview of the Current Chapter and Direction to the Next Chapter	171
	References	172
Chapter 6	Fullerenol-Folic acid Bioconjugate: a potential scope for future study	
6.1	Introduction	175
6.1.1	Further scopes toward bioconjugation	175
6.1.2	Background of study	177
6.2	Experimental	179
6.2.1	Materials	179
6.2.1.1	Stability study of folic acid (FA) solution	179
6.2.1.2	Conjugation study	180
6.2.2	Equipment	180

6.2.2.1	Stability study of folic acid solution	180
6.2.2.2	Conjugation study	180
6.2.3	Methodology	180
6.2.3.1	Preparation of folic acid solution	180
6.2.3.2	Preparation of fulleranol-FA reaction mixtures	181
6.3	Results & Discussion	181
6.3.1	Stability and degradation of FA	181
6.3.2	Comparative study: toward the possibility of F10-FA and F36-FA hybrid molecules	185
6.4	Summary of the Current Chapter and Direction to the Next Chapter	188
	References	189
Chapter 7	Conclusions & Recommendations for Future Research	
7.1	Findings and Implications	190
7.2	Recommendations for Future Studies	193
7.2.1	Industrial scale-up of the proposed method of synthesis	193
7.2.2	Enhancing the sensitivity and selectivity of the fullerenol/folic acid-FR α biosensor	193

List of Scheme & Figures

Scheme No.	Scheme Detail	Page No.
1.0	Different methods proposed for the synthesis of fullerenols in the previous reports (Wang et al., 2015)	4
Figure No.	Figure Details	Page No
1.0	Graphical representation summarizing the research statement and scopes of the research	4
2.1	Components and the involved mechanism of a conventional electrochemical biosensor	15
2.2	Function of fullerene (C ₆₀) at the interface of recognition site and electrode	15
2.3	Calibration curve of the glucose biosensor containing 1.7 µg C ₆₀ /mg of electrode material. Experimental conditions: 10 mM phosphate buffer, pH 7.5, under argon, at +350 mV vs. Ag/AgCl (Gavalas and Chaniotakis, 2000).	18
2.4	Frequency response of the glucose biosensor against different concentration of glucose (Chang and Shih, 2000).	19
2.5	Cyclic voltammogram of GOx/C ₆₀ -Fc-CS-IL-GCE in the absence of glucose (a) in the presence of 1.0 M glucose (b) and in the presence of 5.0 M glucose (c) at pH 7.0 PBS and at 100 mV/s (Zhilei <i>et al.</i> , 2010)	21
2.6	Response time with relation to potential difference when the concentration of urea was changed step by step from 10 ⁻⁵ to 10 ⁻¹ M (A), observed potential vs. urea concentration ranges from 10 ⁻⁵ to 10 ⁻¹ M (B) (Saeedfar <i>et al.</i> , 2013).	25

Figure No.	Figure Details	Page No.
2.7	C ₆₀ -anti-human IgG coated quartz crystal electrode for IgG (Pan and Shih, 2004)	26
2.8	Calibration curve corresponding to the chronoamperometric responses of the proposed biosensor at different concentrations of glutathione (Carano <i>et al.</i> , 2002)	28
2.9	Effect of dosage of C ₆₀ cast onto a GC electrode: a) 5 μL; b) 10 μL; c) 15 μL; d) 20μL (Tan <i>et al.</i> , 2003)	33
2.10	Usage of functionalized C ₆₀ in different types of biosensors [1999-2013]	36
2.11	Trend of using functionalized C ₆₀ for biosensor devices over the last decade (based on the reports discussed in the subsections 2.2.1-2.2.6 of the thesis)	36
2.12	Mechanism of bubble formation and collapse with the expansion and contraction of ultrasound wave through aqueous medium	43
3.1	Greener and cleaner ultrasonic cavitation strategy to synthesize fullerenol in a facile and faster way as compared to other conventional method	71
3.2	Synthesis of water soluble fullerenol via acoustic cavitation induced by ultrasound at ambient temperature and within 1 h reaction time in the presence of dil. H ₂ O ₂ (30%).	72

Figure No.	Figure Details	Page No.
3.3	(a) Dark brown dispersion immediately after ultrasonication, (b) Separation of unreacted C ₆₀ from C ₆₀ (OH) _n . mH ₂ O using toluene and (c) Clear top layer of toluene after 10 times of repeated washing. Here, n = 8 and m = 2 which were finally determined by elemental analysis and TGA (d) Experimental set-up for the synthesis of C ₆₀ (OH) _n . mH ₂ O	74
3.4	FTIR spectra of (a) product C ₆₀ (OH) _n . mH ₂ O, (b) pristine C ₆₀ and (c) pristine C ₆₀ (OH) ₁₂ .	76
3.5	IR spectra of C ₆₀ (OH) _n . mH ₂ O obtained via ultrasonication (a) in presence of dil. H ₂ O ₂ (30%), (b) in Type II pure H ₂ O without any H ₂ O ₂ .	76
3.6	TGA chart for measuring the weight loss (wt.%) of C ₆₀ (OH) ₈ . 2H ₂ O	80
3.7	Particle size measurements: (a) C ₆₀ (OH) ₈ . 2H ₂ O/DMSO solution (collected as supernatant after centrifugation), (b) C ₆₀ (OH) ₈ . 2H ₂ O/DMSO suspension (0.33 mg/mL).	81
3.8	(a) AFM image shows the topography of C ₆₀ (OH) ₈ . 2H ₂ O particles on mica substrate within a scan area of 1 μm x 1 μm; particles under scanning line are marked with red cross. (b) Topography vs. distance chart for thickness measurement where C ₆₀ (OH) ₈ . 2H ₂ O particles show a consistent width of around 150 nm and the average height of the particles under scanning line is in between 135 to 155 nm.	82
3.9	SEM image of C ₆₀ (OH) ₈ . 2H ₂ O (20 KV, magnification of 30000 x)	83

Figure No.	Figure Details	Page No.
3.10	(a) C ₆₀ (OH) ₈ ·2H ₂ O after drying, (b) C ₆₀ (OH) ₈ ·2H ₂ O in DMSO (0.33 mg/mL), *(c) Color of different fullerenols previously reported [*Reprinted from Kokubo <i>et al.</i> (2008)]	84
3.11	Possible reaction paths in ultrasound-assisted synthesis of fulleranol in the presence of dil. H ₂ O ₂ (30%).	86
4.1	(a) Three-electrode set-up used in the experiments, (b) Circuit diagram showing the connections among the three electrodes, (c) VersaSTAT3 potentiostat used for cyclic voltammetry	106
4.2	Steps of modifying a GCE (a) mirror finish texture of the active surface of a bare GCE, (b) modifying GCE by drop casting FA _{PBS} onto its active surface, (c) GCE modified with FA _{PBS} (drop casted and then dried at room temperature), (d) the mirror finish texture of GCE's active surface area is no longer retained after the CV scan of the modified GCE	108
4.3	Polishing of the surface of GCE (faced onto the alumina paste) in a pattern of number '8' on the alumina paste	109
4.4	(a) Different parts of the Ag/AgCl (sat. KCl) reference electrode used in this study, (b) Ag/AgCl (sat. KCl) dipped inside 1 M KCl solution when not in use	111
4.5	Reversible voltammogram of Fe(CN) ₆ ^{3-/4+} redox couple solution (containing 1 mM K ₃ Fe(CN) ₆ and 0.1 M KCl) at a scan rate of 75 mV/s	117

Figure No.	Figure Details	Page No.
4.6	Voltammograms of bare GCE in 0.01 M PBS at a scan rate of 75 mV/s when N ₂ gas was purged for different duration (15 min and 30 min)	119
4.7	(a) cyclic voltammogram of GCE/FA _{H2O} at different concentration of FA dispersion prepared only in H ₂ O, (b) <i>i</i> _{pa} vs. concentration of FA	121
4.8	Effect of scan rates on the anodic peak current (<i>I</i> _{pa}) of GCE/FA _{H2O}	123
4.9	Effect of scan rates on the anodic peak current (<i>I</i> _{pa}) of GCE/FA _{PBS}	123
4.10	(a) <i>I</i> _{pa} vs. <i>v</i> ^{1/2} plot and (b) <i>I</i> _{pa} vs. <i>v</i> plot for GCE/FA _{H2O}	124
4.11	(a) <i>I</i> _{pa} vs. <i>v</i> ^{1/2} plot and (b) <i>I</i> _{pa} vs. <i>v</i> plot for GCE/FA _{PBS}	126
4.12	Multiscan CV of GCE/FA _{H2O} at different scan rates	129
4.13	Multiscan CV of GCE/FA _{PBS} at different scan rates	131
4.14	Electrode-solution interface for an ideal reversible reaction	133
4.15	The irreversible reaction (oxidation) of FA at the surface of GCE	134
4.16	Electrode-solution interface for the irreversible electron transfer mechanism during oxidation of FA at GCE	134

Figure No.	Figure Details	Page No.
5.1	Cyclic voltammetry of GCE/FA _{PBS} in 0.01 M PBS recorded on five consecutive days at a scan rate of 100 mV/s	156
5.2	CV of bare GCE, GCE/PBS, GCE/C ₆₀ (OH) ₈ .2H ₂ O, GCE/FR α and bare GCE in presence of FR α as an analyte in PBS	158
5.3	CV of GCE/FA _{PBS} /C ₆₀ (OH) ₈ .2H ₂ O at different scan rates	159
5.4	Plot of I _{pa} vs. v ^{1/2} for GCE/FA _{PBS} /C ₆₀ (OH) ₈ .2H ₂ O	161
5.5	Plot of I _{pa} vs. v for GCE/FA _{PBS} /C ₆₀ (OH) ₈ .2H ₂ O	161
5.6	CV for the detection of 1 nM FR α with GCE/FA _{PBS} /C ₆₀ (OH) ₈ .2H ₂ O in 0.01 M PBS at a scan rate of 100 mV/s	162
5.7	CV of GCE/FA _{PBS} /C ₆₀ (OH) ₈ .2H ₂ O before and after 7 days in the presence of 1 nM FR α in 0.01 M PBS at a scan rate of 100 mV/s	165
5.8	CV of GCE/FA _{PBS} /C ₆₀ (OH) ₈ .2H ₂ O and GCE'/FA _{PBS} /C ₆₀ (OH) ₈ .2H ₂ O in the presence of 1 nM FR α in 0.01 M PBS at a scan rate of 100 mV/s	166
5.9	Chronoamperometry: current vs. time (I-t) for GCE/FA _{PBS} /C ₆₀ (OH) ₈ .2H ₂ O at an applied voltage of 0.9 V for the addition of 500-1400 pM FR α at a time interval of 60 s in 0.01 M PBS	167
5.10	Plot of anodic peak current vs. concentration of FR α in a linear range	168

Figure No.	Figure Details	Page No.
5.11	Chronoamperometry of GCE/FA _{PBS} /C ₆₀ (OH) ₈ .2H ₂ O at an applied voltage of 0.9 V for the addition of FR α , HS and BSA at varying concentrations* and at a time interval of 60 s in 0.01 M PBS	169
5.12	Linear range of current obtained from chronoamperometry for the addition of FR α in 0.01 M PBS before adding HS and BSA as interfering molecules	169
6.1	Molecular structure of folic acid (Off <i>et al.</i> , 2005)	177
6.2	Absorption spectra of unstirred aqueous solution of FA recorded for five days	182
6.3	Absorption spectra of stirred aqueous solution of FA recorded for five days	182
6.4	Comparative absorption spectra of unstirred and stirred aqueous solution of FA	184
6.5	UV-Vis spectra of the F10-FA reaction mixtures	185
6.6	UV-Vis spectra of the F36-FA reaction mixtures	186
6.7	UV-Vis spectra of the F44-FA reaction mixtures	187

List of Tables

Table No.	Table Details	Page No.
1.0	Distribution of the major contents in this thesis	7
2.1	Comparison of K_m among different types of glucose biosensor (Zhilei <i>et al.</i> , 2010).	22
2.2	Comparative study of glucose limit in the blood serum samples (Zhilei <i>et al.</i> , 2010).	23
2.3	Analytical results of the C_{60} -anti-human IgG coated quartz crystal electrode (Pan and Shih, 2004).	27
3.1	Empirical formula of $C_{60}(OH)_n$ synthesized in the presence of dil. H_2O_2 (30%)	78
3.2	Empirical formula of $C_{60}(OH)_n$ synthesized only in the presence of type II pure H_2O	79
3.3	Solubility of $C_{60}(OH)_8 \cdot 2H_2O$ in comparison to C_{60} in different solvents	85
4.1	Peak currents and peak potentials for the reversible reaction of $Fe(CN)_6^{3-/4-}$ redox couple	117

Table No.	Table details	Page No.
4.2	Anodic peak currents (I_{pa}) and peak potentials (V) recorded at different concentrations of FA	121
5.1	The composition of different protein molecules present in the purchased HS (as received from Sigma-Aldrich product data sheet for the product coded ERM DA470KIFCC)	150
5.2	Anodic peak potential and the corresponding anodic peak current obtained from the CV on five consecutive days	156
5.3	Anodic peak potential and the corresponding anodic peak current obtained from the CV at different scan rates for GCE/ $FA_{PBS}/C_{60}(OH)_8 \cdot 2H_2O$ (in comparison with GCE/ FA_{PBS})	159
5.4	Comparative values of E_{pa} and I_{pa} for different modified GCE in the absence and presence of $FR\alpha$	163
5.5	Values of current vs. concentration for $FR\alpha$ while added with HS and BSA in 0.01 M PBS	170

List of Equations

Equation No.	Equation	Page No.
2.1	$\text{H}_2\text{O} \leftrightarrow \text{H}\cdot + \cdot\text{OH}$	50
2.2	$\text{H}\cdot + \text{H}\cdot \leftrightarrow \text{H}_2$	50
2.3	$\cdot\text{OH} + \cdot\text{OH} \leftrightarrow \text{H}_2\text{O}_2$	50
2.4	$\text{H}\cdot + \text{O}_2 \leftrightarrow \text{HO}_2\cdot$	50
2.5	$\text{H}\cdot + \text{HO}_2\cdot \leftrightarrow \text{H}_2\text{O}_2$	50
2.6	$\text{HO}_2\cdot + \text{HO}_2\cdot \leftrightarrow \text{H}_2\text{O}_2 + \text{O}_2$	50
2.7	$\text{H}_2\text{O}\cdot + \cdot\text{OH} \leftrightarrow \text{H}_2\text{O}_2 + \text{H}\cdot$	50
4.1	$\text{Na}^+(\text{aq}) + \text{e}^- = \text{Na}(\text{s})$ [half reaction, reduction, potential E^0 (V) = - 2.71V]	114
4.2	$\text{K}^+(\text{aq}) + \text{e}^- = \text{K}(\text{s})$ [half reaction, reduction, potential E^0 (V) = - 2.92V]	114
4.3	$\text{Cl}_2(\text{g}) + 2\text{e}^- = 2\text{Cl}^-(\text{aq})$ [half reaction, reduction, potential E^0 (V) = 1.36 V]	114
4.4	$\Delta E = E_{\text{pa}} - E_{\text{pc}} \sim 0.059/n$	116
4.5	$\text{Fe}^{4+} \rightleftharpoons [\text{Fe}]^{3+} + \text{e}^-$	116
4.6	$I_{\text{p}} = 2.69 \times 10^5 n^{3/2} A D^{1/2} v^{1/2} C$	118
4.7	$I_{\text{pa}} (\mu\text{A}) = 0.0173 (\mu\text{M}) + 1.3827$	121
4.8	$I_{\text{pa}} (\mu\text{A}) = 1.3151 v^{1/2} (\text{mV/s}) + 15.196$	125
4.9	$I_{\text{pa}} (\mu\text{A}) = 0.106v (\text{mV/s}) + 18.27$	125
4.10	$I_{\text{pa}} (\mu\text{A}) = 8.6514 v^{1/2} (\text{mV/s}) - 40.199$	126
4.11	$I_{\text{pa}} (\mu\text{A}) = 0.5332 v^{1/2} (\text{mV/s}) - 7.67$	126
5.1a	$\text{FA}_{(\text{depletion})} = f[\text{FR}\alpha_{(\text{overexpression})}]$	147

5.1b	$FA_{(\text{depletion})} \propto FR\alpha_{(\text{overexpression})}$	147
5.2	$I_{pa} (\mu A) = 3.5935v^{1/2} - 4.8216$	160
5.3	$I_{pa} (\mu A) = 0.2112v + 9.46$	160

List of Symbols

K_m	Michaelis-Menten constant
vP	Vapor pressure
Δp	Difference in pressures
Δp_c	Tensile strength of liquid
v	Scan rate

List of Abbreviations

AFM	Atomic force microscopy
Ag	Silver
Au	Gold
BDD	Boron doped electrode
BLM	Self-assembled bilayer lipid membrane
BSA	Bovine serum albumin
BSC	Biosafety cabinet
C ₆₀	Buckminster fullerene/fullerene
C ₆ H ₆	Benzene
C ₆₀ O _n	Fullerene epoxide
C ₆₀ (OH) _n	Fullerol, fullerenol
CHI-SH	Thiolated chitosan
CH ₂ Cl ₂	Dichloromethane
CNT	Carbon nanotube
-COOH	Carboxyl group
C ₆₁ (COOEt) ₂	Cyclopropafullerene-C ₆₀ -dicarboxylic acid diethyl ester
C ₆₁ (COOH) ₂	Cyclopropafullerene-C ₆₀ -dicarboxylic acid
C _n @SWNT	Synthesized modified fullerenes
CE	Counter electrode
CS	Chitosan
CS ₂	Carbon-di-sulfide

CV	Cyclic voltammetry
CNT	Carbon nanotube
CS	Chitosan
DI	Deionized water
DFT	Density functional theory
DLS	Dynamic light scattering
DMSO	Dimethyl sulfoxide
DON	Deoxynivalenol
DPV	Differential pulse voltammetry
DWCNTs	Double-walled carbon nanotubes
EIS	Electrochemical impedance spectroscopy
ESR	Electron spin resonance
FA	Folic acid
FA _{H2O}	Folic acid dispersion prepared only in water
FA _{PBS}	Folic acid solution prepared in PBS
FA _{PBS} /C ₆₀ (OH) ₈ .2H ₂ O	Glassy carbon electrode modified with a mixture of folic acid (prepared in PBS) and synthesized C ₆₀ (OH) ₈ .2H ₂ O (prepared in DI water) solutions
Fc	Ferrocene
F _{ox}	Oxidized folic acid
FISPE	C ₆₀ impregnated screen printed electrode
FE-SEM	Field emission scanning electron microscopy
FR	Folate receptor

FR α	Folate receptor alpha
FTIR	Fourier transform infrared spectroscopy
F10	C ₆₀ (OH) ₁₀ ·5H ₂ O
F36	C ₆₀ (OH) ₃₆ ·8H ₂ O
F44	C ₆₀ (OH) ₄₄ ·8H ₂ O
G (IgG)	Immunoglobulin
GC	Glassy carbon
GCE	Glassy carbon electrode
GCE'	Different glassy carbon electrode
GOx	Glucose oxidase
HO ₂ '	Hydroperoxy radical
H ₂ O ₂	Hydrogen peroxide
Hb	Hemoglobin
HER	Hydrogen evolution reaction
HIVP	HIV-1 protease
HS	Human serum
IL	Ionic liquid
ITO	Indium tin oxide
IUPAC	International Union of Pure and Applied Chemistry
JCM1649	16S rDNA extracted from <i>Escherichia coli</i>
LSV	Linear sweep voltammetry
Mb	Myoglobin
MNPs	Magnetite nanoparticles

miRNA	Micro RNA
MRI	Magnetic resonance imaging
MSDS	Material safety data sheet
MWCNT	Multi-walled carbon nanotube
NaOH	Sodium hydroxide
-NH ₂	Amino group
NMR	Nuclear magnetic resonance
PB	Au-polypyrrole [PPy]/Prussian blue
PBS	Phosphate buffered saline
PGE	Pyrolytic graphite electrode
PTC-NH ₂	3,4,9,10-perylenetetracarboxylic dianhydride
P(MMA-co-St)/O-MMT	Poly(methyl methacrylate-co-styrene)/montmorillonite
PDGF-BB	Platelet-derived growth factor B-chain
PTC	Phase transfer catalysts
-O	Epoxide
-OH	Hydroxy group
OER	Oxygen evolution reaction
OMC	Ordered mesoporous carbon
ORR	Oxygen reduction reaction
ox-CNOs	Carbon nano-onions
PDDA	Poly(diallyldimethylammonium) chloride
PDGF-BB	Platelet-derived growth factor B-chain
PSS	Poly(sodium-4-styrenesulfonate)

PtZONS	Zinc oxide (ZnO) nanospheres
PZ	Piezoelectric
Pt	Platinum
QCM	Quartz crystal microbalance
SCCa	Squamous cell carcinoma antigen
SAW	Surface acoustic wave immunosensor
SHE	Standard hydrogen electrode
SH-SAW	Shear horizontal surface acoustic wave
SEM	Scanning electron microscopy
SEM-EDS	Scanning electron microscopy with energy dispersive X-ray spectroscopy
SWCNT	Single walled carbon nanotube
SWV	Square wave voltammetry
RE	Reference electrode
ROS	Reactive oxygen species
R.S.D	Relative standard deviation
TBAH	Tetrabutylammonium hydroxide
TGA	Thermogravimetric analysis
UV	Ultraviolet
WE	Working electrode

Chapter 1

Introduction: Research Statement & Thesis Outline

1.1 Research Statement

In this report, an innovative and potential technique of synthesizing fulleranol from pristine C₆₀ has been proposed where ultrasonication plays a vital role in hydroxylating pristine C₆₀ in an aqueous medium which upon quantification reveals the possible structure of the potential fulleranol moiety that could be generated by the technique of ultrasonication. The current study shows that by the proposed method of synthesis eight hydroxyl groups (-OH) could be attached to C₆₀. In the application part of this study, the synthesized fulleranol has been applied in developing a biosensor for the detection of a cancer biomarker, folate receptor alpha (FR α) which showed a stable and reproducible biosensing of FR α up to 1 nM at a sensitivity of 3 $\mu\text{A/nM}\cdot\text{cm}^2$. In addition to that, to provide the scopes of future studies to enhancing the sensitivity of the proposed biosensor, an additional comparative study has been presented at the end of the main experimental works, where the possibility of π - π conjugation between three reference fullerenols and folic acid molecules has been discussed with a view to preparing a fulleranol-folic acid hybrid biomolecule.

1.1.1 Motivation of the current research

Every individual or group research is intrigued by the scopes of random possibilities lying underneath certain existing challenges in any particular field of research. Conclusions received from others' studies provide us with diverse schemes to investigating further possibilities, sometimes to rethinking the existing methods/methodologies and redefining a process or phenomenon. Current studies presented in this thesis were also intrigued by an underlying possibility of preparing polyhydroxylated fullerene via only ultrasonication technique, where in the previous studies only hydration was accounted as the reason why fullerene dissolves in an aqueous medium during ultrasonic dispersion, thus the other possibility of

hydroxylation remained overlooked. It is quite interesting to note that there are sufficient reports providing the information about generation of hydroxy groups ($-OH$) during ultrasonication, hence, not only the phenomena of hydration of C_{60} molecules to be considered during its ultrasonic dispersion in aqueous medium but also the possibility of hydroxylation of fullerene molecule is eminent therein, thus further studies along with a detailed quantitative analysis are still in demand to investigate the generation of any potential fullerenol moiety and its possible molecular structure, which has been considered the main motivation of the current study.

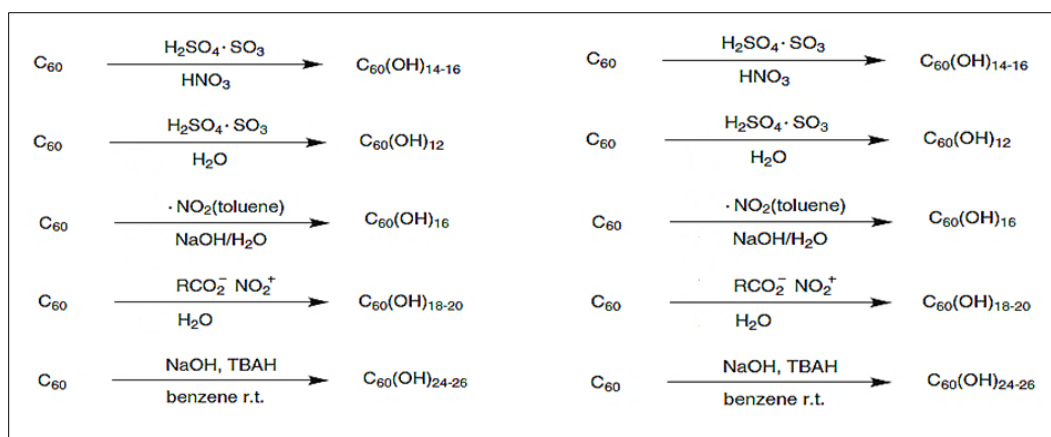
1.1.2 Research problems and questions

In the field of nano-material science and technology Buckminster fullerene (C_{60}), the third allotrope of carbon, nowadays, has been attaining stupendous attention among the scientific communities owing to its interesting physicochemical properties; for instances, nanoparticles of C_{60} have high surface to volume ratio which could be a useful physical property in deriving advanced functional materials from C_{60} via chemical synthesis, it can undergo six distinct one-electron reversible reductions forming stable intermediates which is an outstanding chemical property of C_{60} compared to its other contemporary carbon nanomaterials and this chemical property could also be exploited in synthesizing hybrid biomolecules through bioconjugation as well as in developing potential nanobiosensors, so the applications could be enormous in the fields of physical, chemical and biological sciences.

Although, copious reports based on C_{60} and its functionalization have already provided us with the information about the possibilities and the challenges needed to overcome in utilizing the potential of C_{60} , the scopes of functionalizing this third allotrope of carbon and its useful applications in various fields of material science as well as in biological science are still less explored compared to other contemporary carbon allotropes, e.g., graphene, carbon nanotubes, etc. C_{60} is very stable nanomaterial but at the same time due to its sparing solubility in water and/or aqueous medium makes its use limited in inorganic and organic chemistry as well. Addition of water soluble functional groups, e.g. groups ($-OH$), carboxyl ($-COOH$), amino ($-NH_2$) can enhance the solubility of C_{60} in aqueous medium where some promising reports are available explaining the techniques of functionalization with the aforementioned

radicals/functional groups, still every technique has been associated with some difficulties in synthesis and purification process as well as prolonged time of reaction, thus the application of C₆₀ and its derivatives is still less explored compared to other carbon nanomaterials not only due to its low solubility in water but also owing to the lack of a facile and faster way of functionalizing C₆₀ with potential water soluble functional groups. Therefore, the necessity to developing a more facile technique of functionalizing C₆₀ is still in demand. On this context, this report is designed to develop an innovative method of functionalizing C₆₀ with -OH groups via ultrasound-assisted technology concerning the current demand for the more facile technique of synthesizing 'polyhydroxylated C₆₀' (fullerenol).

Compared to C₆₀, fullerenols are more useful in biological applications due to their water solubility and biocompatibility. Hence, in recent studies fullerenols are being addressed as potential candidates to be used as an antioxidant, a nanocarrier in drug delivery, a mediator in biosensing, even as an interfacial materials or buffer layer in photovoltaic cells (Cao *et al.*, 2016; Semenov *et al.*, 2016; Wang *et al.*, 2015; Chen *et al.*, 2012). However, generally for any biological application a material of interest not only needed to be water soluble and biocompatible but also it is important that the material is free from impurity. Common methods reported previously for the synthesis of various fullerenols mostly involve either acid hydrolysis in presence of other hydroxylating reagents e.g. NaOH, KOH or application of phase transfer catalyst (PTC) (Scheme 1.0). Fullerenols produced using hazardous strong acids, strong alkali reagents and PTC often resulted into impurities in the final product which as reported by others were difficult to remove completely from fullerenols (Wang *et al.*, 2015). The other shortcoming associated to the previous methods also incorporate long duration of reaction which varied from at least 16 h to 4 days. It is also important to note that the use of strong acid makes it a hazardous method for the synthesis of fullerenols.



Scheme 1.0 Different methods proposed for the synthesis of fullerlenols in the previous reports (Wang *et al.*, 2015)

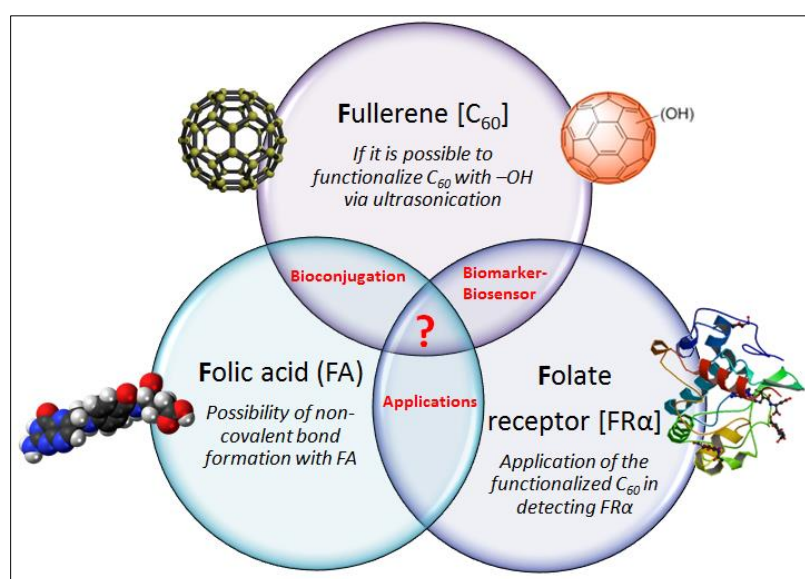


Figure 1.0 Graphical representation summarizing the research statement and scopes of the research

Based on these existing problems related to the previous methods of fullerlenol synthesis this research work is designed to provide answers to the following research questions as well as the possibilities associated with them (Fig. 1.0),

- Whether it is possible to functionalize fullerene with hydroxy groups ($-\text{OH}$) groups only via ultrasonication in an aqueous medium?
- If possible, what could be the molecular structure of the synthesized fullerlenol?
- Whether there could be any potential application(s) of the synthesized fullerlenol prepared by the proposed method of ultrasonication?

1.1.3 Objectives of the research

1. Functionalizing C₆₀ with –OH groups in an aqueous medium in the presence of hydrogen peroxide (H₂O₂) via ultrasonication and quantifying the structure of synthesized polyhydroxylated C₆₀ (fullerenol).
2. Developing a biosensor based on folic acid and the synthesized fullerenol in detecting a cancer biomarker folate receptor alpha (FR α).
3. Evaluating the selectivity and reproducibility of the proposed biosensor.
4. Investigating the possibility of non-covalent bond formation between folic acid and reference fullerenol moieties as part of the future studies toward enhancing the robustness of the proposed biosensor.

1.1.4 Outcomes of the research

The current studies in this research have come up with the following outcomes and novelties,

- An innovative, more facile and cost-effective technique for the preparation of hydroxylated C₆₀ containing eight –OH groups.
- A potential electrochemical biosensor based on a new combination of ligand/receptor (folic acid)-mediator (synthesized fullerenol) for the detection of cancer.
- Directions toward the possibility of facile bioconjugation between folic acid and fullerenols as a further scope stemmed from the findings of the current work.

It is worth mention here that although many methods of fullerenol synthesis have been proposed previously but most of them are not commercially feasible due to long duration of reaction and requirement of more hazardous reagents and multiple steps for purification and synthesis of fullerenols. Fullerenols could be different types based on the number of -OH groups attached to C₆₀ molecule and a specific, industrially scalable method for every fullerenol is currently in high demand. The proposed method shows a handy protocol to prepare a fullerenol which is occupied with eight -OH groups and there is a possibility that the attachment of -OH groups could be increased on further scale-up of the proposed method. Considering this, the proposed method shows the potential for the preparation of fullerenol containing less to more (2-12) -OH groups by

the technique of ultrasonication. In terms of cost-effectiveness the proposed method requires less reagents as well as does not need any PTC for the synthesis, which together offers less cost for the synthesis compared to the previous methods. Current method could be an industrially viable process as it is a green technique of synthesis, offers less processing time coupled with the requirement of less reagents (only 30% H₂O₂) for synthesis as well as easy purification and separation.

1.2 Outline of the Thesis

According to the objectives of the research works, this thesis has been structured into four experimental chapters along with a literature review in the beginning of the thesis and a conclusion pointing out the major findings. Among the four experimental chapters, the first three chapters are structured based on the core experimental works conducted related to the synthesis and application of the synthesized fulleranol. The purpose of the fourth experimental chapter is to provide the findings of some preliminary works in order to evidence further scopes of the current research. Thus, the fourth experimental chapter will basically be considered as the chapter for an empirical discussion toward the future studies (Table 1.0).

For a better understanding, every individual chapter is ended up with the key points or findings and guidance toward the next chapter. Unfamiliar terms and techniques, where necessary, have been narrated prior to the experimental discussion in order to make the contents apprehensive. Every core experimental chapter in this thesis is represented by a graphical abstract in the beginning to emphasize the objective(s) and outcome(s) of every individual chapter.

1.3 Guide to the Next Chapter

The next chapter (chapter 2) of this thesis contains the literature review relevant to the current works. The literature review chapter is discussed in two main sections: the first one about the background studies on functionalized fullerene and its potential applications in biosensing, whereas the next one is to review the application of ultrasound in functionalizing nanomaterials as well as to functionalize C₆₀.

Table 1.0 Distribution of the major contents in this thesis

No. of Chapters	Contents	Percentage of major contents (%)									
		10	20	30	40	50	60	70	80	90	100
1	Research summary										
2	Literature review: fullerene based biosensor	BS/D									
	Literature review: scope of ultrasound					BS/D					
3	Experimental: synthesis	BS/D	E								
4	Experimental: validation	BS/D	E								
5	Experimental: application	BS/D	E								
6	Future direction based on experimentations	BS/D				E					
7	Conclusion										

BS/D = Background Study and/or Discussion

E = Experimental

References:

Cao, T., Wang, Z., Xia, Y., Song, B., Zhou, Y., Chen, N., & Li, Y. (2016). Facilitating electron transportation in perovskite solar cells via water-soluble fullereneol interlayers. *ACS Applied Materials & Interfaces*, 8(28), 18284-18291.

Chen, Z., Ma, L., Liu, Y., & Chen, C. (2012). Applications of functionalized fullerenes in tumor theranostics, *Theranostics*, 2(3), 238–250.

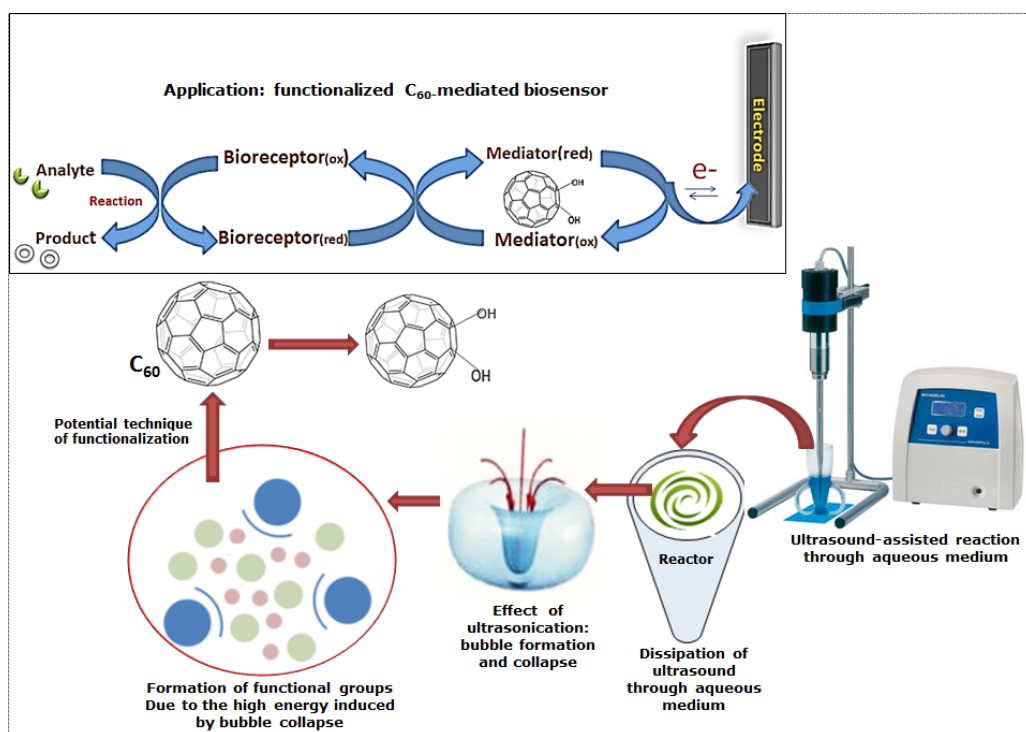
Semenov, K. N., Charykov, N. A., Postnov, V. N., Sharoyko, V. V., Vorotyntsev, I. V., Galagudza, M. M., & Murin, I. V. (2016). Fullerenols: Physicochemical properties and applications. *Progress in Solid State Chemistry*, 44(2), 59-74.

Wang, Z., Wang, S., Lu, Z., & Gao, X. (2015). Syntheses, structures and antioxidant activities of fullereneols: knowledge learned at the atomistic level. *Journal of Cluster Science*, 26(2), 375-388.

Chapter 2

Literature Review

Graphical Abstract



Abstract

Ultrasonication is nowadays being considered as an alternative green and energy efficient technology for not only to produce a diverse size and shape of nanoparticles but also to synthesize multifunctional hybrid nanoparticles. The product and yield of an ultrasound-assisted synthesis process mostly depend on the underlying mechanism of ultrasonication, where several factors should be taken into consideration while designing the synthesis process of nanoparticles by the technique of ultrasonication. Most of the reports on synthesizing and functionalizing nanoparticles by ultrasonication are based on the mechanism of acoustic cavitation of ultrasound. The advantages associated with ultrasound-assisted synthesis technique encompass less time of reaction, cost-effective method, easy handling and maintenance. The application of ultrasound in functionalizing various materials has progressively been gaining its popularity in chemical synthesis and processing of even various nanomaterials. This chapter will review some of the recent promising applications of acoustic cavitation in functionalizing nanomaterials, as well as a brief description will be conveyed on the several factors that should be considered while designing an ultrasound-assisted synthesis process both on lab-scale and on an industrial level for bulk production. With this increasing demand for the use of ultrasonication in the chemical synthesis process, a new scope could be explored to functionalize a carbon nanomaterial, known as Buckminster fullerene (C_{60}) with hydroxy groups (-OH) by the technique of ultrasonication. Functionalization of C_{60} is also nowadays becoming important due to its potential application as an electron mediator in a biosensor. This review also discusses various approaches that have been reported for C_{60} derivatives and their applications in the fabrication of different types of biosensors. On this context, this chapter will also discuss the potential of ultrasonication in functionalizing C_{60} with -OH groups in an aqueous medium along with the application of functionalized C_{60} in various biosensors.

2.1 Outline of the Background Studies

This chapter will present a summarized discussion on the prospects of functionalized C_{60} and the potential of ultrasonication in functionalizing nanomaterials based on the previously reported studies. To provide clear information regarding the background of the current work this chapter on literature review is outlined as follows:

- The aspects and prospects of functionalized C_{60} in the field of electrochemistry, as in biosensor
- The potential of ultrasonication or acoustic cavitation in functionalizing nanomaterials
- In relation to the potential of the acoustic cavitation, the possibility of hydroxylating C_{60} to fulleranol via ultrasonication technique

2.2 Functionalized C_{60} and its Application in Biosensing

Designing a biosensor for versatile biomedical applications is a sophisticated task and how dedicatedly functionalized (C_{60}) can perform on this stage is a challenge for today's and tomorrow's nanoscience and technology. Since the invention of biosensor, many ideas and methods have been invested to upgrade the functionality of biosensors. Due to special physicochemical characteristics, the novel carbon material "fullerene" adds a new dimension to the construction of highly sensitive biosensors. The prominent aspects of C_{60} explain its outstanding performance in biosensing devices as a mediator, e.g. C_{60} in organic solvents exhibits 5 stages of reversible oxidation/reduction, and hence C_{60} can work either as an electrophile or nucleophile. C_{60} is stable and its spherical structure produces an angle strain which allows it to undergo characteristic reactions of addition to double bonds (hybridization which turns from sp^2 to sp^3). However, elemental C_{60} individually is difficult to be used very effectively in the construction of highly sensitive biosensors for the detection of different analytes due to its sparing solubility in aqueous solution. But, prospective benefits could be achieved through the manipulation/modification of C_{60} into its potential derivatives. Hence, research studies are being conducted worldwide to invent a variety of methods of C_{60} functionalization with a purpose of incorporating it effectively in biosensor devices. The different functionalization methods include modification of C_{60} into water soluble

derivatives and conjugation with enzymes and/or other biomolecules, e.g. urease, glucose oxidase, haemoglobin, myoglobin (Mb), conjugation with metals e.g. gold (Au), chitosan (CS), ferrocene (Fc), etc. to enhance the sensitivity of biosensors. The state-of-the-art research on C₆₀ functionalization and its application in sensor devices has proven that C₆₀ can be implemented successfully in preparing biosensors to detect glucose level in blood serum, urea level in urine solution, haemoglobin, immunoglobulin, glutathione in real sample for pathological purpose, to identify doping abuse, to analyze pharmaceutical preparation and even to detect cancer and tumor cells at an earlier stage. Employing fullerene-metal matrix for the detection of tumor and cancer cells is also possible by the inclusion of C₆₀ in single-walled carbon nanotubes (SWCNTs) known as peapods as well as in double-walled carbon nanotubes (DWCNTs), to augment the effectiveness of biosensors.

After the first successful presentation of biosensor by Leland C. Clark in 1962, numerous researches have been executed by the scientific communities worldwide to advance the functionality of this device for the detection of different types of biomolecules. Nowadays we find a variety of biosensors based on distinctive physicochemical detectors, which are now being used in food analysis, environmental monitoring, drug delivery and diagnosis of health-related issues, toxicity measurement, protein engineering, DNA sequencing, genetic analysis, cellular localization, cell identification and sorting, detection of pathogens, remote sensing of airborne bacteria and other biomedical applications (Bosi *et al.*, 2003; Jensen *et al.*, 1996). Some of the examples: carbon nanotube (CNT)/teflon matrix based glucose biosensor, glucose biosensor based on incorporation of laccase in CNT/chitosan matrix (Pumera *et al.*, 2007), glucose nanobiosensor prepared with a bilayer of the poly(diallyldimethylammonium) chloride (PDDA) and poly(sodium-4-styrenesulfonate) (PSS) on 3-mercapto-1-propanesulfonic acid-modified gold (Au) electrode (Ahmed *et al.*, 2010; Pumera *et al.*, 2007). Other types of biosensors are highly sensitive amperometric cholesterol biosensor using platinum (Pt) zinc oxide (ZnO) nanospheres (PtZONS) (Ahmed *et al.*, 2010), multi-walled carbon nanotube (MWCNT) based biosensor [ChO/polyaniline/MWCNT] for choline detection (Pumera *et al.*, 2007), insulated MWNT electrode biosensor and Pt-MWNT biosensor for ultra-sensitive detection of DNA (Pumera *et al.*, 2007; Zhu *et al.*, 2005; Li *et al.*, 2003), CNT and MWNT based immunosensors (Pumera *et al.*, 2007) and silver (Ag) nanoparticle

based biosensor for the detection of squamous cell carcinoma antigen (SCCa) to diagnose cervical cancer (Zhao *et al.*, 2014).

After the discovery of C₆₀, a drastic change in the research of biosensors has taken place. The unique topological attribution and electrochemical properties of C₆₀ e.g. photo-thermal effect, structural angle strain, the ability to accommodate multiple electrons and endohedral metal atoms, long-living triplet state, singlet oxygen production, as well as ability to act as an electron acceptor with a dual nature of electrophilic and nucleophilic characteristics have derived a sharp interest among researchers to investigate the possibilities of using this material as a mediator in biosensor devices (Biju, 2014; Baena *et al.*, 2002). The outcome shows promising applications, whereby C₆₀ and its derivatives has been successfully used in developing biosensors for the detection of various biomolecules, such as glucose, urea, proteins as well as doping agents, such as dexamethasone, prednisolone, etc. in real samples. The application is not only limited in these areas, it frames in the high possibility to detect cancer cells at the earlier stage as well. It has been reported that C₆₀ derivatives can be used effectively in the photoacoustic imaging of cancer and tumor cells (Chen *et al.*, 2012).

Functionalizing C₆₀ in a successful way for some of the specific purposes poses a big challenge for the researchers nowadays. Modern nanotechnology in coalition with other genre of science and technology has been engaged to do this since the discovery of fullerene. A bulk of research works and investigations implies that in order to incorporate C₆₀ derivatives or modified C₆₀ into biosensors, they need to possess a functional group that can easily interact with biomolecules (Baena *et al.*, 2002). Two functional groups i.e. amine and carboxylic acid play very important role to create a liaison between C₆₀ and biomolecules. Also, C₆₀ molecules functionalized with hydroxy groups can be effective mediators in biosensor applications (Chung *et al.*, 2011). Depending on the area of application, the method of functionalization and the types of derivatives to be produced may vary. In fact, based on the type of biosensor (amperometric, potentiometric, optical, piezoelectric, etc.) and nature of analyte (protein, antigen, etc.) the target is to modify the elemental C₆₀ with necessary functional groups so that it is efficient in providing an amiable environment that will allow sufficient electron transfer between the analyte and the electrodes of biosensor.

Numerous research efforts support that functionalized C₆₀ could be a suitable nanomaterial to enhance the sensitivity, selectivity and reproducibility of biosensors. The scope of this review is limited to those remarkable efforts of developing biosensors using functionalized C₆₀ and its derivatives.

2.2.1 Role of C₆₀ in biosensor

A biosensor can be defined as an analytical device which can be used to detect and measure the presence and amount of an analyte by combining a biological component with a physicochemical detector (Chambers *et al.*, 2008). Based on the area of application, biosensors can be of different types e.g. optical biosensor, calorimetric biosensor, piezoelectric biosensor, etc; where compared to other types of biosensors, electrochemical biosensors have widely been adopted for biological sample analysis due to their easy set-up and the advantage of acquiring a range of useful electroanalytical information from them. Fig. 2.1 shows the common configuration of an electrochemical biosensor which comprises of five general steps for its functionality. Similar to other conventional sensors, biosensors also possess a recognition site and a transducer. The recognition site responds to the presence of the analyte and the transducer converts this response into a different kind of energy that is amplified, processed and converted into the desired format of signal.

In a biosensor, a biological component is used in the recognition site (enzymes, antibodies, organelles, microorganisms, tissues and cells). C₆₀ is used as a mediator between the recognition site and electrode of a biosensor to amplify the rate of electron transfer produced due to the biocatalytic or biochemical reaction of analyte in contact with the biological component at the recognition site (Perumal and Hashim, 2014; Zhang *et al.*, 2000; Davis *et al.*, 1995). The function of C₆₀ at the interface of recognition site and electrode can be represented as shown in the following diagram (Fig. 2.2).

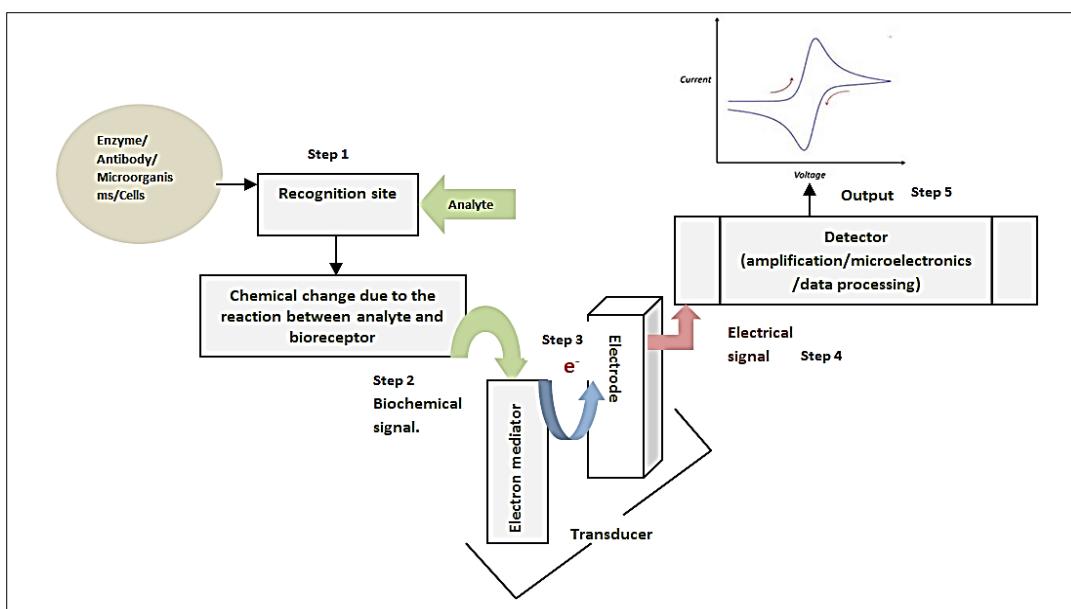


Figure 2.1 Components and the involved mechanism of a conventional electrochemical biosensor

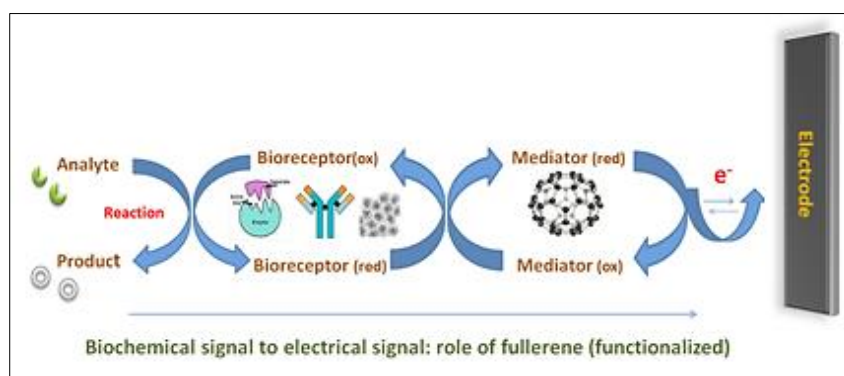


Figure 2.2 Function of fullerene (C_{60}) at the interface of recognition site and electrode

A robust biosensor must be reproducible along with the quality of having a remarkable degree of specificity to an analyte as well as a high sensitivity to detect the target analyte even at a very low concentration. To achieve this target of robustness, a number of methods has been brought by the researchers using distinct types of molecules to functionalize C_{60} to increase its functionality in a biosensor. From the view point of C_{60} chemistry, functionalized C_{60} can be categorized into two basic types: exohedral, where substituents are intercalated outside the cage; endohedral, where the molecules are trapped inside the cage (Hirsch, 1993). It is found that exohedrally functionalized fullerenes bearing organic or organometallic functional groups attached to the exterior

of the carbon cage are more diverse and accessible class of C₆₀ molecules than endohedral metallofullerenes. This type of functionalized C₆₀ has been considered very effective for biosensors and photoconductors (Loboda, 2013; Britz *et al.*, 2004). Also, a comparative study toward the electrochemical properties of functionalized C₆₀-Pd incorporated into different carbon nanostructures e.g. SWCNTs, MWCNTs, and oxidized carbon nano-onions (ox-CNOs) states that this type of composites can exhibit good electrochemical stability under multicyclic voltammetric conditions and give fast current responses upon potential changes (Gradzka *et al.*, 2013).

Britz *et al.* (2004) synthesized modified fullerenes (C_n@SWNT), the cyclopropafullerene-C₆₀-dicarboxylic acid diethyl ester, C₆₁(COOEt)₂ and the cyclopropafullerene-C₆₀-dicarboxylic acid, C₆₁(COOH)₂ and then mixed with purified SWNTs in carbon-di-sulfide (CS₂). The fullerene-SWNT mixtures were then immersed in CO₂ under supercritical condition. From the analysis it has been found that C₆₀ with ester groups can enter SWNTs much easily than C₆₀ with hydrogen bonded carboxylic groups. This technique of filling nanotubes with functionalized C₆₀ at low temperature (50 °C) has offered a new structure of fullerene-CNTs which could be applied in the fabrication of biosensor. The nanotube-C₆₀ host-guest interaction also has proved that altering the functional groups of C₆₀ can enhance or inhibit encapsulation, as compared to elemental C₆₀ (Gradzka *et al.*, 2013; Britz *et al.*, 2004). Zhuo *et al.* (2008) proposed a nanocomposite electrode system based on the synergistic effect of ordered mesoporous carbon (OMC) and C₆₀. The OMC-C₆₀ glassy carbon electrode (GCE) showed more favorable electron transfer kinetics in comparison to OMC/Glassy Carbon (GC) electrode. This investigation emphasized that modified C₆₀ or C₆₀ mediated electrode can offer an electrochemical sensing platform to detect biomolecules.

The function of C₆₀ has also been appreciated in the study of Tien *et al.* (1997) where they have investigated light-induced voltage and current generated by a self-assembled bilayer lipid membrane (s-BLM) doped with C₆₀. The C₆₀ containing s-BLM acts as a molecular device which actuates the redox reaction across the substrate-hydrophobic lipid bilayer-aqueous solution junction. The cyclic voltammetry confirmed that C₆₀ embedded in the BLM can perform as an excellent electron carrier/mediator and hence are useful in developing electrochemical biosensors. Later on, Szyman´ska *et al.* (2001) developed an electrochemical sensor following Tien's method for the detection of

neutral odorant. C₆₀ saturated s-BLM formed on a freshly cleaved metallic surface was employed for the sensing of odorant molecules and again it proved that the presence of functionalized C₆₀ or C₆₀ modified electrodes can facilitate the charge transmission in an electrochemical sensor system. Recent investigation confirms that the modification of biosensor electrode by means of integration of gold nanoparticles and fullerenols can enhance the performance of biosensors (Lanzellotto *et al.*, 2014). Also, a recent review on nanodiagnostics for the detection of pathogens has underlined that C₆₀ modified immobilized C₆₀-enzymes/antibodies/proteins can be a good sensor material for the detection of various biological species (Shinde *et al.*, 2012).

2.2.2 Application of functionalized C₆₀ in glucose biosensor

Generally, glucose is determined by the conventional electrochemical method, but biological species such as ascorbic acid, uric acid, tyrosine, galactose and cysteine in the blood sample cause interference to the detection of glucose (Biju, 2014; Chuang and Shih, 2001). To overcome this limitation, C₆₀ has been assigned in the fabrication of different types of glucose biosensors, e.g. C₆₀ coated piezoelectric sensor and C₆₀ based amperometric biosensor.

C₆₀ mediated biosensor for glucose detection was first claimed by Gavalas and Chaniotakis (2000), where varying amounts of C₆₀ were immobilized to develop an amperometric biosensor against glucose oxidase (GOx) enzyme. Trial was conducted with immobilized C₆₀ from 0.6 to 1.7 µg and GOx stabilized with diethylaminoethyl-dextran was used as the model enzyme. Their observation demonstrates that the sensitivity of biosensor increases with an increase in the amount of immobilized C₆₀ (Fig. 2.3). The response time was found to be in between 120 s and 300 s and was varying with the concentration of glucose in the solution (Gavalas and Chaniotakis, 2000).

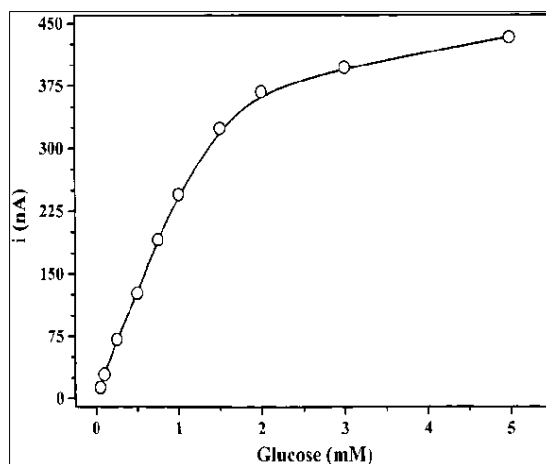


Figure 2.3 Calibration curve of the glucose biosensor containing 1.7 μg C_{60} /mg of electrode material. Experimental conditions: 10 mM phosphate buffer, pH 7.5, under argon, at +350 mV vs. Ag/AgCl (Gavalas and Chaniotakis, 2000)

Chang and Shih (2000) proposed a piezoelectric glucose biosensor based on fullerene-cryptand-22. This biosensor was developed by coating fullerene-cryptand-22 on piezoelectric (PZ) quartz crystal with silver plated metal electrodes. The fullerene-cryptand-22-coated PZ quartz crystal was placed in the working cell containing a solution of glucose. The frequency of PZ crystal device was measured in this glucose solution. After the injection of GOx enzyme into the cell containing glucose solution, a decrease in the frequency shift was observed due to the adsorption of gluconic acid molecules on the C_{60} -cryptand-22 coated PZ quartz crystal. Gluconic acid is produced due to the oxidation of glucose molecules in the presence of GOx enzyme. A decrease in the frequency shift is a desired outcome since PZ crystals are very sensitive to the pressure difference that results from the adsorption of any foreign molecules onto their surface. The device showed a frequency change only when glucose was present in the aqueous solution. It also showed good reproducibility since the adsorption of gluconic acid molecules onto C_{60} -cryptand-22 was completely reversed after introducing pure water. The lower limit of linearity (LLL) was found to be approximately 1×10^{-5} M, which indicates the detection limit of a biosensor as shown in Fig. 2.4. Whereas, the range of glucose concentration in blood sample is within 10^{-2} – 10^{-3} M. It implies that the proposed biosensor has high sensitivity to glucose molecules and can be employed to detect glucose in biological samples.

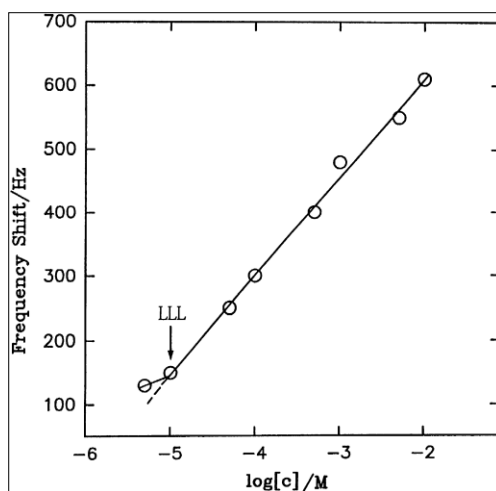


Figure 2.4 Frequency response of the glucose biosensor against different concentration of glucose (Chang and Shih, 2000)

Analytical results demonstrate that the proposed biosensor is very selective to the glucose molecules and showed no interference in its performance that generally occurs due to the presence of other biological species found in the blood or urine samples. Also, the device showed nearly no response to other inorganic species such as Na^+ , NH_4^+ and Cu^{2+} . An optimum frequency shift was observed at around pH 6 and at a temperature of 30 °C. These findings resulted into a first attempt of developing a sensitive glucose biosensor using C_{60} and PZ crystal detector (Chang and Shih, 2000). A similar attempt was also reported by Chen *et al.* (2007) to detect L-amino acid esters in aqueous solution by functionalizing C_{60} with cryptand-22.

Chuang and Shih (2001) developed another glucose biosensor using immobilized C_{60} -glucose oxidase enzyme coated on porous silica plates to create an active platform for the enzymatic reaction of glucose molecules and C_{60} -coated piezoelectric quartz crystal for the sensing of biochemical changes occurred due to this reaction. The oxidation of glucose under the catalytic activity of immobilized GOx enzyme produces gluconic acid, which was detected by a C_{60} -coated PZ quartz crystal sensor. Analytical results have shown that more the C_{60} -glucose oxidase present, more the oxidation of glucose that takes place in the solution. To determine the reproducibility and stability of the C_{60} -enzyme coated porous silica plates, the experimental trials were repeated seven times and the consumption of oxygen was found to be almost the same in all the measurements. Also, the C_{60} /PZ biosensor showed a high reproducibility with a relative

standard deviation (R.S.D) of 2.12 %. This reproducibility was checked with a series of 10 repetitive injections of 5×10^{-3} M glucose. The optimum frequency shift of glucose oxidation was observed at pH 7.0 which is the desirable range of pH for the physiological activity of the enzyme. The device showed its best performance at a temperature of 30 °C, which is similar to the optimum temperature desired for solvated glucose oxidase enzyme. To prevent the thermal denaturation of enzyme, this optimum temperature is an important factor. The shelf-life of this biosensor was found to be 93 days with an effectiveness of 88 % of its initial performance. The proposed PZ crystal biosensor with immobilized enzyme, C₆₀-glucose oxidase has shown a good selectivity to glucose and can overcome the interference raised due to the presence of various biological species in the sample, e.g. Na⁺ and K⁺ ions, galactose, cysteine, tyrosine, ascorbic acid, urea and creatine. Analytical results also showed that this PZ crystal biosensor with two pieces of immobilized enzyme-coated silica plates can detect the presence of glucose nearly up to 3.9×10^{-5} M in an aqueous solution of glucose, where the concentration limit of glucose in the blood is found to be within 10^{-2} to 10^{-3} M. The frequency response of C₆₀-coated PZ quartz crystal glucose biosensor against the coating load of C₆₀ was examined and the result showed that excessive coating is not necessary for the sensitive response of biosensor; in fact, excessive loading of C₆₀ can make unstable oscillation or even oscillation failure to the glucose biosensor. It is visualized that the proposed biosensor can show good sensitivity using a moderate amount of C₆₀ coating on PZ crystals (Chuang and Shih, 2001).

An excellent approach was accomplished by Zhilei *et al.* (2010) to fabricate glucose biosensor using C₆₀ along with ferrocene (Fc), chitosan (CS) and ionic liquid (IL). In this, GOx has been used as a catalyst for the oxidation of glucose which was detected by the electrodes. For the successful immobilization of enzyme, it is essential to nurture a biocompatible environment to allow the electron transfer between the GOx and the electrodes. Fullerenes in conjugation with Fc, CS and IL have been employed to fulfil this requirement. The modified GCE i.e. GOx/C₆₀-Fc-CS-IL-GCE has shown a precise voltammogram both in the presence (at different concentrations) and absence of glucose as shown in Fig. 2.5 (Zhilei *et al.*, 2010).

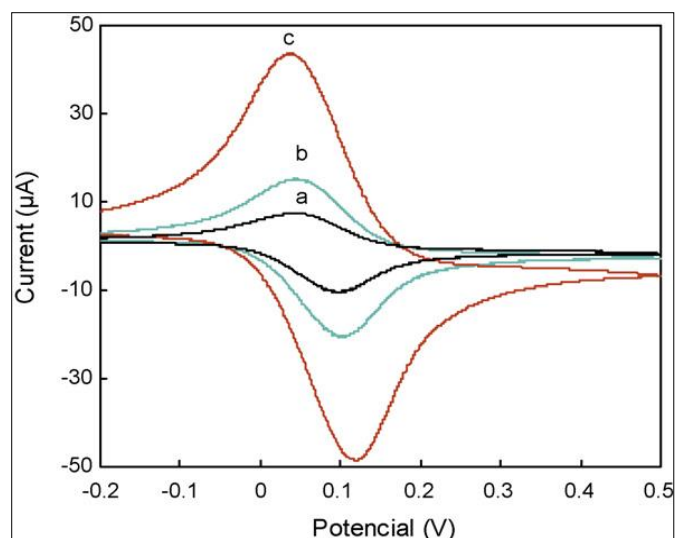


Figure 2.5 Cyclic voltammogram of GOx/C₆₀-Fc-CS-IL-GCE in the absence of glucose (a) in the presence of 1.0 M glucose (b) and in the presence of 5.0 M glucose (c) at pH 7.0 PBS and at 100 mV/s (Zhilei *et al.*, 2010)

The analytical results showed a very fast response time which was less than 0.752 s to reach 95 % of the maximum steady state current. The Michaelis-Menten Constant (K_m) of GOx was found to be 0.03 mM for this biosensor which indicates high bioelectrocatalytic activity of immobilized GOx toward glucose oxidation. Their observation implies that this is a satisfactory value of K_m and better than any other values of K_m derived from other glucose biosensors at that time. Table 2.1 represents the performance of this C₆₀ based glucose biosensor in comparison to others developed for the same purpose.

Table 2.1 Comparison of K_m among different types of glucose biosensor (Zhilei *et al.*, 2010)

Type of glucose biosensor	Analytical value of K_m (mM)
GO _x /C ₆₀ -Fc-CS-IL-GCE	0.03
Sol-gel organic-inorganic hybrid material	20
Pt nanoparticles/mesoporous carbon matrix	10.8
GO _x immobilized at chitosan and Au nanoparticles	10.5
Boron doped carbon nanotube modified electrode	15.19
Single-walled carbon nanotube modified electrode	8.5
Ferrocene-modified multi walled carbon nanotube nanocomposites	3.12
Immobilization of osmium complex and glucose oxidase onto carbon nanotubes modified electrode	0.91

The smallest value of K_m for GO_x/C₆₀-Fc-CS-IL-GCE (Table 2.1) represents the synergistic performance of C₆₀, Fc, CS and IL that were used to build this biosensor. In this combination, C₆₀ plays an important role as a mediator. Due to its electro-catalytic properties, C₆₀ helps to activate the oxidation of glucose molecules in the presence of GO_x and stimulates the electrochemical reaction, which is a must for getting a successful output from any amperometric biosensors. Observations confirmed that the sensor can detect glucose in the human blood serum more easily, selectively and precisely, and the performance is equivalent to the conventional hexokinase method (Zhilei *et al.*, 2010) as shown in Table 2.2.

Table 2.2 Comparative study of glucose limit in the blood serum samples (Zhilei *et al.*, 2010)

Samples	Glucose found by the proposed method (mM)	Glucose found by the hexokinase method (mM)
Serum 1	8.41 ± 0.12	8.37 ± 0.11
Serum 2	3.23 ± 0.09	3.25 ± 0.13
Serum 3	3.66 ± 0.06	3.70 ± 0.09
Serum 4	4.53 ± 0.10	4.51 ± 0.15
Serum 5	5.11 ± 0.11	5.05 ± 0.12

2.2.3 Application of functionalized C₆₀ in urea biosensor

The first piezoelectric-C₆₀ biosensor for urea detection was reported by Wei and Shih (2001), where they have suggested that fullerene-cryptand-22 can be used as a coating material on the surface of PZ quartz crystal to detect the presence of urea in an aqueous solution. They proved that similar to glucose biosensor, it can also be applicable for the detection of urea in the blood sample since the device showed a good sensitivity to urea in an aqueous solution with a detection limit of $\leq 10^{-4}$ M. The main purpose of using C₆₀ with cryptand-22 is to make an insoluble compound for coating on the PZ crystal and also to enhance the absorption of NH₄⁺ that results from the catalytic hydrolysis of urea by solvated urease or immobilized C₆₀-urease enzyme used. To test the comparative efficiency of this sensor, both the solvated urease and immobilized C₆₀-urease were used separately to crack the urea in an aqueous solution and the frequency response was observed under both of these conditions. Similar performance was observed under both conditions proving that C₆₀-urease can be an alternative to the solvated urease in biosensing of urea molecules. The immobilized C₆₀-urease membrane showed a similar performance when solvated urease was used in the biosensor. The performance of this urea biosensor based on C₆₀-cryptand coated PZ crystal detector and immobilized C₆₀-urease membrane does not get blocked due to the

presence of other biological species, organic and inorganic molecules e.g. creatinine, glucose, glycine, serum, ascorbic acid, acetic acid, Na⁺, K⁺, etc. Optimal frequency response was observed at pH 8 and at a temperature of 30 °C. The immobilized C₆₀-urease membrane was reusable 20 times and the signal of the biosensor was found to be 96 % after repeated application in one day (Wei and Shih, 2001).

A potentiometric urea biosensor was fabricated by Saeedfar *et al.* (2013) to measure the amount of urea in the urine sample. The sensor used in this experiment was a C₆₀-urease bio-conjugate on an acrylic based hydrogen ion sensitive membrane, which has shown its stability for up to 140 days. C₆₀ was functionalized with carboxyl (–COOH) groups by sonication, heat, and ultraviolet (UV) radiation. Urease enzyme was then immobilized onto the C₆₀-COOH derivative to devise the potentiometric biosensor for the quantitative identification of urea. Analysis with real samples of diluted urine solution has shown promising results, comparable to that of a standard UV-Vis method. The difference between the C₆₀-urease bio-conjugate sensor and standard UV-Vis method was found to be less than 5 %, which confers a degree of reliability to the C₆₀ that it can be used as an effective nanomaterial in the construction of such biosensors. This C₆₀-based electrode showed good sensitivity and response time which was found to be 2 min for each determination and the responses were constant within the dynamic range area as shown in Fig. 2.6 (Saeedfar *et al.*, 2013).

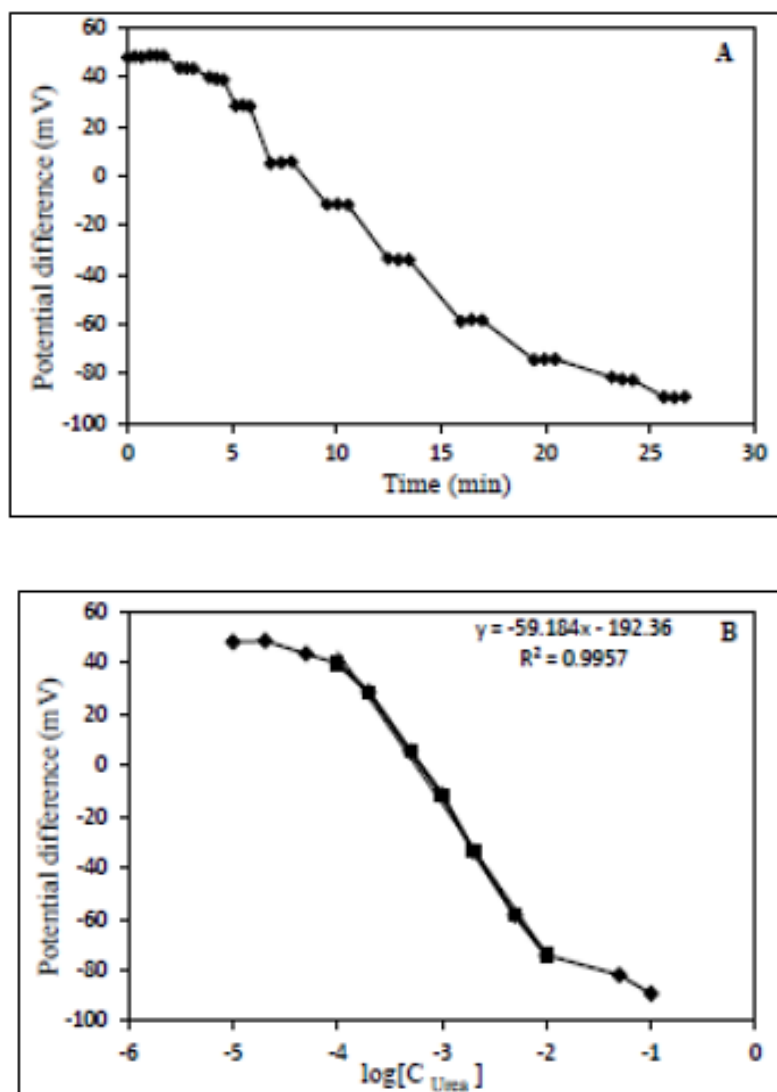


Figure 2.6 Response time with relation to potential difference when the concentration of urea was changed step by step from 10^{-5} to 10^{-1} M (A), observed potential vs. urea concentration ranges from 10^{-5} to 10^{-1} M (B) (Saeedfar *et al.*, 2013)

Analytical results revealed that after 140 days, the sensitivity of biosensor was decreased by 5 %. Storage condition affected the performance of this type of sensors. The activity of the enzyme decreased with time ensuing a diminution in the sensitivity at a rate of 2.18×10^{-2} Δ mV/decade per day. However, this eventually highlights that C_{60} can be a key component in the fabrication of biosensors to detect urea and possibly other biomolecules generated due to the metabolism in our body.

2.2.4 Application of functionalized C₆₀ in immunosensors

Copious research works reported on developing C₆₀-based immunosensors can help in the diagnosis of different types of biological disorders caused due to any malfunction in the metabolism of our body (Liao and Shih, 2013; Sheng *et al.*, 2013; Chang and Shih, 2008; Chou *et al.*, 2008; Chang and Shih, 2007; Zhang *et al.*, 2006; Pan and Shih, 2004; Carano *et al.*, 2002). Besides, some of them showed the potential of C₆₀based immunosensors in the detection of microorganisms such as *Escherichia coli* in the real samples (Li *et al.*, 2013; Guo *et al.*, 2012).

Pan and Shih (2004) used antibody immobilized C₆₀ to detect immunoglobulin G (IgG) and haemoglobin (Hb) in an aqueous solution. Both these bio-species have vital roles in human immune system; therefore, their detection is useful in diagnosing any disorder in immunity. In this study, C₆₀-antibody coated-quartz crystals were prepared to detect IgG and hemoglobin in aqueous solution. The C₆₀-antibody coated-quartz crystals were obtained by coating C₆₀ firstly on quartz crystals combined with silver (Ag)-plated metal electrodes and followed by adsorption of antibodies, e.g., anti-human IgG and anti-hemoglobin in aqueous solution (Fig. 2.7). The obtained analytical results by using the immobilized C₆₀-anti-IgG coated PZ crystal sensor have been depicted in Table 2.3.

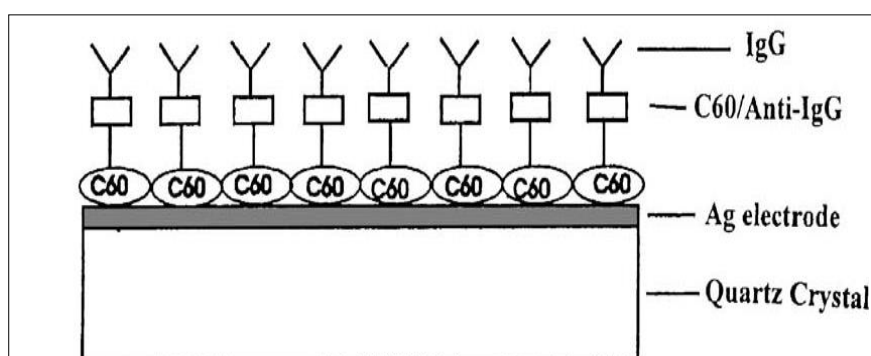


Figure 2.7 C₆₀-anti-human IgG coated quartz crystal electrode for IgG (Pan and Shih, 2004)

Moreover, the immobilized C₆₀-anti-hemoglobin coated piezoelectric biosensor showed a good linear response frequency to the concentration of Hb with a sensitivity and detection limit of 1.56×10^4 Hz/(mg/mL) and $<10^{-4}$ mg/mL respectively. The most successful feature of this PZ crystal immunosensor based on immobilized C₆₀

antibodies is that various common organic and inorganic bio-species in the blood, e.g., cysteine, ascorbic acid, uric acid, tyrosine, urea, Na⁺, K⁺ and Ca²⁺ have shown very minimal interference to the sensitivity of this biosensor (Pan and Shih, 2004).

Table 2.3 Analytical results of the C₆₀-anti-human IgG coated quartz crystal electrode (Pan and Shih, 2004)

Controlling factors	Analytical results
Effect of concentration of IgG	≤10 ⁻⁴ mg/ml (in aqueous solution).
Effect of temperature	Adsorption of IgG on the biosensor increases at lower temperature (e.g. <30 °C); similar effect was observed in the activity of some of the bio-species.
Effect of pH	Operates well at 6.7 which is close to the optimum pH for the physiological activity of most of the bio-species, e.g. enzymes, proteins and antibodies (7.0).
Reproducibility	High reproducibility with a relative standard deviation (R.S.D.) of 3.6 %.
Lifetime	85 % after 7 days.
Selectivity	Small interfering factors (ca. 10 ⁻² to 10 ⁻³) for various interfering bio-species and a quite high selectivity (ca. 0.96–0.99) of IgG solution.

A similar type of observation was reported by Liao and Shih (2013) with C₆₀-myoglobin (C₆₀-Mb), C₆₀-Hb and C₆₀-gliadin coated piezoelectric (PZ) quartz crystal immunosensors. The optimum frequency response for these anti-protein PZ-immunosensors was observed at pH 7.0 and at a temperature around 30 °C Sensitivity of C₆₀-Mb, C₆₀-Hb and C₆₀-gliadin PZ-immunosensors were 1.43×10³, 2.59×10³ and 8.05×10³ Hz/(mg/mL) respectively and their detection limits were 4.36×10⁻³, 3.23×10⁻³ and 1.98×10⁻³ mg/mL respectively. The interference due to other biological species found in the human blood e.g. cysteine, tyrosine, urea, glucose, ascorbic acid and metal ions was negligible (Liao and Shih, 2013).

Glutathione is an enzyme which is considered as a powerful scavenger of free radicals. It plays an important role in our immune system by making proteins and chemicals required for body metabolism and helps in tissue building and repairing. Carano *et al.* (2002) fabricated an amperometric biosensor to detect glutathione. C₆₀ was functionalized to dipyrrolo C₆₀ in line with glutathione reductase to act as a redox mediator for the detection of glutathione. The biosensor has shown a fast and reproducible response to glutathione. A characteristic change in the cathodic current with successive addition of glutathione was observed (Fig. 2.8).

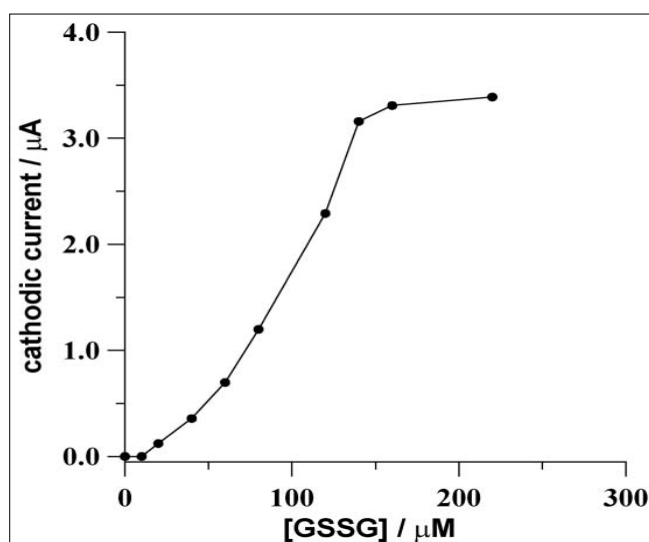


Figure 2.8 Calibration curve corresponding to the chronoamperometric responses of the proposed biosensor at different concentrations of glutathione (Carano *et al.*, 2002)

Numerous approaches have been considered the development of immunosensors based on C₆₀ derivatives or immobilized C₆₀ since they can strongly adsorb proteins e.g. Hb, Mb, gliadin, etc. One of these approaches focused on the development of surface acoustic wave immunosensor (SAW) based on the immobilized C₆₀-protein (Chang and Shih, 2007). Both C₆₀-Hb and C₆₀-Mb were used to study the response of this biosensor against the presence of anti-Hb and anti-Mb in solution. Anti-Hb is a biomarker of megaloblastic anemia cells and anti-Mb is found in polymyositis patient's blood. Instead of quartz crystal microbalance (QCM) transducer, SAW transducer has been employed as it can offer a better operation frequency which is up to 1 GHz, whereas QCM can perform up to 30 MHz. Three strategies were followed to detect anti-Hb and anti-Mb using SAW transducer: first, C₆₀-Hb-coated SAW immunosensor was applied to detect anti-Hb antibody in solution; then immobilized C₆₀-Mb SAW immunosensor

was employed to detect anti-Mb antibody in solution; finally, a dual channel immunosensor with both C₆₀-Hb and C₆₀-Mb was employed to detect and monitor the amount of anti-Hb and anti-Mb antibodies in the solution, simultaneously. The first one showed sensitivity of 140 Hz/(μg/mL); detection limit of 0.32 μg/ml and good reproducibility with a standard deviation of about 2.1 %. The activity of immobilized C₆₀-Hb SAW crystals was found to be 80 % after 10 days. This biosensor was found to be very selective to the anti-Hb antibody (ca. 0.94-1.03) and minimal response was observed for other interfering agents such as glucose, tyrosine, Na⁺, K⁺, Ca₂⁺, etc. (ca. 0.02-0.06). The optimum performance was observed at a temperature of 27 °C and at a pH of 7.3. The immobilized C₆₀-Mb-coated SAW biosensor also showed a good sensitivity of 1.27 kHz/(μg/mL) with a detection limit of 0.035 μg/mL. The dual channel SAW immunosensor showed its capability to detect both anti-Hb and anti-Mb antibodies simultaneously with good sensitivity (Chang and Shih, 2007).

To detect insulin present in aqueous solution, Chang and Shih (2008) developed a shear horizontal surface acoustic wave (SH-SAW) immunosensor based on C₆₀/anti-insulin antibody which showed a similar level of performance. The sensitivity of this immunosensor was found to be 130 Hz/pM with detection limits 0.58 pM for insulin within the normal human insulin concentration range. The interference due to the common inorganic and organic bio-species present in blood sample was found to be negligible in this immunosensor. Also, it has shown excellent reproducibility with a R.S.D of 2.24%.

Sheng *et al.* (2013) proposed a modified approach where functionalized C₆₀ was used with Hb. To understand the electrochemistry of Hb, they have introduced a fullerene-nitrogen doped carbon nanotubes and chitosan (C₆₀-NCNTs/CHIT) composite matrix. Hb was immobilized on this composite matrix to develop Hb/C₆₀-NCNT/CHIT/GC electrode. Their ultimate target was to study how such a configuration based on redox protein in conjugation with C₆₀-NCNTs/CHIT could contribute in the performance of an immunosensor. This proved that immobilized Hb/C₆₀-NCNT/CHIT/GC can perform a faster electron transfer process which can be applied to determine hydrogen peroxide (H₂O₂) in biological and pharmaceutical samples. The synergistic effect of C₆₀ and NCNT plays a vital role behind this electron transfer between the protein and electrode, besides CS and C₆₀-NCNT together elevate the protein stability in this

device. The above biosensor has shown nearly 95 % of its initial activity even after 2 months of storage (Sheng *et al.*, 2013).

The results obtained from the work of Zhang *et al.* (2006) also support this i.e. C₆₀ can facilitate electron transfer between the redox proteins and the electrode. They developed C₆₀-MWCNT on GC electrode and used that electrode to detect Hb. For a comparative study, cyclic voltammogram of both bare MWCNT film on GC electrode and C₆₀-MWCNT film on GC electrodes was obtained. The peak current was much higher in case of C₆₀-MWCNT film on GC electrode which indicates that due to the presence of C₆₀ in MWCNT, Hb receives a favorable environment for its redox reaction. Also, the adsorption behavior for both MWCNT film and C₆₀-MWCNT film was studied to understand the effect of C₆₀ in this type of biosensor. The cyclic voltammogram as a function of time showed that the cathodic peak current increased in parallel with the scan time and reached saturation implying that there is a gradual and more stable adsorption of Hb on the electrode surface. Whereas, MWCNT film electrode initially showed a higher cathodic current but it decreased rapidly over time which indicates an unstable adsorption of Hb on the electrode surface. This confirms that C₆₀ can ensure a facile electrochemical deal between the electrode and the redox site of proteins, e.g., Hb, Mb, gliadin, etc. (Zhang *et al.*, 2006). Another interesting finding by Guo *et al.* (2012) states that polyhydroxylated C₆₀ derivatives can reduce the oxidant damage caused due to the attack by H₂O₂ in Hb electrochemical biosensors. This adds a great advantage in the functionality of biosensor and it ensures a favourable microenvironment for the direct electrochemistry and electrocatalysis of Hb.

A very recent attempt on the development of an electrochemical immunosensor for sensitive detection of *Escherichia coli* 0157:H7 using C₆₀-based biocompatible platform has been reported by Li *et al.* (2013). Previously Shiraishi *et al.* (2007) reported that C₆₀ impregnated screen printed electrode (FISPE) can be used to detect 16S rDNA extracted from *Escherichia coli* (JCM1649). In these days, the detection of *Escherichia coli* is very important in clinical diagnostics, food safety testing and environmental monitoring. In this connection, analysis of 16S rDNA from *Escherichia coli* which has a significant role in phylogenetic research and electrochemical DNA sensor fields. Shiraishi *et al.* (2007) used the approach of mixing carbon ink with C₆₀ benzene solution to generate C₆₀ ink which was then impregnated onto the electrode

surface and the resultant sensor was employed to detect 16S rDNA. It has been reported as a novel method of electrochemically detecting 16S rDNA by using C₆₀-ink. Li *et al.* (2013) assembled a sandwich type electrode by immobilizing C₆₀, Fc, thiolated chitosan (CHI-SH), Au nanoparticles coated SiO₂ nanocomposites (Au-SiO₂), avidin (SA) and biotinylated capture antibodies of *Escherichia coli* 0157: H7 (bio-Ab₁) onto the surface of GCE to make a modified electrode, bio-Ab₁/SA/Au-SiO₂/CHI-SH/Fc/C₆₀ to detect *Escherichia coli* 0157:H7. The sensitivity of this immunosensor was found to have a detection limit of 15 CFU/mL which is below the commonly accepted threshold concentration in clinical diagnosis. It means that this type of biosensor can offer a subtle measurement in the detection of *Escherichia coli* in real samples.

The effect of C₆₀ in developing highly sensitive deoxynivalenol (DON) immunosensor was visualized by Zhilei *et al.* (2011). For the detection of DON in food samples, they made a sensitive electrochemical immunosensor using GCE and a composite prepared from C₆₀, Fc and IL. This biosensor showed high sensitivity, selectivity and shelf-life of about 180 days. To investigate the effect of C₆₀ as well as IL in this type of biosensor, they have also examined the device without using C₆₀ and IL. The results showed that when C₆₀ and IL were used, the sensitivity of biosensor increases substantially which is twice than that of a biosensor without C₆₀ and IL. Due to its unique electrochemical properties, C₆₀ promotes electron transfer on the surface of modified electrodes and helps to increase the sensitivity of biosensor (Zhilei *et al.*, 2011).

2.2.5 Application of functionalized C₆₀ in the analysis of drugs

The advantages of C₆₀'s electrochemical properties have also been utilised to determine the amount of drugs in various clinical and pharmacological studies. C₆₀ modified gold electrode (C₆₀/Au) has been proven to detect prednisolone in human urine or whole blood sample, a potential application during the investigation of doping cases by athletes (Goyal *et al.*, 2009a). Better result was obtained by using SWNTs instead of C₆₀ in case of triamcinolone detection, which is also considered as a doping agent (Goyal *et al.*, 2009b). The reason behind this could be that the electrocatalytic interaction of SWNT with the drug triamcinolone was more compatible compared to C₆₀. Nevertheless, C₆₀ exhibited significant performance in the detection of

dexamethasone (Goyal *et al.*, 2009c). In the determination of prednisolone in human blood and urine samples, C₆₀/Au modified indium tin oxide (ITO) electrode showed a quite impressive voltammogram. The anodic peak current gave a sharp and a significant peak rise in the voltammogram when C₆₀/Au electrode was used rather than bare ITO electrode. Although the stability of Au modified ITO (Au/ITO) electrode was found to be better than that of C₆₀/Au electrode (4.78 % after 10 days for C₆₀/Au electrode and 3.35 % after 15 days for Au/ITO electrode), it was also observed that the sensitivity of C₆₀/Au was much better than that of Au/ITO electrode. It again demonstrates the advantage of using C₆₀ in biosensing as the electrocatalytic activity of C₆₀ as well as Au promotes the oxidation of prednisolone and increases the rate of electron transfer (Goyal *et al.*, 2009a).

Dexamethasone is a glucocorticoid class of steroid and is immensely used in the pharmaceutical formulations. It is used, for the treatment of cancer to reduce the side-effects of antitumor therapy; to alleviate high altitude illness; for viral infections, respiratory diseases, gastrointestinal diseases; to cure skin disorders and nervous system abnormalities, etc. Due to the strong efficacy of dexamethasone to these diseases, it is very much required to determine its dosage to ensure the safety limit of its use for any treatment. Moreover, dexamethasone is also considered to be a doping agent among the athletes. Goyal *et al.* (2009c) developed a biosensor to determine this dexamethasone in human plasma which is a simple and rapid methodology in comparison to other available methods. They introduced C₆₀ modified edge plane pyrolytic graphite electrode (PGE) to form a reproducible and stable biosensor. Due to the presence of fullerene, this biosensor showed acceleration in the electrocatalytic reduction of dexamethasone, which brought a significant peak current indicating a higher sensitivity toward dexamethasone. This study was carried out with both commercial and real samples and ascertained that C₆₀-PGE can offer better quantitative results for dexamethasone in the pharmaceutical preparations and doping investigations (Goyal *et al.*, 2009c).

Many investigations reiterate that functionalized C₆₀ mediated electrode surface can enhance the electrical signal toward voltammetric outputs. The voltammetric study carried out by Tan *et al.* (2003) to detect L-cysteine using GCE modified by C₆₀ strongly support this postulate. L-cysteine, commercially known as E920 is widely used in food

industries as an antioxidant and in pharmaceutical industries as a biomarker which can assist to investigate the biomolecular structure and dynamics. The modified electrode was prepared by casting C_{60} containing dichloromethane (CH_2Cl_2) solution onto the surface of clean GC electrode which was then applied to detect and measure the presence of L-cysteine in two types of samples, alcovite (100 mg L-cysteine per pill) and casamino acid (90% L-cysteine and 10% lactose). Both these samples contained a known amount of cysteine which was provided by the manufacturer. Other samples of root beer syrup and soya bean milk were spiked with L-cysteine to do a comparative study. Voltammetric study showed that the obtained current from the oxidation of cysteine is a function of C_{60} dosage and higher current was observed with an increase in the coating of C_{60} . The observed results have been shown in Fig. 2.9.

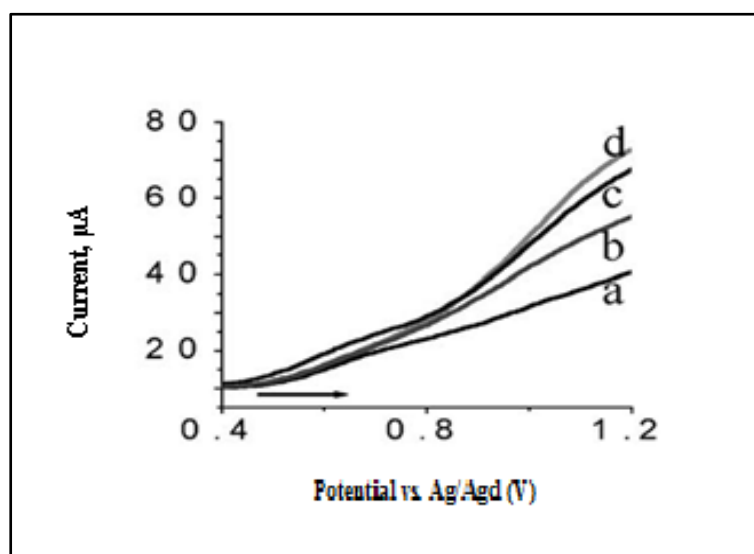


Figure 2.9 Effect of dosage of C_{60} cast onto a GC electrode: a) 5 μ L; b) 10 μ L; c) 15 μ L; d) 20 μ L (Tan *et al.*, 2003)

The presence of C_{60} microcrystals on the surface of GC improved the oxidation current of L-cysteine. This biosensor also has good reproducibility and selectivity to the determination of L-cysteine and presents a distinctive scenario where C_{60} mediated electrode is used in mediating the irreversible oxidation of a species in an aqueous media (Tan *et al.*, 2003).

2.2.6 Application of functionalized C₆₀ in the detection of cancer cells

Usage of C₆₀ is increasing gradually due to its potential physicochemical features, for example, in the detection and treatment of chronic diseases such as cancer (Orlova *et al.*, 2013; Chen *et al.*, 2012; Rassoly and Jacobson, 2006), to detect and target DNA strain in real samples (Xu *et al.*, 2009) and to investigate the nature of HIV (Ros and Prato, 1999; Friedman *et al.*, 1993). It has been suggested that C₆₀ derivatives can be used effectively as inhibitors of HIV-1 protease (HIVP) since C₆₀ possesses steric and chemical reciprocity with the active site of HIVP (Friedman *et al.*, 1993). Recent research on the application of C₆₀ is focused on its use as a biosensor material for cancer detection at earlier stages (Han *et al.*, 2013; Chen *et al.*, 2012). The objective is to fabricate the easiest and the simplest electrochemical system which enables to detect the presence of cancer and its extent inside the human body. The challenge is that it should be selective and specific to the biomarkers of various types of cancer and tumor cells along with a good reproducibility and user-friendly configuration, so that it can stand as an effective tool for the early detection and measurement of cancer in comparison to other available methods.

Han *et al.* (2013) established a biosensor which composed of multi-labelled C₆₀ nanohybrid molecules derived from the supramolecular interaction between C₆₀ and amino functionalized 3,4,9,10-perylenetetracarboxylic dianhydride (PTC-NH₂) and was employed for the early diagnosis, treatment and prognosis of cancer by detecting cancer related protein known as platelet-derived growth factor B-chain (PDGF-BB). In this investigation PTC-NH₂ was dispersed in the nano C₆₀ suspension to obtain amino functionalized nano-C₆₀ (PTC-NH₂-C₆₀). The resultant product was functionalized C₆₀ nanoparticles with amino and thiol groups (FC₆₀-NPs). This biosensor was found to be highly sensitive and selective toward PDGF-BB with satisfactory reproducibility and a R.S.D of 4.79%, also the interfering biological species have almost negligible influence to this detection. The stability of this aptasensor was found to be 95.2% of its initial performance after one week and 86.7% of its initial performance after four weeks (Han *et al.*, 2013).

Recently, it has been proved that the C₆₀ derivatives i.e. polyhydroxy fullerenes (PHF; C₆₀(OH)_xO_yNa_z) and carboxy fullerenes (CF; C₆₀(C(COOH)₂)₃) can be used in photo-acoustic imaging of tumor and cancer cells (Chen *et al.*, 2012). A mechanical scanning

photo-acoustic system has been developed by the researchers. A higher photo-acoustic image of the functionalized C₆₀ was obtained after laser irradiation and a notable result was found out when the study was conducted on tumor-bearing mice. Distinctive images were observed between tumor and non-tumor regions after the injection of polyhydroxy fullerene. This observation adds a new dimension to the application of functionalized C₆₀ that it can act as an *in vivo* biosensor material to detect cancer and tumor cell lines. Due to the excellent response of C₆₀ and its derivatives to photo-acoustic imaging, it is now conceived that C₆₀ can be used as a diagnostic and therapeutic agent to these diseases in the near future.

2.2.7 Functionalized C₆₀ based biosensor: over ten years of its development

Overall, the key aspects of various biosensors based on C₆₀ derivatives and the prospects of functionalized C₆₀ as an effective nanomaterial to ramp up the sensitivity and functionality of biosensor devices have been discussed. It is visualized that due to its excellent electron accepting capacity and its ability to accelerate charge separation in any electrochemical process, C₆₀ and its derivatives can be used in various types of biosensors, e.g., potentiometric, amperometric, piezoelectric, etc. The novel characteristics of C₆₀ have already been appreciated (Umeyama, 2008; Martin, 2006; Sotiropoulou *et al.*, 2003; Forró and Mihály, 2001). The gist is, C₆₀ performs as a ‘nano negotiator’ between the recognition site and the electrodes to complete the deal of electron transfer which ultimately produces an electric signal that appears as a final output after being amplified by the detector. When C₆₀ is functionalized by any selective molecules or radicals, it becomes more active to bind and pass the electrons. However, the function of C₆₀ is still under investigation and it is essential to know that what might be the other promising advantages of using C₆₀ in biosensor devices other than facilitating the rate of electron transfer.

From this review it is also visualized that most of the investigations (~44.4 %) are focused in developing the immunosensors, to the best of our knowledge (Fig. 2.10). Following this, much of the work concentrates in developing glucose biosensors. In fact glucose and urea biosensors were the initial type of biosensors based on functionalized fullerene. Later on, it has been expanded to the field of clinical and pharmacological studies and to the field of cancer and tumor cells detection. At present, functionalized

C₆₀ has received attention in detecting cancer and tumor cells. A comparative scenario has been shown in Fig. 2.10.

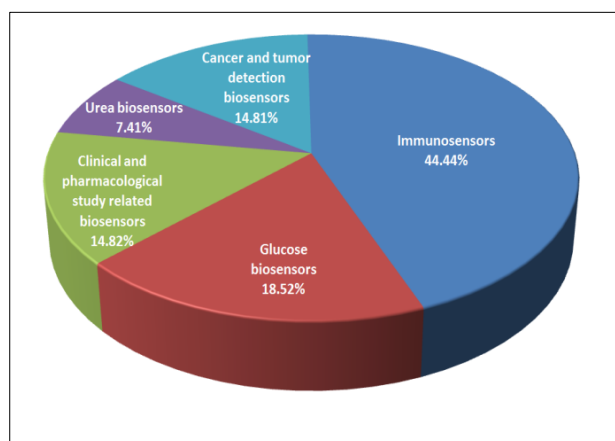


Figure 2.10 Usage of functionalized C₆₀ in different types of biosensors [1999- 2014]

However, considering the intensity of research that focusses on the development of novel and potential biosensors over the last decade, it is realised that biosensors using functionalized C₆₀ are on the rise in between 2002 to 2009 (Fig. 2.11).

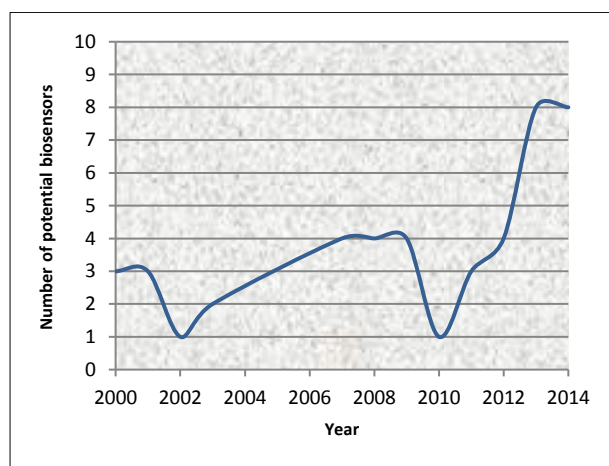


Figure 2.11 Trend of using functionalized C₆₀ for biosensor devices over the last decade (based on the reports discussed in the subsections 2.2.1-2.2.6 of the thesis)

This may be due to that before 2002 the potential aspects of C₆₀ in biosensing applications were not completely familiar to the researchers. Since 2002 a gradual surge in the investigations and approaches were directed on the development of biosensors using C₆₀ derivatives. More importantly, the number of C₆₀ based biosensors developed

decreasing after 2009 (Fig. 2.11) which might be due to the rapid fashion of using various types of other nanomaterials such as SWCNT, MWCNT, graphene, Au nanoparticles, Pt nanoparticles, etc. for similar purpose. Nevertheless, this is a temporary scenario and the statistical results clearly show that after 2010, the utilisation of functionalized fullerenes in developing biosensors has attained a sharp increase and this trend ultimately asserts that C₆₀ could be a promising nanomaterial in the field of biosensors and a good proportion of research investigations (Pilehvar and De Wael, 2015) are still under progress to exploit its potentiality to the fullest.

On this context, recently a number of methods for the hydroxylation of C₆₀ have been developed, and thus polyhydroxylated C₆₀ has recently become a potential candidate in this avenue of functionized C₆₀ and its application in biosensor. The attachment of -OH groups not only make C₆₀ water soluble but also contribute to additional biochemical properties to the hydroxylated C₆₀ moieties, e.g. free radical scavenging and electrocatalytic sensitivity. The solubility of polyhydroxylated C₆₀ varies from 0.01 to 64.9 mg/mL (Chaban *et al.*, 2017; Kokubo *et al.*, 2011) based on the number (n= 2-44) of attached -OH groups onto C₆₀; the more the number of -OH groups the more is the solubility as reported. However, in preparing a biosensor solubility is not only the concern. In fact, a fullereneol molecule having more -OH groups can show very good solubility but might not play active role in the electrochemical reaction occurring between the ligand and analyte at the electrode-solution interface due to steric hindrance caused by the presence of more -OH groups crowded onto C₆₀. In this regard, besides developing more facile techniques to hydroxylating C₆₀ with different number of -OH groups, it is also important to investigate the role of different fullereneols prepared by different methods for the detection of different bio-analytes. Thus, it could be an extended and emerging field of research concerning the application of C₆₀, functionalized with different -OH groups, in different biosensors in order to understand their comparative performance in terms of the attached -OH groups onto C₆₀. Although various methods of synthesizing polyhydroxylated C₆₀ have been proposed in the past years, but biosensor based on different fullereneols are scarcely reported by researchers, where only a few studies reported to date on this domain are unable to provide us a very detailed and comprehensive comparative features in terms of the sensitivity, LOD, specificity, stability, and reproducibility of different fullereneol-based biosensors. A significant study was conducted by Hang *et al.* (2014) where polyhydroxylated C₆₀ was

found to detect DNA upto 1 fM as a result of the increased loading of DNA probe on the polyhydroxylated (n= 24-26) C₆₀. However, this report was not associated with a detailed information about the specificity and sensitivity of the proposed biosensor. Prior to that, another study reported by Zhuo et al. (2013) showed that C₆₀ hydroxylated with eight -OH groups has a significant electrocatalytic effect on hydrogen evolution reaction (HER) indicating that hydroxylated C₆₀ has the potential to perform as an electrocatalyst or as a mediator in electroanalytical studies. Although this study showed very significant electrochemical behavior of C₆₀(OH)₈ in a (-)ve potential window of voltammetric analysis but how the same hydroxylated C₆₀ would behave under a (+)ve potential window remains unexplained. The sensitivity, LOD, specificity, stability, reproducibility will vary diversely based on several factors, e.g. method of synthesis of polyhydroxylated C₆₀ and preparation of biosensor, type of biosensor, type of analyte, ligand, electrolyte and supporting materials, and applied potential, etc. In addition, which make it more challenging that the geometrical configuration of a polyhydroxylated C₆₀ moiety or the geometric orientation of the -OH groups onto C₆₀ may form different isomers, which makes this idea more interesting that how different isomers of a polyhydroxylated C₆₀ moiety may act in a particular biosensor. Thus, it becomes a potential area to focus on further research of functionalizing C₆₀ and its application in biosensor. Considering the rising demand of more studies in this domain, the current study was designed for not only to realise a more facile as well as a green technique to functionalize C₆₀ with -OH groups but also to investigate the function of the as-synthesized polyhydroxylated C₆₀ in detecting a cancer biomarker, folate receptor alpha (FR α).

2.2.8 Prospects of the functionalized C₆₀ based biosensors

Scientific community is engaged to upgrade the biosensor technology using C₆₀ derivatives with a view to implement it commercially and conveniently in the diagnosis of various diseases. The icosahedron molecular structure of C₆₀ has a unique combination of 20 hexagons and 12 pentagons where the carbons are both sp² and sp³ hybridized. Thus, based on the electrochemical environment C₆₀ and its derivatives may act both as electrophile and nucleophile, which make it a suitable and potential candidate for a diverse type of biosensors compared to its contemporary carbon

nanomaterials. It is appreciable that the salient features of C₆₀ have brought several prospects in clinical diagnosis and pharmaceutical applications, but further research is required for its overall development as a biosensor. There are tons of examples of developing biosensors using distinct combination of nanomaterials besides C₆₀ and almost every sensor has some good aspects. The competition lies mainly between the C₆₀ and other nano moieties, e.g. SWCNT, MWCNT, Au nanoparticles, silver nanoparticles, platinum nanoparticles, etc. However, behind the success scenario, all these different types of biosensors may also have some limitations which might be still unseen or unconsidered by the researchers unless they are involved in the diagnosis for practical cases. This is because any new technology not only brings bright scopes but also bears some tentative obstructions that may cause both pros and cons to its application in real life cases. Numerous investigations and trials are still waiting to exploit the unique properties of C₆₀ in the field of biosensing. Surely, this is not a challenge anymore because all the experimental findings and discussions reveal that C₆₀ is able to perform as an active material in various types of biosensor devices for the detection and measurement of different types of biomolecules. The major issue that should be examined now is, how conveniently it can be incorporated in a biosensor and how robustly it can deliver its performance under different experimental conditions, to detect and measure different types of biomolecules, in comparison to other potential nanoparticles based biosensors that have been proposed so far for the similar purpose. Certainly, C₆₀ based biosensors can offer high sensitivity, selectivity and good reproducibility in biosensing and bio-imaging but that does not comprehend all the features of a biosensor required particularly for point of care diagnosis. It must be cost-effective and should consist of an easy to handle configuration. Proper chemical modification and bioconjugation of C₆₀ molecules can bring more development in biosensing and bio-imaging but at the same time it also encompasses high cost. This is because C₆₀ itself is a costly nanomaterial and for its functionalization and then finally for the fabrication of all the materials and components into a biosensor system different types of other chemicals and tools are required which are costly too. From all these perspectives, C₆₀ biosensors can successfully be employed in real sample diagnosis. The rapid development and attention in the research of functionalizing C₆₀ and cutting-edge biosensor technology over the past few years emphasized the possibility that in the near future C₆₀ based biosensors can be appeared as an effective device in biosensing and bio-imaging of various diseases and numerous research works are still in progress

on this issue to achieving comprehensive C₆₀ based biosensors which will be robust, convenient to use and commercially worth for point-of-care diagnosis of diseases.

2.3 Ultrasonication: A Potential Technique of Functionalization

2.3.1 Acoustic cavitation

Cavitation, in general, is a phenomenon of repeated formation and collapse of voids occupied with vapour in a bulk liquid medium due to the rapid change of pressure inside the liquid medium as a result of any physico-mechanical effect. The change of pressure leads to a negative pressure drop which creates small vacuum zone(s) inside the liquid and initiates the formation of vapor cavities (Brennen, 2013; Franc and Michele, 2006). The rotating propeller of a submarine inserts cavitation in the bulk liquid around the propeller blades; this phenomenon is well explained by Bernoulli's law which states that an increase in the speed of a fluid occurs simultaneously with a decrease in pressure or a decrease in the fluid's potential energy (Apfel, 1997). A rotating propeller under water develops positive pressure on the front side of the blades and consequently a negative pressure on the other side of the blades, leading to propeller cavitation. Another practical example of cavitation is known as 'pump cavitation'; when liquid is pumped through pipes, the impeller of the pump undergoes cavitation due to the development of a relatively low pressure around the eye of the impeller, this low pressure may cause due to any blockage in the pipe, poor piping design or poor suction conditions. Not only in man-made objects, but also in some natural phenomenon cavitation could be observed. For example, when a waterfall drops from a higher height on the rocks then at the contact zone between the rocks and the falling water the rapid pressure drop causes cavitation near the rock surface, that could also be the reason that if someone stands under a water fall dropping from a higher height the person will feel a piercing sensation on the skin when the water falls on the skin, as transient cavitation may occur instantly on the skin.

Acoustic cavitation is also standing on the basic concept of cavitation, when high frequency sound wave (20 kHz-1 GHz), coined as ultrasound, passes through a liquid medium (e.g. water, aqueous solvent, and pure organic or inorganic solvent), the resulting cavitation is termed to be acoustic cavitation. In this case, high frequency

sound waves, applied in the liquid medium, when dissipate through the liquid medium via ‘expansion and rarefaction’ of the sound waves that causes rapid change of pressure inside the bulk liquid. Thus, the expansion or rarefaction of waves creates negative pressure zones inside the bulk liquid medium, and results in ‘micro vacuum zones’ also known as ‘hot spots’, where at that point of pressure difference inside the liquid medium microbubbles are formed. These bubbles start to grow as long as the local pressure (p) within the micro vacuum zones remains lower than the saturated vapor pressure (p_V) of the liquid, at a certain magnitude of $p_V - p$ (Δp), where Δp reaches the magnitude of the tensile strength of the liquid, (Δp_c), a rapid adiabatic compression of bubble ultimately results in a bubble collapse. This whole phenomenon takes place within milliseconds of time and continues until the source of energy (ultrasound) remains to maintain the negative pressure zones inside the liquid (Brennen, 2013; Capote and de Castro 2007).

Interestingly, while cavitation is considered as one of the reasons for the corrosion and erosion of metals or any solid surfaces in contact with the liquid wherein it occurs (Lei *et al.*, 2017; Kwok *et al.*, 2016; Taillon, 2016; Karimi and Martin, 1986), on the contrary in the field of sonochemistry it is considered as a potential phenomenon to be exploited for various applications in the field of physical chemistry, industrial processes and healthcare as well. The collapse of microbubbles is associated with the formation of shock-waves and micro-jets which have widely been studied in the fields of both physical chemistry and sonochemistry (Ashokkumar, 2010). While cavitation occurs in liquid which is in contact to some solid surface, high speed liquid jets appear as the resultant of cavitation, these liquid jets straightway hit the solid surface in contact at a speed of around 400 km/h (Capote and de Castro, 2007) which is nearly the speed (431 km/h) of the sports car that currently holds the ‘fastest road production car’ record in the Guinness World Record ("*Production car speed record*", n.d.). Solid surface continuously exposed to these high speed liquid jets undergoes severe corrosion; eventually it damages the machine or system. Due to this fact, cavitation is an important topic of study in the corrosion engineering. While in the field of sonochemistry, acoustic cavitation taking place only inside the bulk liquid media, not at the contact zone of the liquid and a solid surface, holds much attention because the energy generated due to the collapse of bubbles has a great impact on the chemical species present in the liquid medium, that could even result in the potential physical and/or

chemical changes of the species. Due to this fact, in the field of sonochemistry cavitation is an important phenomenon that is being exploited for various applications, e.g., controlling the particle size and shape of nanoparticles, processing materials e.g. synthesis and functionalization, extraction of materials, cleaning, dispersion, welding, medical scanning, etc. (Krasulya *et al.* 2014; Xu *et al.*, 2013; Suslick and Price, 1999).

On this context, to be noted that based on the applied technique of generating cavitation, there could be different types of cavitation including acoustic cavitation, hydrodynamic cavitation, optic cavitation and particle cavitation. Similar to acoustic cavitation, hydrodynamic cavitation is associated to the tension in the liquid media and is generated by pressure variations due to the change in the geometry of the system. Optic and particle cavitation are the result of local deposition of energy via pulse laser and elementary particles, respectively (Ashokkumar, 2010). In this work, acoustic cavitation was employed in functionalizing C₆₀ molecule, hence the review will be limited to the importance of acoustic cavitation and its applications in synthesizing and functionalizing materials. Prior to that discussion, a brief summary of bubble dynamics will help to understand the impact of cavitation that could occur on the materials present in the liquid medium during ultrasonication.

The dynamics of a single microbubble, the mechanism of bubble collapse and what is the real scenario that takes place during a bubble collapse are the core concerns specifically in the area of ultrasonic cavitation and more widely in the field of (ultra)sonochemistry. Formation and collapse of bubbles could be explained on the concepts of both physics and chemistry; although not all aspects of bubble formation and collapse are yet fully understood and rationalized by the conventional methods, hence in the field of sonochemistry ‘bubble dynamics’ is still a subject that demands more explanation to the depth of this phenomenal consequence of ultrasound while passing through a liquid media. The most well-known concept of bubble growth and collapse explains (Brennen, 2013; Capelo-Martínez, 2009; Capote and de Castro, 2007) that an initially spherical bubble continues to grow through a successive cycle of expansion and contraction of the applied field of ultrasound, then finally gains an optimum radius of its size in the bulk medium (Fig. 2.12), where it reaches the ultimate condition of $\Delta p = \Delta p_c$ and then collapse.

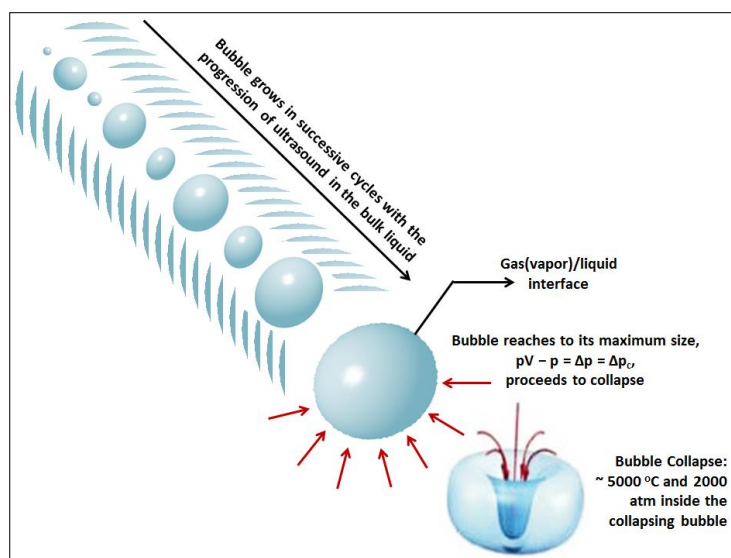


Figure 2.12 Mechanism of bubble formation and collapse with the expansion and contraction of ultrasound wave through aqueous medium

Till to date, all the established theories and methods (based on both theoretical and analytical studies) in bubble dynamics and sonochemistry imply that a collapsing bubble is the source of intense heat and pressure which may rise to 5000 °C and 2000 atm respectively; such a higher temperature could be compared to the temperature of the surface of sun, and the pressure generated could be compared to the pressure felt at the deepest part of ocean i.e. Mariana trench (Brennen, 2013; Capote, 2007). However, the hot spots are transient and compared to the bulk volume they are enormously smaller and the energy released from the bubble collapse is immediately dissipated through the bulk, hence no significant effect on the surrounding environment and/or damage to the reactor occur. Due to this interesting feature ‘cavitation’ is also termed as ‘cold boiling’ (Capote, 2007). The generation of transient immense heat and pressure inside the hot spots featuring ‘cold boiling’ makes up thermodynamically favorable environment for the formation of radicals from the solvent of the bulk medium. Hence, ultrasonication has even been applied to functionalize a number of materials and in the next section of this chapter it will be discussed elaborately.

While talking about the applications of ultrasound, it is to be considered that on a real scenario not only one single bubble is generated inside the liquid medium, scores of microbubbles are produced within a millisecond of time at a time, hence their cumulative energy with respect to the derivative of time could be a subject of special interest in the future studies with a view to solving the current energy crisis in the world.

Since a collapsing bubble is the immense source of heat and energy, on this context some spectacular ideas came into describing the potential effects of bubble formation and collapse, such as 'plasma theory', 'electrical theory' and 'fusion theory'. Mason (2015) in his personal review on sonochemistry recalled one of those renowned postulates known as 'the electrical theory related to bubble collapse' where it was conceived that charge formation could occur at the surface of microbubbles which may result into an intense electrical field of approximately 10^{11} V/m. Plasma theory assumes that the extreme conditions of heat inside a collapsing bubble indicate the formation of microplasma inside the collapsing bubbles; this theory has later been supported by spectroscopic studies of both single bubble and multibubbles sonoluminescence that non-equilibrium plasma may exist inside a collapsing bubble (Nikitenko, 2014; Flannigan and Suslick, 2005; Lepoint-Mullie *et al.*, 1996). Hua *et al.* (1995) suggested that under such condition it could be very obvious that ultrasonic cavitation in water can produce supercritical water. Fusion theory proposes an interesting possibility of generating nuclear fusion of atoms inside the collapsing bubbles. Given the extreme temperature and pressure conditions of a collapsing bubble, initially this idea was thought to be very potential; however, this idea raised interesting arguments in the field of sonochemistry and the possibility is still under investigation (Taleyarkhan *et al.*, 2002).

Acoustic cavitation depends on several factors, where the effect of cavitation also affects the outcome of the reaction or the physical changes that may occur in the reactor (Capelo-Martínez, 2009; Capote and de Castro, 2007; Raso *et al.*, 1996). Hence, it is essential to take note about all the controlling factors prior to the application of ultrasonic cavitation for any of the applications.

Applied frequency is one of the most important variables in selecting the power of ultrasonication. Trivially, it might be conceived that the higher the frequency the higher the cavitation, but in practice it has been observed that with the increase of frequency of the ultrasound the cavitation threshold increases due to the short span of rarefaction phase of the wave, which ultimately takes longer time for the bubbles to form within that short rarefaction cycles. Thus, an increase in frequency will require an increase in intensity or higher amplitude to provide the threshold energy for the bubbles to form at higher frequency. Because of this, ultrasonication from 20 to 50 kHz is mostly used for cleaning, synthesis and for other common sonochemical applications in the processing

of materials. This also implies the effect of intensity as well, since intensity is directly proportional to the square of amplitude, and thus increasing the amplitude will increase the intensity and hence the sonochemical effect. However, there is a minimum intensity at which the cavitation threshold for a particular system is obtained, beyond that limit of intensity a very high power will be dissipated throughout the liquid medium which can result in the formation of more bubbles. Formation of more bubbles not necessarily offers better sonochemical effect, rather it affects in an opposite manner; while more bubbles are formed under higher intensity and amplitude they tend to coalesce to each other and form even larger bubbles. This causes larger bubbles impossible to collapse within the rarefaction cycles as the larger the bubbles the more the time it would take for the adiabatic compression of the gas trapped inside the bubbles and finally the collapse may not be achievable at a certain applied frequency, especially when the applied frequency is also higher. Hence, it is not essential to use higher frequency, higher intensity and higher amplitude in order to gain better sonochemical effect for a particular system; rather it might cause the erosion of the transducer over time.

Any 'particular system' may entail one or more particular solvent(s), dissolved gas inside the solvent, temperature and external pressure applied on the solvent. Since it requires a minimum energy or negative pressure to pull apart the solvent molecules from each other to create a void inside the liquid medium, the viscosity of solvent also plays an important role on the cavitation threshold. Higher viscosity solvent will require more energy to experience cavitation phenomenon during ultrasonication, but at the same time solvent vapor pressure is another critical factor to consider as the lower the vapor pressure the easier is to form the voids inside the liquid medium. A higher vapor pressure solvent rather will require less power to experience cavitation. While considering about the vapor pressure as one of the controlling factors to cavitation, consequently the effect of applied temperature and external pressure together also become vital factors during ultrasonication, as the vapor pressure of a solvent is temperature and pressure dependent. At lower acoustic intensity, cavitation is favored by the increase of temperature. Thus, using higher vapor pressure solvent and higher temperature might sound good to increase the sonochemical effect, but then under such circumstances, where the vapor pressure of liquid is high and the temperature as well, more bubbles cause 'bubble hindrance' toward the transmission of sound wave inside the liquid media which weakens the effect of ultrasonic energy and results in reduced

cavitation effect on the system. Hence, a lower temperature or normal room temperature ensures a favorable condition for cavitation and where possible, alternative solvents able to accomplish the same purpose but have lower vapor pressure should be chosen to acquire the maximum benefit of cavitation. However, in order to obtain a desired sonochemical effect, while a higher vapor pressure solvent is required to use the values of amplitude and frequency have to be lowered or optimized to a level such that the formation and collapse of bubbles can happen within the rarefaction cycles of the sound wave.

In summary, the value of the applied frequency, intensity, amplitude of ultrasound along with the type of solvent used, temperature and pressure for the system, all should be taken into consideration prior to design any ultrasound-assisted system. So, the applied ultrasound energy passing throughout the liquid medium neither form too small bubbles that may dissolve in the bulk liquid before approaching to cavitation nor form too large of them so they coalesce to each other or need longer beyond the time of a rarefaction cycle.

Apart from the above-discussed factors, the dissolved gas, e.g. trapped air has reported to have significant effect on the cavitation threshold (Rooze *et al.*, 2013; Capote and de Castro, 2007). Trapped air or any other gas molecules act as ‘gas pockets’ inside the liquid media. These gas pockets are the weak zones in the network of continual intermolecular bonds and perform as nucleation sites to boost up the cavitation phenomenon. Thus, the presence of gas pockets reduces the required energy needed to form the cavitation bubbles, however, the shock waves released from the collapse of these bubbles are found to result in lower intensity. It might be considered as an interesting avenue to explore, the effect of different trapped gas at their different vapor pressure and different concentration inside the bulk liquid, not only on the sonochemical phenomena but also how they may affect the yield of any reaction or physical change of the materials under ultrasonication.

2.3.2 Application of ultrasonication in functionalizing nanoparticles

Ultrasonication technology has become popular due to the fact that it is now being considered as an alternative green and energy efficient technique for synthesizing and

functionalizing nanomaterials. Not only to produce a diverse size and shape of nanoparticles, but also ultrasonic cavitation has been proved as one of the efficient green techniques in producing a range of useful multifunctional hybrid nanoparticles which have potential applications in various fields of science and technology (Manickam and Ashokkumar, 2014).

The application of ultrasonic treatment is not limited to the production of controlled size and shape of nanoparticles, rather nowadays it is extended to functionalizing and producing multifunctional hybrid nanoparticles. The physical phenomenon of ultrasonication ultimately contributes in controlling the chemical properties of particles. Previous reports supported that ultrasonication could be a very useful technique in the field of analytical chemistry. There are copious reports on the sonochemical synthesis of nanoparticles, optimizing the physical properties of material via ultrasonic treatment and functionalizing materials via acoustic cavitation generated during ultrasonication. The following review provides an account on some of those useful reports.

In a series of reports, delivered by Gonzalez *et al.* (2011), Banerjee *et al.* (2012), Bastami and Entezari (2010), Akhbari and Morsali (2012), Safarifard and Morsali (2012), Neppolian *et al.* (2012), Bastami and Entezari (2012), synthesis of various nanoparticles, e.g., Co-Sn-graphite, zinc oxide, manganese oxide, titanium oxide, copper oxide, Pt-graphene oxide (GO)-TiO₂ and manganese oxide by using ultrasonication were reported. An innovative approach of applying ultrasonication in association with three-electrode electrochemical system was proposed by Mancier *et al.* (2010), where the synthesis of Cu-Ag core-shell nanoparticle was achieved via sonoelectrochemical technique and the sonotrode was used as the working electrode. The synthesis technique followed an integrated strategy of both sonochemistry and electrochemistry, where an ultrasonic horn with a tunable power from 7 to 100 W was employed in producing copper-silver core-shell nanoparticles.

Application of acoustic cavitation via the technique of ultrasonication has also been employed in functionalizing and/or modifying magnetic nanoparticles. As magnetic nanoparticles possess both magnetic and chemical functional parts, hence it becomes advantageous in medical diagnosis and treatment, waste water treatment, magnetic immunoassay, cancer therapy, biomedical engineering and information technology. Gopi *et al.* (2012) reported that magnetic hydroxyapatite has potential in treating bone

cancer which could be functionalized with magnetite nanoparticles (MNPs) via an ultrasound irradiation at 35 kHz at 320 W. Wang *et al.* (2010) reported that one of the most popular magnetic nanoparticles i.e. Fe_3O_4 , which has enormous applications in catalysis, preparing sensor and magnetic storage devices and magnetic resonance imaging (MRI), its catalytic activity could be enhanced by ultrasonic cavitation technique.

While considering the nanoparticles, the benefits obtained via ultrasonic treatment in optimizing the functionality of nanocomposites should not be ignored as well, as nanocomposites also nowadays are offering potential applications in aerospace, automotive, electronics and biotechnology, hence their functionality and activity vary based on the applications. In a study reported by Ghows *et al.* (2012), it was shown that the ultrasonic treatment of CdS nanoparticles and CdS/TiO₂ nanocomposites using an ultrasonic horn of 20 kHz at 55 W at a constant temperature 55 °C resulted in well-crystallized nanoparticles from the mixture. In other report, exfoliated structure of poly(styrene-co-methyl-methacrylate/Montmorillonite [p(MMA-co-St)/O-MMT] nanocomposites were obtained via ultrasonic-assisted emulsion polymerization technique (Bhanvase *et al.*, 2012), Au-polypyrrole [PPy]/Prussian blue (PB) nanocomposite was synthesized via a one-step sonochemical approach without using any reductant and stabilizer and the synthesized nanocomposite was employed in fabricating highly sensitive and stable H₂O₂ biosensor (Lu *et al.*, 2012). Similarly, synthesis of chitosan/gold nanocomposites and magnesium-aluminium-layered double hydroxides nanocomposite were reported by Ou *et al.* (2011) and Chang *et al.* (2011), where sonochemically synthesized nanocomposites showed better activity in oxidizing CO to CO₂ and a high adsorption capacity for fluoride, respectively. Contemporarily, a one-step synthesis method at high yield of chromium dioxide nanowire was reported by Zhou *et al.* (2011), where the proposed method could be an alternative to the solid-state reaction technique which involves multi-steps in synthesizing the CrO₂ nanowires.

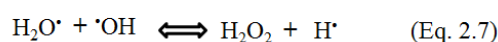
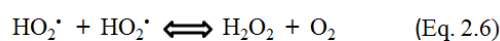
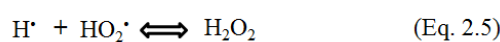
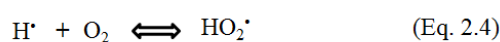
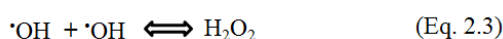
2.3.3 C₆₀ to fullereneol via ultrasonic cavitation: a longstanding overlooked idea and its prospects

In the current context of this work, where the main objective is to develop a facile and green technique of functionalizing C₆₀, the role of ultrasound could be considered to

prepare exohedrally functionalized C₆₀. The prospect of ultrasonication or acoustic cavitation has been remarked as one of the energy-efficient and green technique in synthesizing or functionalizing various materials (Mason, 2000, 2003, 2007; Gedanken, 2004). C₆₀ as a nanoparticle becomes more useful while functionalized with –OH, –COOH, –NH₂ functional groups. Among them, polyhydroxylated C₆₀ or fulleranol is being mentioned in various studies as a potential candidate to be used as an antioxidant, free radical scavenger, a drug carrier and as a nanomediator in detecting biomarker (Djordjevic *et al.*, 2015; Borović *et al.*, 2014; Slavic *et al.*, 2013; Pinteala *et al.*, 2009; Đorđević *et al.*, 2008; Chiang *et al.*, 1995). The spherical molecule of C₆₀ represents a truncated icosahedron structure built up with 12 pentagons and 20 hexagons of carbon rings, where the carbons in the pentagon are single bonded but interestingly at the junction of pentagon and hexagon the carbons are double bonded. Hence, the molecular structure of C₆₀ contains both sp² and sp³ hybridized carbons, as a result of this fact, C₆₀ behaves as an electron deficient alkene due to the unsaturated delocalization of π electrons throughout the icosahedron structure (Curl, 1997). Because of this physicochemical property of C₆₀, it reacts with electron rich species, and this is where the possibility of hydroxylation of C₆₀ molecule appears via ultrasonication in aqueous medium.

To explore the possibility, first to be noted is the outcome of acoustic cavitation while ultrasound energy is applied through an aqueous medium, or simply through water. What happens to the water molecules under acoustic cavitation, the knowledge of that phenomenon will clear the scope of producing fulleranol via ultrasonication. In fact, the outcome of ultrasonication in a liquid medium is quite phenomenal from the view point of energy generation, which results due to the high temperature and pressure of a collapsing bubble, which has been discussed in the previous sections of this chapter. Under such an extreme condition of heat and pressure inside the collapsing bubbles, potential radicals and functional groups formed from the water vapors which have been reported and supported in several studies (Ince *et al.*, 2001; Gong *et al.*, 1998; Luche *et al.*, 1997). The continuous process of bubble formation and collapse thus ultimately results in a pool of ·OH and H· inside the aqueous medium. Under such a thermodynamically favorable condition for the generation of free radicals, due to the presence of a pool of active hydroxyl radicals, C₆₀ molecules while present in water (or in an aqueous medium) may also undergo certain reaction(s). Although in the previous

studies it was shown that the generation of $\cdot\text{OH}$ and $\text{H}\cdot$ radicals are responsible in making C_{60} molecules dispersed in an aqueous medium via hydration but the possibility of forming potential fulleranol moieties under the same condition was not carefully observed, thus a potential facile pathway toward producing fulleranol directly from pristine C_{60} via ultrasonication in an aqueous medium has long been left overlooked. However, the generation of active radicals is not very straightforward, rather it follows multiple steps. Gong and Hart (1998) described that the reaction mechanisms that could possibly occur in a simple sonochemical system in water alone may follow seven steps,



More elaborately to explain the above-mentioned steps, the radicals produced in the first place from the breakdown of water molecules under ultrasonication are $\cdot\text{OH}$ and $\text{H}\cdot$ (Eq. 2.1). The production of $\cdot\text{OH}$ radicals carries much importance in accomplishing a targeted reaction compared to $\text{H}\cdot$ radicals. The parent radicals, $\cdot\text{OH}$ and $\text{H}\cdot$, formed in the initial stage, proceed to the inter-combination of radicals, thus forming hydrogen peroxide (H_2O_2) and secondary radicals e.g. hydroperoxyl ($\text{HO}_2\cdot$) (Eq. 2.2-2.7). The reaction is spontaneous in presence of oxygen (Rooze *et al.*, 2013). In presence of oxygen the secondary radicals further generate H_2O_2 . The series of radical formation and combination results in not only the potential $-\text{OH}$ groups but also H_2O_2 , hydrogen and oxygen gases. In previous studies, C_{60} was dispersed in aqueous solution by ultrasonic dispersion where the reason behind the dispersion was mentioned as the hydration of C_{60} molecules due to the presence of water as well as the generation of OH radicals or $-\text{OH}$ groups. Consequently, C_{60} becomes C_{60} dispersion in water. However, the possibility of hydroxylation of C_{60} under such condition has been neglected so far. While considering the possibility of hydroxylation of C_{60} by ultrasonic cavitation, it is also an important fact which provides supports toward the ideas that hydrogen peroxide which is being produced by the recombination of $\cdot\text{OH}$ and $\text{H}\cdot$ radicals break down into

further $\cdot\text{OH}$ and $\text{H}\cdot$ radicals, thus promoting the total amount of $\cdot\text{OH}$ radicals in the aqueous medium under ultrasonication.

While the possibility of hydroxylation of C_{60} is bright based on empirically established reaction mechanisms (Manickam and Ashokkumar, 2014; Capelo-Martínez, 2009; Capote and de Castro, 2007; Ince *et al.*, 2001), some important points derived from the thermodynamics of the ultrasound-assisted reaction coupled with bubble dynamics may propose differently. It is anticipated that at the final stage of bubble collapse the rate of bubble collapse is higher than the rate of reaction (Capote and de Castro, 2007; Franc and Michel, 2006). Hence, if hydroxylation occurs to the C_{60} moiety the rate of hydroxylation will be dependent on the bubble dynamics although it is practically difficult to quantify the kinetics of the reaction rate under such conditions. However, as cavitation is also dependent on the vapor pressure and viscosity of the solvent as well as temperature of the bulk liquid plays a vital role in controlling the bubble formation and collapse phenomenon, hence optimizing the sonochemical system to produce a desired yield is required. While a sonochemical system is already designed with a specific solvent, then the vapor pressure and viscosity become fixed for that system with that choice of solvent. In that case, the main variables that will have impact on the rate of hydroxylation or overall yield of the reaction are the temperature of the solvent during ultrasonication, amplitude and frequency of the sonotrode; thus, selecting the best frequency and amplitude as well as maintaining the desired temperature in the reactor during ultrasonication are important measures to produce a desired product out of the effect of acoustic cavitation during ultrasonication. It has long been believed that ultrasonication of C_{60} in water or aqueous medium turns this ‘tough to dissolve’ C_{60} into C_{60} dispersion due to the hydration of C_{60} by surrounding water molecules via H-bonding or via the charge transfer from water molecule to C_{60} , but it has been a long standing doubt whether the ultrasound-assisted dispersion of C_{60} in water is actually the result of any chemical changes to C_{60} moiety occurring during ultrasonication (Prylutsky *et al.*, 2014; Labille *et al.*, 2009; Brant *et al.*, 2005). Not only the generation of $\cdot\text{OH}$ radicals during ultrasonication raise this doubt but also the presence of unsaturated delocalized π electrons in the truncated icosahedron structure of C_{60} makes this assumption stronger that during acoustic cavitation hydroxylation may occur to the C_{60} molecule resulting in potential fulleranol moieties. However, this doubt was not carefully investigated so far and till to date lacks sufficient evidence to support the

assumption. Hence, in this work, the possibility for C₆₀ to functionalize with hydroxy groups (-OH) via ultrasound-assisted reaction in an aqueous medium in the presence of hydrogen peroxide (H₂O₂) has been investigated. The investigation was both qualitative and quantitative which comprised of three objectives, first to observe whether hydroxylation occurs to C₆₀ molecule during acoustic cavitation; second, to determine the most possible structure of the fulleranol synthesized via ultrasound-assisted technique, and finally to develop a method where the values of the reaction parameters were optimized to propose a reproducible facile synthesis technique for fulleranol(s).

2.4 Key Points of the Review and Direction to the Next Chapter

- Derivatives of C₆₀ could be considered as potential candidates to produce bio-functional hybrid materials for detecting biomarkers.
- Ultrasonication could be considered as a potential facile technique to functionalize C₆₀ with -OH functional groups.
- In the next chapter, a qualitative and quantitative discussion will be delivered toward the investigation of hydroxylating C₆₀ with -OH functional groups via ultrasonication.

References

Ahmed, M., Pan, C., Gan, L., Nawaz, Z., & Zhu, J. (2010). Highly sensitive amperometric cholesterol biosensor based on Pt-incorporated fullerene-like ZnO nanospheres. *Journal of Physical Chemistry C*, 114, 243-250.

Akhbari, K., & Morsali, A. (2012). Thallium (I) supramolecular polymer with Tl⁺... π secondary interactions; preparation of nano-structures by sonochemical method as a new precursor for preparation of Tl₂O₃ with nano-structural surface. *Journal of Organometallic Chemistry*, 700, 125-131.

Apfel, R. E. (1997). Sonic effervescence: A tutorial on acoustic cavitation. *The Journal of the Acoustical Society of America*, 101(3), 1227-1237.

Ashokkumar, M. (Ed.). (2010). *Theoretical and experimental sonochemistry involving inorganic systems*. Springer Science & Business Media.

Banerjee, P., Chakrabarti, S., Maitra, S., & Dutta, B. K. (2012). Zinc oxide nanoparticles—sonochemical synthesis, characterization and application for photo-remediation of heavy metal. *Ultrasonics Sonochemistry*, 19(1), 85-93.

Bastami, T. R., & Entezari, M. H. (2012). Synthesis of manganese oxide nanocrystal by ultrasonic bath: Effect of external magnetic field. *Ultrasonics Sonochemistry*, 19(4), 830-840. Bastami, T. R., & Entezari, M. H. (2010). Sono-synthesis of Mn₃O₄ nanoparticles in different media without additives. *Chemical Engineering Journal*, 164(1), 261-266.

Bhanvase, B. A., Pinjari, D. V., Gogate, P. R., Sonawane, S. H., & Pandit, A. B. (2012). Synthesis of exfoliated poly (styrene-co-methyl methacrylate)/montmorillonite nanocomposite using ultrasound-assisted in situ emulsion copolymerization. *Chemical Engineering Journal*, 181, 770-778.

Biju, V. (2014). Chemical modifications and bioconjugate reactions of nanomaterials for sensing, imaging, drug delivery and therapy. *Chemical Society Reviews*, 43(3), 744-764.

Baena, J. R, Gallego, M. & Valcarcel, M. (2002). Fullerenes in the analytical sciences', *TrAC Trends in Analytical Chemistry*, 21(3), 187-198.

Borović, M. L., Ičević, I., Kanački, Z., Žikić, D., Seke, M., Injac, R., & Djordjević, A. (2014). Effects of fulleranol C₆₀(OH)₂₄ nanoparticles on a single-dose doxorubicin-induced cardiotoxicity in pigs: an ultrastructural study. *Ultrastructural Pathology*, 38(2), 150-163.

Bosi, S., Ros, T.D., Spalluto, G. & Prato, M. (2003). Fullerene derivatives: An attractive tool for biological applications. *European Journal of Medicinal Chemistry*, 38(11–12), pp. 913–923.

Brant, J., Lecoanet, H., Hotze, M., & Wiesner, M. (2005). Comparison of electrokinetic properties of colloidal fullerenes (n-C₆₀) formed using two procedures. *Environmental Science & Technology*, 39(17), 6343-6351.

Brennen, C. E. (2013). *Cavitation and bubble dynamics*. Cambridge University Press.

Britz, D. A., Khlobystov, A. N., Wang, J., O'Neil, A. S., Poliakoff, M., Ardavan, A., & Briggs, G. A. D. (2004). Selective host–guest interaction of single-walled carbon nanotubes with functionalised fullerenes. *Chemical Communications*, 61(2), 176-177.

Capelo-Martínez, J. L. (Ed.). (2009). *Ultrasound in chemistry: analytical applications*. John Wiley & Sons.

Capote, F. P., & de Castro, M. L. (2007). *Analytical applications of ultrasound* (Vol. 26). Elsevier.

Carano, M., Cosnier, S., Kordatos, K., Marcaccio, M., Margotti, M., Paolucci, F., Prato, M., & Roffia, S. (2002). A glutathione amperometric biosensor based on an amphiphilic

fullerene redox mediator immobilised within an amphiphilic polypyrrole film, *Journal of Materials Chemistry*, 12(7), 1996–2000.

Chaban, V. V., & Fileti, E. E. (2017). Which fullerenols are water soluble? Systematic atomistic investigation. *New Journal of Chemistry*, 41(1), 184-189.

Chambers, J.P., Arulanandam, B.P., Matta, L.L., Weis, A. & Valdes, J.J., (2008). Biosensor recognition elements. *Current Issues in Molecular Biology*, 10 (1-2), 1-12.

Chang, M. S., & Shih, J. S. (2000). Fullerene-cryptand-coated piezoelectric crystal membrane glucose enzyme sensor. *Sensors and Actuators, B: Chemical*, 67(3), 275–281.

Chang, H. W., & Shih, J. S. (2007). Surface acoustic wave immunosensors based on immobilized C60-proteins, *Sensors and Actuators, B: Chemical*, 121(2), 522–529.

Chang, H. W., & Shih, J. S. (2008). Insulin surface acoustic wave immunosensor based on immobilized C-60/anti-insulin antibody. *Journal of the Chinese Chemical Society*, 55(2), 318–325.

Chang, Q., Zhu, L., Luo, Z., Lei, M., Zhang, S., & Tang, H. (2011). Sono-assisted preparation of magnetic magnesium–aluminum layered double hydroxides and their application for removing fluoride. *Ultrasonics Sonochemistry*, 18(2), 553-561.

Chen, C. H., Chang, H. W., & Shih, J. S. (2007). Optical isomer piezoelectric crystal sensor for l-amino acid esters based on immobilized C60-lipase enzyme. *Sensors and Actuators, B: Chemical*, 123(2), 1025–1033.

Chen, Z., Ma, L., Liu, Y., & Chen, C. (2012). Applications of functionalized fullerenes in tumor theranostics, *Theranostics*, 2(3), 238–250.

Chiang, L. Y., Lu, F. J., & Lin, J. T. (1995). Free radical scavenging activity of water-soluble fullerenols. *Journal of the Chemical Society, Chemical Communications*, (12), 1283-1284.

Chou, F. F., Chang, H. W., Li, T. L., & Shih, J. S. (2008). Piezoelectric crystal/surface acoustic wave biosensors based on fullerene C60 and enzymes/antibodies/proteins. *Journal of the Iranian Chemical Society*, 5(1), 1-15.

Chuang, C. W., & Shih, J. S. (2001). Preparation and application of immobilized C60-glucose oxidase enzyme in fullerene C60-coated piezoelectric quartz crystal glucose sensor, *Sensors and Actuators, B: Chemical*, 81(1), 1–8.

Chung, D. J., Seong, M. K., & Choi, S. H. (2011). Radiolytic synthesis of -OH group functionalized fullerene structures and their biosensor application. *Journal of Applied Polymer Science*, 122(3), 1785-1791.

Davis, J., Huw Vaughan, D., & Cardosi, M. F. (1995). Elements of biosensor construction. *Enzyme and Microbial Technology*, 17(12), 1030–1035.

Da Ros, T., & Prato, M. (1999). Medicinal chemistry with fullerenes and fullerene derivatives. *Chemical Communications*, 8, 663-669.

Djordjevic, A., Srdjenovic, B., Seke, M., Petrovic, D., Injac, R., & Mrdjanovic, J. (2015). Review of synthesis and antioxidant potential of fullerene nanoparticles. *Journal of Nanomaterials*, 16(1), 280.

Dorđević, A., & Bogdanović, G. (2008). Fullerenol: a new nanopharmaceutic?. *Archive of Oncology*, 16(3-4), 42-45.

Flannigan, D. J., & Suslick, K. S. (2005). Plasma formation and temperature measurement during single-bubble cavitation. *Nature*, 434(7029), 52-55.

Franc, J. P., & Michel, J. M. (2006). *Fundamentals of cavitation* (Vol. 76). Springer Science & Business Media.

Friedman, S. H., Decamp, D. L., Sijbesma, R. P., Srdanov, G., Wudl, F., & Kenyon, G. L. (1993). Inhibition of the HIV- 1 protease by fullerene derivatives: Model building

studies and experimental verification. *Journal of the American Chemical Society*, 115(5), 6506–6509.

Gavalas, V. G. & Chaniotakis, N. A. (2000). [60]Fullerene-mediated amperometric biosensors, *Analytica Chimica Acta*, 409(1), 131–135.

Gedanken, A. (2004). Using sonochemistry for the fabrication of nanomaterials. *Ultrasonics Sonochemistry*, 11(2), 47-55.

Ghows, N., & Entezari, M. H. (2012). Sono-synthesis of core-shell nanocrystal (CdS/TiO₂) without surfactant. *Ultrasonics Sonochemistry*, 19(5), 1070-1078.

Goyal, R. N., Oyama, M., Bachheti, N., & Singh, S. P. (2009a). Fullerene C₆₀ modified gold electrode and nanogold modified indium tin oxide electrode for prednisolone determination. *Bioelectrochemistry*, 74(2), 272-277.

Goyal, R. N., Gupta, V. K. & Chatterjee, S. (2009b). A sensitive voltammetric sensor for determination of synthetic corticosteroid triamcinolone, abused for doping, *Biosensors and Bioelectronics*, 24(12), 3562–3568.

Goyal, R. N., Gupta, V. K. & Chatterjee, S. (2009c). Fullerene-C₆₀-modified edge plane pyrolytic graphite electrode for the determination of dexamethasone in pharmaceutical formulations and human biological fluids. *Biosensors and Bioelectronics*, 24(6), 1649–1654.

Gong, C. & Hart, D. P. (1998). Ultrasound induced cavitation and sonochemical yields. *The Journal of the Acoustical Society of America*, 104(5), 2675-2682.

González, J. R., Alcántara, R., Nacimiento, F., & Tirado, J. L. (2011). CoSn-graphite electrode material prepared by using the polyol method and high-intensity ultrasonication. *Electrochimica Acta*, 56(27), 9808-9817.

Gopi, D., Ansari, M. T., Shinyjoy, E., & Kavitha, L. (2012). Synthesis and spectroscopic characterization of magnetic hydroxyapatite nanocomposite using

ultrasonic irradiation. *Spectrochimica Acta Part A: Molecular and Biomolecular Spectroscopy*, 87, 245-250.

Gradzka, E., Winkler, K., Borowska, M., Plonska-Brzezinska, M. E. & Echegoyen, L. (2013). Comparison of the electrochemical properties of thin films of MWCNTs/C 60-Pd, SWCNTs/C60-Pd and ox-CNOs/C60-Pd, *Electrochimica Acta*, 96, 274–284.

Han, J., Zhuo, Y., Chai, Y., Yuan, R., Xiang, Y., Zhu, Q., & Liao, N. (2013). Multi-labeled functionalized C₆₀ nanohybrid as tracing tag for ultrasensitive electrochemical aptasensing. *Biosensors and Bioelectronics*, 46, 74-79.

Hang, L., Wang, Q., Gao, F., Shi, J., & Gao, F. (2014). A high-performance DNA biosensor using polyhydroxylated fullerenol as 3D matrix for probe immobilization. *Electrochemistry Communications*, 47, 84-87.

Hirsch, A. (1993). The chemistry of the fullerenes: an overview. *Angewandte Chemie International Edition*, 32(8), 1138-1141.

Hua, I., Hoechemer, R. H., & Hoffmann, M. R. (1995). Sonolytic hydrolysis of p-nitrophenyl acetate: the role of supercritical water. *The Journal of Physical Chemistry*, 99(8), 2335-2342.

Ince, N. H., Tezcanli, G., Belen, R. K., & Apikyan, I. G. (2001). Ultrasound as a catalyzer of aqueous reaction systems: the state of the art and environmental applications. *Applied Catalysis B: Environmental*, 29(3), 167-176.

Jensen, A. W., Wilson, S. R. & Schuster, D. I. (1996). Biological applications of fullerenes, *Bioorganic and Medicinal Chemistry*, 4(6), 767–779.

Karimi, A., & Martin, J. L. (1986). Cavitation erosion of materials. *International Metals Reviews*, 31(1), 1-26.

Kokubo, K., Shirakawa, S., Kobayashi, N., Aoshima, H., & Oshima, T. (2011). Facile and scalable synthesis of a highly hydroxylated water-soluble fullerene as a single nanoparticle. *Nano Research*, 4(2), 204-215.

Krasulya, O., Shestakov, S., Bogush, V., Potoroko, I., Cherepanov, P., & Krasulya, B. (2014). Applications of sonochemistry in Russian food processing industry. *Ultrasonics Sonochemistry*, 21(6), 2112-2116.

Kwok, C. T., Man, H. C., Cheng, F. T., & Lo, K. H. (2016). Developments in laser-based surface engineering processes: with particular reference to protection against cavitation erosion. *Surface and Coatings Technology*, 291, 189-204.

Labille, J., Masion, A., Ziarelli, F., Rose, J., Brant, J., Villiéras, F., Pelletier, M., Borschneck, D., Wiesner, M.R., & Bottero, J.Y. (2009). Hydration and dispersion of C60 in aqueous systems: the nature of water– fullerene interactions. *Langmuir*, 25(19), 11232-11235.

Lanzellotto, C., Favero, G., Antonelli, M. L., Tortolini, C., Cannistraro, S., Coppari, E., & Mazzei, F. (2014). Nanostructured enzymatic biosensor based on fullerene and gold nanoparticles: preparation, characterization and analytical applications. *Biosensors and Bioelectronics*, 55, 430-437.

Liao, Y.-H., & Shih, J.-S. (2013). Piezoelectric quartz crystal anti-protein immunosensors based on immobilized fullerene C60-proteins. *Journal of the Chinese Chemical Society*, 60(11), 1387–1395.

Li, J., Koehne, J., Chen, H., Cassell, A., Ng, H. T., Fan, W., Ye, Q., Han, J. & Meyyappan, M. (2003). Carbon nanotube nanoelectrode array as an electronic chip for ultrasensitive label-free DNA detection. *Nano Letters*, 3(5), 597–602.

Li, Y., Fang, L., Cheng, P., Deng, J., Jiang, L., Huang, H., & Zheng, J. (2013). An electrochemical immunosensor for sensitive detection of Escherichia coli O157: H7 using C60 based biocompatible platform and enzyme functionalized Pt nanochains tracing tag. *Biosensors and Bioelectronics*, 49, 485-491.

Lei, Y., Chang, H., Guo, X., Li, T., & Xiao, L. (2017). Ultrasonic cavitation erosion of 316L steel weld joint in liquid Pb-Bi eutectic alloy at 550° C. *Ultrasonics Sonochemistry*, 39, 77-86.

Lepoint-Mullie, F., De Pauw, D., Lepoint, T., Supiot, P., & Avni, R. (1996). Nature of the “extreme conditions” in single sonoluminescing bubbles. *The Journal of Physical Chemistry*, 100(30), 12138-12141.

Loboda, O., (2013). Quantum-chemical studies on porphyrins, fullerenes and carbon nanostructures. Berlin Heidelberg: Springer.

Lu, X., Li, Y., Zhang, X., Du, J., Zhou, X., Xue, Z., & Liu, X. (2012). A simple and an efficient strategy to synthesize multi-component nanocomposites for biosensor applications. *Analytica Chimica Acta*, 711, 40-45.

Luche, J. L. (1997). A few questions on the sonochemistry of solutions. *Ultrasonics Sonochemistry*, 4(2), 211-215.

Mancier, V., Rouse-Bertrand, C., Dille, J., Michel, J., & Fricoteaux, P. (2010). Sono and electrochemical synthesis and characterization of copper core–silver shell nanoparticles. *Ultrasonics Sonochemistry*, 17(4), 690-696.

Manickam, S., & Ashokkumar, M. (Eds.). (2014). *Cavitation: a novel energy-efficient technique for the generation of nanomaterials*. CRC Press.

Martín, N. (2006). New challenges in fullerene chemistry. *Chemical Communications*, 20, 2093-2104.

Mason, T. J. (2000). Large scale sonochemical processing: aspiration and actuality. *Ultrasonics Sonochemistry*, 7(4), 145-149.

Mason, T. J. (2003). Sonochemistry and sonoprocessing: the link, the trends and (probably) the future. *Ultrasonics Sonochemistry*, 10(4), 175-179.

Mason, T. J. (2007). Sonochemistry and the environment—Providing a “green” link between chemistry, physics and engineering. *Ultrasonics Sonochemistry*, 14(4), 476-483.

Mason, T. J. (2015). Some neglected or rejected paths in sonochemistry—A very personal view. *Ultrasonics Sonochemistry*, 25, 89-93.

Merouani, S., Ferkous, H., Hamdaoui, O., Rezgui, Y., & Guemini, M. (2015). A method for predicting the number of active bubbles in sonochemical reactors. *Ultrasonics Sonochemistry*, 22, 51-58.

Metin, R., Cairós, C., & Troia, A. (2015). Sonochemistry and bubble dynamics. *Ultrasonics Sonochemistry*, 25, 24-30.

Nikitenko, S. I. (2014). Plasma formation during acoustic cavitation: toward a new paradigm for sonochemistry. *Advances in Physical Chemistry*, 2014.

Neppolian, B., Bruno, A., Bianchi, C. L., & Ashokkumar, M. (2012). Graphene oxide based Pt–TiO₂ photocatalyst: ultrasound-assisted synthesis, characterization and catalytic efficiency. *Ultrasonics Sonochemistry*, 19(1), 9-15.

Ou, K. L., Yu, C. C., Liu, Y. C., Yang, K. H., Wang, C. C., & Chen, Q. Y. (2011). Sonoelectrochemical synthesis of chitosan/gold nanocomposites for application in removing toxic materials in mainstream smokes. *Materials Research Bulletin*, 46(12), 2333-2337.

Orlova, M. A., Trofimova, T. P., Orlov, A. P., & Shatalov, O. A. (2013). Perspectives of fullerene derivatives in PDT and radiotherapy of cancers. *British Journal of Medicine and Medical Research*, 3(4): 1731-1756.

Pan, N. Y., & Shih, J. S. (2004). Piezoelectric crystal immunosensors based on immobilized fullerene C₆₀-antibodies. *Sensors and Actuators, B: Chemical*, 98(2–3), 180–187.

Perumal, V., & Hashim, U. (2014). Advances in biosensors: Principle, architecture and applications. *Journal of Applied Biomedicine*, 12(1), 1-15.

Pilehvar, S., & De Wael, K. (2015). Recent advances in electrochemical biosensors based on fullerene-C₆₀ nano-structured platforms. *Biosensors*, 5(4), 712-735.

Pinteala, M., Dascalu, A., & Ungurenasu, C. (2009). Binding fullerenol C₆₀(OH)₂₄ to dsDNA. *International Journal of Nanomedicine*, 4, 193.

Pumera, M., Sánchez, S., Ichinose, I. & Tang, J. (2007). Electrochemical nanobiosensors. *Sensors and Actuators, B: Chemical*, 123(2), 1195–1205.

Production car speed record. (n.d). In Wikipedia. Retrieved August 17, 2017, from https://en.wikipedia.org/wiki/Production_car_speed_record

Prylutskyy, Y.I., Petrenko, V.I., Ivankov, O.I., Kyzyma, O.A., Bulavin, L.A., Litsis, O.O., Evstigneev, M.P., Cherepanov, V.V., Naumovets, A.G. & Ritter, U. (2014). On the origin of C₆₀ fullerene solubility in aqueous solution. *Langmuir*, 30(14), 3967-3970.

Raso, J., Manas, P., Pagan, R., & Sala, F. J. (1999). Influence of different factors on the output power transferred into medium by ultrasound. *Ultrasonics Sonochemistry*, 5(4), 157-162.

Rasooly, A., & Jacobson, J. (2006). Development of biosensors for cancer clinical testing. *Biosensors and Bioelectronics*, 21(10), 1851–1858.

Rooze, J., Rebrov, E. V., Schouten, J. C., & Keurentjes, J. T. (2013). Dissolved gas and ultrasonic cavitation—a review. *Ultrasonics Sonochemistry*, 20(1), 1-11.

Saeedfar, K., Heng, L. Y., Ling, T. L., & Rezayi, M. (2013). Potentiometric urea biosensor based on an immobilised fullerene-urease bio-conjugate. *Sensors*, 13(12), 16851-16866.

Safarifard, V., & Morsali, A. (2012). Sonochemical syntheses of a nano-sized copper (II) supramolecule as a precursor for the synthesis of copper (II) oxide nanoparticles. *Ultrasonics Sonochemistry*, 19(4), 823-829.

Semenov, K. N., Charykov, N. A., Postnov, V. N., Sharoyko, V. V., Vorotyntsev, I. V., Galagudza, M. M., & Murin, I. V. (2016). Fullerenols: Physicochemical properties and applications. *Progress in Solid State Chemistry*, 44(2), 59-74.

Sheng, Q., Liu, R., & Zheng, J. (2013). Fullerene–nitrogen doped carbon nanotubes for the direct electrochemistry of hemoglobin and its application in biosensing. *Bioelectrochemistry*, 94, 39-46.

Shinde, S. B., Fernandes, C. B., & Patravale, V. B. (2012). Recent trends in in-vitro nanodiagnostics for detection of pathogens. *Journal of Controlled Release*, 159(2), 164-180.

Shiraishi, H., Itoh, T., Hayashi, H., Takagi, K., Sakane, M., Mori, T. & Wang, J. (2007). Electrochemical detection of E. coli 16S rDNA sequence using air-plasma-activated fullerene-impregnated screen printed electrodes. *Bioelectrochemistry*, 70(2), 481–487.

Slavic, M., Djordjevic, A., Radojicic, R., Milovanovic, S., Orescanin-Dusic, Z., Rakocevic, Z., Spasic, M.B., & Blagojevic, D. (2013). Fulleranol C₆₀(OH)₂₄ nanoparticles decrease relaxing effects of dimethyl sulfoxide on rat uterus spontaneous contraction. *Journal of Nanoparticle Research*, 15(5), 1650.

Sotiropoulou, S., Gavalas, V., Vamvakaki, V., & Chaniotakis, N. A. (2002). Novel carbon materials in biosensor systems. *Biosensors and Bioelectronics*, 18(2–3), 211–215.

Szymańska, I., Radecka, H., Radecki, J., & Kikut-Ligaj, D. (2001). Fullerene modified supported lipid membrane as sensitive element of sensor for odorants. *Biosensors and Bioelectronics*, 16(9–12), 911–915.

Suslick, K. S., & Price, G. J. (1999). Applications of ultrasound to materials chemistry. *Annual Review of Materials Science*, 29(1), 295-326.

Tan, W. T., Bond, A. M., Ngooi, S. W., Lim, E. B., & Goh, J. K. (2003). Electrochemical oxidation of l-cysteine mediated by a fullerene-C60-modified carbon electrode, *Analytica Chimica Acta*, 491(2), 181–191.

Taleyarkhan, R. P., West, C. D., Cho, J. S., Lahey, R. T., Nigmatulin, R. I., & Block, R. C. (2002). Evidence for nuclear emissions during acoustic cavitation. *Science*, 295(5561), 1868-1873.

Taillon, G., Pougoum, F., Lavigne, S., Ton-That, L., Schulz, R., Bousser, E., Savoie, S., Martinu, L., & Klemberg-Sapieha, J. E. (2016). Cavitation erosion mechanisms in stainless steels and in composite metal–ceramic HVOF coatings. *Wear*, 364, 201-210.

Tien, H. T., Wang, L. G., Wang, X., & Ottova, A. L. (1997). Electronic processes in supported bilayer lipid membranes (s-BLMs) containing a geodesic form of carbon (fullerene C60). *Bioelectrochemistry and Bioenergetics*, 42(2), 161–167.

Wang, N., Zhu, L., Wang, D., Wang, M., Lin, Z., & Tang, H. (2010). Sono-assisted preparation of highly-efficient peroxidase-like Fe₃O₄ magnetic nanoparticles for catalytic removal of organic pollutants with H₂O₂. *Ultrasonics Sonochemistry*, 17(3), 526-533.

Wei, L. F., & Shih, J. S. (2001). Fullerene-cryptand coated piezoelectric crystal urea sensor based on urease. *Analytica Chimica Acta*, 437(1), 77–85.

Xu, K., Huang, J., Ye, Z., Ying, Y., & Li, Y. (2009). Recent development of nanomaterials used in DNA biosensors. *Sensors*, 9(7), 5534–5557.

Xu, H., Zeiger, B. W., & Suslick, K. S. (2013). Sonochemical synthesis of nanomaterials. *Chemical Society Reviews*, 42(7), 2555-2567.

Zhang, H., Fan, L., & Yang, S. (2006). Significantly accelerated direct electron-transfer kinetics of hemoglobin in a C₆₀-MWCNT nanocomposite film. *Chemistry - A European Journal*, 12(27), 7161–7166.

Zhang, S., Wright, G., & Yang, Y. (2000). Materials and techniques for electrochemical biosensor design and construction. *Biosensors and Bioelectronics*, 15(5–6), 273–282.

Zhao, Q., Duan, R., Yuan, J., Quan, Y., Yang, H., & Xi, M. (2014). A reusable localized surface plasmon resonance biosensor for quantitative detection of serum squamous cell carcinoma antigen in cervical cancer patients based on silver nanoparticles array. *International Journal of Nanomedicine*, 9, 1097.

Zhilei, W., Zaijun, L., Xiulan, S., Yinjun, F., & Junkang, L. (2010). Synergistic contributions of fullerene, ferrocene, chitosan and ionic liquid towards improved performance for a glucose sensor. *Biosensors and Bioelectronics*, 25(6), 1434-1438.

Zhilei, W., Xiulan, S., Zaijun, L., Yinjun, F., Guoxiao, R., Yaru, H., & Junkang, L. (2011). Highly sensitive deoxynivalenol immunosensor based on a glassy carbon electrode modified with a fullerene/ferrocene/ionic liquid composite. *Microchimica Acta*, 172(3-4), 365-371.

Zhuo, J., Wang, T., Zhang, G., Liu, L., Gan, L., & Li, M. (2013). Salts of C₆₀ (OH)₈ electrodeposited onto a glassy carbon electrode: surprising catalytic performance in the hydrogen evolution reaction. *Angewandte Chemie International Edition*, 52(41), 10867-10870.

Zhou, M., Guo, J., Guo, L., & Bai, J. (2008). Electrochemical sensing platform based on the highly ordered mesoporous carbon-fullerene system. *Analytical Chemistry*, 80(12), 4642–4650.

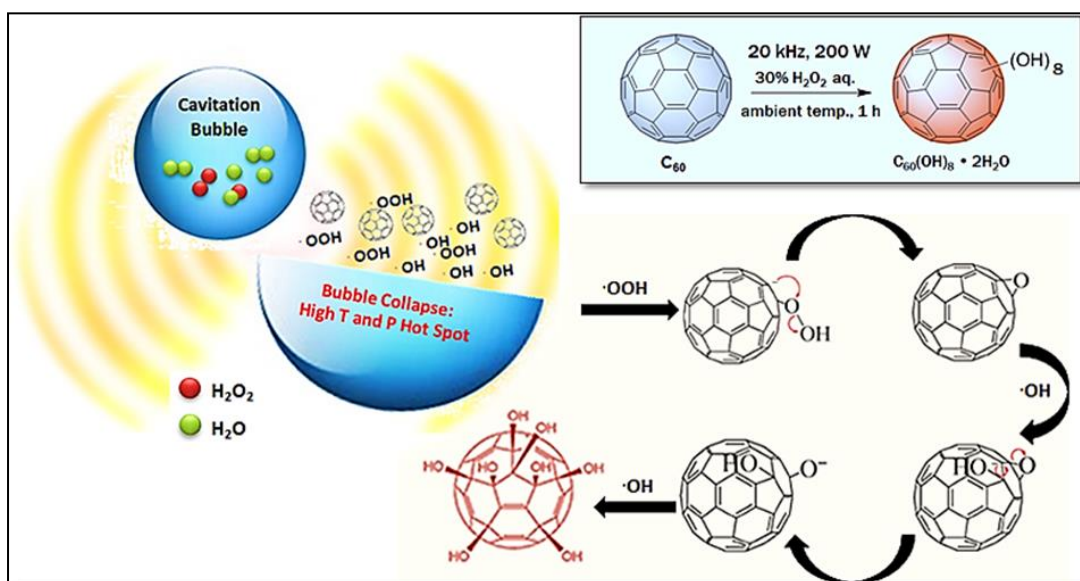
Zhou, S. M., Zhu, G. Y., Wang, Y. Q., Lou, S. Y., & Hao, Y. M. (2011). Sonochemical preparation of massive CrO₂ nanowires. *Chemical Engineering Journal*, 174(1), 432-435.

Zhu, N., Chang, Z., He, P., & Fang, Y. (2005). Electrochemical DNA biosensors based on platinum nanoparticles combined carbon nanotubes. *Analytica Chimica Acta*, 545(1), 21–26.

Chapter 3

Hydration or Hydroxylation: direct synthesis of fulleranol from pristine fullerene [C₆₀] via acoustic cavitation in presence of hydrogen peroxide

Graphical Abstract



Abstract

A greener and cleaner approach providing less energy requirement and avoiding the use of any toxic or corrosive reagents/solvents for the synthesis of potential fullerene moieties $[C_{60}(OH)_n \cdot mH_2O]$ has been proposed in this investigation, where pristine fullerene (C_{60}) in dil. H_2O_2 (30%) associated aqueous media was ultrasonicated (20 kHz, 200 W) at 30% amplitude for 1 h. Attachment of hydroxy groups ($-OH$) was investigated by Fourier transform infrared spectroscopy (FTIR) and the quantification of $-OH$ groups attached to C_{60} cage was conducted by elemental analysis. The number of secondary bound water molecules (mH_2O) with each fullerene molecule $[C_{60}(OH)_n]$ was measured by thermogravimetric analysis (TGA) and the estimated average structure of the fullerene was calculated to be $C_{60}(OH)_8 \cdot 2H_2O$. The synthesized fullerene was moderately soluble in water and dimethyl sulfoxide (DMSO). The size of the synthesized $C_{60}(OH)_8 \cdot 2H_2O$ particles determined by both atomic force microscopy (AFM) and dynamic light scattering (DLS) analysis was found to be in the range of 135-155 nm. The proposed ultrasound-assisted acoustic cavitation technique encompasses a one-step facile reaction strategy, requires less time for the reaction, and reduces the number of solvents required for the separation and purification of $C_{60}(H_2O)_8 \cdot 2H_2O$ which could be scalable for the commercial synthesis of fullerene moieties in future.

3.1 Introduction

Discovery of fullerene (C_{60}) by Sir Harold Kroto and his group in 1985 (Smalley, 1997; Kroto *et al.*, 1985) pioneered a new chapter of ‘fullerene chemistry’ in the domain of carbon allotropes and gradually this new area of chemistry provided versatile fullerene (C_{60}) derivatives (Bosi *et al.*, 2003) having potential features that could be exploited in numerous technological applications. Fullerene C_{60} , specifically known as Buckminster fullerene, is a carbon allotrope and has been incessantly reported as a potential carbon nanomaterial useful for various biological and metallurgical applications (Tagmatarchis and Shinohara, 2001; Da Ros and Prato, 1999; Prato, 1997). But owing to its insolubility in most of the organic and inorganic solvents (Martin, 2006; Hirsch, 1993), it becomes difficult to employ for many prospective studies. This ‘tough to dissolve’ feature could be overcome by introducing various hydrophilic functional groups on C_{60} cage (Semenov *et al.*, 2011; Partha and Conyers, 2009; Periya *et al.*, 2004; Richardson *et al.*, 2000; Wang *et al.*, 1999; Lamparth and Hirsch, 1994). Fullerenol; also known as fullerol, polyhydroxylated fullerene, hydroxylated fullerene, is one of the most commonly pronounced water-soluble fullerene derivatives (Đorđević and Bogdanović, 2008) that has been derived by hydroxylation of C_{60} molecule in various ways (both solvent-associated and solvent-free methods) over past years. Ever since the first preparation of fullerenol, it has been a great challenge to increase the attachment of more number of hydroxy groups ($-OH$) onto C_{60} cage as well as to make the synthesis simpler and faster than before. The attachment of the largest number of $-OH$ groups [$C_{60}(OH)_{44} \cdot 8H_2O$] has been reported by Kokubo *et al.* (2011). Zhang *et al.* (2003) reported on synthesizing $C_{60}(OH)_{27.2}$ by mechanochemical means where potassium hydroxide was used as a hydroxylation reagent with C_{60} and mixed vigorously in a ball mill. Wang *et al.* (2005) reported another solvent-free reaction path to obtain $C_{60}(OH)_{16}$ using dil. H_2O_2 (30%) and sodium hydroxide mixture. Use of alkali was very common in almost all the previously reported successful methods for the preparation of fullerenol along with other chemicals, e.g., sulfuric acid (H_2SO_4), nitric acid (HNO_3), various solvents e.g., toluene (C_7H_8), benzene (C_6H_6), tetrahydrofuran (THF) and phase transfer catalysts (PTC) e.g., tetrabutylammonium hydroxide (TBAH) (Chiang *et al.*, 1996; Chiang *et al.*, 1994; Li *et al.*, 1993). Methods proposed by Zhang *et al.* (2004), Alves *et al.* (2006), Kokubo *et al.* (2008), Lu *et al.* (2010), Zhang *et al.* (2010), Wang

et al. (2010), to prepare fullerenols with different number of –OH groups were also associated with the use of H₂O₂, NaOH and in some cases PTC as well. However, previous methods were proved to be successful for producing a moderate to highly soluble fullereneol, but those methods had the difficulties in removing the impurities obtained from NaOH, PTC which contaminated the synthesized fullereneol (Wang *et al.*, 2010; Matsubayashi *et al.*, 2009). In some cases, the higher solubility of fullereneol was due to the presence of Na⁺ impurity introduced during the synthesis (Alves *et al.*, 2006).

Also, the reaction time was much longer with these methods (from several hours to days) to generate and then to incorporate –OH groups onto C₆₀ cage. On this context, developing a simpler and faster approach of synthesizing fullereneol tailored by using a minimum number of reagents and customized with easy purification and separation steps, is being an urge in ‘fullerene chemistry’. In this investigation, a facile method has been demonstrated to overcome the above-mentioned barriers to a greater extent by direct ultrasonication of C₆₀ in presence of dil. H₂O₂ (30%).

Several studies (Hu *et al.*, 2008; Fang *et al.*, 1996; Makino *et al.*, 1983) evidence that ultrasonication in H₂O₂ associated aqueous medium results in the formation of hydroxyl radicals (·OH) which generate hydrated C₆₀ as C₆₀@{H₂O}_n (Labille, *et al.*, 2009; Rivelino *et al.*, 2006; Ko *et al.*, 2004). Alternatively, it will be advantageous if this formation of ·OH radicals can be tuned to form potential fullereneol moieties as well rather than just leaving it as hydrated C₆₀. Based on this, in this study, the ultrasound induced acoustic cavitation strategy has been explored, whereby with optimal ultrasonic variables (30% amplitude and 1 h sonication at pulse mode) the pristine C₆₀ was functionalized with –OH groups in aqueous medium in the presence of dil. H₂O₂ (30%). Following the synthesis, quantitative analysis was conducted with the functionalized C₆₀ to determine the average structure of fullereneol that could be potentially derived by this ultrasound-assisted acoustic cavitation technique.

It is worth to mention here that synthesizing fullereneol using H₂O₂ as a hydroxylation reagent has been practiced before but in association with other solvents and/or reagents and PTC as well (Kokubo *et al.*, 2008; Wang *et al.*, 2005). Looking at this, the proposed method herewith is a simpler technique which avoids the usage of multiple reagents/solvents as well as PTC and thus it is an approach to produce fullereneol more

easily and efficiently in comparison to the reported ones so far. Fig. 3.1 represents the chronological development on the methods proposed for the synthesis of fulleranol over years and the salient features of the technique proposed in this study in comparison. Only dil. H₂O₂ (30%) has been used as a hydroxylation reagent and no other supporting reagents and/or solvents or PTC were used for synthesis. Besides, reaction time was reduced to 1 h and unreacted C₆₀ was only present as an impurity and the separation of which was easy after the reaction.

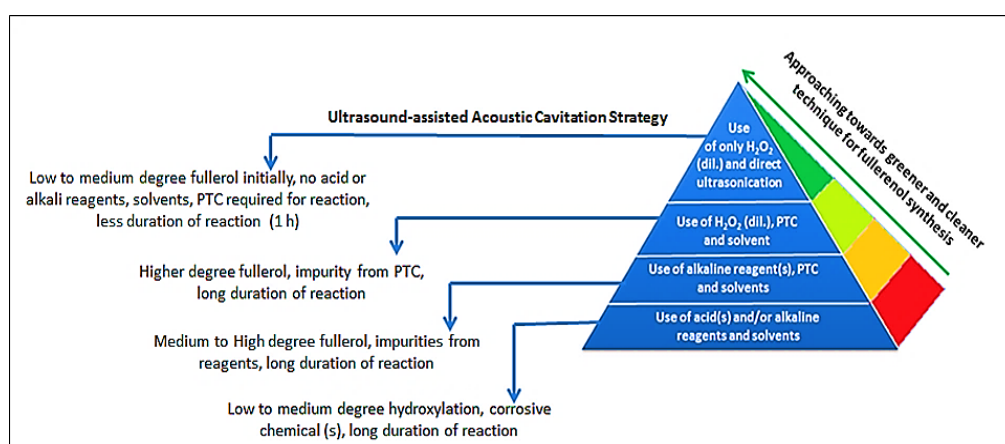


Figure 3.1 Greener and cleaner ultrasonic cavitation strategy to synthesize fulleranol in a facile and faster way as compared to other conventional method

In the present method, direct ultrasonication induces cavitation bubbles in the liquid H₂O₂ and C₆₀ containing aqueous media. Continuous formation and then their collapse generates high energy transient ‘hot spots’ inside the liquid medium which dissociates water molecules into hydrogen and hydroxyl radicals. These hydroxyl radicals in turn combine and form H₂O₂. Further disassociation of H₂O₂ due to the effect of acoustic cavitation generates –OOH anion and/or ·OH radicals which exohedrally get attached to C₆₀ cage by either nucleophilic attack or successive radical addition, respectively (Wang *et al.*, 2015; Zhu *et al.*, 2013; Chang *et al.*, 2012; Goswami *et al.*, 2003; Ko and Baek, 2002). Fig. 3.2 represents the experimental conditions followed in the synthesis of fulleranol in this study.

The attachment of –OH groups onto C₆₀ cage was identified by Fourier transform infrared spectroscopy (FTIR) and the number of –OH groups and bound water molecules were determined by elemental analysis and thermogravimetric analysis

(TGA). The common formula of fulleranol is $C_{60}(OH)_n$, where n is the number of $-OH$ groups attached to each C_{60} cage and the number could vary from 2 to 44 (Kokubo *et al.*, 2011; Meier and Kiegiel, 2001; Kokubo *et al.*, 2008).

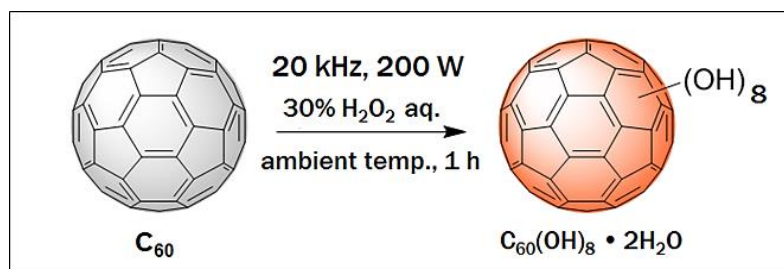


Figure 3.2 Synthesis of water soluble fulleranol via acoustic cavitation induced by ultrasound at ambient temperature and within 1 h reaction time in the presence of dil. H_2O_2 (30%).

However, the presence of $-OH$ groups on C_{60} cage also binds some water molecules, and the number of bound water molecules increases with an increase in the number of $-OH$ groups attached to each C_{60} moiety. Therefore, the most accurate formula of fulleranol molecule that could be obtained practically is $C_{60}(OH)_n \cdot mH_2O$ (Wang *et al.*, 2015; Kokubo *et al.*, 2008) where m is the number of secondary bound water molecules associated with each fulleranol moiety. Elemental analysis along with TGA clearly support that the average structure of synthesized fulleranol obtained by the present ultrasound-assisted technique is $C_{60}(OH)_8 \cdot 2H_2O$.

3.2 Experimental

3.2.1 Materials & equipments for the synthesis

Pristine C_{60} (98%) was purchased from Sigma Aldrich (USA) and used as a starting material to synthesize fulleranol. Hydrogen peroxide (H_2O_2) aqueous solution (30% reagent grade) from R&M chemicals (UK) was used as a hydroxylation reagent. Type II pure water (TOC <50 ppb) was obtained from a Milli-Q system (Merck Millipore Integral 5, France). Bandelin Sonoplus (UW 3200, 20 kHz, 200 W, Germany) with titanium horn sonotrode (MS 73) was employed to introduce ultrasound. Graduated

centrifuge tube (50 mL, angle 60° conical bottom) was used as reactor or treatment vessel. A refrigerated circulator water bath (Julabo F34-ED, Germany) was used to maintain the reaction temperature which was close to ambient temperature during ultrasonication. Toluene (AR grade) was obtained from R&M Chemicals (Malaysia) for the separation and purification of unreacted C₆₀ from C₆₀(OH)₈·2H₂O. Dimethyl sulfoxide (DMSO) was obtained from Wako Pure Chemical Industries, Ltd (Japan) to check the solubility of synthesized fulleranol. After separation and purification, C₆₀(OH)₈·2H₂O dispersion was dried in a freeze dryer (Christ Alpha 1-2 LDplus, Germany).

3.2.2 Methods of characterization

The formation and attachment of –OH groups onto C₆₀ cage was identified by FTIR (JASCO FT/IR-4100). Quantification of the attached –OH groups was attained by elemental analysis using Yanaco, CHN corder MT-6. TGA was performed in Mettler Toledo (TGA/DSC 1/LF/1100, Switzerland) to measure the amount of secondary bound water molecules with C₆₀(OH)₈. Particle size of C₆₀(OH)₈·2H₂O in solution was measured by Photal, FPAR-1000HR. The thickness of C₆₀(OH)₈·2H₂O particles was examined by 5500 Agilent Technologies Atomic force microscopy (AFM) System (USA) using an ultra-sharp tip (non-contact high resonance frequency, nanosensor probe). Morphological study was carried out using Quanta 400 (USA) field emission scanning electron microscopy (FE-SEM).

3.3 Methodology

3.3.1 Synthesis of C₆₀(OH)_n· mH₂O

Pure C₆₀ (200 mg) was added into 30% H₂O₂ (20 mL) and subjected to ultrasonication (30% amplitude, 200 W, pulse mode) for 1 h at ambient temperature. As discussed in the subsection 2.3.1 of chapter 2 in this thesis that higher frequency and amplitude not necessarily result in the formation of effective cavitation bubbles rather it may increase the cavitation threshold, thus more higher amplitude (i.e. intensity) would be required at a higher frequency to obtain a similar sonochemical effect compared to a lower

frequency ultrasonication. This is a reason that most of the sonochemical synthesis as well as sonochemical applications are designed within a frequency range of 20-50 kHz (Capote, F. P and de Castro, 2007). Hence, in this study a frequency of 20 kHz at 200 W with an amplitude of 30% was found to be the best selection for the synthesis of fulleranol via acoustic cavitation. At the selected frequency and amplitude, the sonochemical effect on C_{60} in 30% H_2O_2 was observed within 30 min of ultrasound irradiation where the heterogeneous mixture of C_{60} in H_2O_2 became dispersed, however to completely disperse all the C_{60} the irradiation was continued for another 30 min. Initially C_{60} in aqueous H_2O_2 was immiscible and was a colorless heterogeneous mixture which turned into light brown after 30 min of ultrasonication. Following this, in the next 30 min of ultrasonication it turned into a complete dark brown dispersion (Fig. 3.3a). Thus, 1 h sonication finally resulted in a completely dark brown dispersion of C_{60} in H_2O_2 .

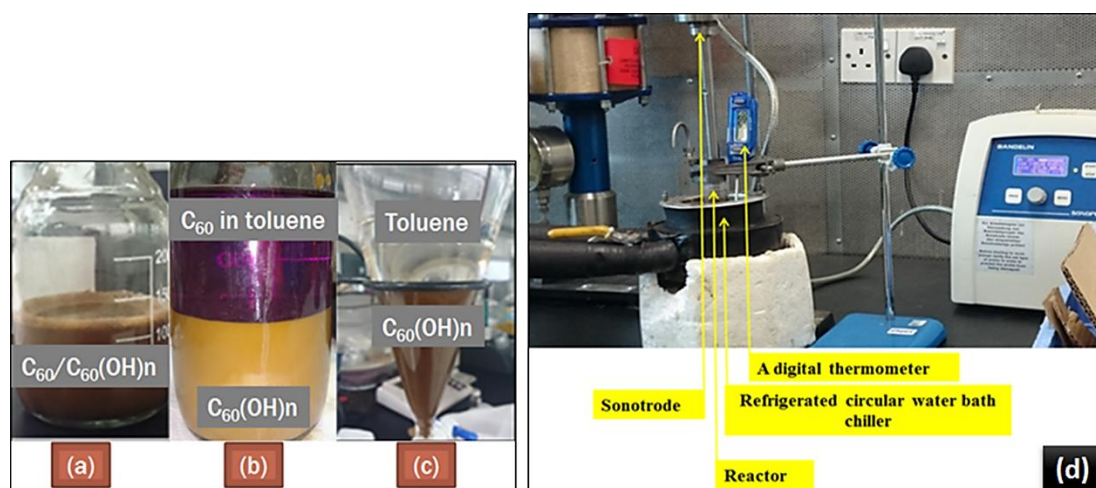


Figure 3.3 (a) Dark brown dispersion immediately after ultrasonication, (b) Separation of unreacted C_{60} from $C_{60}(OH)_n$ in H_2O_2 using toluene and (c) Clear top layer of toluene after 10 times of repeated washing. Here, $n = 8$ and $m = 2$ which were finally determined by elemental analysis and TGA (d) Experimental set-up for the synthesis of $C_{60}(OH)_n$ in H_2O_2

To avoid a rapid increase in the temperature owing to ultrasound dissipation through the liquid media, the reactor was fitted with a refrigerated circulator water bath which maintained the temperature inside the reactor near to ambient temperature (Fig. 3.3d).

3.3.2 Separation and purification of $C_{60}(OH)_n \cdot mH_2O$

Since pure C_{60} was used as the starting material to synthesize fullereneol and no other reagents were used except 30% H_2O_2 for hydroxylation, thus after the reaction it was easier to separate the impurity i.e. unreacted C_{60} than the reported methods. After washing the dark brown dispersion with an equal volume of toluene for 10 times, unreacted C_{60} was separated from $C_{60}(OH)_n \cdot mH_2O$. After adding toluene in the dispersion, two separated layers were formed immediately; the bottom layer was dark brown and the upper one was initially dark purple due to the dissolution of unreacted C_{60} particles into toluene layer (pristine C_{60} is soluble in toluene and gives purple color solution) (Fig. 3.3b). Washing with toluene was repeated until the dark purple top layer turned into colorless toluene indicating the complete removal of unreacted C_{60} from the brown layer (Fig. 3.3c). The dark brown dispersion containing $C_{60}(OH)_n \cdot mH_2O$ was then separated from toluene layer and dried in a freeze dryer for 30 h ($-40\text{ }^\circ\text{C}$, 0.12 mbar). To avoid any potential damage to the physicochemical properties of the synthesized fullereneol, the purified fullereneol was dried by the method of freeze drying where a complete removal of water could be achieved without subjecting to any heating. Thus, any potential physicochemical damage that could be caused by the prolonged heat-associated drying was also avoided. Moreover, in terms of the duration of drying, method of freeze drying required lesser time (30 h) compared to vacuum drying (3 days) for the synthesized fullereneol.

3.4 Results and Discussion

3.4.1 Identification of $-OH$ groups

For identifying the functional group(s), dried $C_{60}(OH)_n \cdot mH_2O$ was analyzed by FTIR (Fig. 3.4a). A clear broad peak at 3395 cm^{-1} within a range of $3600\text{--}3100\text{ cm}^{-1}$ indicates the characteristic O–H stretching which does not appear in the IR spectrum of pristine C_{60} (Fig. 3.4b) but has been reported to be present also in the IR spectra of pristine $C_{60}(OH)_{12}$ (Fig. 3.4c) (Kokubo *et al.*, 2008), which initially confirms the attachment of $-OH$ groups onto C_{60} cage after functionalization.

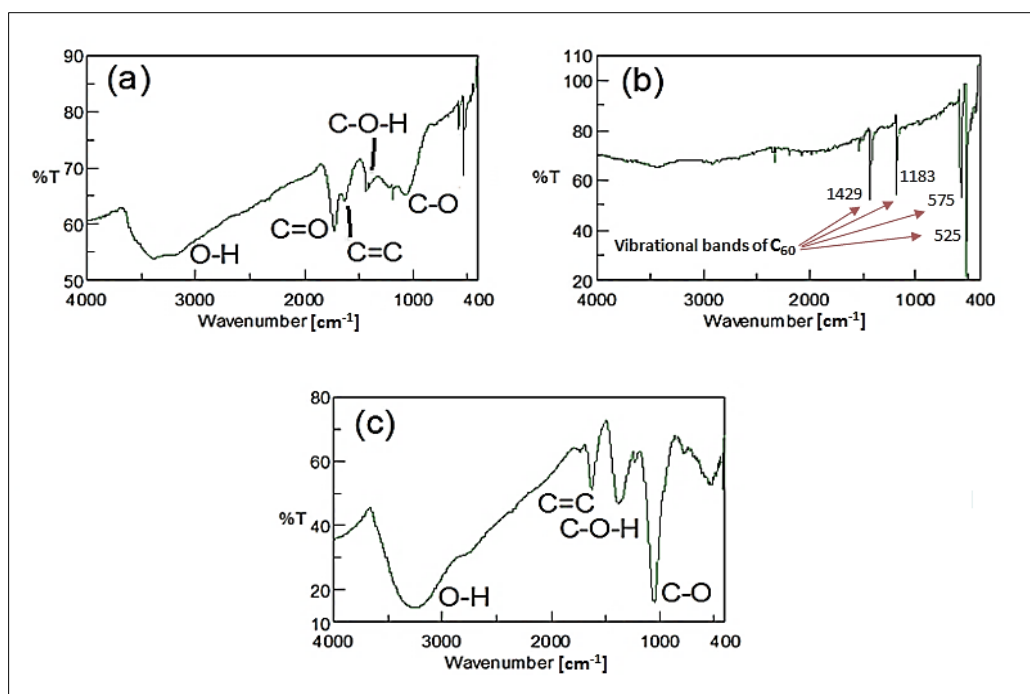


Figure 3.4 FTIR spectra of (a) $C_{60}(OH)_n \cdot mH_2O$, (b) pristine C_{60} and (c) pristine $C_{60}(OH)_{12}$.

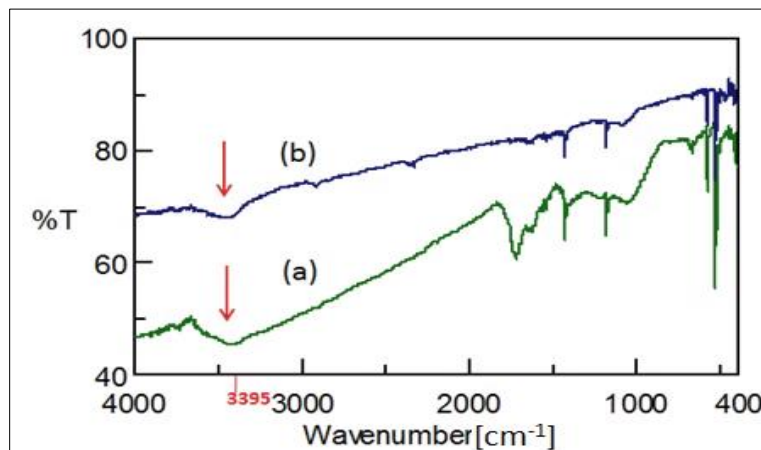


Figure 3.5 IR spectra of $C_{60}(OH)_n \cdot mH_2O$ obtained via ultrasonication (a) in presence of dil. H_2O_2 (30%), (b) in Type II pure H_2O without any H_2O_2 .

This peak was not intense when C_{60} was ultrasonicated in Type II pure water (H_2O) under the same experimental conditions but in the absence of any H_2O_2 (Fig. 3.5b), indicating that usage of H_2O_2 in aqueous media will be a more efficient approach to introduce $-OH$ groups onto C_{60} cage rather than only using H_2O for the synthesis of fulleranol in this ultrasound-assisted technique.

Peaks at 1625, 1427 and 1057 cm^{-1} (Figs. 3.4a and 3.5a) could possibly be attributed to the bond stretching of C=C, C–O–H and C–O respectively (Indeglia *et al.*, 2014; Husebo *et al.*, 2004). Indeglia *et al.* (2014) emphasized that the presence of C–O bond stretching is inevitable in all the fullereneols which perhaps indicates the formation of hemiketal groups prior to the hydroxylation onto C_{60} cage. While sonication only with water, these significant peaks which display the characteristic bond stretching of fullereneol were absent in the IR spectra (Fig. 3.5b) which again supports that to synthesize fullereneol moieties by this ultrasound strategy the presence of H_2O_2 plays an important role in intensifying the hydroxylation. Additional peaks at 575 and 525 cm^{-1} found out in the finger print region ($<1000 \text{ cm}^{-1}$) in the IR spectra of $\text{C}_{60}(\text{OH})_n \cdot m\text{H}_2\text{O}$ (Fig. 3.4a and Fig. 3.5a) are the characteristic peaks of pure C_{60} , where pure C_{60} shows four non-degenerate mode of vibrations in the IR spectra (Menéndez and Page, 2000) at 525 cm^{-1} , 575 cm^{-1} , 1183 cm^{-1} and 1429 cm^{-1} (Figure 3.4b). Therefore, peaks observed at 525 and 575 in the fingerprint region of the IR spectra of $\text{C}_{60}(\text{OH})_n \cdot m\text{H}_2\text{O}$ are not attributed to any potential functional group(s) except that there could have been a trace amount of unreacted C_{60} remains with $\text{C}_{60}(\text{OH})_n \cdot m\text{H}_2\text{O}$ during the separation and purification which is possibly responsible for these peaks in the IR spectra of $\text{C}_{60}(\text{OH})_n \cdot m\text{H}_2\text{O}$. We cannot rule out this possibility especially when we scale-up this method for the mass production of $\text{C}_{60}(\text{OH})_n \cdot m\text{H}_2\text{O}$.

3.4.2 Estimation of the number of –OH groups and the structure of fullereneol

IR spectra alone are not enough to determine and confirm the –OH groups, their numbers and the structure of fullereneol. Therefore, elemental analysis (CHN method), which is recommended as an efficient method to derive the molecular formula of an unknown hydrocarbon (Fadeeva *et al.*, 2008; Thompson *et al.*, 2008; Etherington *et al.*, 2001; Gnaiger *et al.*, 1984) was conducted to determine the composition and an average structure of $\text{C}_{60}(\text{OH})_n \cdot m\text{H}_2\text{O}$. Number of bound water molecules (m) with $\text{C}_{60}(\text{OH})_n$ structure was calculated by TGA. After the ultrasound-assisted functionalization of pure C_{60} , the average composition of C and O (C: 82.6 wt%, O: 17.2 wt%) in $\text{C}_{60}(\text{OH})_n$ was first obtained from SEM-EDS analysis. In pure C_{60} no trace of oxygen (C: 100%) was detected before the reaction which forecasts the formation and presence of some oxygen containing functional group(s) in the functionalized C_{60} . However, EDS cannot

analyze the presence and composition of hydrogen present in a sample. The composition and structure of $C_{60}(OH)_n$ was finally deduced from elemental analysis (Table 3.1).

In the elemental analysis of fullerenols if the product is pure single isomer and can be purified totally, the difference should be within 0.4%, but generally the product fullereneol is a mixture of many isomers and it is far difficult to separate the isomers from each other. Therefore, from our many synthetic experiences even the reaction condition is completely the same as much as we can, the difference in elemental analysis is somewhat large even the chemical and physical properties of the fullereneol are essentially the same. Due to this, the average molecular formula of fullereneol is always estimated within 1% error of elemental analysis [Tables 3.1 and 3.2].

Table 3.1 Empirical formula of $C_{60}(OH)_n$ synthesized in the presence of dil. H_2O_2 (30%)

	%C	%H	H_2O (wt. %)*
Experimentally obtained	80.52	0.96	5.58
Estimated average structure [based on the known molecular weight of different fullerenols] calculated for-			
$C_{60}(OH)_2 \cdot 8H_2O$ (MW 898 amu)	80.18	2.02	16.0
$C_{60}(OH)_4 \cdot 6H_2O$ (MW 896 amu)	80.36	1.80	12.1
$C_{60}(OH)_6 \cdot 4H_2O$ (MW 894 amu)	80.54	1.58	8.1
$C_{60}(OH)_8 \cdot 2H_2O$ (MW 892 amu)	80.72	1.35	4.0
$C_{60}(OH)_{10} \cdot 1H_2O$ (MW 908 amu)	79.30	1.33	2.0
$C_{60}(OH)_{10} \cdot 0H_2O$ (MW 890 amu)	80.91	1.13	0

*Measured by TGA, difference between exp. and calc. should be within $\pm 1\%$

From elemental analysis it became evident that the number of $-OH$ groups attached to each C_{60} cage is $n=8$. The composition (C: 80.52%, H: 0.96%) obtained from elemental analysis is similar to the composition that was calculated theoretically for the structure of $C_{60}(OH)_8$ and thus the structure of $C_{60}(OH)_n$ synthesized by the present ultrasound

strategy has been calculated as $C_{60}(OH)_8$ (Table 3.1). Similarly, elemental analysis was conducted to estimate the number of $-OH$ groups that could possibly be attached while sonicating pristine C_{60} only in type II pure H_2O without adding any H_2O_2 . By this, the number of $-OH$ groups that could be attached to C_{60} cage is only 2 ($n=2$) (Table 3.2), which again supports the role of H_2O_2 in intensifying the hydroxylation.

Table 3.2 Empirical formula of $C_{60}(OH)_n$ synthesized only in the presence of type II pure H_2O

	%C	%H	H_2O (wt. %)*
Experimentally obtained	92.41	0.57	1.4
Estimated average structure [based on the known molecular weight of different fullerenols] calculated for-			
$C_{60}(OH)_2 \cdot 2H_2O$ (MW 790 amu)	91.14	0.76	4.6
$C_{60}(OH)_2 \cdot 1H_2O$ (MW 772 amu)	93.27	0.52	2.3
$C_{60}(OH)_4 \cdot 0H_2O$ (MW 788 amu)	91.37	0.51	0

*Measured by TGA, difference between exp. and calc. should be within $\pm 1\%$

Formation and the attachment of $-OH$ groups were further confirmed by TGA (Fig. 3.6). The weight loss (wt. %) of $C_{60}(OH)_8 \cdot 2H_2O$ was observed from room temperature to $900^\circ C$ at a rate of $10^\circ C/min$ under N_2 flow at $20 mL/min$. An initial weight loss (5.58 wt. %) was observed from room temperature to $100^\circ C$ which indicates the loss of bound water molecules. Since the number of $-OH$ groups attached to C_{60} cage is less than 10, the weight loss (5.58 wt. %) for secondary bound water in $C_{60}(OH)_8$ could be observed from room temperature to $100^\circ C$ (kokubo *et al.*, 2011). From this percentage of weight loss, the number of bound water molecules associated with each $C_{60}(OH)_8$ molecule was calculated to be 2 ($m=2$) which is shown in Table 3.1 as well in estimating the complete structure of the synthesized fulleranol. Since there are only two molecules of bound water associated to each $C_{60}(OH)_8 \cdot 2H_2O$, hence the effect of bound water on FTIR and elemental analysis was negligible.

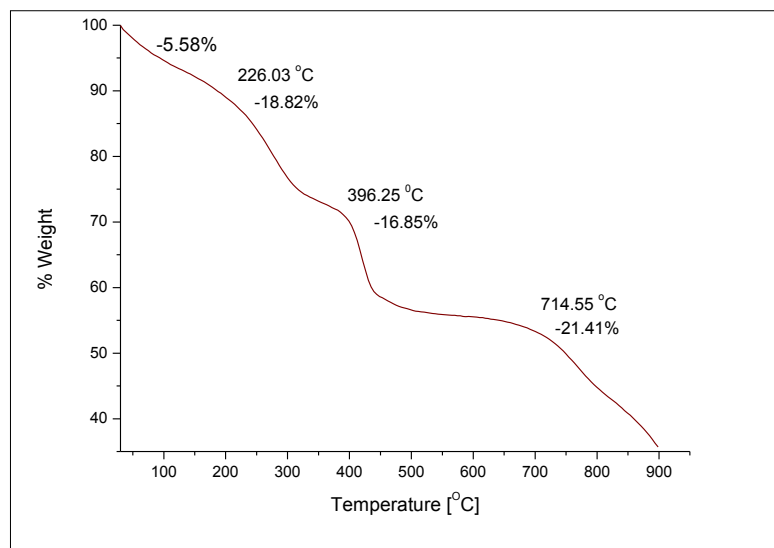


Figure 3.6 TGA chart for measuring the weight loss (wt. %) of $C_{60}(OH)_8 \cdot 2H_2O$

After the decomposition of bound water, the degradation continued to around 226 °C, which could be due to some of the intermediates such as epoxy or hemiketal oxygen and/or carbonyl oxygen generated during ultrasound-assisted reaction (Indeglia, 2014; Husebo *et al.*, 2004; Chiang *et al.*, 1993). These intermediates may be present in $C_{60}(OH)_8 \cdot 2H_2O$ in trace amounts but possibly will not hinder the characteristic physical and chemical properties of $C_{60}(OH)_8 \cdot 2H_2O$. However, a detailed understanding on these intermediates present in fullerene is not yet fully accomplished which encourages further studies. Dehydration of –OH groups (16.85 wt.%) attached to the C_{60} molecular cage mostly occurred in the second step of TGA at around 396 °C, the value of which is very close to the theoretically calculated (15.2%) for the dehydration of 8 –OH groups. Degradation observed at around 714 °C is due to the sublimation of C_{60} molecules. Together, with elemental analysis, TGA result manifests that C_{60} could be successfully functionalized to fullerene by ultrasound-assisted hydroxylation in the presence of aq. H_2O_2 and the average structure of fullerene derived from these studies is $C_{60}(OH)_8 \cdot 2H_2O$.

In applying this ultrasound technique for the production of fullerene, it is also necessary to explore the yield of the prepared $C_{60}(OH)_8 \cdot 2H_2O$. In this work, the yield was verified by repeating the experiments three times. The yield of $C_{60}(OH)_8 \cdot 2H_2O$ was investigated based on both the amount of $C_{60}(OH)_8 \cdot 2H_2O$ obtained after drying and the

amount of unreacted C₆₀ separated after reaction. The yield was found to be varying in between 2.18-4.04%. There is always a possibility of material loss during the process of drying, specially directly from liquid to solid state, which should be considered in any future work when reproducing the proposed method of preparing C₆₀(OH)₈·2H₂O. The yield achieved is not high though on the laboratory scale, even so by optimizing the reaction conditions, selecting different solvents for separation and purification, improving the drying method to avoid any loss of the material the yield of C₆₀(OH)₈·2H₂O could be increased by the proposed ultrasound method.

3.4.3 Particle size measurements

Usually the particles of fullerenols having fewer number of –OH groups have been reported to be aggregative and the particle size may vary in a range of 50–300 nm (Husebo *et al.*, 2004). DLS analysis and AFM scanning were carried out to investigate the size and the morphology of C₆₀(OH)₈·2H₂O particles respectively. For particle size measurements, C₆₀(OH)₈·2H₂O was dissolved in DMSO (0.33 mg/mL). As a polar aprotic solvent DMSO can dissolve both polar and nonpolar compounds. C₆₀(OH)₈·2H₂O in DMSO initially formed a suspension which was then centrifuged (TOMY, LC-200) for 5 min at 7500 rpm to obtain a clear solution of C₆₀(OH)₈·2H₂O in DMSO. Both the suspension and the solution (collected as supernatant after centrifugation) were analyzed for particle size measurements by DLS method.

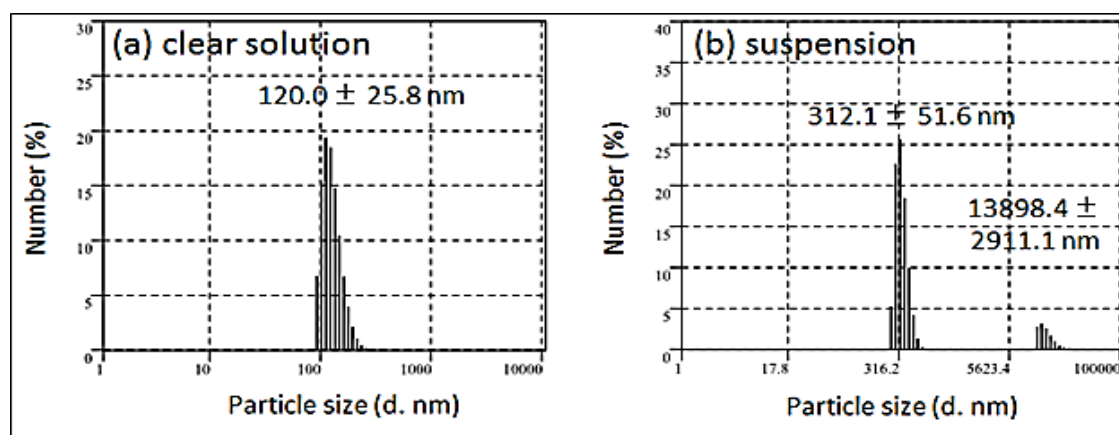


Figure 3.7 Particle size measurements: (a) C₆₀(OH)₈·2H₂O/DMSO solution (collected as supernatant after centrifugation), (b) C₆₀(OH)₈·2H₂O/DMSO suspension (0.33 mg/mL).

The average particle size of $C_{60}(OH)_8 \cdot 2H_2O$ in the suspension was found to be larger (312 nm) (Fig. 3.7b) than in the solution (120 nm) (Fig. 3.7a). Also, larger sized particles of about $13.9 \mu m$ could be seen in the suspension (Fig. 3.7b) which could either be due to the highly aggregative nature of $C_{60}(OH)_8 \cdot 2H_2O$ along with some intermediates possibly present as described in the earlier section of this study or due to the presence of trace amounts of unreacted pristine C_{60} which remains in the sample even after the separation process. Considering these, we infer that $C_{60}(OH)_8 \cdot 2H_2O$ when dispersed in DMSO contains particles of wider range of sizes and thus could be considered as a ‘polydispersed’ suspension, which after centrifugation provides a clear solution of uniform sized particles of $C_{60}(OH)_8 \cdot 2H_2O$ about 120 nm.

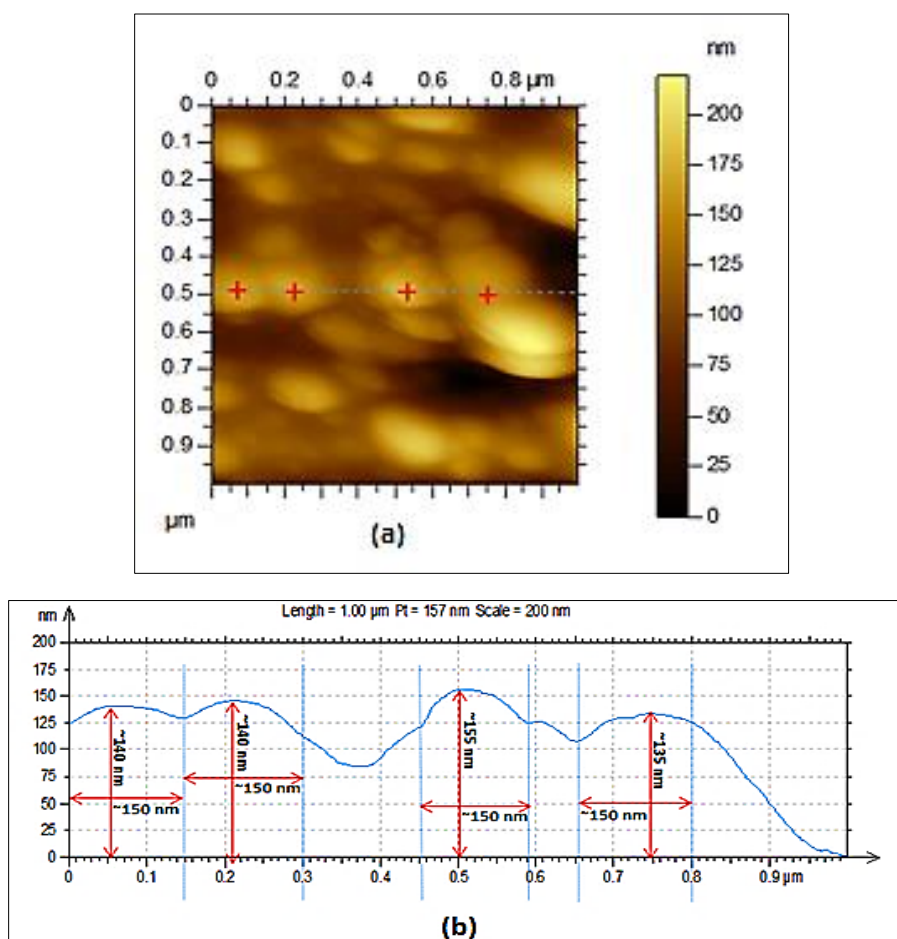


Figure 3.8 (a) AFM image shows the topography of $C_{60}(OH)_8 \cdot 2H_2O$ particles on mica substrate within a scan area of $1 \times 1 \mu m^2$ particles under scanning line are marked with red cross. (b) Topography vs. distance chart for thickness measurement where $C_{60}(OH)_8 \cdot 2H_2O$ particles show a consistent width of around 150 nm and the average height of the particles under scanning line is in between 135 to 155 nm.

The particle size was further verified by topography vs. distance chart (Fig. 3.8b) obtained from AFM analysis of $C_{60}(OH)_8 \cdot 2H_2O$. The cross section of AFM image shows that the width of the particles is around 150 nm and the height of the particles may vary from 135 to 155 nm (Fig. 3.8b). This indicates that the synthesized $C_{60}(OH)_8 \cdot 2H_2O$ particles could be considered spherical in shape having a diameter in a range of 135-155 nm. The average width and height of the particles obtained from AFM analysis are congruent with the particle sizes (120 ± 25.8 nm and 312 ± 51.6 nm) obtained by DLS analysis for the saturated solution of $C_{60}(OH)_8 \cdot 2H_2O$ in DMSO (Fig. 3.7a) and suspension of $C_{60}(OH)_8 \cdot 2H_2O$ in DMSO (Fig. 3.7b) respectively. $C_{60}(OH)_8 \cdot 2H_2O$ is considered as the first member from polyhydroxylated fullerene group which shows solubility in water at lower concentration but at the same time forms aggregates when dispersed in water or DMSO. Therefore, some larger particles in the suspension of $C_{60}(OH)_8 \cdot 2H_2O$ /DMSO could be observed. This aggregation has been observed in both AFM and SEM images. The image (Fig. 3.8a) and height profile (Fig. 3.8b) received from AFM analysis reveal that individual particles of $C_{60}(OH)_8 \cdot 2H_2O$ are actually not finely separated from each other rather they are assembled in the form of nearly spherical shaped aggregates having a range of sizes.

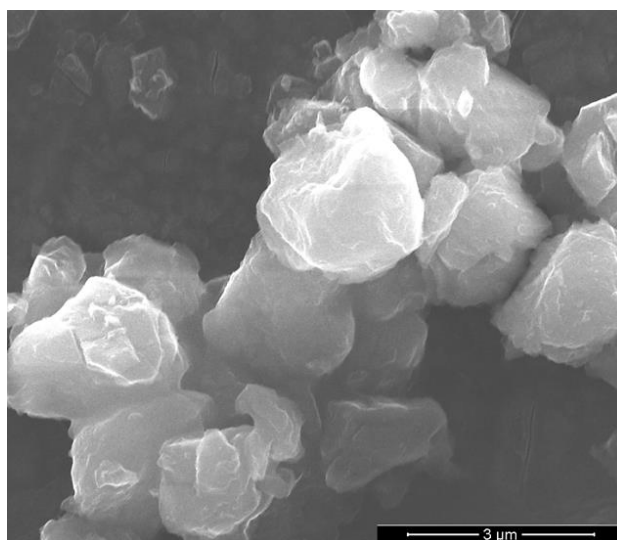


Figure 3.9 SEM image of $C_{60}(OH)_8 \cdot 2H_2O$ (20 kV, magnification of 30000 x)

The SEM image (Fig. 3.9) provides further understanding on the aggregation of synthesized $C_{60}(OH)_8 \cdot 2H_2O$ particles when they are in powder form. In the powder form of $C_{60}(OH)_8 \cdot 2H_2O$, particles are much more aggregative and can even show larger

size than 300 nm, but when they are dispersed in solvent(s) aggregation becomes less effective. This nature of aggregation decreases with an increase in the number of –OH groups attached to each C₆₀ molecule as well (Kokubo *et al.*, 2011). Even though C₆₀(OH)₈·2H₂O exhibits amphiphilic behavior, it is moderately polyhydroxylated; as a result, the interaction potential between the particles becomes more effective than the intermolecular hydrogen bond potential which ultimately causes Brownian aggregation, and could result in a variable size of self-assembled C₆₀(OH)₈·2H₂O particles in the suspension (Liu *et al.*, 2011; Zhang *et al.*, 2010).

3.4.4 Color and solubility

C₆₀(OH)₈·2H₂O obtained after separation, purification and drying was not completely black rather it was nearly brown (Fig. 3.10a). While dispersed in DMSO it gave a dark brown color suspension (Fig. 3.10b). Fullerenol having more than 10 –OH groups is observed to be dark brown in color, and the color gradually shifts from dark brown to yellow with an increase in the number of –OH groups (Fig. 3.10c) as previously reported (Kokubo *et al.*, 2008). Solubility of C₆₀(OH)₈·2H₂O was also examined both in water and in organic solvents i.e. DMSO, toluene and benzene (Table 3.3).

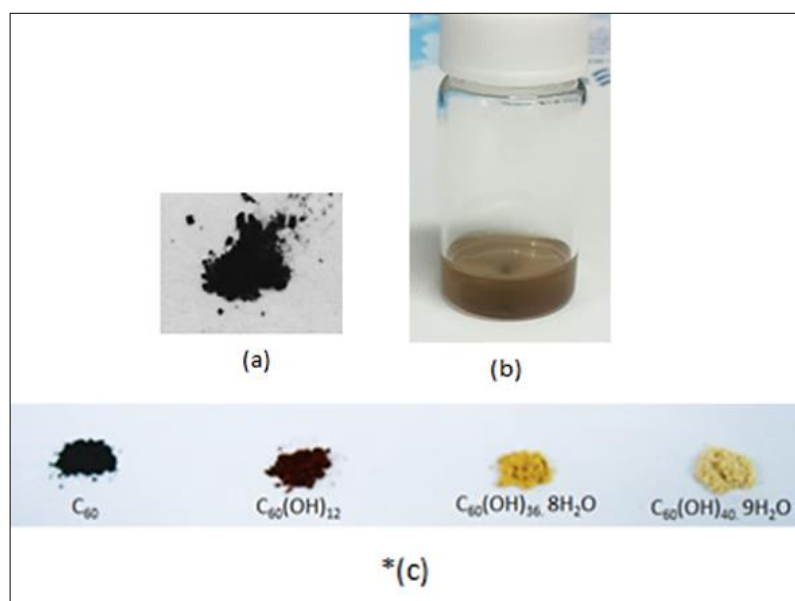


Figure 3.10 (a) C₆₀(OH)₈·2H₂O after drying, (b) C₆₀(OH)₈·2H₂O in DMSO (0.33 mg/mL), *(c) Color of different fullerenols previously reported [*Reprinted from Kokubo *et al.* (2008)]

Table 3.3 Solubility of $C_{60}(OH)_8 \cdot 2H_2O$ in comparison to C_{60} in different solvents

	Water	DMSO	Toluene	Benzene
Fullerene (C_{60})	X	X	O	O
Fullerenol [$C_{60}(OH)_8 \cdot 2H_2O$]	O*	O*	X	X

X = not soluble, O = soluble, *soluble at lower conc. of 0.33 mg/mL

It is noteworthy to mention here that $C_{60}(OH)_8 \cdot 2H_2O$ moderately dissolves in water at lower concentration owing to its amphiphilic nature. It was found to be soluble in DMSO but did not show any solubility in toluene and benzene solvents. On the other hand, pure C_{60} dissolves both in toluene and benzene but does not show any solubility in water and DMSO. The solubility value of $C_{60}(OH)_8 \cdot 2H_2O$ was measured in DMSO where 1 mg of $C_{60}(OH)_8 \cdot 2H_2O$ was dissolved in 1 mL of DMSO by sonication, then after centrifugation the precipitate was removed from the solution carefully by decantation, after drying the separated residue the calculated solubility for $C_{60}(OH)_8 \cdot 2H_2O$ was found to be ~0.33 mg/mL.

3.4.5 Reaction pathways

Acoustic cavitation generated from ultrasonication is being regarded to bring forth the chemical reactions inside a liquid media (Raso *et al.*, 1999). When acoustic cavitation is induced throughout the liquid media (30% H_2O_2 in this case) it produces cavitation bubbles, upon continuous ultrasonication these bubbles form and collapse randomly. These bubbles' collapse produces transient local hot spots with intense local heat and pressure inside the liquid media which assist in high-energy chemical reactions among the molecules either trapped inside the cavitation bubbles or present in the liquid media (Rooze *et al.*, 2013; Suslick and Price, 1999).

In this investigation, due to ultrasound induced acoustic cavitation radicals such as $\cdot\text{OH}$, $\cdot\text{OOH}$ and $\cdot\text{H}$ could originate from H_2O and H_2O_2 molecules (Mason, 2015; Villeneuve *et al.*, 2009; Hu *et al.*, 2008;). Especially the formation of $\cdot\text{OH}$ radicals due to the thermal decomposition of aqueous media has been found to be evident by electron spin resonance (ESR) and spin trapping (Fang *et al.*, 1996; Riesz and Kondo, 1992; Buettner *et al.*, 1987; Christman *et al.*, 1987; Makino *et al.*, 1983) studies. H_2O_2 is thermodynamically unstable and dissociates into H_2O and O_2 under thermal decomposition. During ultrasonic cavitation the molecules of H_2O and H_2O_2 are trapped inside the microbubbles, and when the bubbles collapse with an enormous amount of heat (several thousand degrees Kelvin) and pressure (hundreds of atmosphere) (Kohno *et al.*, 2011; Leonelli *et al.*, 2010), these molecules decompose to $\cdot\text{OH}$ and $\cdot\text{OOH}$ radicals (Gong and Hart, 1998; Mark *et al.*, 1998).

Reaction may progress in two path ways simultaneously (Fig. 3.11); $\cdot\text{OH}$ radicals as reactive oxygen species (ROS) attach onto C_{60} cage and give fulleranol (Path I), and/or $\cdot\text{OH}$ and $\cdot\text{OOH}$ radicals attack the electron deficient C_{60} double bonds in a nucleophilic reaction leading to the formation of fullerene epoxide [C_{60}O_n] as an intermediate in the first stage (Path II) which is similar to the mechanism of Bingel reaction (Chang *et al.*, 2012; Hirsch, 1999). Further, the repeated attack of $\cdot\text{OH}$ (or $\cdot\text{OOH}$) on C_{60}O by $\text{S}_{\text{N}}2$ reaction results in the polyhydroxylated fullerene or fulleranol.

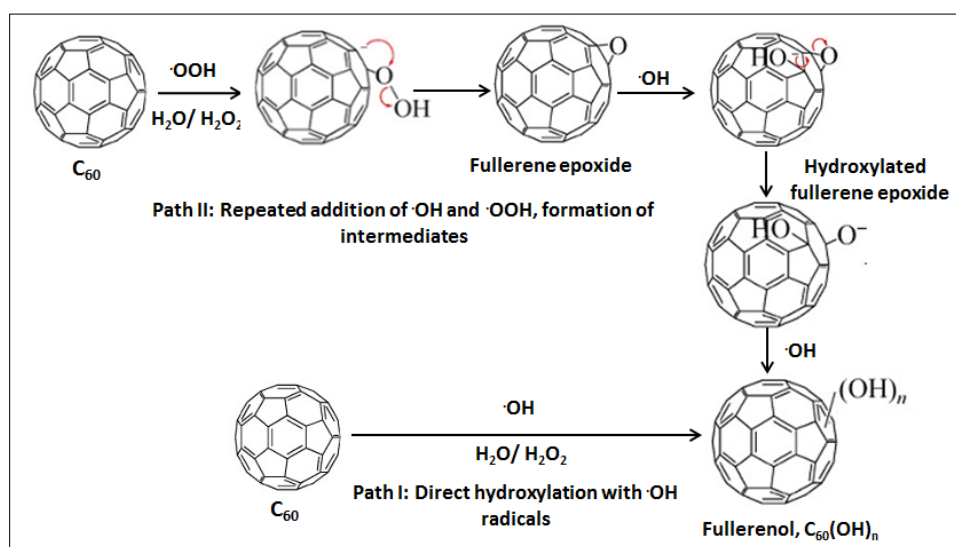


Figure 3.11 Possible reaction paths in ultrasound-assisted synthesis of fulleranol in the presence of dil. H_2O_2 (30%).

Repeated epoxidation may take place which produces other successive epoxide groups e.g., $C_{60}O_2$, $C_{60}O_3$. These could be the possible candidates to generate other intermediates e.g. hydroxylated fullerene epoxide [$C_{60}(OH)_xO_y$] (Kokubo *et al.*, 2011; Goswami *et al.*, 2004) during sonolysis. The subsequent ring opening of $C_{60}(OH)_xO_y$ with $\cdot OH$ can result in the formation of fulleranol as well (Li *et al.*, 1999). The formation of these intermediates during sonolysis of H_2O_2 or H_2O in presence of C_{60} is inevitable, and their presence in the final fulleranol (although in trace amount) cannot be unnoted. However, because of their trace amounts in the fulleranol it is expected not to cause any significant impact.

3.5 Prospects of the Current Finding

To explore the potential applications of fullerenols it is indeed essential to produce high quality fulleranol which means not only 'higher water solubility' but also 'free of any impurity'. Presence of any impurities that generally come from the process of preparation makes it undesirable for any specific biological and metallurgical applications. More importantly the commercial value of fulleranol depends on the presence and percentage of impurities. Moreover, a faster approach is desirable to facilitate the commercial production of fulleranol. The proposed technique for the preparation of hydroxylated C_{60} by ultrasonication in the presence of H_2O_2 is free from using other hydroxylating reagents, i.e. NaOH, H_2SO_4 , and PTC (causes impurities in fulleranol), which is a cleaner approach to produce fulleranol in an easier and a faster way as well. Previously $C_{60}(OH)_{12}$ was used as a starting material to synthesize highly soluble fullerenols [$C_{60}(OH)_{36}$, $C_{60}(OH)_{40}$] by vigorously stirring with dil. H_2O_2 for several days (Kokubo *et al.*, 2008). Similarly, $C_{60}(OH)_8 \cdot 2H_2O$ synthesized by this method could be used as a starting material further to produce fullerenols containing more number of hydroxy groups, e.g. $C_{60}(OH)_{24}$, $C_{60}(OH)_{36}$ and $C_{60}(OH)_{40}$. Moreover, compounds that express specific biochemical functions which are required for diagnostics as well as drug therapy studies can be derivatized from $C_{60}(OH)_8 \cdot 2H_2O$ by conjugating it with other potential functional groups or biomolecules.

Further potential applications for $C_{60}(OH)_8 \cdot 2H_2O$ synthesized by the proposed method of ultrasonication include: as an antioxidant since it offers higher antioxidant activities compared to its neighboring fullerenols having more hydroxy groups, i.e., $C_{60}(OH)_{24}$,

$C_{60}(OH)_{26}$, $C_{60}(OH)_{36}$ (Wang *et al.*, 2015); as an electrochemically active nanomediator since based on the density functional theory (DFT) it has also been found that fullerenols having less hydroxy groups are thermodynamically more stable than those of containing more hydroxy groups due to the symmetric orientation of –OH groups around the C_{60} molecular cage (Li *et al.*, 2013; Zhou *et al.*, 2013); as a light harvesting material in solar cell applications (Singh, 2015); preparation of rich carbon structure of different shapes, sizes and isomeric orientations recently termed as ‘Janus particles’ for various other applications (Liu *et al.*, 2011).

It is anticipated that there must be a substantial difference between the levels of energy generated during continuous ultrasonication and pulse mode ultrasonication which should be taken care of as well in the future investigations. In addition, the duration of ultrasonication may cause a remarkable difference in the structure of fullereneol. Besides the variables of ultrasonication (time, power input), it is equally important to optimize other parameters in future studies, i.e. temperature, size and geometry of treatment vessel, nature and concentration of any dissolved gas, concentration of H_2O_2 , solute to reagents ratio (C_{60} : 30% H_2O_2 , mg/mL) and height of the mixture in the treatment vessel; all of them alone or together can play vital roles in producing fullerenols having different combinations of –OH groups and bound H_2O molecules as well as to increase the yield of $C_{60}(OH)_8 \cdot 2H_2O$ while applying the proposed ultrasound technique for the synthesis.

3.6 Overview of the Current Chapter and Direction to the Next Chapter

Herewith, a more facile and faster approach to prepare fullereneol by ultrasound-assisted hydroxylation of C_{60} only in dil. H_2O_2 (30%) was proposed and the possible structure of fullereneol that could be derived by this technique was quantified. It appears that while doing ultrasonication of pure C_{60} in aqueous medium even only in presence of H_2O_2 it not only leads to the hydration of C_{60} in the reaction medium but also results in the generation of potential fullereneol candidate(s). Upon quantitative analysis which has been identified as $C_{60}(OH)_8 \cdot 2H_2O$. Since no alkali, acids or PTC have been used for the synthesis, the proposed method offers a greener and cleaner approach toward hydroxylation of C_{60} cage. Quantitative studies revealed that this hydroxylation technique assisted by ultrasonication in presence of H_2O_2 can lead to the formation of

fullerenol having an average structure of $C_{60}(OH)_8 \cdot 2H_2O$ and with an average yield of 2 %. $C_{60}(OH)_8 \cdot 2H_2O$ was found to be amphiphilic and thus moderately soluble in water at lower concentration and it could further be exploited as a starting material to prepare highly water soluble fullerenol moieties. Presence of aq. H_2O_2 intensifies the hydroxylation and enhances the number of hydroxy groups ($n=8$) on C_{60} cage in comparison to the hydroxy groups obtained ($n=2$) while applying the same ultrasonication but only in the presence of pure water. This indicates that H_2O_2 plays a vital role in the hydroxylation and could be potential to obtain fullerenol moieties by this method, even the yield could be increased by varying the concentration of H_2O_2 . The proposed technique encompasses a one-step reaction strategy, requires less time for the reaction, offers a greener and cleaner approach providing less energy requirement and avoiding the use of any toxic or corrosive reagents for synthesis, and reduces the number of solvents required for the separation and purification of $C_{60}(OH)_8 \cdot 2H_2O$. Hence this potential approach should further be investigated to scale-up mass production of fullerenol moieties for a wider range of technological applications.

In this thesis, one of the potential applications of the synthesized $C_{60}(OH)_8 \cdot 2H_2O$ in association with folic acid (FA) will be investigated in preparing a folate receptor ($FR\alpha$) biosensor. In doing so, first it is essential to study the electrochemical behavior of FA in a specific solvent suitable for the detection of $FR\alpha$, hence the next chapter will demonstrate a comparative study toward the electrochemical behavior of FA in both aqueous medium and buffer solution, to select the best experimental condition for the detection of $FR\alpha$, while using FA as the ligand/receptor to target $FR\alpha$.

References

- Alves, G. C., Ladeira, L. O., Righi, A., Krambrock, K., Calado, H. D., Gil, R. P. D. F., & Pinheiro, M. V. B. (2006). Synthesis of C₆₀ (OH) 18-20 in aqueous alkaline solution under O₂-atmosphere. *Journal of the Brazilian Chemical Society*, 17(6), 1186-1190.
- Bosi, S., Da Ros, T., Spalluto, G., & Prato, M. (2003). Fullerene derivatives: an attractive tool for biological applications. *European Journal of Medicinal Chemistry*, 38(11), 913-923.
- Buettner, G. R. (1987). Spin trapping: ESR parameters of spin adducts 1474 1528V. *Free Radical Biology and Medicine*, 3(4), 259-303.
- Capote, F. P., & de Castro, M. L. (2007). Analytical applications of ultrasound (Vol. 26). Elsevier.
- Chang, W. W., Li, Z. J., Yang, W. W., & Gao, X. (2012). Reactions of anionic oxygen nucleophiles with C₆₀ revisited. *Organic Letters*, 14(9), 2386-2389.
- Chiang, L. Y., Upasani, R. B., Swirczewski, J. W., & Soled, S. (1993). Evidence of hemiketals incorporated in the structure of fullerols derived from aqueous acid chemistry. *Journal of the American Chemical Society*, 115(13), 5453-5457.
- Chiang, L. Y., Wang, L. Y., Swirczewski, J. W., Soled, S., & Cameron, S. (1994). Efficient synthesis of polyhydroxylated fullerene derivatives via hydrolysis of polycyclosulfated precursors. *The Journal of Organic Chemistry*, 59(14), 3960-3968.
- Chiang, L. Y., Bhonsle, J. B., Wang, L., Shu, S. F., Chang, T. M., & Hwu, J. R. (1996). Efficient one-flask synthesis of water-soluble [60] fullerrenols. *Tetrahedron*, 52(14), 4963-4972.

Christman, C. L., Carmichael, A. J., Mossoba, M. M., & Riesz, P. (1987). Evidence for free radicals produced in aqueous solutions by diagnostic ultrasound. *Ultrasonics*, 25(1), 31-34.

Da Ros, T., & Prato, M. (1999). Medicinal chemistry with fullerenes and fullerene derivatives. *Chemical Communications*, (8), 663-669.

Dorđević, A., & Bogdanović, G. (2008). Fullerenol: a new nanopharmaceutic? *Archive of Oncology*, 16(3-4), 42-45.

Etherington, K. J., Rodger, A., & Hemming, P. (2001). CHN microanalysis: A technique for the 21st century. *LabPlus International*, 26, 1-2.

Fadeeva, V. P., Tikhova, V. D., & Nikulicheva, O. N. (2008). Elemental analysis of organic compounds with the use of automated CHNS analyzers. *Journal of Analytical Chemistry*, 63(11), 1094-1106.

Fang, X., Mark, G., & von Sonntag, C. (1996). OH radical formation by ultrasound in aqueous solutions Part I: the chemistry underlying the terephthalate dosimeter. *Ultrasonics Sonochemistry*, 3(1), 57-63.

Gnaiger, E., & Bitterlich, G. (1984). Proximate biochemical composition and caloric content calculated from elemental CHN analysis: a stoichiometric concept. *Oecologia*, 62(3), 289-298.

Gong, C., & Hart, D. P. (1998). Ultrasound induced cavitation and sonochemical yields. *The Journal of the Acoustical Society of America*, 104(5), 2675-2682.

Goswami, T. H., Nandan, B., Alam, S., & Mathur, G. N. (2003). A selective reaction of polyhydroxy fullerene with cycloaliphatic epoxy resin in designing ether connected epoxy star utilizing fullerene as a molecular core. *Polymer*, 44(11), 3209-3214.

Goswami, T. H., Singh, R., Alam, S., & Mathur, G. N. (2004). Thermal analysis: a unique method to estimate the number of substituents in fullerene derivatives. *Thermochimica Acta*, 419(1), 97-104.

Hirsch, A. (1993). The chemistry of the fullerenes: an overview. *Angewandte Chemie International Edition*, 32(8), 1138-1141.

Hirsch, A. (1999). Principles of fullerene reactivity. In *Fullerenes and Related Structures*. Springer Berlin Heidelberg.

Hu, Y., Zhang, Z., & Yang, C. Measurement of hydroxyl radical production in ultrasonic aqueous solutions by a novel chemiluminescence method. *Ultrasonics Sonochemistry*, 2008, 15(5), 665–672.

Husebo, L. O., Sitharaman, B., Furukawa, K., Kato, T., & Wilson, L. J. (2004). Fullerenols revisited as stable radical anions. *Journal of the American Chemical Society*, 126(38), 12055-12064.

Indeglia, P. A., Georgieva, A., Krishna, V. B., & Bonzongo, J. C. J. (2014). Physicochemical characterization of fullereneol and fullereneol synthesis by-products prepared in alkaline media. *Journal of Nanoparticle Research*, 16(9), 2599.

Kroto, H. W., Heath, J. R., O'Brien, S. C., Curl, R. F., & Smalley, R. E. (1985). C₆₀: Buckminsterfullerene. *Nature*, 318(6042), 162-163.

Ko, W. B., & Baek, K. N. (2002). The oxidation of fullerenes (C₆₀ and C₇₀) with various oxidants by ultrasonication. *Physics of the Solid State*, 44(3), 410-412.

Ko, W. B., Heo, J. Y., Nam, J. H., & Lee, K. B. (2004). Synthesis of a water-soluble fullerene [C₆₀] under ultrasonication. *Ultrasonics*, 41(9), 727-730.

Kohno, M., Mokudai, T., Ozawa, T., & Niwano, Y. (2011). Free radical formation from sonolysis of water in the presence of different gases. *Journal of Clinical Biochemistry and Nutrition*, 49(2), 96-101.

Kokubo, K., Matsubayashi, K., Tategaki, H., Takada, H., & Oshima, T. (2008). Facile synthesis of highly water-soluble fullerenes more than half-covered by hydroxyl groups. *ACS Nano*, 2(2), 327-333.

Kokubo, K., Shirakawa, S., Kobayashi, N., Aoshima, H. & Oshima, T. (2011). Facile and scalable synthesis of a highly hydroxylated water-soluble fullereneol as a single nanoparticle. *Nano Research*, 4(2), 204-215.

Labille, J., Masion, A., Ziarelli, F., Rose, J., Brant, J., Villiéras, F., Pelletier, M., Borschneck, D., Wiesner, M.R., & Bottero, J. Y. (2009). Hydration and dispersion of C₆₀ in aqueous systems: the nature of water–fullerene interactions. *Langmuir*, 25(19), 11232-11235.

Lamparth, I., & Hirsch, A. (1994). Water-soluble malonic acid derivatives of C₆₀ with a defined three-dimensional structure. *Journal of the Chemical Society, Chemical Communications*, (14), 1727-1728.

Leonelli, C., & Mason, T. J. (2010). Microwave and ultrasonic processing: now a realistic option for industry. *Chemical Engineering and Processing: Process Intensification*, 49(9), 885-900.

Li, J., Takeuchi, A., Ozawa, M., Li, X., Saigo, K., & Kitazawa, K. (1993). C₆₀ fullerol formation catalysed by quaternary ammonium hydroxides. *Journal of the Chemical Society, Chemical Communications*, (23), 1784-1785.

Li, T., Li, X., Huang, K., Jiang, H., & Li, J. (1999). Synthesis and characterization of hydroxylated fullerene epoxide—an intermediate for forming fullerol. *Journal of Central South University of Technology*, 6(1), 35-36.

Li, X. J., Yang, X. H., Song, L. M., Ren, H. J., & Tao, T. Z. (2013). A DFT study on structure, stability, and optical property of fullereneols. *Structural Chemistry*, 24(4), 1185-1192.

Liu, Y., Zhang, G., Niu, L., Gan, L., & Liang, D. (2011). Assembly of Janus fullerene: a novel approach to prepare rich carbon structures. *Journal of Materials Chemistry*, 21(38), 14864-14868.

Lu, Y. A. O., Feng, K. A. N. G., Qiyun, P. E. N. G., & Xinlin, Y. A. N. G. (2010). An improved method for fullerene preparation based on dialysis. *Chinese Journal of Chemical Engineering*, 18(5), 876-879.

Makino, K., Mossoba, M. M., & Riesz, P. (1983). Chemical effects of ultrasound on aqueous solutions. Formation of hydroxyl radicals and hydrogen atoms. *The Journal of Physical Chemistry*, 87(8), 1369-1377.

Mark, G., Tauber, A., Laupert, R., Schuchmann, H. P., Schulz, D., Mues, A., & von Sonntag, C. (1998). OH-radical formation by ultrasound in aqueous solution—Part II: Terephthalate and Fricke dosimetry and the influence of various conditions on the sonolytic yield. *Ultrasonics Sonochemistry*, 5(2), 41-52.

Mason, T. J. (2015). Some neglected or rejected paths in sonochemistry—A very personal view. *Ultrasonics Sonochemistry*, 25, 89-93.

Martín, N. (2006). New challenges in fullerene chemistry. *Chemical Communications*, (20), 2093-2104.

Matsubayashi, K., Kokubo, K., Tategaki, H., Kawahama, S., & Oshima, T. (2009). One-step synthesis of water-soluble fullereneols bearing nitrogen-containing substituents. *Fullerenes, Nanotubes and Carbon Nanostructures*, 17(4), 440-456.

Meier, M. S., & Kiegiel, J. (2001). Preparation and characterization of the fullerene diols 1, 2-C₆₀(OH)₂, 1, 2-C₇₀(OH)₂, and 5, 6-C₇₀(OH)₂. *Organic Letters*, 3(11), 1717-1719.

Menéndez, J., & Page, J. B. (2000). Vibrational spectroscopy of C₆₀. In *Light Scattering in Solids VIII* (pp. 27-95). Springer Berlin Heidelberg.

Partha, R., & Conyers, J. L. (2009). Biomedical applications of functionalized fullerene-based nanomaterials. *International Journal of Nanomedicine*, 4, 261-275.

Periya, V. K., Koike, I., Kitamura, Y., Iwamatsu, S. I., & Murata, S. (2004). Hydrophilic [60] fullerene carboxylic acid derivatives retaining the original 60 π electronic system. *Tetrahedron Letters*, 45(45), 8311-8313.

Prato, M. (1997). [60] Fullerene chemistry for materials science applications. *Journal of Materials Chemistry*, 7(7), 1097-1109.

Raso, J., Manas, P., Pagan, R., & Sala, F. J. (1999). Influence of different factors on the output power transferred into medium by ultrasound. *Ultrasonics Sonochemistry*, 5(4), 157-162.

Richardson, C. F., Schuster, D. I., & Wilson, S. R. (2000). Synthesis and characterization of water-soluble amino fullerene derivatives. *Organic Letters*, 2(8), 1011-1014.

Rivelino, R., Maniero, A. M., Prudente, F. V., & Costa, L. S. (2006). Theoretical calculations of the structure and UV-Vis absorption spectra of hydrated C 60 fullerene. *Carbon*, 44(14), 2925-2930.

Riesz, P., & Kondo, T. (1992). Free radical formation induced by ultrasound and its biological implications. *Free Radical Biology and Medicine*, 13(3), 247-270.

Rooze, J., Rebrov, E. V., Schouten, J. C., & Keurentjes, J. T. (2013). Dissolved gas and ultrasonic cavitation—a review. *Ultrasonics Sonochemistry*, 20(1), 1-11.

Semenov, K. N., Charykov, N. A., & Keskinov, V. N. (2011). Fullerenol synthesis and identification. Properties of the fullerenol water solutions. *Journal of Chemical & Engineering Data*, 56(2), 230-239.

Singh, S. P. (Ed.). (2015). *Light Harvesting Nanomaterials*. Bentham Science Publishers.

Smalley, R. E. (1997). Discovering the fullerenes. *Reviews of Modern Physics*, 69(3), 723.

Suslick, K. S., & Price, G. J. (1999). Applications of ultrasound to materials chemistry. *Annual Review of Materials Science*, 29(1), 295-326.

Tagmatarchis, N., & Shinohara, H. (2001). Fullerenes in medicinal chemistry and their biological applications. *Mini Reviews in Medicinal Chemistry*, 1(4), 339-348.

Thompson, M. (2008). CHNS elemental analysers. AMCTB of The Royal Society of Chemistry, 4.

Villeneuve, L., Alberti, L., Steghens, J. P., Lancelin, J. M., & Mestas, J. L. (2009). Assay of hydroxyl radicals generated by focused ultrasound. *Ultrasonics Sonochemistry*, 16(3), 339-344.

Wang, I. C., Tai, L. A., Lee, D. D., Kanakamma, P. P., Shen, C. K. F., Luh, T. Y., Cheng, C. H., & Hwang, K. C. (1999). C60 and water-soluble fullerene derivatives as antioxidants against radical-initiated lipid peroxidation. *Journal of Medicinal Chemistry*, 42(22), 4614-4620.

Wang, S., He, P., Zhang, J. M., Jiang, H., & Zhu, S. Z. (2005). Novel and efficient synthesis of water-soluble [60] fulleranol by solvent-free reaction. *Synthetic Communications*, 35(13), 1803-1808.

Wang, F. F., Li, N., Tian, D., Xia, G. F., & Xiao, N. (2010). Efficient synthesis of fulleranol in anion form for the preparation of electrodeposited films. *ACS Nano*, 4(10), 5565-5572.

Wang, Z., Wang, S., Lu, Z., & Gao, X. (2015). Syntheses, structures and antioxidant activities of fullerenols: knowledge learned at the atomistic level. *Journal of Cluster Science*, 26(2), 375-388.

Zhang, P., Pan, H., Liu, D., Guo, Z. X., Zhang, F., & Zhu, D. (2003). Effective mechanochemical synthesis of [60] fullerols. *Synthetic Communications*, 33(14), 2469-2474.

Zhang, J. M., Yang, W., He, P., & Zhu, S. Z. (2004). Efficient and convenient preparation of water-soluble fullerenol. *Chinese Journal of Chemistry*, 22(9), 1008-1011.

Zhang, G., Liu, Y., Liang, D., Gan, L., & Li, Y. (2010). Facile synthesis of isomerically pure fullerenols and formation of spherical aggregates from C₆₀(OH)₈. *Angewandte Chemie International Edition*, 49(31), 5293-5295.

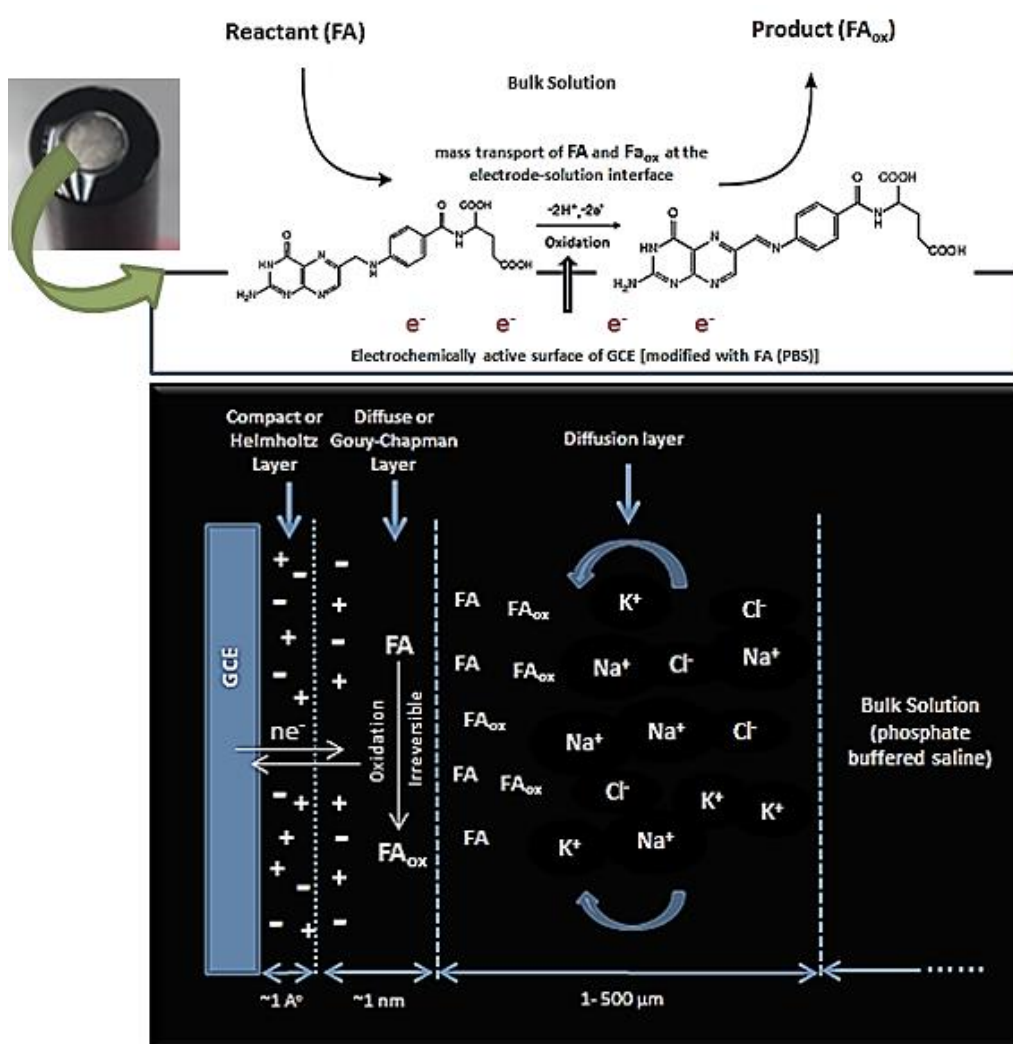
Zhu, S. E., Li, F., & Wang, G. W. (2013). Mechanochemistry of fullerenes and related materials. *Chemical Society Reviews*, 42(18), 7535-7570.

Zhuo, J., Wang, T., Zhang, G., Liu, L., Gan, L., & Li, M. (2013). Salts of C₆₀(OH)₈ electrodeposited onto a glassy carbon electrode: surprising catalytic performance in the hydrogen evolution reaction. *Angewandte Chemie International Edition*, 52(41), 10867-10870.

Chapter 4

A comparative study on the electrochemical behavior of folic acid dispersion vs. folic acid solution by cyclic voltammetry

Graphical Abstract



Abstract

Cellular uptake of folic acid (one of the essential nutrients for human body) in human body is regulated by the glycoprotein folate receptor alpha (FR α). Due to this fact, recently folic acid has immensely been proposed to be used as FR α -specific ligand in developing biosensors for the detection of cancer. The problem associated to using folic acid in a biosensor is that folic acid is sensitive to heat and light, and unstable in its solution form which may affect the reaction at the electrode surface of a biosensor. The instability of FA in its solution form is dependent both on the type and pH of the solvent. As a result, its electrocatalytic activity may vary based on the different types of biosensor and the materials used in preparing the biosensor. In most of the cases, for the detection of FR α , it requires to choose an electrolyte which can provide a similar physiological condition with respect to the value of pH and other physiological ions. Therefore, phosphate buffered saline (PBS) has widely been used in most of the studies for detecting FR α in presence of folic acid and/or in association with other mediators. On this context, it will be interesting to observe the electrochemical behavior of folic acid in PBS prior to designing the synthesized fulleranol, [C₆₀(OH)₈.2H₂O], mediated biosensor for the detection of FR α . In the current chapter, a comparative study on the electrochemical behavior of folic acid dispersion in water and folic acid solution in PBS was conducted by cyclic voltammetry to determine the best one for the detection of FR α . The information obtained from this study provided useful insights on whether folic acid should be prepared in water or PBS for the detection of FR α while the biosensor to be designed based on the folic acid- synthesized C₆₀(OH)₈.2H₂O mixture. Cyclic voltammetry of folic acid on glassy carbon electrode (GCE) showed that although folic acid dispersion prepared in water had more advantages in regard to the absence of other ions that may potentially appear in PBS due to the presence of Na⁺ and K⁺ salts, but the anodic current for the oxidation of folic acid was unable to maintain any linear correlation with the scan rates for folic acid dispersion, indicating unstable oxidation of folic acid at GCE, whereas the anodic peak current for the oxidation of folic acid while prepared in PBS showed a linear regression coefficient of $R^2 \sim 0.93$ with respect to varying the scan rates, implying that folic acid solution prepared in PBS should be considered for designing the folic acid and synthesized C₆₀(OH)₈.2H₂O mediated FR α biosensor in this study.

4.1 Introduction

Folic acid (FA) belonging to vitamin B9 class (molecular formula and weight: $C_{19}H_{19}N_7O_6$ and 441.40 g/mol, respectively) has widely been reported as a biomolecule which has high affinity toward a potential biomarker of cancer progression in human cell termed as folate receptor alpha (FR_{α}). Due to this fact, FA in its conjugated form with other materials has been reported to be useful in diagnosing carcinoma and for drug delivery (Bhunja *et al.*, 2016; Li *et al.*, 2016; Qiao *et al.*, 2016; Bettio *et al.*, 2006; Parker *et al.*, 2005; A and Lee, 2000; Lee and Philip, 1994; Sudimack and Lee, 2000). In developing FA based biosensor, it is important first to study the electrochemical behavior of FA itself. As FA is temperature and heat sensitive, hence may degrade easily, thus impose the necessity to investigating its electrochemical response under different electrochemical techniques prior to designing and developing a biosensor. In the previous studies, the electrochemical behavior of FA as well as the detection of FA in pharmaceutical samples was carried out by different electroanalytical methods, e.g. differential pulse voltammetry (DPV), electrochemical impedance spectroscopy (EIS), square wave voltammetry (SWV), linear sweep voltammetry (LSV), and cyclic voltammetry (CV) (Lavanya *et al.*, 2016; Ananthi *et al.*, 2015; Taherkhani *et al.*, 2014; Maiyalagan *et al.*, 2013; Vaze and Srivastava 2007; Wei *et al.*, 2006). The information obtained from those studies were further used for the detection of various analytes (Arvand *et al.*, 2017; Zhang *et al.*, 2016; Qiao *et al.*, 2015; Yardim and Entürk, 2014; Mirmoghtadaie *et al.*, 2013; Unnikrishnan *et al.*, 2011; Jiang *et al.*, 2009; Ojani *et al.*, 2009). Among the different electroanalytical methods, CV has widely been used for the detection of FA or for the development of FA-based biosensor established on both the reduction and oxidation of FA. Among these electroanalytical techniques CV has become very popular due to its advantageous features over other methods; several information e.g., whether the anodic/cathodic reaction is reversible/irreversible, reaction mechanism, rate constant of the reaction, and the number of electrons takes part in an oxidation/reduction reaction could easily be derived for an electroactive species from a single or multiple cycle cyclic voltammetry scan of that species (Heinze, 1984; Nicholson, 1965). Also, the detection limit for an analyte in the cyclic voltammetry could be measured up to ppm level, the detection is fast and it is possible to study the electrochemical behavior of almost all the materials based on the experimental set-up, which includes selection of electrodes, electrolytes, potential

window for scan, scan rates and the applied voltage. Hence, CV is being used and recommended by others (Bollella *et al.*, 2017; Mahadevan and Fernando, 2017; Torati *et al.* 2016; Wang *et al.* 2016; Jiang *et al.*, 2009; Rusling and Suib, 1994; Kissinger and Heineman, 1983) as a facile and useful electroanalytical technique for both qualitative and quantitative analysis. In this study, cyclic voltammetry method has been adopted to study the electrochemical behavior of FA prepared only in water as dispersion (FA_{H2O}) and prepared in phosphate buffered saline (FA_{PBS}) as a solution.

Folic acid has voltammetric response both in the positive and negative potential window meaning that FA undergoes both cathodic reduction and anodic oxidation under electrochemical analysis. FA shows anodic oxidation current in the positive potential window and cathodic reduction in the negative potential window (as per the IUPAC convention of sign of potentials). It is suggested that for the quantitative analysis, the anodic oxidation of FA could be more reliable compared to its cathodic reduction, given the fact that the cathodic reduction of FA produces multiple peaks and not all of them are well-defined for quantitative analysis, whereas anodic oxidation peak of FA has been reported to be useful for the both qualitative and quantitative analysis (Akbar *et al.*, 2016). Also, in the negative potential window, under certain electrochemical conditions, e.g. pH and applied voltage, the quantitative analysis of an electrochemically active species or analyte could be inhibited due to the contribution of peak currents generated by oxygen evolution reaction (OER) or hydrogen evolution reaction (HER) from the water redox couple (Canales *et al.*, 2015; Lamas-ardisana *et al.*, 2015; Laursen *et al.*, 2012). However, in designing an electrochemical system or developing a method for the detection of any particular analyte, there are several other controlling factors that should be taken into consideration, e.g. applied voltage on the working electrode (WE) and the scan rate of cyclic voltammetry (CV), type and material of what the WE as well as the supporting electrodes are made of, type and pH of the electrolyte, solvent(s) used to prepare the sample solution, and temperature of the bulk solution during analysis. For the purpose of detection, in deciding whether an electrochemical analysis is to be performed in the negative or positive potential window that not only depends on the intrinsic electrochemical properties of a chemical species but also on these controlling factors. In addition, it is also essential to understand the targeted analyte's chemical interaction with other electroactive species in the system. For instance, if the targeted analyte interacts with the redox active site of FA, then for

the detection of the analyte the cathodic reduction of FA should be considered as the control. On the other hand, if the analyte of interest shows an interaction with the oxidation site of FA, then the voltammetric measurements are suggested to be performed in the positive potential for the detection of analyte.

FA has a very low solubility in water, only about 1.6 mg/L (Wu *et al.*, 2010), and the solubility could be increased in an acidic or alkaline medium. FA has intensively utilized mostly in the healthcare products and bio-research, where too acidic or alkaline solution of FA may not always be a good choice to apply on a real biological sample not only because it may affect the biological sample but also FA has been reported to be soluble but eventually degradable in a more acidic or alkaline aqueous solution (Yardim and Entürk, 2014). Therefore, particularly for the detection of any biological analyte or in developing a biosensor it is suggested to maintain a pH of the FA solution as well as the electrolyte medium close to that of the physiological fluid (Maiyalagan *et al.*, 2013). To maintaining the pH similar to the pH (7.2-7.4) of our biological fluid system (blood, plasma, serum), a buffer as a solvent is recommended for FA. For this purpose, PBS has amply been used in previous reports due to its easy preparation and storage method, most importantly because it resembles the ionic and pH condition of the physiological fluid (serum, plasma) in human body (Araoyinbo *et al.*, 2013). However, different buffer solutions have different types of cations and anions and their concentrations also vary based on their different methods of preparation, which may potentially affect the detection of any particular analyte. To avoid the possibility of ionic hindrance from the buffer ions, it is also recommended preparing a dispersion of FA only in water, where possible, without violating the targeted analysis of an analyte. Although there have been numerous studies on the detection of FA and also using FA for the detection of cancer biomarker, where different solvents or buffers have been used to prepare the FA solution, still there is lack of studies whether choosing FA dispersion prepared only in water (FA_{H2O}) or FA solution prepared in PBS (FA_{PBS}) could be better for the detection of biological analytes. With a view to reviewing the matter, before developing a FA based biosensor for the detection of FR α , a comparative electrochemical study of FA_{H2O} and FA_{PBS} was conducted via CV. In the current chapter, the electrochemical behavior of FA is being investigated based on its anodic oxidation in the positive potential window, since the anodic oxidation of FA produced more consistent and a well-defined anodic current irrespective of other controlling

factors mentioned above. The IUPAC convention of sign of the potential and current was followed during all the CV scans in this study.

The position of anodic/oxidation peak potential of FA on a voltammogram may vary based on the type of solvent used to prepare a solution/dispersion of FA as well as the electrolyte chosen for the electrochemical system, type of electrode materials (working, counter and reference electrodes); peak current (whether oxidation or reduction) may also vary in its intensity based on the concentration of FA in a particular solvent. Besides, pH value of the electrolyte solution which plays a vital role in the voltammetric expression of FA. Ojani *et al.* (2009) showed that CV of FA at its different concentration in NaOH (0.1 M) in the presence of Nickel/Poly (o-anisidine) modified carbon paste electrode (Ni/POA/CPE) produces oxidation peak current which significantly varies in its intensity with an increase in the concentration of FA in NaOH. Although the current vs. concentration of FA produced a linear calibration curve in this study, the oxidation peak potential varied with different concentrations as well. In another study (Yardim and Entürk, 2014), comparative CV of FA solution (700 µg/mL in NaOH) in Britton-Robinson (BR) buffer (pH 6.0) as the electrolyte and at a scan rate of 100 mV/S was conducted both at boron-doped diamond electrode (BDD) and glassy carbon electrode (GCE), where FA produced twin oxidation peaks in the positive potential window. At the BDD electrode, the oxidation peaks were observed at 0.94 V and 1.15 V, whereas at GCE the oxidation peaks were found at 0.73 V and 0.99 V, implying the oxidation peak potential is dependent on the type of working electrode and in a wider potential window it can produce two successive anodic peaks of FA due to the oxidation of FA. In relation to this, choosing a wider potential window (2.0 or -2.0 V) may provide further useful information about the electrochemical behavior of an electroactive species; in that case it is also important to consider the stability of the electrodes under that wider potential range. Not all the electrodes can perform well in a broader potential window as the electrode material itself may undergo oxidation or reduction based on the applied voltage in a broader potential window, resulting in electrode corrosion or damage which affects the electrochemical analysis of a targeted species in an electrochemical system. Based on these facts, the working potential window should carefully be chosen for an electrochemical system. In the above study, both at BDD and GCE electrode, the peak potential shifted upon repetitive CV analysis of FA, implying that the electrochemical reaction of FA onto the selected working

electrode was irreversible. This irreversible oxidation behavior of FA was again reported by Arvand *et al.*, (2017), where the CV of FA (1×10^{-4} M) at 100 mV/s and at a gold modified carbon paste electrode (GNPs/CPE) produced anodic oxidation current at 0.62 V, also the anodic oxidation current was significantly dependent on pH showing an increment in the oxidation current with the increase of pH (5.5-7.5). Relating to the intensity of peak currents, it is very important to prepare a homogenous suspension/solution of FA prior to its usage for any electroanalytical method. This is because heterogenous distribution of FA could result in irregular intensity in the peak current as the peak current could highly be dependent on the concentration of FA. Since FA shows low solubility in water in most of the cases, a solution of FA is prepared in an acidic or alkaline aqueous medium in presence of some alkali or acid, e.g. NaOH, HCl, etc. to increase the solubility of FA in the aqueous medium prior to the electrochemical analysis. However, there has been no particular comparative study on the electrochemical behavior of FA dispersion (prepared only in H₂O) vs. FA solution (prepared in PBS). Based on the recent reports (Bhunja *et al.*, 2016; Li *et al.*, 2016; Qiao *et al.*, 2016; Parker *et al.*, 2005; Bettio *et al.*, 2006.), due to the rising possibilities of FA to be used as an electroactive species in developing biosensors for the detection of cancer biomarkers FR α , it is now quite essential to make such a comparative study. Herein, prior to the investigation of the electrocatalytic behavior of FA dispersion vs. FA solution, a series of experiments were first conducted to select the potential window, scan rate, concentration of FA for the cyclic voltammetry. The results showed that FA solution prepared in PBS is comparatively reliable for the quantitative purposes, when all the measurements of the electrochemical behavior of FA were performed at a scan rate 100 mV/s, in a positive potential window at room temperature in oxygen-free solution. The anodic oxidation peak of FA vs. varying scan rates showed a regression coefficient (R^2) of 0.08 for FA_{H₂O}, whereas for FA_{PBS} it was calculated to be 0.93, indicating that the anodic oxidation of FA follows not only a linear correlation with the varying scan rates for FA_{PBS} but also it offers better regression coefficient compared to FA_{H₂O}. In the following study, this finding will be explained through a series of quantitative analysis via CV of both FA_{H₂O} and FA_{PBS}.

4.2 Experimental

4.2.1 Materials & Equipments

Folic acid (FA) was purchased from Sigma Aldrich (China). Type II pure water (TOC <50 ppb) was used from a Milli-Q system (Merck Millipore Integral 5, France) for the preparation of all the samples and cleaning of electrodes. Phosphate buffered saline (PBS) tablet [1 tablet in 200 mL DI water to prepare 0.01M PBS of pH 7.4 which contains 0.0027 M potassium chloride (KCl) and 0.137 M sodium chloride (NaCl)] was purchased from Sigma–Aldrich (Switzerland) and was used as the electrolyte. Potassium hexacyanoferrate (III) [$\text{K}_3\text{Fe}(\text{CN})_6$] (ReagentPlus, ~ 99%, China) and potassium chloride (ReagentPlus, 99%, USA) were purchased from Sigma Aldrich and used to prepare the standard solution of ferrocyanide/ferricyanide redox couple [$\text{Fe}(\text{CN})_6^{3-/4-}$] which was used in studying a standard voltammetric curve for the bare glassy carbon working electrode.

Glassy carbon electrode (GCE, CHI 104) was used as a working electrode (WE) in all the electrochemical analysis along with silver/silver chloride (Ag/AgCl) saturated in potassium chloride (sat. KCl) as a reference electrode (RE) and platinum (Pt) wire as counter electrode (CE). All the electrodes were purchased from CH instruments, Inc. (USA) including the polishing kit (CHI120) containing the alumina powder (0.1 μm) for polishing the GCE prior to all the electrochemical analyses.

Nitrogen (minimum N_2 99.9999%) gas (HiQ[®] 5.0 ZERO) used to remove dissolved oxygen from the electrolyte solution was purchased from Linde, Malaysia.

The potentiostat/galvanostat (VersaSTAT3 equipped with VersaStudio software package) for the electroanalytical studies was purchased from Princeton Applied Research (AMETEK- AMT, USA).

An ultrasonic bath sonicator (KERRY Ultrasonics Ltd, England) was used for the homogeneous mixing of folic acid in water to prepare folic acid dispersion.

4.2.2 Methodology

4.2.2.1 Selection of electrodes

Three-electrode system was used for all the electrochemical analysis in this work, where a working electrode (WE) plays vital role as the electrochemical reaction (oxidation/reduction) of the targeted material or an analyte takes place onto the active surface of WE. In a three-electrode electrochemical system the WE is used along with two other electrodes generally known as reference electrode (RE) and counter electrode (CE). The role of RE is to maintain a constant potential with the WE during the electrochemical analysis. The CE is used for completing the circuit for WE so the current flows from WE to counter electrode and vice versa. In a three-electrode system, therefore, the cell voltage (ΔE) or the potential of WE is always measured with respect to a stable RE which has a known potential value, whereas the current at the WE is measured with respect to the CE (Mabboil 1983). Fig. 4.1 shows a typical three-electrode system (Fig. 4.1a), the potentiostat used in the current study (Fig 4.1c) and a simplified circuit diagram (Fig 4.1b) representing the three-electrode set-up with the potentiostat.

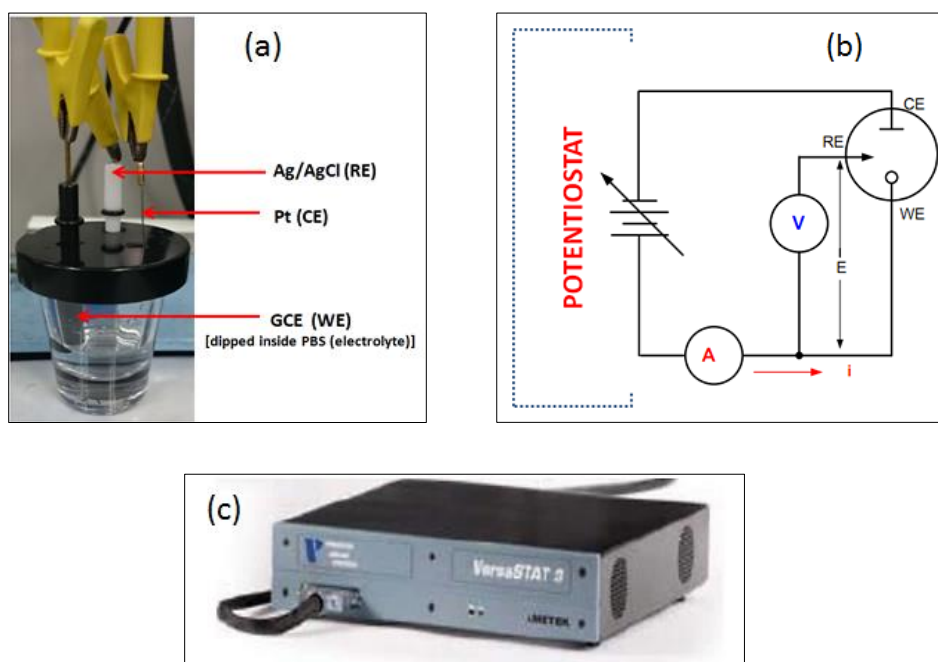


Figure 4.1 (a) Three-electrode set-up used in the experiments, (b) Circuit diagram showing the connections among the three-electrode, (c) VersaSTAT3 potentiostat used for cyclic voltammetry

Care must be taken in selecting the electrodes, especially the WE so that the electrodes should be inert to the air, materials, chemicals and electrolyte to be used in the electrochemical analysis. In addition, the electrodes should be durable enough to withstand the applied potential and be able to perform in a wide range of potential without being deteriorated. Considering these factors, in the current experiment, GCE was used as the working electrode as glassy carbon is mostly inert to many materials, non-toxic, comparatively cheaper than gold (Au) and platinum (Pt) electrode, and can perform in a wide potential range, and thus being considered widely for the development of biosensor (Pocard *et al.* 1992). Similarly, RE should also be carefully chosen as the potential at the WE is maintained by the RE during in electroanalytical chemistry. Hence, in this work, Ag/AgCl (sat. KCl) was used as the RE since it can perform in a wide range of potential. The standard electrode potential for Ag/AgCl is +0.197 V vs. standard hydrogen electrode (SHE) at 25 °C, referring that it can be stable in a more positive potential window. Further advantages of Ag/AgCl electrode over saturated calomel electrode are; it can withstand even high temperature of up to 100 °C, no toxic material is used to prepare the electrode and a porous Teflon tip at the end of the electrode ensures the durability and its chemical inertness. As for CE, Pt wire is mostly popular due to its electrochemical inertness as well good electrical conductivity, hence was chosen as the CE in this study.

4.2.2.2 Cleaning and pretreatment of electrode

Once the electrodes are selected for the electrochemical analysis of FA, it is vital to pay attention on the cleaning and pretreatment of electrodes. Without having the electrodes cleaned there is a potential risk to obtain an improper voltammogram with undesired peaks and noises. In a three-electrode system the working electrode is generally modified with some electroactive material(s). In some cases, the material itself is a subject of the electrochemical study, whereas in other cases the material is used to modify the electrode for further purpose, e.g. detection of an analyte. In both cases, a homogeneous suspension/solution of the material/compound is used to modify the electrode by simply drop casting it onto the active surface of WE (Fig. 4.2). Since the electrochemical reaction (oxidation/reduction of an electroactive species or analyte) in response to the applied voltage to an electrochemical cell takes place at the working

electrode, hence in obtaining reliable results from the electrochemical analysis one of the major needs is the cleaning of working electrode as well as its proper maintenance.

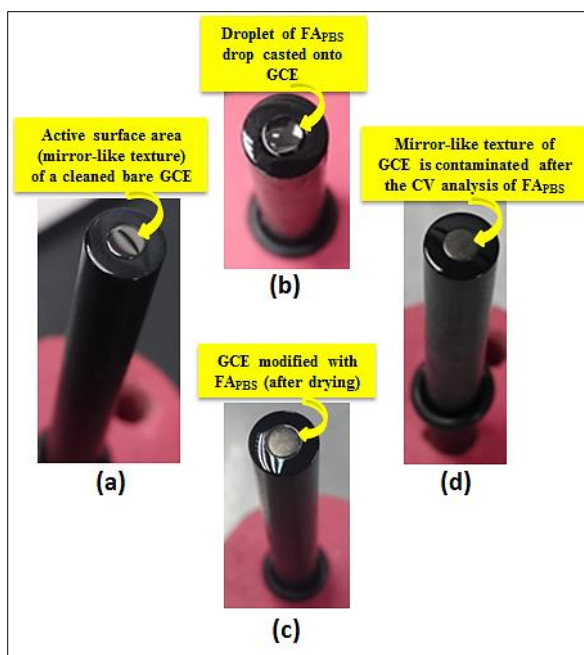


Figure 4.2 Steps of modifying a GCE (a) mirror finish texture of the active surface of a bare GCE, (b) modifying GCE by drop casting FA_{PBS} onto its active surface, (c) GCE modified with FA_{PBS} (drop casted then dried at room temperature), (d) the mirror finish texture of GCE's active surface area is no longer retained after the CV scan of the modified GCE

Typically, the active surface area of a cleaned bare GCE exhibits a mirror-like texture (Fig. 4.2a). After drop casting a material (in this work FA_{PBS}) onto its active surface (Fig 4.2b) and then having the material dried onto its active surface the active surface area of GCE becomes modified with that material (Fig. 4.2c). After CV analysis some residual of the material remains on the surface, also the reaction product or byproduct or even material from the electrolyte may settle onto its active surface, so the active surface area of GCE gains contamination and thus no longer exhibits a mirror-like texture that is usually obtained for a cleaned bare GCE (Fig. 4.2d). The possible sources of WE contamination could be the presence of residual materials or reaction product/byproduct onto its active surface, deposition of airborne material when left outside without any covering, attachment of any material during handling and transfer

of electrode. These contaminations hinder the electrochemical analysis; hence it is necessary to restore the active surface of GCE in between each electroanalytical study to ensure that the obtained current signal is not contributed by any contamination attached to the GCE surface itself.

In this work, for the cleaning of GCE's active surface, a very small amount of alumina powder was placed on a polishing pad and then few drops of DI water was added on the powder to turn it into a small amount of alumina paste. GCE was then held vertically and rubbed continuously for about 1-5 min on the polishing pad (at the zone containing the alumina paste) in a pattern of numeric value 8 (Fig. 4.3). This is a very effective technique of polishing WE as the continuous movement of GCE surface in a pattern of '8' onto the alumina paste for a few minutes can slowly cast away the contaminations from all the corners of its surface.

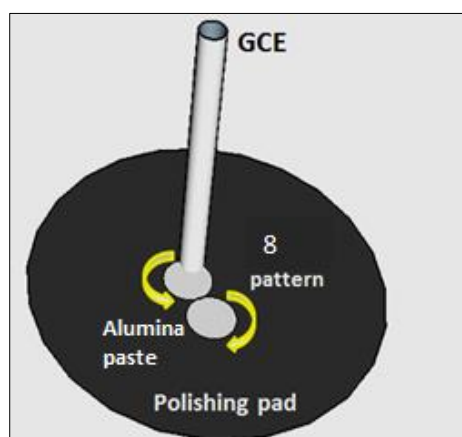


Figure 4.3 Polishing of the surface of GCE (faced onto the alumina paste) in a pattern of number '8' on the alumina paste

After this mechanical polishing, GCE surface was rinsed with abundant DI water to remove away any particles of the alumina powder attached to its surface to confirm any contamination free regeneration of the mirror finish texture of the GCE surface after this cleaning. Time required for this mechanical polishing may vary from 1-5 min or more based on the degree of contamination on the GCE surface, if the degree of contamination is too high then it may require more time to cleaning the GCE by the mechanical method of polishing WE. If mechanical cleaning is not able to remove the contamination from the GCE surface, then an electrochemical pretreatment of GCE

should be followed after the mechanical treatment. In this experiment, mechanical polishing for a maximum of 5 min was good enough to remove any contamination from GCE surface. To confirm that GCE surface was free from contamination, after each cleaning a CV of the cleaned bare GCE was performed in the standard redox couple $\text{Fe}(\text{CN})_6^{3-/4-}$, where for a cleaned GCE the standard reversible voltammogram of the $\text{Fe}(\text{CN})_6^{3-/4-}$ showed a peak to peak separation in a range 60-70 mV, which is the norm and widely accepted a range for a cleaned GCE. Where necessary, when mechanical polishing was not enough to remove the contamination from the GCE surface, an electrochemical pretreatment of GCE was followed afterwards in 0.1 M H_2SO_4 for 25 cycles at a scan rate of 100 mV/s within a potential window -1 V to +1 V. The number of cycles during pretreatment in H_2SO_4 could be chosen as per requirement; if the contamination is hard enough to remove by first 25 cycles, then more cycles could be chosen to ensure a proper cleaning of the electrode. After pretreatment, the cleaned GCE was again scanned in the standard $\text{Fe}(\text{CN})_6^{3-/4-}$ to obtain a peak to peak separation within 60-70 mV. Thus, for every CV measurement the GCE was cleaned and verified in between two consecutive electroanalytical studies.

As for the maintenance of GCE, when not in use, the tip of the GCE was covered with a rubber cap (as provided with the electrode) and stored in a cool dry place, prior to the use the GCE was cleaned every time as per the procedure discussed above.

Similar to GCE, the cleaning and maintenance of both Ag/AgCl (sat. KCl) and Pt electrodes were necessary as they play vital roles in the electrochemical cell as a reference and counter electrode, respectively.

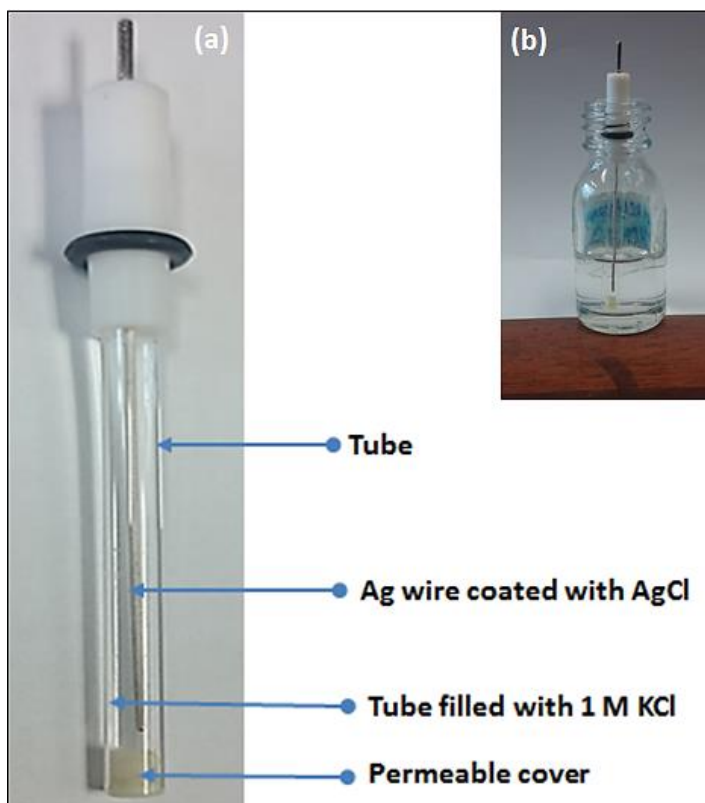


Figure 4.4 (a) Different parts of the Ag/AgCl (sat. KCl) reference electrode used in this study, (b) Ag/AgCl (sat. KCl) dipped inside 1 M KCl solution when not in use

The Ag/AgCl (sat. KCl) electrode is made of Ag wire which is kept inside a Teflon tube filled with 1 M KCl solution and at the end of the tube it is closed by a permeable cover (Fig. 4.4a). It is necessary to keep the electrode dipped inside 1M KCl solution when not in use (whether temporarily or for long time), so it can maintain an equilibrium concentration of ions (Fig. 4.4b). The solution inside the electrode may dry over time if it is not preserved in a standard 1M KCl solution, moreover it may catch contamination very easily because of its semi-permeable membrane if the electrode is not thoroughly washed after every electrochemical analysis. Also, Ag/AgCl (sat. KCl) electrode may lose its activity if it is exposed to light for long period. The possible outcomes are Ag wire can undergo reduction reaction while exposed to light, or may form a black layer of contamination when not preserved in KCl solution as well as causing ionic imbalance due to the dryness of the solution inside the electrode tube. All these will lead to a very noisy current signal. To get rid of these consequences, the Ag/AgCl (sat. KCl) electrode was always preserved in 1 M KCl solution to maintain

the equilibrium of the ions as well as was stored in a cool dark place to avoid any exposure to light and atmosphere while not in use.

Pt electrode was washed thoroughly before and after every electrochemical analysis to avoid any contamination. Although Pt is inert, still it was preserved in a cool dry tube when not in use to avoid any corrosion.

4.2.2.3 Selection of electrolyte solution

PBS of pH 7.4 was selected as a suitable electrolyte in studying the electrochemical behavior of FA, due to its resemblance to physiological fluid. As for the concentration of PBS, for all the electrochemical analysis a low concentration was preferred, since the ions present in the electrolyte may also take part in the anodic and cathodic reaction during the electrochemical analysis of a targeted analyte. This ultimately will cause interference in the expected electrochemical analysis. Now as per the concepts of electrochemistry, which ion will go first to the anode and/or cathode for oxidation/reduction reaction that depends on the ions' position in the electrochemical series based on their redox potentials. The ions at the top of the series act as strong reducing agents being oxidized in an electrochemical cell. An electrolyte solution, for instance PBS, contains more than one anions or cations which may take part in reaction at the working electrode based on the value and direction of the applied potential. Sometimes, therefore, the interference or noise in an electrochemical analysis during the detection of an analyte could also be attributed to the presence of these ions at a very high concentration in the electrolyte solution. These may also be termed as 'solution resistance' which can cause an ohmic drop commonly known as IR drop/IR compensation in electrochemistry. As a result, high concentration of an electrolyte may potentially increase the risk of generating unexpected noise in an electroanalytical method. However, the concentration of an electrolyte should also be chosen in a way so that it is also able to provide the necessary conductive medium within an electrochemical cell in order to maintain the flow of charge transfer between the electrodes.

In this work, the limit of detection of FR α is expected to be in the range of pM-nM, hence PBS with a lower concentration (0.01 M) was chosen as the electrolyte to ensure

that the individual concentration of the ions in the PBS does not contribute in the IR drop during the electrochemical analysis of both FR α and FA. At the same time PBS is also able to maintain a conductive medium providing a physiological condition of pH 7.4 for the detection of FR α . In relation to that, since FA will be applied to detect FR α , therefore all the electrochemical behavior of FA was also studied at the same concentration of PBS as an electrolyte.

4.2.2.4 Selection of potential window

Selecting the potential window for cyclic voltammetry is also very important prior to the electrochemical analysis. Since each cation and anion in the solution will have their individual oxidation and reduction potential values, hence to target an analyte or study the electrochemical behavior of a chemical species the potential window must be chosen carefully. In that case, choosing a broader potential window may ensure that all the signals generated due to the oxidation/reduction of the material of interest could be recorded, but at the same time that might cause some potential damage to the electrodes. This is due to the fact that based on electrode materials, all electrodes have a 'tolerance potential', beyond that potential an electrode can easily be oxidized or reduced causing the damage of the electrode. Another important factor in choosing the potential window, while the electrolyte is an aqueous solution there is a possibility of water redox couple reaction to occur at a certain potential window. Also, the dissolved oxygen in the electrolyte can undergo reaction and contribute background current in the total measured current (Oldham *et al.*, 2011). Considering the above-mentioned conditions, in this work, for studying the electrochemical behavior of FA and all other electrochemical analysis relevant to the detection of FA were performed in a positive potential window (0 to +1 V and 0 to +1.2 V). For the Fe(CN) $_6^{3-/4-}$ redox couple, the potential window was selected from -0.2 to +0.6 V to obtain the standard oxidation/reduction reversible voltammogram for determining the active surface area of GCE.

Within the selected potential window for the electrochemical analysis of FA no ions from PBS buffer possibly could undergo oxidation or reduction reaction as the half-cell

reaction potential of the cations and anions (Eqs. 4.1, 4.2 and 4.3) from the PBS are beyond the range of the selected potential window (Oldham *et al.*, 2011).



As for the electrode potential GCE can perform within a potential range of -1 to +1.2 V. For the Ag/AgCl (sat. KCl) electrode limiting potential is +0.197/0.222 V and for Pt electrode limiting potential is +1 to -0.7 V. Although prior to every electrochemical analysis N₂ gas was purged into the electrolyte solution to remove any dissolved oxygen in order to avoid oxygen reduction reaction (ORR) which may occur at different negative potentials based on the pH (0-14) of the solution (Aguirre *et al.*, 2009), still it is hard to completely avoid oxygen involvement during an electrochemical analysis. Hence, the selected positive potential window within a range of 0-1.2 V in this study was favorable for all the electrochemical analysis of FA, which in the next chapter will also be followed for the detection of FR α based on FA and synthesized C₆₀(OH)₈.2H₂O.

4.2.2.5 Preparation of FA dispersion (FA_{H2O}) and FA solution (FA_{PBS})

The solubility of FA in water is reported to be only 1.6 mg/L (Wu *et al.* 2010) but for the electrochemical study a mixture (whether a dispersion or a solution) needs to be homogeneous. A homogeneous mixture of FA can form a thin film onto GCE where the particles of FA will be homogeneously distributed, thus the current signal will be achieved proportionately with the change in the concentration of FA solution and/or change in the scan rate. Under this condition, prior to an electrochemical analysis, it is suggested to choose either a homogeneous dispersion of FA in water, if that is not satisfactory then a suitable solvent should be selected which will allow the dissolution of FA to a substantial amount for the preparation of a homogeneous FA dispersion/solution. As for FA dispersion in water, 566.38 μM dispersion of FA was prepared by mixing 0.5 mg of FA into 2 mL DI water and then was sonicated in a water bath sonicator for 1 minute; since FA is temperature and light sensitive, it is preferable not to sonicate it for longer time and to avoid any exposure to light. After sonication, a

homogeneous dispersion of $\text{FA}_{\text{H}_2\text{O}}$ was obtained, which was preserved in a dark cool environment and the vial containing $\text{FA}_{\text{H}_2\text{O}}$ dispersion was fully wrapped with aluminum foil to avoid its any further exposure to light and heat.

In the similar way, a solution of FA in PBS was also prepared for the comparative study. FA was readily dissolved in the PBS, first, 0.01 M PBS (pH 7.4) was prepared by dissolving one PBS tablet in 200 mL DI water. Then, 0.5 mg FA was dissolved in 2 mL of 0.01 M PBS (pH 7.4) to obtain 566.38 μM FA_{PBS} . FA_{PBS} was also stored in a dark cool environment and the vial containing FA_{PBS} was fully wrapped with aluminium foil to avoid any exposure to light and heat. This 566.38 μM FA_{PBS} was also used to modify the bare GCE.

Both $\text{FA}_{\text{H}_2\text{O}}$ and FA_{PBS} were used to modify the GCE, and then modified GCE was subjected to cyclic voltammetry to observe the electrochemical behavior of FA.

4.2.2.6 Preparation of a standard redox couple $[\text{Fe}(\text{CN})_6^{3-/4-}]$

A 100 mL solution containing 1 mM $\text{K}_3\text{Fe}(\text{CN})_6$ and 0.1 M KCl was prepared by dissolving together 32.9 mg of $\text{K}_3\text{Fe}(\text{CN})_6$ and 750 mg of KCl in 100 mL DI water. This solution was used as an electrolyte in obtaining a standard reversible voltammogram of $\text{Fe}(\text{CN})_6^{3-/4-}$ redox couple to determine the activity of GCE after having the surface of GCE cleaned and polished and prior to modifying the active surface of GCE with $\text{FA}_{\text{H}_2\text{O}}$ and/or FA_{PBS} .

4.2.2.7 Modifying GCE with FA

5 μL dispersion of $\text{FA}_{\text{H}_2\text{O}}$ was drop casted onto cleaned bare GCE, and then was allowed to dry it on the surface of GCE for 1 h at room temperature. It is recommended not to use any heat for drying since heat may deform and damage the outer supporting material of GCE causing a leakage and sealing failure. After drying the drop casted 5 μL of $\text{FA}_{\text{H}_2\text{O}}$ onto GCE at room temperature, the bare GCE became modified with $\text{FA}_{\text{H}_2\text{O}}$ which to be termed as GCE/ $\text{FA}_{\text{H}_2\text{O}}$. In the same way, GCE modified with FA_{PBS} to be termed as GCE/ FA_{PBS} .

4.3 Results & Discussion

All the electrochemical measurements in this study were performed at room temperature and at atmospheric pressure. The IUPAC convention method was followed thoroughly in expressing and explaining all the voltammograms.

4.3.1 Activity of the cleaned bare GCE

Prior to any electrochemical analysis, the activity of the polished and cleaned bare GCE was first investigated by scanning the bare GCE in a standard $\text{Fe}(\text{CN})_6^{3-/4-}$ redox couple at 75 mV/s. $\text{Fe}(\text{CN})_6^{3-/4-}$ redox couple undergoes reversible oxidation/reduction reaction where the peak to peak separation for the oxidation and reduction reaction of $\text{Fe}(\text{CN})_6^{3-}/\text{Fe}(\text{CN})_6^{4-}$ redox couple certifies the quality of the GCE surface. In an ideal electrochemical condition, a good GCE in a standard electrolyte solution of $\text{Fe}(\text{CN})_6^{3-}/4-$ redox couple will produce a reversible voltammogram where the ratio (I_{pa}/I_{pc}) of the anodic peak current (I_{pa}) and cathodic peak current (I_{pc}) should be ~ 1.0 . The peak potentials also convey very important information in understanding the quality of GCE. Theoretically, for a reversible redox couple's anodic and cathodic reactions, the number of electrons transferred at the electrode could be measured by using Eq. 4.4 (Oldham, 2011).

$$\Delta E = |E_{pa} - E_{pc}| \sim 0.059/n \quad (\text{Eq. 4.4})$$

Where, for a single electron transferred oxidation/reduction reversible reaction the value of n is 1 (Eq. 4.5). The reversible reaction of $\text{Fe}(\text{CN})_6^{3-/4-}$ couple is associated to 1 electron transfer, implying that peak to peak potential difference should ideally be ~ 0.059 V.



Although theoretically an electroactive GCE as a working electrode should produce a peak to peak separation of 59 mV in a standard $\text{Fe}(\text{CN})_6^{3-/4-}$ solution for a single electron transfer reaction, practically it is very difficult to achieve that value due to the uncompensated resistance or IR drop that may occur in the sample during any

electrochemical analysis, considering the fact that the value of peak to peak separation in the range of 60-70 mV for a single electron transfer at GCE surface in a standard $\text{Fe}(\text{CN})_6^{3-/4-}$ redox couple solution is widely accepted and generally followed. Therefore, prior to every electrochemical analysis the GCE surface was mechanically polished every time followed by checking in the $\text{Fe}(\text{CN})_6^{3-/4-}$ redox couple solution. Where necessary, an electrochemical pretreatment of GCE was conducted after the mechanical polishing to renew the GCE. For the electrochemical pretreatment, bare GCE (in a three-electrode system) was scanned for 25 cycles in 0.1 M H_2SO_4 at a scan rate of 100 mV/s within a potential window of -1 V to +1 V.

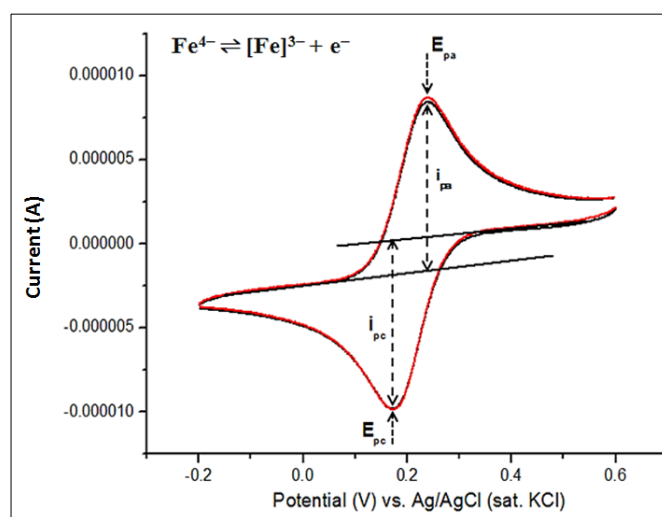


Figure 4.5 Reversible voltammogram of $\text{Fe}(\text{CN})_6^{3-/4-}$ redox couple solution (containing 1 mM $\text{K}_3\text{Fe}(\text{CN})_6$ and 0.1 M KCl) at a scan rate of 75 mV/s

Table 4.1 Peak currents and peak potentials for the reversible reaction of $\text{Fe}(\text{CN})_6^{3-/4-}$ redox couple

E_{pa} (V)	E_{pc} (V)	$E_{pa} - E_{pc}$ (V)	I_{pa} (μA)	I_{pc} (μA)	I_{pa}/I_{pc}
0.24	0.17	0.07 (70 mV)	9.97	10	0.99 ~ 1.0
0.23	0.17	0.06 (60 mV)	9.83	9.98	0.98 ~ 1.0

Fig. 4.5 shows a multicycle (2 cycles) voltammogram of bare GCE obtained at a scan rate of 75 mV/s in $\text{Fe}(\text{CN})_6^{3-/4-}$ redox couple and the value of $E_{\text{pa}}-E_{\text{pc}}$ was obtained in a range of 60-70 mV. The voltammograms obtained from 2 cycles of CV scans for the bare GCE in the $\text{Fe}(\text{CN})_6^{3-/4-}$ redox couple coincides providing a qualitative measure that the GCE was properly cleaned so that the standard voltammogram of the redox remained same over 2 cycles. The ratio of the peak currents was calculated for the peak to peak separation obtained at a value of both 60 mV and 70 mV. Table 4.1 shows that when peak to peak separation was 60 mV (very close to the theoretical value of 59 mV), the ratio of I_{pa} and I_{pc} was 1.05. While the peak to peak separation was 70 mV, the ratio of I_{pa} and I_{pc} remains still 1.0, indicating that the GCE was in good condition so within the acceptable range (60-70 mV) of peak to peak separation the ratio of I_{pa} and I_{pc} always remained ~ 1.0 . Thus, the activity of the GCE was always checked after every cleaning and before every electroanalytical study.

4.3.2 Calculating the active surface area of GCE

For a reversible one electron transfer redox couple oxidation/reduction reaction, Randles-Sevcik equation (Eq. 4.6) is used to measure the active surface area of a working electrode. In the equation, I_p is the peak current (given that $I_{\text{pa}}/I_{\text{pc}} \approx 1.0$) in amperes (A), n is the number of electrons transferred or participated during the oxidation or reduction of an electrochemically active species, A is the active surface area of the working electrode in cm^2 , D is the diffusion coefficient of the electrochemically active species in cm^2/s , v is the scan rate in V/s , C is the concentration of the electrochemically active species in the bulk solution in moles/cm^3 .

$$I_p = 2.69 \times 10^5 n^{3/2} A D^{1/2} v^{1/2} C \quad (\text{Eq. 4.6})$$

The reversible reaction of $\text{Fe}(\text{CN})_6^{3-/4-}$ redox couple is associated with one electron transfer ($n=1$) where $I_p \approx 10$ as observed in Table 4.1. The diffusion coefficient of ferro/ferricyanide ions [$\text{Fe}(\text{CN})_6^{3-/4-}$] (Eq. 4.5) is obtained from the literature, where $D = 7.60 \times 10^{-6} \text{ cm}^2/\text{s}$ (Konopka and McDuffie, 1970). For the CV analysis of $\text{Fe}(\text{CN})_6^{3-/4-}$ the scan rate was 0.075 V/s (75 mV/s) and C was $10^{-6} \text{ moles}/\text{cm}^3$ (1 mM). In this study based on the empirical values obtained from the CV scan of $\text{Fe}(\text{CN})_6^{3-/4-}$ the active surface area of GCE was determined to be 0.049 cm^2 ($\sim 5 \text{ mm}^2$).

4.3.3 Effect of N₂ purging

Prior to the electrochemical analysis, it was necessary to remove the dissolved oxygen from the solution. Apparently, presence of dissolved oxygen may not cause any hindrance in the electrochemical analysis unless the following conditions are applicable for an electrochemical cell.

- The value of the applied voltage on the working electrode and the selected potential window are favorable for the OER and/or HER evolution.
- The dissolved oxygen may potentially react with the electrolyte solution, or with the analyte of interest present in the electrolyte, or may react with the material which is being used to modify the GCE.

To avoid any of the above-mentioned circumstances, it is essential to purge an inert gas (N₂/Ar) to degas the dissolved oxygen from the electrolyte prior to the electroanalytical study. In this work, N₂ gas was purged throughout PBS to remove the dissolved oxygen out of it as well as a continuous flow of N₂ (also known as N₂ blanket) gas was maintained over PBS during all the CV scan in order to eliminating the scope of further oxygen dissolution during the electroanalytical study.

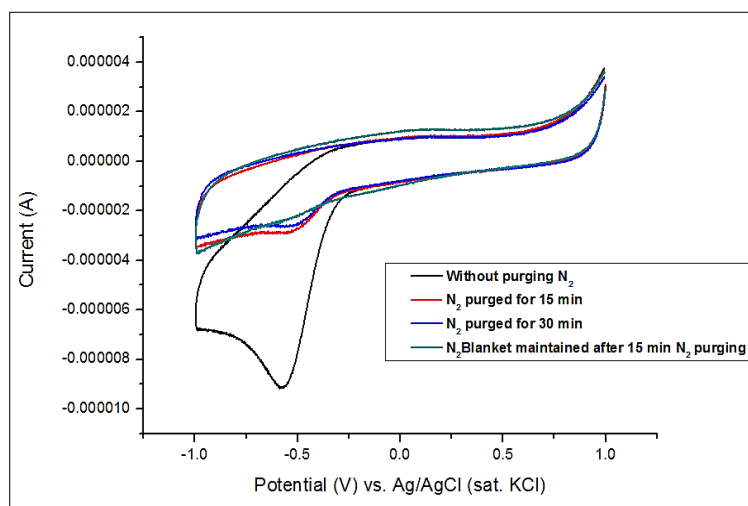


Figure 4.6 Voltammograms of bare GCE in 0.01 M PBS at a scan rate of 75 mV/s when N₂ gas was purged for different duration (15 min and 30 min)

The time of N₂ purging and its effect on the CV of PBS at bare GCE was recorded, and the resulting voltammograms (Fig. 4.6) showed that when the dissolved oxygen gas was not removed by purging N₂ the voltammogram of PBS buffer produced a cathodic

peak current at around -0.58 V which is due to the presence of O₂ in the solution. This cathodic peak current gradually decreased when N₂ was purged for 15 min and 30 min, and finally disappeared when a N₂ blanket was maintained over PBS electrolyte during the CV scan. However, it was an interesting observation that the effect of N₂ purging for 15 min and 30 min had a subtle difference in the voltammogram of bare GCE in PBS. Therefore, prior to all the electrochemical analysis, N₂ gas was continuously purged for 15 min throughout the electrolyte and then a N₂ blanket was maintained over the electrolyte solution during the electrochemical analysis.

4.3.4 Electrochemical behavior of FA: dispersion (FA_{H2O}) vs. solution (FA_{PBS})

4.3.4.1 Effect of concentration

Generally, the effect of concentration on cyclic voltammetry is very straightforward, the more the material the more the flow of electrons will result due to the oxidation or reduction reaction of the material present on the surface of GCE or present as an analyte in the electrolyte. With an increase in the concentration, the oxidation or reduction current increases and vice versa, so a linear correlation is expected between the peak currents (I_{pa} and/or I_{pc}) and concentration of the material(s) used to modify the working electrode. Still, it is a primary concern to check the effect of concentration for a particular chemical species and for a specific electrochemical cell, as based on the type of the compound and electrochemical system the linear correlation of current vs. concentration could be suspended. While the GCE is modified with FA, the voltammetric response of the modified GCE depends not only on the electrochemical properties of FA but also on the physicochemical properties of FA to a greater extent. FA particles can rearrange themselves on the GCE surface to provide space for more FA when added onto the GCE surface. The extent to which FA particles rearrange themselves in forming a self- assembled monolayer onto the active surface of GCE could be influenced by the increase or decrease in the concentration of FA.

For investigating the effect of very high to low concentration on the cyclic voltammogram of FA, 566.38 μM FA_{H2O} was diluted 10 folds in DI water to produce 56.64, 5.6 and 0.56 μM FA_{H2O}. GCE/ FA_{H2O} at different concentrations of FA_{H2O} were scanned in 0.01 M PBS (pH 7.4) at a scan rate of 75 mV/s in the positive potential

window (Fig. 4.7a). A well-defined anodic peak current (I_{pa}) due to the oxidation of FA appeared and the anodic peak current decreased with the decrease in the concentration of FA in water; a linear correlation (Eq. 4.7) was obtained by plotting the anodic peak current vs. concentration of FA (Fig. 4.7b) in explaining the effect of concentration on I_{pa} of FA, where the coefficient of determination (R^2) was calculated to be 0.9965.

$$I_{pa} (\mu A) = 0.0173 (\mu M) + 1.3827 \quad (\text{Eq. 4.7})$$

R^2 is a useful statistical measure which explains how closely the variables are fitted on the regression line. In another way R^2 value represents a degree of linear correlation and is expressed between 0-1, as the R^2 value approaches very close to 1 the model is said to be very good fit of a linear correlation model.

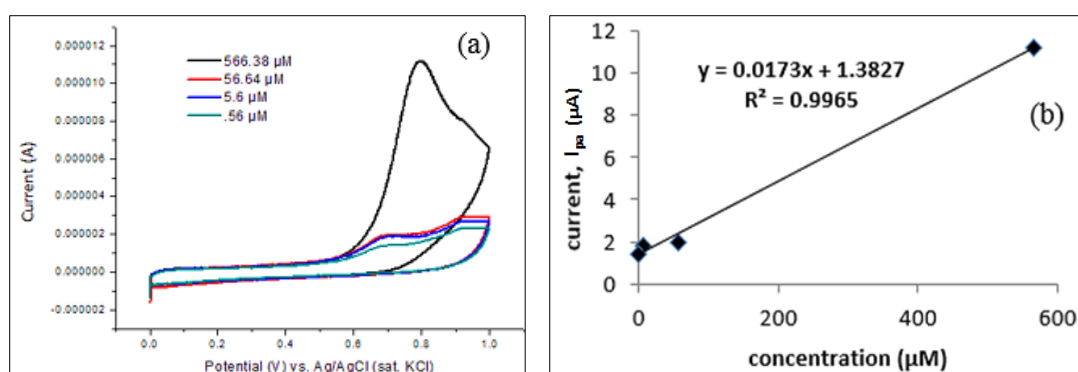


Figure 4.7 (a) Cyclic voltammogram of GCE/FA_{H₂O} at different concentrations of FA dispersion prepared only in H₂O, (b) i_{pa} vs. concentration of FA

Table 4.2 Anodic peak currents (I_{pa}) and peak potentials (V) recorded at different concentrations of FA

Concentrations, μM	E_{pa} V	I_{pa} μA
566.38	0.80	11.2
56.64	0.70	2
5.6	0.70	1.8
0.56	0.70	1.4

Table 4.2 shows that at higher concentration the anodic peak current is the highest among all the four used concentrations. Interesting observation was recorded for the anodic peak potential of GCE/FA_{H₂O} which was constant at very low concentration. The possible reason could be due to the formation of a more stable homogeneous dispersion of FA in H₂O was achieved at the low concentration as compared to its high concentration. Although at lower concentrations the peak potential was found to be constant, but the intensity of the anodic peak current decreased at a substantial amount (ac. 88%) from the concentration of 566.38 μ M to 0.56 μ M, indicating that at such a lower concentration it will be hard to quantify the electrochemical system for a targeted analyte. This is because a biosensor could be built on both electrochemical outputs that the peak current will increase and decrease in the presence of an analyte. In the latter case, it would be difficult to quantify the decreased value of the peak current for the analyte if the peak current in the absence of an analyte itself shows a very weak and low intensity of I_{pa} . In addition, one of the vital things while dealing with FA is that FA may leach out easily from the GCE surface into the electrolyte solution, although FA has a self-assembling capability onto the surface of GCE by adsorption, where the adsorption is rather physisorption than chemisorption and hence there remains a possibility of the desorption of some FA particles from the GCE over the duration of electrochemical scanning. Therefore, if the initial concentration of FA is very low which will cause a drop in the anodic current or sometimes no response at all due to the diffusion of FA particles from the modified GCE surface when it is immersed into the electrolyte. Considering these facts, a higher concentration of FA (566.38 μ M) was selected to prepare GCE/FA_{H₂O} and GCE/FA_{PBS} for the rest of the electroanalytical studies in this work.

4.3.4.2 Effect of scan rate (v): comparative study

Scan rate (v) is one of the major parameters that govern the voltammogram of a specific material or an electrochemical system. As with the increase/decrease of scan rate the voltammetric shape, peak current intensity, peak potential and the level of noise may be affected in a significant manner. Once the concentration of the material is selected for voltammetric study the next essential measurement should be the selection of a suitable scan rate.

Effect of scan rate on two different modified working electrodes, GCE/FA_{H2O} and GCE/FA_{PBS}, were measured at scan rates of 25, 50, 75, 100 and 125 mV/s. As there is a possibility that the I_{pa} may slightly differ at the same scan rate even for inter-day CV scans due to the reason of FA desorption from GCE surface over a long period of electroanalytical scan, therefore all the voltammetric scans at varying scan rates both for GCE/FA_{H2O} and GCE/FA_{PBS} were conducted within 24-48 h to ensure the reliability of the voltammetric signals.

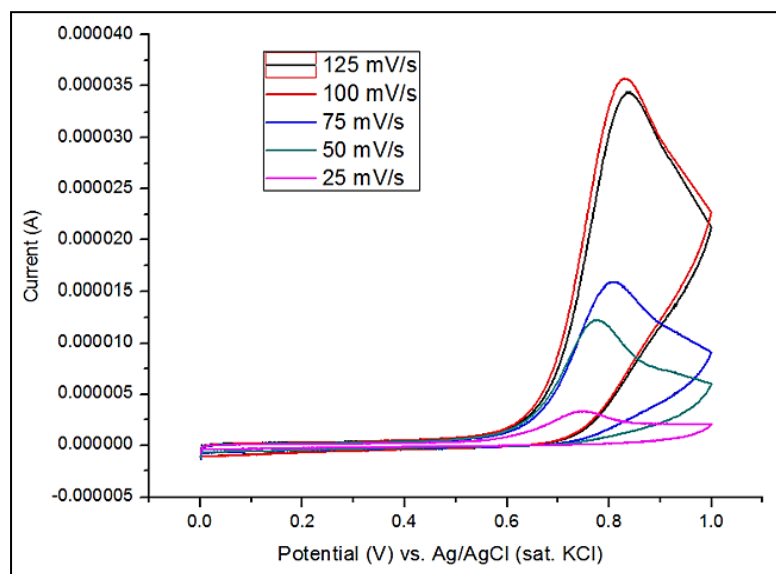


Figure 4.8 Effect of scan rates on the anodic peak current (I_{pa}) of GCE/FA_{H2O}

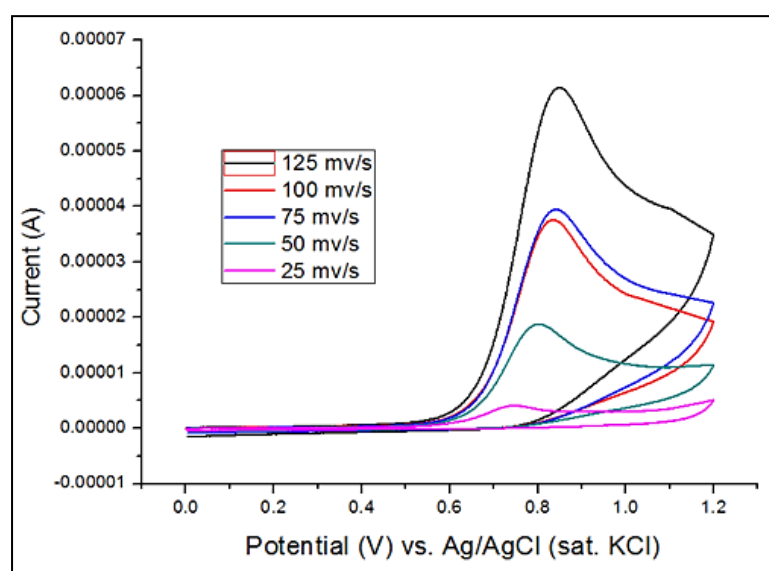


Figure 4.9 Effect of scan rates on the anodic peak current (I_{pa}) of GCE/FA_{PBS}

Scan rate dependence of an electrochemical reaction provides us the useful information about the reaction kinetics. If the peak current increases with the voltage sweep while the peak potential remains same that provides a clue of fast electron transfer kinetics at the working electrode. On the other hand, a quasi-reversible or irreversible process will show a shift in the peak potential values with the change of scan rate. The voltammogram of GCE/FA_{H2O} and GCE/FA_{PBS} showed one electron transfer reaction irrespective of the values of scan rates (Figs. 4.8 and 4.9), where I_{pa} increased with an increase in scan rate and the E_{pa} slightly shifted toward more positive potential with an increase in the scan rate, providing further information that the reaction kinetics at the GCE surface for GCE/FA_{H2O} and GCE/FA_{PBS} follow slow electron transfer kinetics.

To understand the reaction mechanism of GCE/FA_{H2O} and GCE/FA_{PBS} with regard to the varying scan rates, both I_{pa} vs. $v^{1/2}$ and I_{pa} and v were plotted for GCE/FA_{H2O} and GCE/FA_{PBS}.

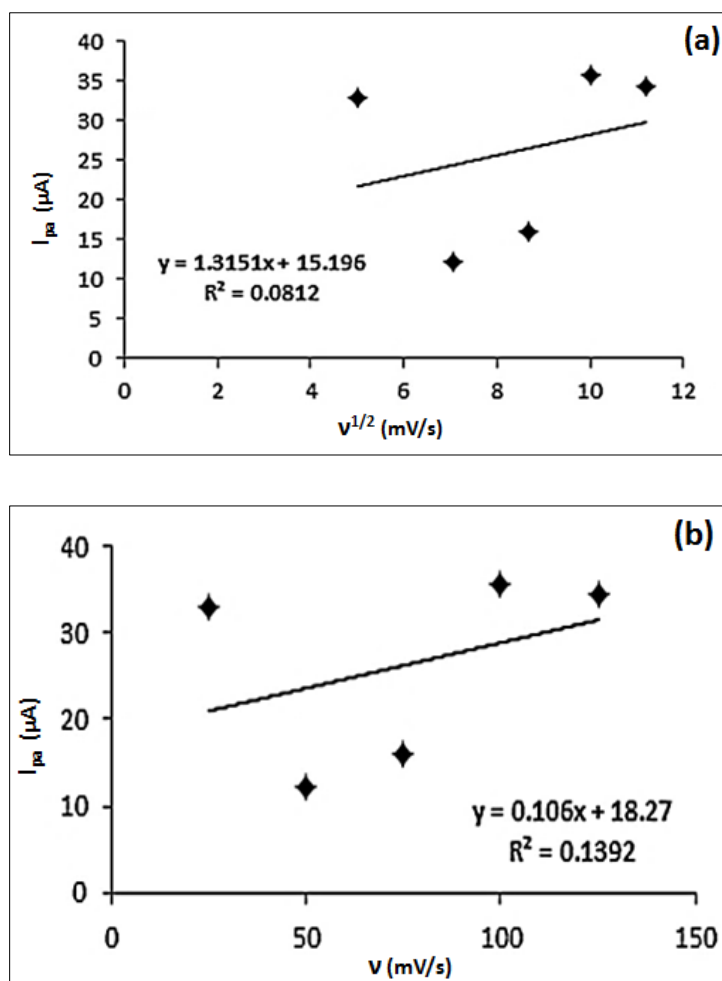


Figure 4.10 (a) I_{pa} vs. $v^{1/2}$ plot and (b) I_{pa} vs. v plot for GCE/FA_{H2O}

For GCE/FA_{H2O} the linear regression equations (Eq. 4.8 and 4.9) were obtained from I_{pa} vs. $v^{1/2}$ plot and I_{pa} vs. v plot (Figs. 4.10a and 4.10b), where the values of coefficient of determination were calculated to be $R^2=0.0812$ and $R^2 = 0.1392$ respectively.

$$I_{pa} (\mu A) = 1.3151v^{1/2} (\text{mV/s}) +15.196 \quad (\text{Eq. 4.8})$$

$$I_{pa} (\mu A) = 0.106v (\text{mV/s}) +18.27 \quad (\text{Eq. 4.9})$$

The values of R^2 show that the reaction kinetics of GCE/FA_{H2O} is either diffusion or adsorption controlled, where the progress of oxidation of FA with the varying scan rate was unable to produce a linear correlation for I_{pa} in respect to the varying scan rate. One possible reason to this could be due to the low solubility of FA in water making it difficult to restore the homogeneity of FA dispersion, hence the amount of FA onto the active surface of GCE varied. Moreover, FA could drop off from the surface of GCE and thus could cause this deviation from linearity. Loss of material from the working electrode surface during electrochemical analysis has been a very common issue reported by others (Moyo *et al.*, 2012; Li *et al.*, 2011; House *et al.*, 2007). Some remedies to this problem were suggested by others where using a polymer as a binder could hold the material firmly onto the electrode surface. Another solution is to select a suitable solvent which will facilitate the very homogeneous dispersion of the material of interest.

While using a binder, it has to be not only very specific to FA but also to GCE, otherwise the binder may also drop off from the GCE surface including FA. During selecting a binder care should be taken on this matter that it must be inert to the electrolyte and the analyte as well otherwise it will certainly hinder the desired electrochemical reaction of FA at GCE. A binder can enhance the attachment of FA to the GCE surface but at the same time, in some cases, for the detection of protein or other biomolecules, it can block the active functional groups present in FA or inhibit the interaction between FA and the analyte. Thus, using a binder could be a solution but does not ensure the sensitive detection of the material of interest. Given these facts, the use of any binder was avoided in this current study as GCE modified with FA will later be used for the detection of a cell membrane glycoprotein FR α .

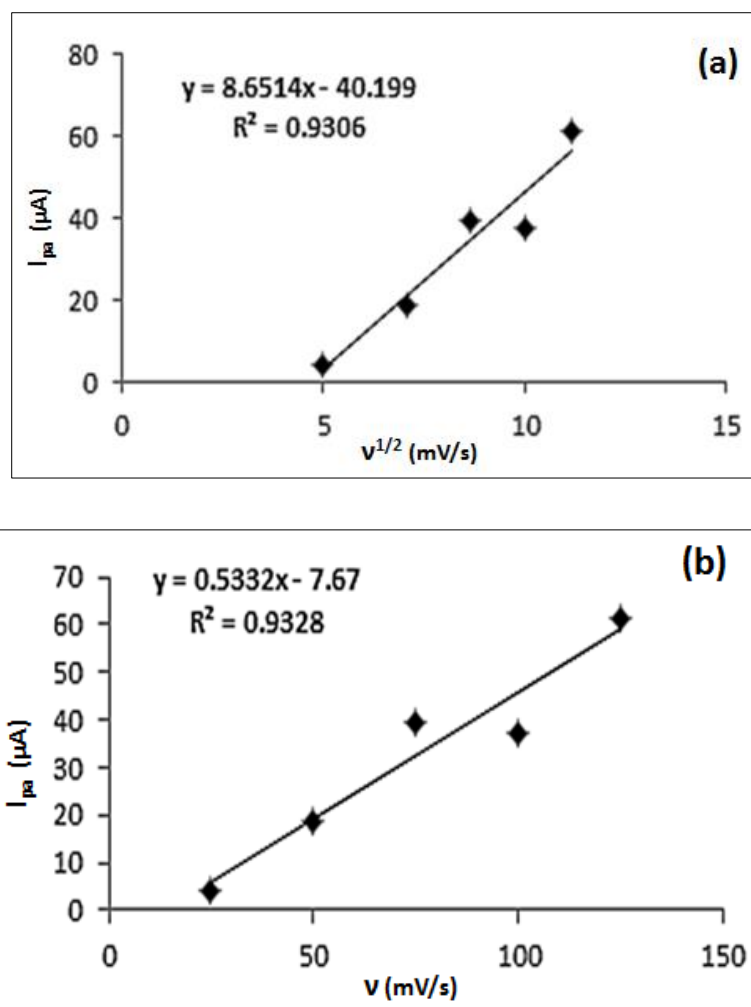


Figure 4.11 (a) I_{pa} vs. $v^{1/2}$ plot and (b) I_{pa} vs. v plot for GCE/ FA_{PBS}

On the other hand, GCE/ FA_{PBS} electrode showed a good linear correlation for I_{pa} vs. $v^{1/2}$ and I_{pa} vs. v (Figs. 4.11a and 4.11b). The linear regression equations (Eqs. 4.10 and 4.11) from I_{pa} vs. $v^{1/2}$ and i_{pa} vs v plots showed $R^2= 0.9306$ and $R^2= 0.9328$, respectively, where in both cases $R^2 \sim 1.0$, implying that the reaction might be partially diffusion controlled and partially adsorption controlled.

$$I_{pa} (\mu A) = 8.6514 v^{1/2} (mV/s) - 40.199 \quad (\text{Eq. 4.10})$$

$$I_{pa} (\mu A) = 0.5332 v^{1/2} (mV/s) - 7.67 \quad (\text{Eq. 4.11})$$

The assumptions that could be derived from the above-discussed empirical studies are as follows,

- a) The reaction is mostly but not solely diffusion controlled, where adsorption may play some roles in the overall electrochemical process associated with the oxidation of FA at GCE.
- b) The reaction is mostly but not solely adsorption controlled, where diffusion also plays some roles in the oxidation of FA at GCE.
- c) The reaction is both diffusion and adsorption controlled due to the fact that $R^2 = 0.93\sim 1.0$.

Under such circumstances, where it is ambiguous whether diffusion or adsorption is playing the vital role in the reaction kinetics of FA at GCE, a suitable scan rate could be chosen based on the information to be acquired from Figs. 4.8 and 4.9. From Figs. 4.8 and 4.9, it is quite evident that I_{pa} increases both for GCE/FA_{H2O} and GCE/FA_{PBS} with the increase in v . This increment was regular from 25 mV/s to 75 mV/s. However, for GCE/FA_{H2O}, I_{pa} was slightly decreased at 125 mV/s than at 100 mV/s, whereas for GCE/FA_{PBS}, I_{pa} was slightly decreased at 100 mV/s than at 75 mV/s. This observation comes with the useful information regarding the stability of FA on the modified GCE surface with the increase of scan rate. We can see that starting from 100 mV/s both GCE/FA_{H2O} and GCE/FA_{PBS} can show a slight deviation in the I_{pa} . Besides FA desorption from the GCE surface into the bulk electrolyte, another possible reason for this deviation could be attributed to the uncertainty at the noise level associated with the higher scan rates in an electrochemical system. At higher scan rate we increase the possibility of higher signal to noise ratio which means the system may face some disturbance due to the applied voltage at the working electrode. There are also other potential sources of noise in an electrochemical system, e.g., noise generated by the potentiostat itself and perturbation from the surrounding environment near the electrochemical system.

However, both too lower and higher scan rate may cause undesired voltammogram or voltammetric response. An increase in I_{pa} with an increase in v follows the rule of diffusion. A diffusion bilayer exists near to the GCE during electrochemical analysis, where the width of diffusion bilayer increases as the scan rate increases. When the width of diffusion bilayer increases the concentration gradient between the GCE and the bulk solution, it advocates more mass transfer from the bulk to the electrode surface and vice versa, resulting in an increased peak current. From this point of view, it might seem that if we increase the scan rate as high as possible that will produce a higher peak current

to design a good or robust electrochemical system. On a practical scenario, the more the scan rate the more the noise may occur in the system, hence the higher current generated may not always be considered for an accurate quantitative analysis. On the other hand, a very slow scan rate will reduce the diffusion bilayer near to the GCE surface resulting in a poor current signal due to the reduced mass transfer from the bulk electrolyte solution to the electrode and vice versa. In such a case it will be difficult to measure the I_{pa} for the detection of an analyte. Considering the facts discussed above, the scan rate of an electrochemical system should be optimized in a way so that it does not incur potential noise as well as can produce a significant value of I_{pa} for both qualitative and quantitative analysis of an electrochemical active species. The comparative study of GCE/FA_{H2O} and GCE/FA_{PBS} shows that the scan rate within a range of 75-100 mV/s could be considered for the quantitative analysis, where the 100 mV/s is able to produce a more significant signal of I_{pa} but the scan rate higher than 100 mV/s may include the potential noise in the electrochemical signal of I_{pa} . Bearing the above discussed facts and based on the comparative study of GCE/FA_{H2O} and GCE/FA_{PBS}, a scan rate of 100 mV/s to be followed for further electrochemical studies of GCE/FA_{H2O} and GCE/FA_{PBS} as well as for the detection of FR α in the next chapter of this study.

For more understanding toward the voltammetric response of both GCE/FA_{H2O} and GCE/FA_{PBS}, multi-cycles voltammogram at different scan rates for each electrode was recorded. Generally, for the quantitative purpose first and second scans are considered during data acquisition. However, multiple cycles can provide us useful information not only about the material's stability onto GCE but also a guideline about how many cycles for a specific electrochemical system could be valid for quantitative purpose and at what cycle the electrochemical reaction reaches the equilibrium. Based on these information in some cases the data obtained even from the third and the fourth cycles could be useful for quantitative analysis depending on the purpose of the electrochemical analysis.

In this work, while studying the comparative electrochemical behavior of GCE/FA_{H2O} and GCE/FA_{PBS}, four voltammetric cycles were recorded to obtain the information of the stability of GCE/FA_{H2O} and GCE/FA_{PBS} onto the active surface of GCE. Fig. 4.12 shows that GCE/FA_{H2O} maintains a well-defined I_{pa} both at higher and lower scan rates on the first cycle of CV. A significant noise was observed on the second cycle of

scanning at a scan rate of 125 mV/s. Nevertheless, at higher scan rates (125 mV/s-100 mV/s), I_{pa} decreases with the progress of further cycles but still provides a well-defined oxidation peak of FA up to four cycles.

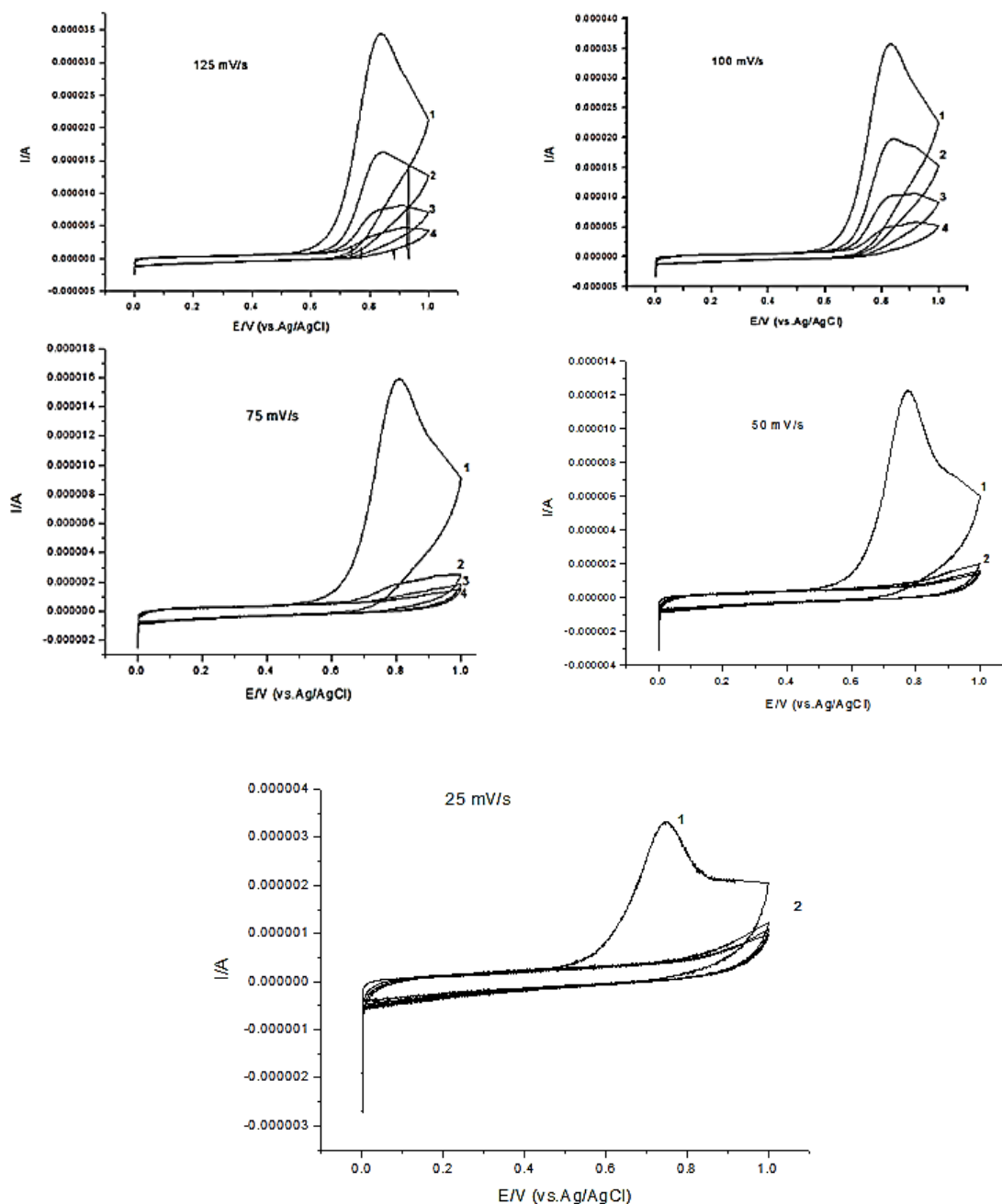


Figure 4.12 Multiscan CV of GCE/FA_{H2O} at different scan rates

At the scan rate of 75 mV/s anodic peak current became weak in intensity on the second cycle. At further slower scan rates of 50 and 25 mV/s, after the first cycle no oxidation peak was observed, implying that at slow scan rates after the first cycle almost all the FA onto GCE surface gets oxidized leaving no more FA onto GCE surface to go under further electrochemical reactions for the succeeding cycles. This may be due to that at slow scan rates the width of the diffusion bilayer becomes narrower as compared to that of a high scan rates and thus it takes longer time than the higher scan rates to oxidize FA onto GCE to produce a complete one cycle voltammogram. Thus, there is also a possibility for FA to leach out from the GCE surface during completing one cycle of voltammogram at a very slower scan rates. As a result, no further oxidation peak current was observed at 50 and at 25 mV/s after the first cycle of voltammetry.

Moving to the multicycle voltammogram profile of GCE/FA_{PBS} (Fig. 4.13), it was interesting to observe that GCE/FA_{PBS} showed more stable voltammograms in contrast to GCE/FA_{H₂O} both at higher and at lower scan rates.

The anodic oxidation of FA at GCE was continued up to three cycles scanning from 125 mV/s-50 mV/s, compared to GCE/FA_{H₂O} which was significant provided with the information of homogeneous distribution of FA onto GCE when it was modified with FA_{PBS}. In PBS, all the FA could homogeneously distribute and the adsorption of FA onto GCE was better when prepared in PBS solution. In H₂O the FA molecules are surrounded by only hydrogen bonds from water molecules and by the intermolecular Van der Waals forces, whereas in PBS the ionic poles of a FA molecule are more exposed to the cations and anions from the PBS which creates an ionic tension among the FA molecules and facilitates to self-assemble the FA particles onto GCE surface. Hence, comparatively a more homogeneous and stable coating of FA is achieved when FA solution is prepared in PBS and used to modify GCE. This assumption is also supported by the results obtained from I_{pa} vs. v plots (Fig. 4.11), where a linear correlation between the anodic peak current and scan rate was achieved.

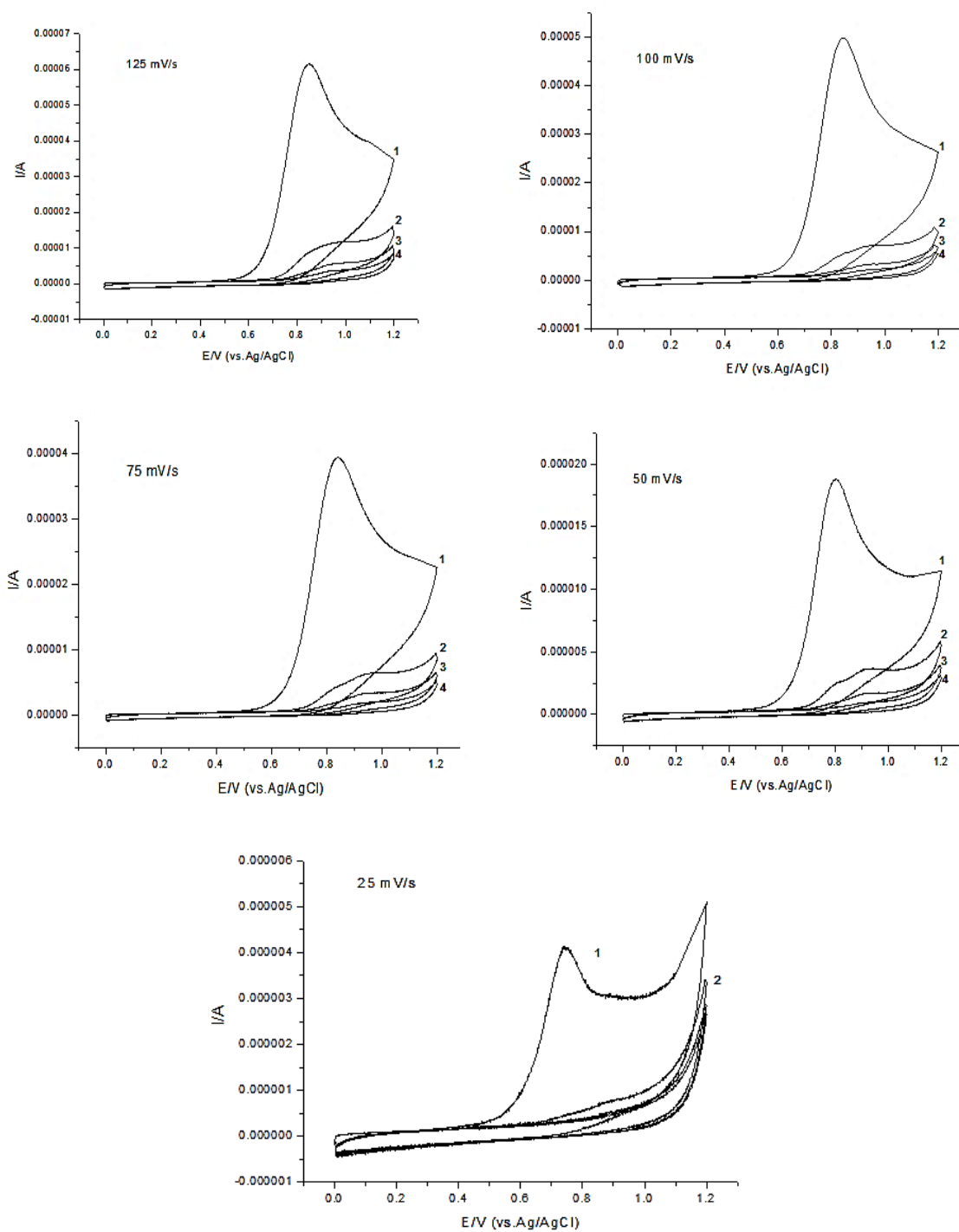


Figure 4.13 Multiscan CV of GCE/FA_{PBS} at different scan rates

Based on the above studies, it could be inferred that when FA_{H2O} is used the first cycle should be taken for the quantification purpose, whereas at higher scan rate up to 3 cycles could be used for quantification. Considering the physicochemical stability of FA_{H2O}

vs. FA_{PBS} based on the electroanalytical observations obtained from CV analysis, it is apprehended that FA_{PBS} could be preferable to be used for the detection of $FR\alpha$, at $50 \text{ mV/s} \leq \nu \leq 125 \text{ mV/s}$.

The analytical information discussed above for both FA_{H_2O} and FA_{PBS} shows that compared to FA dispersion prepared only in water FA solution prepared in PBS can produce a more stable, reliable and mathematically comprehensible results based on the effect of scan rate, multi-cycle analysis and linear dependence of I_{pa} in relation to the varying scan rates. Hence, hereinafter FA solution prepared in PBS will be considered to be the suitable one for the detection of $FR\alpha$ at a suitable scan rate of 100 mV/s , where at 100 mV/s scan rate the anodic peak current response is higher enough for quantification, as well as lower the risk of FA desorption from the surface of GCE into the electrolyte.

4.3.5 Reaction mechanism

The electron transfer process at the working electrode is described based on the concept of forming an electric double layer at and near to the electrode surface which forms when a voltage or electric energy is supplied on the electrode that is being dipped into an electrolyte or conductive liquid. Electrochemical reaction kinetics at the working electrode surface, whether oxidation or reduction, is guided by other phenomenon e.g. the mass transfer of ions from the bulk to the electrode, interfacial chemistry between the solution and electrode interface, adsorption and desorption energy of the material to be analyzed, heterogeneous rate of electron transfer, any side reactions, deposition of any products or byproducts onto the electrode followed by any side reaction(s).

When the voltage is applied on the working electrode, a diffusion layer is formed between the bulk solution and the electrode surface where the movement of the ionic species (cations and anions), both from the electrode surface toward the solution and from the solution toward the electrode surface, is dominated by the mass transport phenomena. On this context, it is better to illuminate the fact that the mass transport phenomenon that is the flow of ions from the bulk solution to the electrode surface and vice versa is mostly governed by diffusion within the diffusion bilayer; however, the

other two techniques of mass transport, e.g. migration and convection may also have some effects on the movements of ions based on different experimental conditions.

In relation to the diffusion layer, an electric double layer is formed at the electrode-solution interface. Electric double layer concept is well-explained by two popular models known as Helmholtz and Gouy-Chapman models (Oldham et al, 2011). According to the electric double layer concept, within a very minimum distance (1 \AA to -1 nm) between the GCE and PBS (electrolyte solution) the electric double layer is divided into two sublayers, termed as compact and diffuse layer. The compact layer is at contact with the GCE, also known as the Helmholtz layer. The adjacent diffuse layer is known as Gouy-Chapman layer. The charge distributions of FA and potential changes are the phenomenon occurring in this zone, hence coined as electric double layer. Next to the electric double layer, the diffusion layer is the zone where the transfer of chemical species or ions to and from the electrode and the bulk electrolyte takes place through migration and/or diffusion.

Figs. 4.14 and 4.16 are presented here to show the schemes of a standard electric double layer environment and the electric double layer of the GCE modified with FA_{PBS}, respectively.

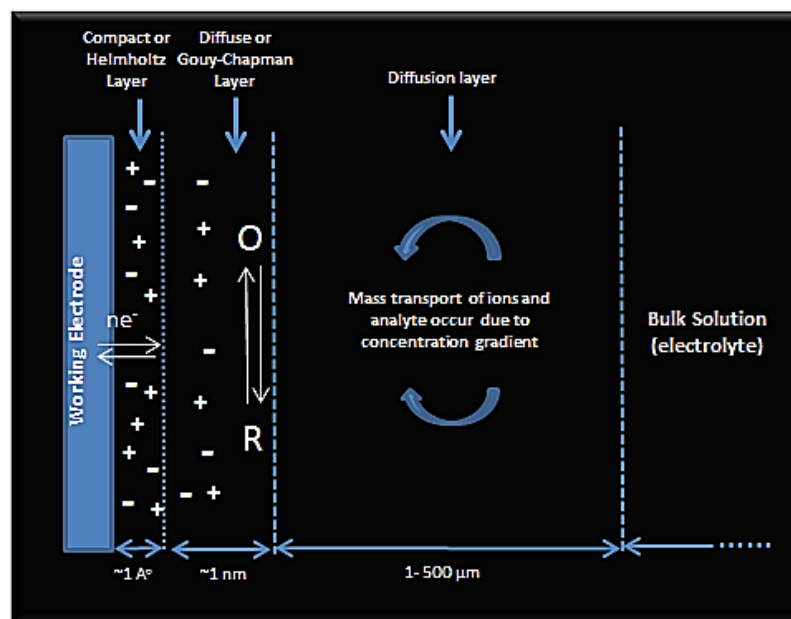


Figure 4.14 Electrode-solution interface for an ideal reversible reaction

Fig. 4.14 represents an ideal electric double layer model where a reversible reaction occurs at the electrode surface under the applied voltage. A very common example of this type of reaction is the $\text{Fe}(\text{CN})_6^{3-/4-}$ redox couple reaction (Eq. 4.5) which produces a reversible voltammogram (Fig. 4.5). In this ideal situation where, only charge transfer from electrode surface to the electric double layer and vice versa occurs, and no other subsidiary electrochemical/chemical/catalytic phenomenon appears hence the reaction mechanism involves simple electron transfer from electrode to the electrochemically active species in the electrolyte and vice versa, which could be observed during the reversible reaction of $\text{Fe}(\text{CN})_6^{3-/4-}$ redox couple.

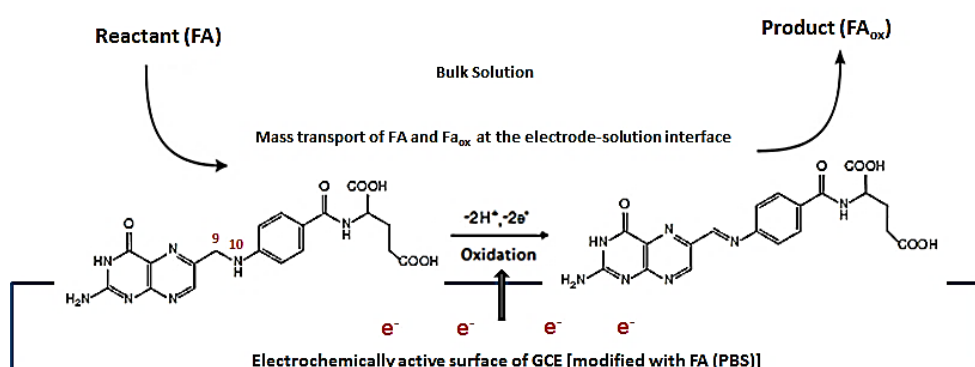


Figure 4.15 The irreversible reaction (oxidation) of FA at the surface of GCE

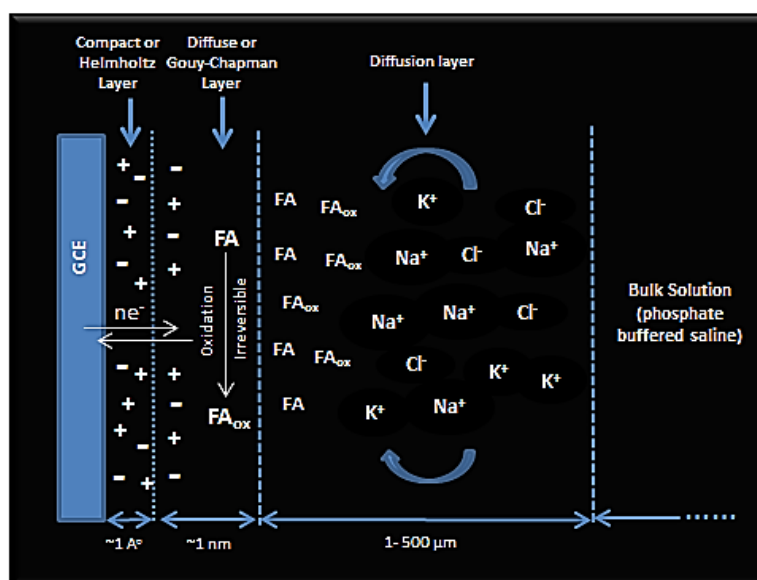


Figure 4.16 Electrode-solution interface for the irreversible electron transfer mechanism during oxidation of FA at GCE

Whereas, the electrochemical oxidation phenomenon of FA occurring in the electric double layer zone is not reversible (Fig. 4.16); in this case the applied voltage or electric energy creates a potential difference between the GCE surface and the electric double layer at GCE, where FA onto GCE surface becomes oxidized. As per previous studies (Yardim and Entürk, 2014; Maiyalagan *et al.*, 2013), the oxidation reaction of FA onto GCE follows 2 electron transfer generating dehydrofolic acid, where the oxidation takes place at C9 and N10 position of the FA molecule (Fig. 4.15). In a blank solution of PBS (in absence of analyte) no electroactive ions take part in this reaction from the bulk solution unless the ions from the electrolyte itself are capable to be reduced/oxidized at the applied voltage at GCE, which in this case, has been ignored by choosing a positive potential window in between 0 to +1.2. The current generated due to the oxidation of FA onto GCE is characterized as the Faradic current. However, in an electrochemical system the measured current is often a combination of both Faradic and background current. The background current could be encountered in an electrochemical system due to IR drop as a result of resistance from the electrolyte solution. Other possibilities e.g. any ions other than the targeted analyte from the electrolyte participating in the reaction at the electrode, the electrode itself undergoes reaction under the applied potential, and current generated due to any impurities present in the solution or onto GCE during an electrochemical analysis may potentially contribute to the background current. In the current study, while all these factors were taken care of prior to and during all the electrochemical analysis of FA, the anodic peak current of FA could be attributed to the Faradic current produced mainly due to the oxidation of FA to dehydrofolic acid. This provides us with the information that charge transfer between the GCE and FA molecules onto GCE is 'the principal' but not necessarily 'the only' phenomenon that governs the entire electrochemical process of FA onto GCE, where there might be some underlying possibilities concurrently taking place therein.

Since FA is pH sensitive the mechanism described here may not follow for the oxidation/reduction of FA at a different pH value in a different three-electrode system. In fact, in the current study there might be some underlying consequences as a result of this irreversible oxidation of FA onto GCE. Further research question could be raised on the matter that what happens to the oxidized FA (FA_{ox}) molecules immediately after their formation on or near to the GCE surface, as till to date (to the best knowledge of the author) no concrete mechanisms have yet been established focusing on this matter

to investigating the other possibilities associated with the oxidation of FA onto GCE and elucidating the underlying phenomenon taking place in the electric double layer for the oxidation of FA onto GCE. In the current electrochemical system, dehydrofolic acid, which is the immediate product generated at the electrode surface due to the oxidation of FA, may deposit onto GCE or undergo further degradation or oxidation/reduction, however in such cases if the secondary reaction(s) of dehydrofolic acid progress in a substantial manner that will produce a corresponding peak to that reaction besides the characteristic oxidation peak of FA.

In the current study by analyzing the voltammogram obtained for the electrochemical change(s) of FA within a positive potential window it is conceived that the electrochemical change of FA to FA_{ox} may follow EC or pseudo ECE mechanism, where a straightforward simple electrode reaction of FA oxidation occurs at GCE which is an electrode-surface-specific reaction (denoted by E). However, there are possibilities for FA and/or for the FA_{ox} to undergo further reaction which could be defined as both electrode reaction(s) in combination with chemical reaction(s) (denoted by C). On this context, further possibilities are that rather than depositing onto GCE it travels through the electric double layer to the diffusion layer where a chemical interaction between the FA_{ox} and the ions of PBS may occur as well. In addition to this, not all the FA onto GCE can finally take part in the oxidation reaction; some may desorb from GCE surface into the bulk. The interesting thing is that the desorbed FA could also travel back to the GCE surface due to the continuous mass transport from the bulk toward the GCE and vice versa. From the above discussion it is evident that while at the electrode interface the main electrochemical reaction is the oxidation of FA, subsequently this reaction could be interfered by other possible phenomena of side reactions and migration of different ions back and forth in between the electrode-solution interface. These assumptions are also supported by the I_{pa} vs. $v^{1/2}$ and I_{pa} vs. v plots (Figs. 4.11a and 4.11b) and linear regression equations (Eq. 4.10 and 4.11) obtained for GCE/FA_{PBS}, where it was observed that the anodic oxidation of FA onto GCE could be partially due to diffusion and partially due to adsorption controlled.

Although, in the current study at a fixed pH of 7.4 in PBS buffer the voltammogram of FA does not exhibit any additional peak toward that assumption of multiple reactions (ECE) but it needs to be noted that the oxidation (even reduction) of FA is highly influenced by pH and the buffer used for electroanalytical purpose. Yardim and Entürk

(2014) showed that the oxidation of FA can produce a two-peak voltammogram in a wider positive potential (> 1.2 V) in BR buffer in highly acidic medium, which eventually disappears in a neutral to alkaline medium resulting in a single well-defined broad oxidation peak. However, the underlying mechanism and the possibilities behind the two-oxidation peaks were still ambiguous and left unexplained. It was also reported that in an aqueous electrolyte solution FA has different ionic forms hence making it possible to even go for six acidic disassociations of FA (Tyagi and Penzkofer 2010). Hence, while designing a FA-based biosensor the other possibilities that the oxidation of FA may follow a pseudo EC or ECE mechanism of reaction(s) should also be considered, where an electrochemical (E) phenomenon could be followed by a successive chemical (C) reaction(s) and then again by an electrochemical (E) reaction(s) where the product(s) of the chemical reaction(s) itself could also be electrochemically active.

4.4 Summary of the Current Chapter and Direction to the Next Chapter

Although $\text{FA}_{\text{H}_2\text{O}}$ is free from other ions (except ions from the water itself) and thus is perceived to help developing a more facile electrochemical system but it is unable to provide a similar pH condition of the physiological fluid, which is one of the important conditions to be followed in designing a biosensor for the detection of $\text{FR}\alpha$. Moreover, the solubility of FA in water is too low to confirm a very homogeneous distribution of FA onto GCE surface which caused a non-linear correlation between the anodic peak current of FA with the varying scan rates. Whereas, for FA_{PBS} , FA molecules could be homogeneously mixed in PBS, hence ensures a more stable as well as homogeneous distribution of FA particles onto GCE surface. The relationship between the anodic peak current (I_{pa}) and scan rate (v) was well analyzed with two models of correlation in this study; I_{pa} vs. $v^{1/2}$ and I_{pa} vs. v , where both the plots generated linear correlation for FA_{PBS} . This provides some interesting information toward further studies that the electrochemical change of FA molecules onto GCE surface is not quite straightforward, bearing in mind that the current observation may differ based on the other variables in a different electrochemical system. Here in the comparative electrochemical study, between $\text{FA}_{\text{H}_2\text{O}}$ and FA_{PBS} , no linear correlation was observed for $\text{FA}_{\text{H}_2\text{O}}$ for its I_{pa} vs. $v^{1/2}$ and I_{pa} vs. v plots emphasizing that $\text{FA}_{\text{H}_2\text{O}}$, if used for the detection purpose, a quantitative analysis will be difficult to achieve for the detection of $\text{FR}\alpha$. Hence, for the fabrication of a FA based FR biosensor, FA_{PBS} will be better compared to $\text{FA}_{\text{H}_2\text{O}}$ for

the quantitative analysis. As for future directions, care should be taken while preparing GCE/ FA_{PBS} for the detection of FR α that FA needs to be dried properly onto GCE so all the FA gets settled properly onto GCE prior to any CV scan for any electroanalytical purposes. It is extremely recommended to dry FA onto GCE at room temperature, as drying by heating will not only degrade the molecular structure of FA but will also affect the shelf-life of GCE. It is also recommended to use the modified GCE immediately after preparation as a long-time exposure and/or storage may reduce the activity of the modified electrode, due to FA degradation, airborne contamination and contamination from handling; as the modified GCE becomes contaminated or deactivated it is no longer suitable for any electrochemical analysis until it is properly cleaned and modified again by repeated polishing and pretreatments. Additional attention to be paid regarding the 'leaching' issue of FA from the GCE surface during electrochemical analysis, as the loss in the signal due to the leaching out of FA from GCE surface into the electrolyte solution can occur. Loss of some of the FA from the GCE surface is almost difficult to avoid in all circumstances, which is applicable for any other materials (even in presence of a binder) used to modify a working electrode. However, the loss could be prevented in a significant manner if special care is given during connecting the modified GCE in the electrochemical system, once all the connections are set the GCE should be then connected to the potentiostat and the scan should be started immediately so that GCE does not need to stay longer time in the electrolyte. This practice will help reducing the loss of FA to a great extent and was followed thoroughly in this study. Also, any vibration or stirring should be avoided (unless that is one of the conditions of the experiments) during the CV scan for an electrochemical analysis.

As a continuation of the outcomes of the current chapter, the next chapter is designed with the following scopes for the detection of FR α by a GCE modified with FA_{PBS} and the synthesized fulleranol [C₆₀(OH)₈.2H₂O].

- Repeatability of the voltammetric response of GCE/FA_{PBS}
- Detection of FR α at CGE modified with FA_{PBS}
- Detection of FR α at GCE modified with both FA_{PBS} and C₆₀(OH)₈.2H₂O
- Calculation and determination of the selectivity, reproducibility, repeatability and the LOD of the proposed biosensor for FR α .

References

- Aguirre, C. M., Levesque, P. L., Paillet, M., Lapointe, F., St-Antoine, B. C., Desjardins, P., & Martel, R. (2009). The role of the oxygen/water redox couple in suppressing electron conduction in field-effect transistors. *Advanced Materials*, 21(30), 3087-3091.
- Akbar, S., Anwar, A., & Kanwal, Q. (2016). Electrochemical determination of folic acid: A short review. *Analytical Biochemistry*, 510, 98-105.
- Ananthi, A., Kumar, S. S., & Phani, K. L. (2015). Facile one-step direct electrodeposition of bismuth nanowires on glassy carbon electrode for selective determination of folic acid. *Electrochimica Acta*, 151, 584-590.
- Araoyinbo, A. O., Nazree Derman, M., Rahmat, A., & Rafezi Ahmad, K. (2013). Electrochemical measurement of PBS using cyclic voltammetry and AAO fabricated at ambient temperature and low potential. *Advanced Materials Research* 795, 654-657.
- Arvand, M., Pourhabib, A., & Giahi, M. (2017). Square wave voltammetric quantification of folic acid, uric acid and ascorbic acid in biological matrix. *Journal of Pharmaceutical Analysis*, 7(2), 110-117.
- Bettio, A., Honer, M., Müller, C., Brühlmeier, M., Müller, U., Schibli, R., Groehn, V., Schubiger, A.P., & Ametamey, S.M. (2006). Synthesis and preclinical evaluation of a folic acid derivative labeled with ¹⁸F for PET imaging of folate receptor-positive tumors. *Journal of Nuclear Medicine*, 47(7), 1153-1160.
- Bhunia, S. K., Maity, A. R., Nandi, S., Stepensky, D., & Jelinek, R. (2016). Imaging cancer cells expressing the folate receptor with carbon dots produced from folic acid. *ChemBioChem*, 17(7), 614-619.
- Bollella, P., Schulz, C., Favero, G., Mazzei, F., Ludwig, R., Gorton, L., & Antiochia, R. (2017). Green synthesis and characterization of gold and silver nanoparticles and their application for development of a third generation lactose biosensor. *Electroanalysis*, 29(1), 77-86.
- Canales, C., Gidi, L., & Ramírez, G. (2015). Electrochemical activity of modified glassy carbon electrodes with covalent bonds towards molecular oxygen reduction. *International Journal of Electrochemical Science*, 10, 1684-1695.

- Heinze, J. (1984). Cyclic voltammetry— “electrochemical spectroscopy”. New analytical methods (25). *Angewandte Chemie International Edition*, 23(11), 831-847.
- House, J. L., Anderson, E. M., & Ward, W. K. (2007). Immobilization techniques to avoid enzyme loss from oxidase-based biosensors: a one-year study. *Journal of Diabetes Science and Technology*, 1(1), 18-27.
- Jiang, X. L., Li, R., Li, J., & He, X. (2009). Electrochemical behavior and analytical determination of folic acid on carbon nanotube modified electrode. *Russian Journal of Electrochemistry*, 45(7), 772-777.
- Kissinger, P. T., & Heineman, W. R. (1983). Cyclic voltammetry. *Journal of Chemical Education*, 60(9), 702.
- Konopka, S. J., & McDuffie, B. (1970). Diffusion coefficients of ferri- and ferrocyanide ions in aqueous media, using twin-electrode thin-layer electrochemistry. *Analytical Chemistry*, 42(14), 1741-1746.
- Lamas-Ardisana, P. J., Fanjul-Bolado, P., & Costa-García, A. (2015). Hydrogen evolution: Electrochemical pretreatment for voltammetric analysis with gold electrodes. *Electroanalysis*, 27(5), 1073-1077.
- Laursen, A.B., Varela, A.S., Dionigi, F., Fanchiu, H., Miller, C., Trinhammer, O.L., Rossmeisl, J., & Dahl, S. (2012). Electrochemical hydrogen evolution: Sabatier's principle and the volcano plot. *Journal of Chemical Education*, 89(12), 1595-1599.
- Lavanya, N., Fazio, E., Neri, F., Bonavita, A., Leonardi, S. G., Neri, G., & Sekar, C. (2016). Electrochemical sensor for simultaneous determination of ascorbic acid, uric acid and folic acid based on Mn-SnO₂ nanoparticles modified glassy carbon electrode. *Journal of Electroanalytical Chemistry*, 770, 23-32.
- Lee, R. J., & Low, P. S. (1994). Delivery of liposomes into cultured KB cells via folate receptor-mediated endocytosis. *Journal of Biological Chemistry*, 269(5), 3198-3204.
- Li, H., Cheng, Y., Liu, Y., & Chen, B. (2016). Fabrication of folic acid-sensitive gold nanoclusters for turn-on fluorescent imaging of overexpression of folate receptor in tumor cells. *Talanta*, 158, 118-124.

- Li, S., Singh, J., Li, H., & Banerjee, I. A. (Eds.). (2011). Biosensor nanomaterials. John Wiley & Sons.
- Mabbott, G. A. (1983). An introduction to cyclic voltammetry. *Journal of Chemical Education*, 60(9), 697.
- Mahadevan, A., & Fernando, S. (2017). An improved glycerol biosensor with an Au-FeS-NAD-glycerol-dehydrogenase anode. *Biosensors and Bioelectronics*, 92, 417-424.
- Maiyalagan, T., Sundaramurthy, J., Kumar, P. S., Kannan, P., Opallo, M., & Ramakrishna, S. (2013). Nanostructured α -Fe₂O₃ platform for the electrochemical sensing of folic acid. *Analyst*, 138(6), 1779-1786.
- Mirmoghtadaie, L., Ensafi, A. A., Kadivar, M., Shahedi, M. & Ganjali, M. R. (2013). Highly selective, sensitive and fast determination of folic acid in food samples using new electrodeposited gold nanoparticles by differential pulse voltammetry. *International Journal of Electrochemical Science*, 8, 3755-67.
- Moyo, M., Okonkwo, J. O., & Agyei, N. M. (2012). Recent advances in polymeric materials used as electron mediators and immobilizing matrices in developing enzyme electrodes. *Sensors*, 12(1), 923-953.
- Nicholson, R. S. (1965). Theory and application of cyclic voltammetry for measurement of electrode reaction kinetics. *Analytical Chemistry*, 37(11), 1351-1355.
- Ojani, R., Raoof, J. B., & Zamani, S. (2009). Electrocatalytic oxidation of folic acid on carbon paste electrode modified by nickel ions dispersed into poly (o-anisidine) film. *Electroanalysis*, 21(24), 2634-2639.
- Oldham, K., Myland, J., & Bond, A. (2011). Electrochemical science and technology: fundamentals and applications. John Wiley & Sons.
- Parker, N., Turk, M. J., Westrick, E., Lewis, J. D., Low, P. S., & Leamon, C. P. (2005). Folate receptor expression in carcinomas and normal tissues determined by a quantitative radioligand binding assay. *Analytical Biochemistry*, 338(2), 284-293.
- Pocard, N. L., Alsmeyer, D. C., McCreery, R. L., Neenan, T. X., & Callstrom, M. R. (1992). Doped glassy carbon: a new material for electrocatalysis. *Journal of Materials Chemistry*, 2(8), 771-784.

Qiao, J., Dong, P., Mu, X., Qi, L., & Xiao, R. (2016). Folic acid-conjugated fluorescent polymer for up-regulation folate receptor expression study via targeted imaging of tumor cells. *Biosensors and Bioelectronics*, 78, 147-153.

Qiao, W., Li, Y., Wang, L., Li, G., Li, J., & Ye, B. (2015). Electrochemical behavior of daphnetin and its sensitive determination based on electrochemically reduced graphene oxide modified electrode. *Journal of Electroanalytical Chemistry*, 749, 68-74.

Rusling, J. F., & Suib, S. L. (1994). Characterizing materials with cyclic voltammetry. *Advanced Materials*, 6(12), 922-930.

Sudimack, J., & Lee, R. J. (2000). Targeted drug delivery via the folate receptor. *Advanced Drug Delivery Reviews*, 41(2), 147-162.

Taherkhani, A., Jamali, T., Hadadzadeh, H., Karimi-Maleh, H., Beitollahi, H., Taghavi, M., & Karimi, F. (2014). ZnO nanoparticle-modified ionic liquid-carbon paste electrode for voltammetric determination of folic acid in food and pharmaceutical samples. *Ionics*, 20(3), 421-429.

Torati, S. R., Reddy, V., Yoon, S. S., & Kim, C. (2016). Electrochemical biosensor for Mycobacterium tuberculosis DNA detection based on gold nanotubes array electrode platform. *Biosensors and Bioelectronics*, 78, 483-488.

Tyagi, A., & Penzkofer, A. (2010). Fluorescence spectroscopic behaviour of folic acid. *Chemical Physics*, 367(2), 83-92.

Unnikrishnan, B., Yang, Y. L., & Chen, S. M. (2011). Amperometric determination of folic acid at multi-walled carbon nanotube-polyvinyl sulfonic acid composite film modified glassy carbon electrode. *International Journal of Electrochemical Science*, 6, 3224-3237.

Vaze, V. D., & Srivastava, A. K. (2007). Electrochemical behavior of folic acid at calixarene based chemically modified electrodes and its determination by adsorptive stripping voltammetry. *Electrochimica Acta*, 53(4), 1713-1721.

Wang, T., Reid, R. C., & Minter, S. D. (2016). A paper-based mitochondrial electrochemical biosensor for pesticide detection. *Electroanalysis*, 28(4), 854-859.

Wei, S., Zhao, F., Xu, Z., & Zeng, B. (2006). Voltammetric determination of folic acid with a multi-walled carbon nanotube-modified gold electrode. *Microchimica Acta*, 152(3), 285-290.

Wu, Z., Li, X., Hou, C., & Qian, Y. (2010). Solubility of folic acid in water at pH values between 0 and 7 at temperatures (298.15, 303.15, and 313.15) K. *Journal of Chemical & Engineering Data*, 55(9), 3958-3961.

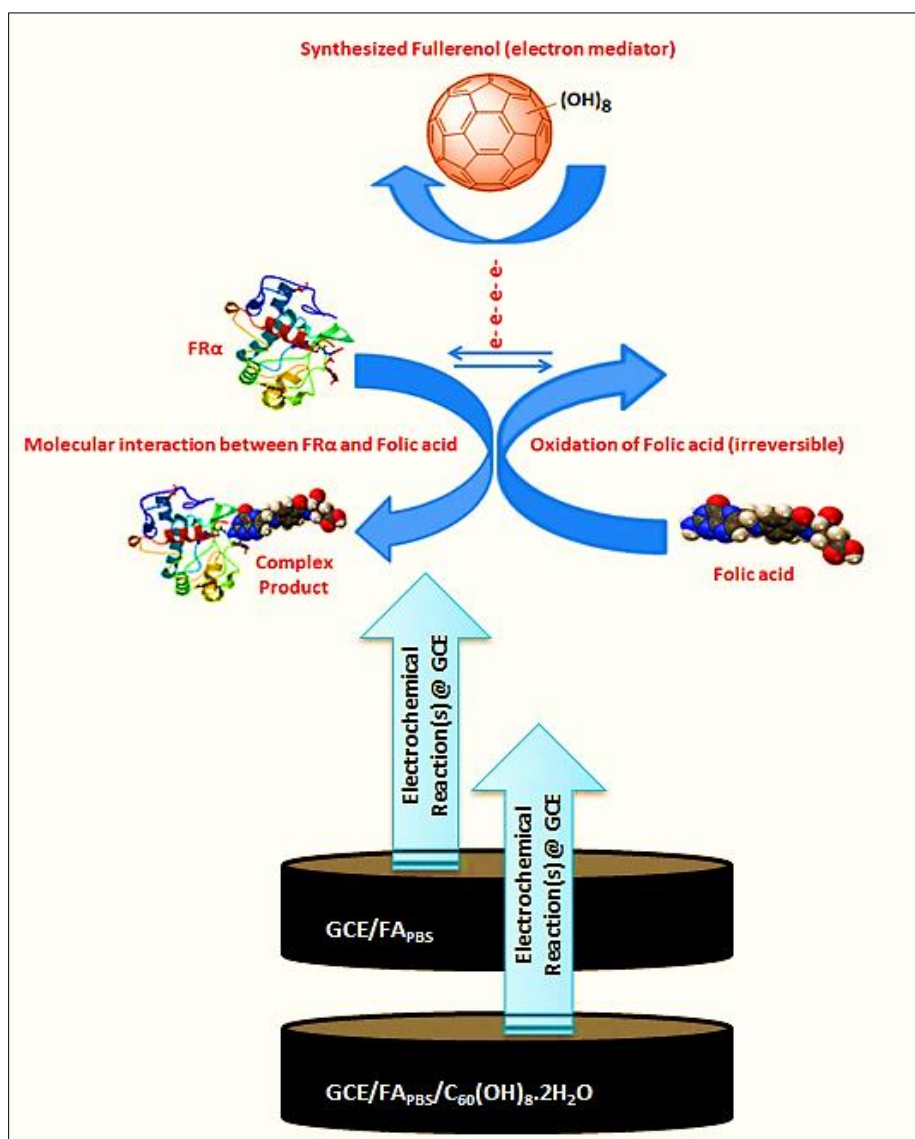
Yardim, Y., & Şenturk, Z. (2014). Electrochemical behavior of folic acid at a boron-doped diamond electrode: Its adsorptive stripping voltammetric determination in tablets. *Turkish Journal of Pharmaceutical Sciences*, 11(1), 87–100.

Zhang, D., Ouyang, X., Ma, W., Li, L., & Zhang, Y. (2016). Voltammetric determination of folic acid using adsorption of methylene blue onto electrodeposited of reduced graphene oxide film modified glassy carbon electrode. *Electroanalysis*, 28(2), 312-319.

Chapter 5

Synthesized fullereneol [$C_{60}(OH)_8 \cdot 2H_2O$]-mediated-folic acid-based biosensor for the detection of folate receptor alpha ($FR\alpha$)

Graphical Abstract



Abstract

Folate receptor alpha (FR α) is a cell-membrane glycoprotein considered as one of the biomarkers for the epithelial-derived cancer. In this study, synthesized fullereneol [C₆₀(OH)₈.2H₂O] prepared by the ultrasonic-assisted technique will be applied to develop a folic acid (FA)- based biosensor for the detection of folate receptor alpha (FR α). The proposed biosensor shows that synthesized C₆₀(OH)₈.2H₂O has the potential to be used as a mediator in fabricating folic acid-based biosensor for the detection of folate receptor alpha, where C₆₀(OH)₈.2H₂O impacts significantly in minimizing the anodic peak current of folic acid in the absence of folate receptor alpha which continues further in the presence of FR α , thus follows a gradual decreasing trend of the anodic peak current in the proposed biosensor. Upon quantitative analysis based on cyclic voltammetry and chronoamperometry, the proposed biosensor showed 93% stability and 86% reproducibility, and the lower limit of detection was limited to 1 nM. Current data underline that C₆₀(OH)₈.2H₂O could be considered as a potential nanomediator in fabricating folic acid-based biosensor for the detection of folate receptor alpha, but for devising a point-of-care diagnostic tool for the early stage detection of cancer, future studies should be undertaken to mitigate few drawbacks. e.g. increasing the stability of folic acid onto glassy carbon electrode as well as establishing a facile way to compose a stronger conjugation between folic acid and synthesized C₆₀(OH)₈.2H₂O without compromising the molecular interaction between folic acid and folate receptor alpha.

5.1 Introduction

5.1.1 FR α as a potential cancer biomarker

Folate receptor alpha, synonymized as FR α , FBP, FOLR1, is a cell-membrane glycoprotein, which is mainly expressed on the apical surface of a subset of polarized epithelial cells (O'Shannessy *et al.*, 2011). In human this protein is encoded by the FOLR1 gene which plays an important role in human metabolism in binding and transporting physiological level of folate into cells which is an essential biomolecule in DNA synthesis and replication, cell division, and growth, and survival. Folic acid is a nutrient for rapidly dividing cancer cells and FR α has high affinity to folic acid or folate; so, during the cancer cell growth an increased uptake of folic acid into the cells often leads to the overexpression of FR α . It has been reported after several observation and investigation that overexpression of FR α could be a prominent sign in epithelial derived tumors and can be related to cancer prognosis. Therefore, it could be considered as a potential biomarker in early stage of cancer progression and diagnosis (Bueno *et al.*, 2001). Specifically, FR α has been investigated widely in diagnosing ovarian, lung, breast, bladder and pancreatic cancer (Cai *et al.*, 2017; Dhawan *et al.*, 2013; O'Shannessy *et al.*, 2012a; O'Shannessy *et al.*, 2012b; Kalli *et al.*, 2008). As a result of numerous cancer study reports, among four genres of folate receptors, e.g., folate receptor alpha, beta, and gamma (Zwicke *et al.*, 2012; O'Shannessy *et al.*, 2011; Shakeri-Zadeh *et al.*, 2010), FR α is the mostly reported a biomarker for identifying malignancy in cancer etiology.

5.1.2 Correlation between FR α and folate/FA in cancer etiology

As a member of the FOLR1 gene family, FR α has high affinity to folic acid (FA) and several reduced folic acid derivatives (folate). These two terms i.e. folic acid (FA) and folate might be confusing in many cases, while these two terms are often used interchangeably. In actual case, folate is the generic term for FA and structurally related compounds that have the biochemical activity of FA, also known as B vitamin or vitamin B9. Folate is the nutrient in cell division mechanism and plays very important role in DNA synthesis and other cell division phenomena. Folate deficiency is associated with increased chromosomal strand breaking and abnormal methylation

reaction in DNA synthesis and replication which is implicated in cancer (Kelemen *et al.*, 2006). Expression of the FR α gene, FOLR1, is regulated by extracellular folate depletion, and thus there is a proportional relation between FR α and folate in cancer etiology which could be expressed as follows:

If, the depletion of extracellular folate or folic acid (FA) = FA_(depletion)

and, overexpression of FR α in cancer cell lines = FR α _(overexpression)

$$FA_{(depletion)} = f[FR\alpha_{(overexpression)}] \quad (\text{Eq. 5.1a})$$

$$\text{where, } FA_{(depletion)} \propto FR\alpha_{(overexpression)} \quad (\text{Eq. 5.1b})$$

Eq. 5.1a implies that the depletion of extracellular folic acid is a function (f) of the amount of FR α in cancer cell lines. In another word, the overexpression of FR α gene, FOLR1, is proportionally regulated by extracellular folate depletion (Eq. 5.1b).

More elaborately, the phenomenon of cancer progression encompasses rapid division of abnormal cells with altered genes which is closely associated with a higher requirement of FA to maintain the DNA synthesis. FR α plays the vital role; it modulates FA uptake from serum to the cells' interior to furnish the continuous demand of FA for rapidly dividing cancer cells under low folate condition. This ultimately results in an overexpression of FR α in the cell membrane. Previous and recent reports on the role of folate receptor show that overexpression of FR α on cell membrane and its presence in the human serum could be a precursor of cancer progression, given the facts that healthy human serum does not contain FR α and its amount on normal cell surface is also restricted to a certain amount which aberrantly increase when the cells undergo cancer progression (Ledermann *et al.*, 2015; O'Shannessy *et al.*, 2013).

This biological correlation has recently been adopted as the main strategy in designing a biosensor for the detection of FR α in view to providing advanced solution toward the early stage detection of cancer. In fact, this correlation has significantly been used in the applications of not only in early stage of cancer diagnosis but also in the receptor-mediated chemotherapy for the treatment and monitoring cancer (Cheung *et al.*, 2016; Assaraf *et al.*, 2014; Salazar and Ratnam 2007; Lu *et al.*, 2004). However, the underlying 'facts and factors' that can explain the mechanism about how FR α binds to folate and folate-conjugated drugs is still subject to further research and investigation.

Meanwhile, several studies have already been reported that FA could perform better as a biorecognition tool in association with a mediator for the detection of FR α , where in most of the cases nanomaterials were highly pronounced as the mediator/nanomediator in developing a receptor-mediated targeting therapy for many cancers e.g. leukemia cells, PC3 cells and ovarian tumor (Huang *et al.*, 2011; Shakeri-Zadeh *et al.*, 2010; Nie *et al.*, 2007).

5.1.3 Application of synthesized fullerol [C₆₀(OH)₈.2H₂O] in the detection of FR α

The performance of a FA-based biosensor for the detection of FR α could be enhanced in association with other nanoparticles (Zwicke *et al.*, 2012). The reason behind using the other nanoparticles in association to FA is that due to the molecular affinity between FA and FR α , FA will interact spontaneously with FR α , where the nanoparticles conjugated or physically attached to FA perform as the electron mediator in enhancing the electrochemical signal generated due to the interaction between FA and FR in a biosensor. However, the mechanism of this interaction is much complex as well as the combination of FA and different nanoparticles in detecting FR α is diverse. In fact, ‘enhancing the electrochemical signal’ not necessarily always refers to the gradual increase of anodic/cathodic current in the presence of an analyte, in some cases it was reported as to rather decreasing gradually in the presence of an analyte. Therefore, in interpreting the sensitivity of a biosensor as well as for the qualitative and quantitative analysis of a targeted analyte, the more appropriate approach is to identify any significant change or shift in the anodic/cathodic peak currents and in the potential.

Nanoparticles, especially carbon nanoparticles have been reported in many studies as the potential nanomediator to enhancing the electrochemical signal generated during a chemical phenomenon occurring at the working electrode surface in fabricating a highly sensitive biosensor. Various combinations of receptor-mediator have been proposed in many studies in developing a highly sensitive and selective electrochemical biosensor for the detection of various bio-analytes (Topkaya *et al.* 2016), where modified fullerene or fullerene derivatives could contribute in charge separation and charge transfer which can enhance the electrochemical signal generated due to the reaction

between the recognition element (FA) and analyte (FR α) in a biosensor. Nevertheless, on this context, the application of fullerene derivatives is still less explored, more specifically, the application of fullerenols synthesized by the recent advanced methods, e.g. synthesis using phase transfer catalyst (PTC) and using the potential technique of ultrasonication, have not yet been taken under any investigations to preparing a biosensor for the detection of FR α . Based on this scenario, in the current study, fulleranol synthesized by the proposed method of ultrasonication has been applied for the preparation of a FA-based biosensor in detecting FR α . Herein, in the combination of receptor-mediator, FA has been used as the receptor which immediately interacts with FR α , where FR α is the bio-analyte and synthesized fulleranol [C₆₀(OH)₈.2H₂O] prepared by ultrasound-assisted technique is being used as the potential nanomediator to investigate whether C₆₀(OH)₈.2H₂O synthesized by the proposed technique of ultrasonication could potentially be used as a mediator/nanomediator in the detection of FR α in association with FA.

As discussed in the chapter 4 of this thesis, the molecular structure of FA is comprised of three major organic counterparts, e.g. pteridine, p-aminobenzolate, and glutamate. The oxidation of FA occurs due to the de-hydrogenation process through losing H⁺ from C9 in the pteridine counterpart and H⁺ from N10 in the p-aminobenzolate counterpart, resulting in the dehydrofolic acid. This characteristic anodic oxidation of FA will be inhibited in the presence of FR α , which interacts mostly with the pteridine and aminobenzolate part of FA and to some extent to the glutamate counterpart as well, resulting either a decrease or increase in the anodic peak current of FA and possibly a shift in the peak potential.

To maintain the physiological condition during the *in vitro* detection of FR α phosphate buffered saline (PBS) at pH 7.4 was used as the electrolyte solution in this study. In addition, in the previous chapter a detailed study was conducted on the suitable technique of preparing FA solution for the detection of FR α , where FA solution prepared in PBS was found to be more reliable to obtain feasible results compared to FA dispersion prepared only in water. Hence, for the detection of FR α , PBS (pH=7.4) was also used in preparing FA solution (FA_{PBS}).

5.2 Experimental

5.2.1 Materials & Equipments

FR α (recombinant) was purchased from Sigma-Aldrich (product code SRP6461 - FOLR1 human1) which is expressed in HEK 293 cells. The product was received in lyophilized form and the calculated molecular weight is 25 kDa (which in its physiological *in vivo* environment has been observed to vary between 33-37 kDa) as provided in the material specification data sheet. In the current study, for the purpose of *in vitro* detection of FR α , its theoretical molecular weight (25 kDa) was used for all the calculations. To avoid denaturation of FR α , the FR α vial (as received) was stored intact at -20 °C [as recommended by the product material safety data sheet (MSDS) as well as the standard procedure of protein sample preparation and storage], the vial was opened only on the day of preparation of FR α solution.

In investigating the specificity in the detection of FR α , human serum (HS) and bovine serum albumin (BSA) were used as interfering molecules. HS (ERMMDA470KIFCC, ERM[®] certified Reference Material) was purchased from Sigma-Aldrich. As per the product data sheet the HS contains multiple proteins (Table 5.1) which therefore was used as an interfering protein sample in determining the selectivity of the FR α biosensor.

Table 5.1 The composition of different protein molecules present in the purchased HS (as received from the Sigma-Aldrich product data sheet for the product coded ERMMDA470KIFCC)

Proteins in Human Serum Sample	α 2 macroglobulin (A2M)	α 1 acid glycoprotein (AAG)	α 1 antitrypsin (AAT)	β -2-microglobulin (B2M)	complement 3c (C3c)	complement 4 (C4)	albumin (ALB)
Certified values (g/L)	1.43	0.617	1.12	0.00217	1.0	0.162	37.2
Proteins in Human Serum Sample	Immunoglobulin A (IgA)	immunoglobulin G (IgG)	immunoglobulin M (IgM)	transferrin (TRF)	transthyretin (TTR)	haptoglobin (HPT)	
Certified values (g/L)	1.80	9.17	0.723	2.36	0.220	0.869	

BSA (lyophilized powder, essentially fatty acid free, Product code: A4612-1G, New Zealand) was purchased from Sigma-Aldrich as well. As recommended by the MSDS and safety handling data sheet of the material, HS vial (as received) and BSA container (as received) were also stored intact at -70 °C and -20 °C, respectively, and were only opened in a sterile condition inside a biosafety cabinet (BSC) during the preparation of HS and BSA solution.

All other chemicals and materials used in this study, e.g., PBS buffer solution, potassium chloride, potassium ferrocyanide, sulfuric acid, N₂ gas, electrode polishing kit, alumina powder for cleaning the working electrode and DI water for preparing samples as well as for cleaning the electrodes were similar as mentioned in chapter 4. For the electrochemical analysis in developing FR α biosensor, three similar electrode set-up was used as mentioned in chapter 4, where glassy carbon electrode (GCE) as the working electrode (WE), silver/silver chloride (Ag/AgCl) saturated in potassium chloride (sat. KCl) the reference electrode (RE) and platinum (Pt) wire as the counter electrode (CE) were used for all the electroanalytical studies. As for equipment, similar potentiostat system mentioned in chapter 4 was used for the detection of FR α in the current study. The entire laboratory consumables required to handling and preparation of all the biological samples, e.g. FR α , HS and BSA, were sterilized in autoclave (Brand – Hirayama, Model – HV110, serial number – 30511070978, country of origin – Japan). Non-heat-resistant consumables which were unable to be autoclaved were disinfected by 70% ethanol where ethanol was purchased from J. Kollins Chemicals. For the accuracy in sample preparation mini benchtop centrifuge machine (FORCE MINI, Korea) was used to rotate the vial prior to the sample preparations, so that no protein sample left at the vial's wall. All the FR α , HA and BSA solutions were prepared inside a biosafety cabinet (BSC) (Brand - Esco, Model - Airstream AC2-4E8, Serial number -2015-105288, type - Class II, country of origin - Singapore).

5.2.2 Methodology

5.2.2.1 Preparation of the modified electrode GCE/FA_{PBS}/C₆₀(OH)₈.2H₂O

566.38 μM FA_{PBS} was prepared as mentioned in section 4.2.2.5 of chapter 4 (0.5 mg FA in 2 mL 0.01 M PBS,). A 280 μM dispersion of the synthesized fullereneol [C₆₀(OH)₈.2H₂O] was prepared by dissolving 0.5 mg of the synthesized fullereneol [C₆₀(OH)₈.2H₂O] in 2 mL DI water by sonication. Upon overnight storage a clear solution of C₆₀(OH)₈.2H₂O was obtained from the dispersion of C₆₀(OH)₈.2H₂O. The solutions of FA_{PBS} and C₆₀(OH)₈.2H₂O were then mixed in a 1:1 volumetric ratio. 5 μL of this FA_{PBS}/C₆₀(OH)₈.2H₂O mixture was then drop casted onto the polished and cleaned GCE surface (peak to peak separation in Fe(CN)₆^{3-/4-} redox couple was in between 60-70 mV always) and was dried for 1 h at room temperature. After drying, the modified GCE holding the coating of FA_{PBS}/C₆₀(OH)₈.2H₂O onto its active surface area was used for the detection of FR α and will be termed hereafter as GCE/FA_{PBS}/C₆₀(OH)₈.2H₂O.

5.2.2.2 Preparation of folate receptor alpha (FR α) solution

FR α is a protein where its careful handling as well standard technique of protein sample preparation and storage were followed for the preparation of FR α solution. In this study, FR α was prepared according to the protocol received with the product manual and MSDS. Prior to the preparation, FR α vial (as received) was stored under -20 °C to avoid protein denaturation.

FR α was prepared under a sterile environment inside a biosafety cabinet (BSC). Prior to the preparation, the UV light inside the BSC was turned on for 30 min to deactivate any microbes inside the BSC followed by purging throughout the cabinet for 3 min. All other materials and consumables used in the preparation of FR α solution were sterilized prior to their use inside the BSC. For items which were not suitable to be autoclaved 70% ethanol solution was used to disinfect those items prior to transfer them inside the BSC. Once all the materials were ready and the BSC as well, the FR α was prepared according to the following steps, where steps (b) and (c) were performed inside a BSC.

- a) The vial (containing 50 µg lyophilized FR α) was centrifuged for 30 s prior to opening the vial.
- b) 50 µg of lyophilized FR α was reconstituted in 1 mL of sterile PBS (pH 7.4) at a concentration of 2 µM (calculated based on the theoretical molecular weight of FR α). A clear transparent solution of FR α in PBS confirmed that the protein structure was well-preserved, whereas a denatured protein solution would rather form a cloudy and foamy solution.
- c) 2 µM of FR α solution was then divided into aliquots of 10 µL, which were then stored at -20 °C for detecting FR α by FA_{PBS}/C₆₀(OH)₈.2H₂O.

5.2.2.3 Preparation of human serum (HS) solution

Care also was taken for the preparation of HS as it has the same risk of getting denatured since it contains a number of cell proteins. Therefore, HS was reconstituted as per the following procedure provided by Sigma-Aldrich, where steps (c) - (f) were performed inside a BSC.

- a) Before preparing the solution of HS, the vial was taken out from the freezer and placed outside for 1 h to unfreeze the material inside the vial.
- b) After 1 h, the bottom of the vial was tapped gently on the surface of a table so that any serum attached to the wall or lid of the vial would be accumulated at the bottom. This is necessary to accurately calculate the weight of the material inside the vial prior to the preparation of the solution,
- c) Since it is difficult to weigh a very small amount of lyophilized powder as there is a certain chance of weight loss during the measurement, hence the amount of lyophilized HS was measured including the vial. First, the vial was weighed including the rubber stopper, then 1 mL of sterile DI water was added into the bottle and the rubber stopper was placed back into place. After adding the sterile water into the vial, it was weighed again and the previous weight was subtracted to calculate the mass of HS, which was 20 mg.
- d) The vial was then left at room temperature for 1 h to allow the serum to completely dissolve in the water. After 1 h, the mixture was turned into a clear

and transparent light yellow colored solution. Any shaking or vigorous mixing was avoided as it might cause foamy solution upon compromising the structure of the protein molecules contained in HS.

- e) Before dividing the solution into small aliquots, the stock solution in the vial was very gently and carefully inverted for 10 times.
- f) The solution was then divided into aliquots of 10 μ L and stored at -20 °C.

5.2.2.4 Preparation of bovine serum albumin (BSA) solution

BSA is commonly used as a standard protein to determine other proteins in protein assay protocols. It can also be used to prevent non-specific binding of proteins as well as an interfering protein molecule in developing a biosensor. BSA could be prepared both in water or PBS based on the purpose of study. In this study, since BSA was used for interference study, similar to human serum, sterile water was used to prepare BSA solution. As for the preparation of BSA, 1 g BSA was dissolved in 100 mL sterile water to produce a 151.5 μ M solution of BSA. The preparation was performed inside a BSC and was allowed to form a stable solution for 1 h. After 1 h the BSA stock solution was divided into aliquots of 10 mL for further use.

5.3 Results & Discussion

5.3.1 Inter-day voltammetric response of GCE/FA_{PBS}

Prior to the modification of GCE by FA_{PBS}/C₆₀(OH)₈.2H₂O for the detection of FR α , inter-day stability of FA_{PBS} was investigated by recording the voltammetric response of GCE/FA_{PBS} for five consecutive days. In the previous chapter it was noted that the peak potential (as a result of the corresponding peak current) of a chemical species may slightly shift if the cyclic voltammetry is conducted on different days, in fact the anodic or cathodic peak potential may also slightly shift if scanned on different days. One of the limiting factors to this fact could be the material itself may not be able to produce a constant value of peak current due to its unstable physical properties. Other limiting factors that may control this situation are the nature of electrolyte solutions, the cleanliness of the electrode, any contamination occurring from the surrounding during electrochemical analysis, due to the low signal to noise ratio. In this study, all the

possible limiting factors were taken into consideration prior to and during any voltammetric studies and necessary measures were taken accordingly to obtain consistent voltammetric data. However, while designing a biosensor for the detection of an analyte, it is still important to check the voltammetric response of a modified electrode on different days to observe the extent of shift of peak potential value in the absence of an FR α , which later will help to understand the reason behind any considerable change if observed in the peak potential when the same modified electrode will be subjected to voltammetric study in the presence of FR α under the same experimental conditions. As in the electrochemistry shift in peak potential is considered as one of the useful primary indicators indicating about whether any reaction is happening at the surface of the working electrode. The reaction at the working electrode may cause either by the oxidation/reduction of the chemical species used to modify the electrode or due to the oxidation/reduction of an analyte at the electrode surface. Therefore, the shift in peak potential provides useful information regarding any chemical reaction occurring at the electrode surface. In this experiment, since FA has the characteristic property of undergoing degradation as well as the coating of FA onto GCE surface may not stay over a longer period, so the shift in peak potential along with the change in the anodic peak current of FA via inter-day cyclic voltammetry was necessary to investigate prior to the detection of FR α . Thus, GCE/FA_{PBS} electrode basically was considered as the main 'control' in the detection of FR α , hence the voltammetry of GCE/FA_{PBS} on different days was recorded and the best value was selected to be followed for the rest of the analyses.

Fig. 5.1 and Table 5.2 present the anodic peak potential (E_{pa}) and the anodic peak current (I_{pa}) recorded for five consecutive days. The voltammograms show that E_{pa} shifted over 5 days in a range of 0.80-0.85 V. However, this shift was observed neither in an ascending or descending order starting from day 1 to day 5, rather it varied randomly within a range of 0.80-0.85 V over 5 days (Table 5.2). Yardim and Şentürk, (2014) reported similar observation that FA in different drug samples exhibited anodic peak current potential from 0.79 to 0.85 V, and the peak potential also varied in a more wider range (0.79-1.0 V) based on different pH. The observed values of E_{pa} therefore comply with the reported data indicating that FA_{PBS} can produce reliable and stable voltammetric response on different days. The mean value of E_{pa} was 0.83 V and the mode was 0.84 V.

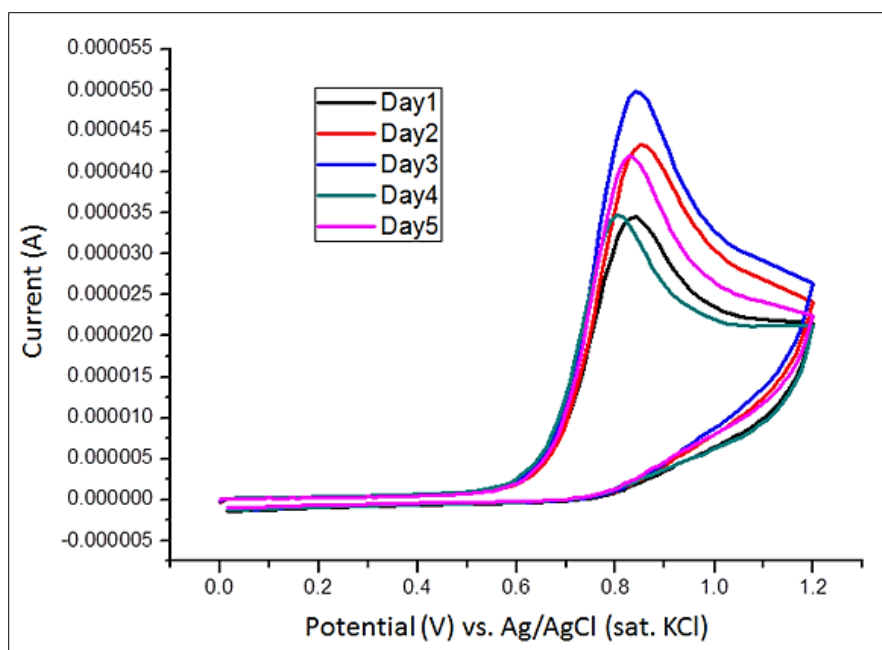


Figure 5.1 cyclic voltammetry of GCE/FA_{PBS} in 0.01 M PBS recorded on five consecutive days at a scan rate of 100 mV/s

Table 5.2 Anodic peak potential and corresponding anodic peak current obtained from the CV on five consecutive days

Day	E_{pa} (V)	i_{pa} (μ A)
1	0.84	34.6
2	0.85	43.3
3	0.84	49.9
4	0.81	34.8
5	0.83	41.8

Nevertheless, for the detection of FR α it is necessary to choose a particular E_{pa} and I_{pa} values for the comparative studies. These selections could be made in two ways; either based on the mean value of E_{pa} since the mean value will provide an average estimation to satisfy all other observed values; or based on the mode of E_{pa} , where the potential which appears the most within five consecutive record should be considered. Here the calculated value of mean and mode was 0.83 V and 0.84 V, respectively, and 0.84 V

was observed both on day 1 and day 3 showing that the most consistent E_{pa} for GCE/FA_{PBS} to be ~0.84 V.

Similarly, a particular I_{pa} for GCE/FA_{PBS} is to be selected for the comparative studies in detecting FR α . Whereas, in this case (Table 5.2), it is neither suggested to take the mean of I_{pa} nor even the mode of I_{pa} should be considered. Since I_{pa} could be affected by several limiting factors as discussed above, therefore taking an average of I_{pa} may encounter errors in the comparative quantitative studies. By considering the mode of I_{pa} from among the 5 days' observation for GCE/FA_{PBS}, it could be observed from Table 5.2 that unlike E_{pa} there is no value of I_{pa} that is repeating on different days. Hence in this case taking the highest value observed for I_{pa} at E_{pa} = 0.84 V to be a valid consideration, given that other experimental conditions were similar for all the measurements, where the electrodes were properly cleaned and then checked in the standard Fe(CN)₆^{3-/4-} redox couple solution in between every analysis, the electrolyte was not contaminated by other materials during handling, the noise level was controlled both from the machine and from the surrounding and the pH of all the solutions used in the experiments were constant throughout at room temperature. In this case the best value of E_{pa} was 0.84 V which appeared both on day 1 and day 3, and the highest I_{pa} at E_{pa} = 0.84 V was observed on day 3 which was 49.9 μ A (Table 5.2). The reason of taking the highest value of I_{pa} is because the lower values of I_{pa} may appear due to the desorption of some FA particles from GCE before or during electrochemical analysis, so taking the lower value may not exhibit the true maximum signal of anodic peak current for GCE/FA_{PBS}. Based on this observation, hereinafter for the detection of FR α the value of E_{pa} and I_{pa} for the GCE/FA_{PBS} should be taken as 0.84 and 49.9 μ A.

5.3.2 Control measurement

Besides GCE/FA_{PBS} taken as one of the controls, prior to the detection of FR α with GCE/FA_{PBS}/C₆₀(OH)₈.2H₂O, other related 'control' experiments' were conducted to ensure that the electrolyte PBS, the solvent used for sample preparation (both H₂O and PBS), synthesized C₆₀(OH)₈.2H₂O and the FR α itself do not individually produce any anodic peak current that may overlap the current signal to be generated due to the interaction between FA and FR α at GCE/FA_{PBS}/C₆₀(OH)₈.2H₂O.

To check whether GCE itself produce any peak current the voltammogram of bare GCE [not modified with FA_{PBS} and C₆₀(OH)₈.2H₂O] in PBS (in the absence of any FR α) was recorded. To ensure that no current was contributed from the PBS (since it contains ions from its salts), bare GCE was modified by drop casting 5 μ L of PBS (GCE/PBS) and then CV was conducted for the modified GCE/PBS and GCE/H₂O electrodes. To understand whether the synthesized C₆₀(OH)₈.2H₂O had any characteristic peak currents, bare GCE was also modified by drop casting 5 μ L of the synthesized C₆₀(OH)₈.2H₂O onto it, then CV was recorded for the modified GCE/C₆₀(OH)₈.2H₂O. To understand whether FR α alone could produce any peak currents, GCE was also modified by drop casting 5 μ L of FR α onto bare GCE (GCE/FR α) and then CV was recorded.

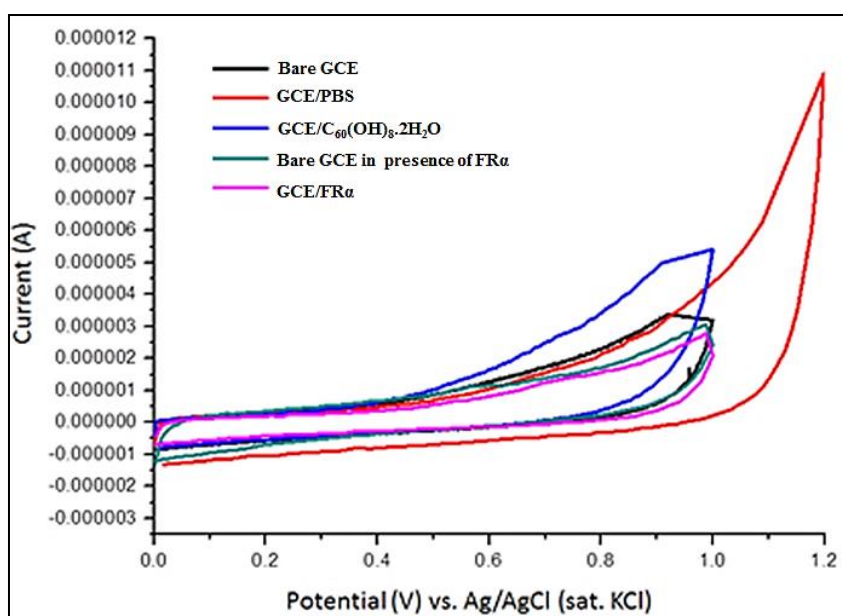


Figure 5.2 CV of bare GCE, GCE/PBS, GCE/C₆₀(OH)₈.2H₂O, GCE/FR α and bare GCE in presence of FR α as an analyte in PBS

Fig. 5.2 shows that bare GCE, GCE/PBS, GCE/C₆₀(OH)₈.2H₂O and GCE/FR α do not show any anodic peak currents on their voltammograms. In addition to this, voltammetric response of bare GCE in presence of FR α in PBS was recorded, which also showed that bare GCE does not show any oxidation/reduction current due to the presence of FR α in the PBS. These observations imply that, in this study, for developing FR α biosensor only the change in the anodic peak current and peak potential of FA will provide sufficient information regarding the molecular interaction between FA and FR α at GCE/C₆₀(OH)₈.2H₂O.

5.3.3 Effect of scan rate on the GCE/FA_{PBS}/C₆₀(OH)₈.2H₂O

The effect of different scan rates on GCE/FA_{PBS}/C₆₀(OH)₈.2H₂O was investigated at 125, 100, 75, 50 and 25 mV/s prior to the detection of FR α (Fig. 5.3). The values of E_{pa} for GCE/FA_{PBS}/C₆₀(OH)₈.2H₂O at different scan rates were found to be almost in the same range (0.79-0.85 V) (Table 5.3) which was observed for GCE/FA_{PBS}.

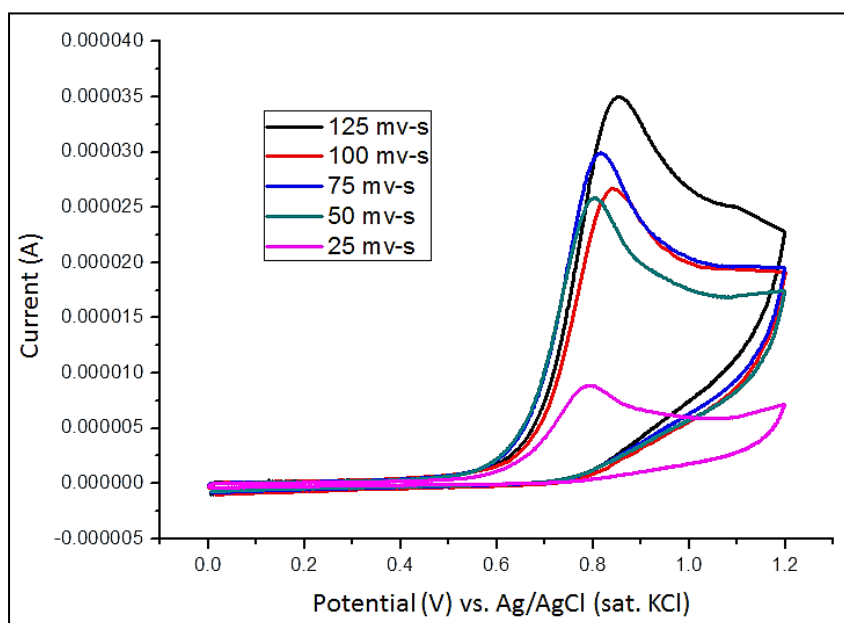


Figure 5.3 CV of GCE/FA_{PBS}/C₆₀(OH)₈.2H₂O at different scan rates

Table 5.3 Anodic peak potential and the corresponding anodic peak current obtained from the CV at different scan rates for GCE/FA_{PBS}/C₆₀(OH)₈.2H₂O (in comparison with GCE/FA_{PBS})

Scan Rate, v (mV/s)	GCE/FA _{PBS} /C ₆₀ (OH) ₈ .2H ₂ O		GCE/FA _{PBS}	
	E _{pa} (V)	I _{pa} (μA)	E _{pa} (V)	I _{pa} (μA)
125	0.85	35	0.85	61.2
100	0.84	26.6	0.84*	49.9*
75	0.81	30	0.84	39.6
50	0.8	26	0.80	18.8
25	0.79	8.9	0.74	4.28

*As determined in section 5.3.1 based on Fig. 5.1

Table 5.3 shows that the intensity of current followed a regular as well as quantifiable trend for GCE/FA_{PBS}/C₆₀(OH)₈.2H₂O compared to GCE/FA_{PBS} at a scan rate range of 125 mV/s-75 mV/s) where the anodic peak current of FA has followed a significant descending trend in presence of C₆₀(OH)₈.2H₂O. As already was found in section 4.3.4.2 based on the investigation into the voltammograms of GCE/FA_{PBS} both at different scan rates of CV and multi-cycle of CV that too high scan rate and too lower scan rate is not feasible to quantify the detection of FR α as too high or low intensity of current at higher and lower scan rate, respectively, could also be attributed to the noise related to the expansion of diffusion bilayer near to the electrode-solution interface and/or uncertainties associated to the desorption of folic acid from GCE surface during electrochemical reaction. Thus, a scan rate of 100 mV/s is suggested in this study of FR α detection. At a scan rate of 100 mV/s (to be followed for all the studies of detecting FR α), the I_{pa} (= 26.6 μ A) for GCE/FA_{PBS}/C₆₀(OH)₈.2H₂O was significantly lower compared to that observed for GCE/FA_{PBS} (I_{pa} = 49.9 μ A). The presence of C₆₀(OH)₈.2H₂O thus contributes a significant effect on lowering the anodic peak current.

The linear regression equations (Eqs. 5.2 and Eq. 5.3) obtained from I_{pa} vs. $v^{1/2}$ and I_{pa} vs. v plots (Figs. 5.4 and 5.5) for GCE/FA_{PBS}/C₆₀(OH)₈.2H₂O showed that the coefficient of determination was: $R^2 = 0.7896$ and $R^2 = 0.7198$, respectively.

$$I_{pa} (\mu A) = 3.5935v^{1/2} - 4.8216 \quad (\text{Eq. 5.2})$$

$$I_{pa} (\mu A) = 0.2112v + 9.46 \quad (\text{Eq. 5.3})$$

From the R^2 values obtained from the linear regression equations for GCE/FA_{PBS}/C₆₀(OH)₈.2H₂O, it could be inferred that unlike GCE/FA_{PBS} the electrochemical reaction taking place at GCE/FA_{PBS}/C₆₀(OH)₈.2H₂O is also partly diffusion and partly adsorption controlled. In chapter 4 of this work, it was shown that the E_{pa} and I_{pa} values for GCE/FA_{PBS} were 0.84 V and 49.9 μ A respectively.

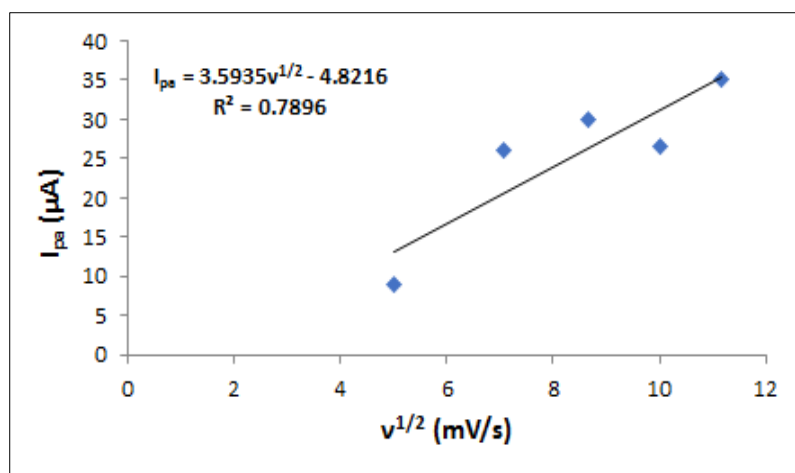


Figure 5.4 Plot of I_{pa} vs. $v^{1/2}$ for GCE/FA_{PBS}/C₆₀(OH)₈.2H₂O

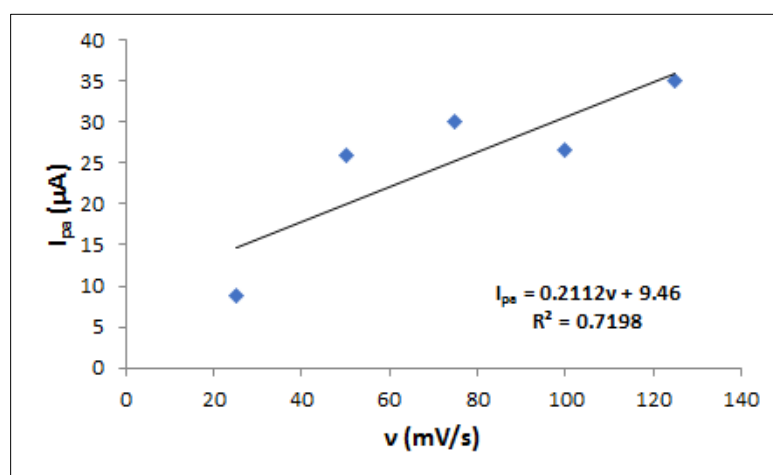


Figure 5.5 Plot of I_{pa} vs. v for GCE/FA_{PBS}/C₆₀(OH)₈.2H₂O

Therefore, the anodic current decreased at a significant value, while a mixture of FA_{PBS} and C₆₀(OH)₈.2H₂O was used to modify GCE. In the control experiment, in Fig. 5.2, it could be noted that C₆₀(OH)₈.2H₂O alone does not exhibit any peak current, but the presence of C₆₀(OH)₈.2H₂O along with FA on the GCE decreases the anodic peak current intensity of FA. In verifying the above finding, when CV was repeated three times for GCE/FA_{PBS}/C₆₀(OH)₈.2H₂O, the mean E_{pa} was obtained at 0.84 V and the I_{pa} was obtained in a range of 20.0-26.7 μ A, where the maximum $I_{pa} = 26.7 \mu$ A at $E_{pa} = 0.84$ V to be followed for the comparative study in detecting FR α .

5.3.4 Detection of FR α

Fig. 5.6 presents the detection of 1 nM FR α in PBS with the modified electrode GCE/FA_{PBS}/C₆₀(OH)₈.2H₂O. The voltammogram shows the detection of FR α by GCE/FA_{PBS} electrode as well. The voltammogram shows that bare GCE and C₆₀(OH)₈.2H₂O do not have any anodic peak current under the current experimental conditions. Table 5.4 summarizes all the values of I_{pa} and E_{pa} obtained from Fig. 5.6 for the detection of FR α .

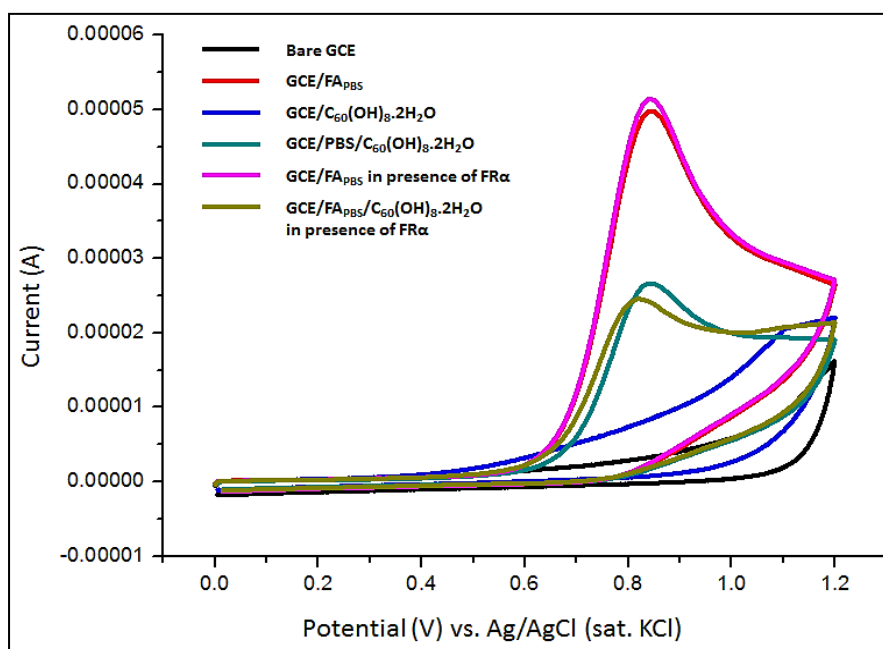


Figure 5.6 CV for the detection of 1 nM FR α with GCE/FA_{PBS}/C₆₀(OH)₈.2H₂O in 0.01 M PBS at a scan rate of 100 mV/s

In the absence of FR α , GCE/FA_{PBS} shows an anodic peak current of I_{pa} = 49.9 μ A at E_{pa} = 0.84, whereas the peak current for GCE/FA_{PBS}/C₆₀(OH)₈.2H₂O decreased by 46.5% (I_{pa} = 26.7 μ A, E_{pa} = 0.84). Since there is no significant shift in the anodic peak potential and hence it is deemed that C₆₀(OH)₈.2H₂O did not form any covalent or ionic bond with FA, but the decrease in the current indicates that there might have some hydrogen bond formation or simple pi-pi conjugation between them when mixed together (Mignon *et al.*, 2005).

Table 5.4 Comparative values of E_{pa} and I_{pa} for different modified GCE in the absence and presence of FR α

Scan rate, v (mV/s)	E_{pa} (V)	I_{pa} (μ A)
Bare GCE	No peak potential	No peak current
GCE/FA _{PBS}	0.84	49.9
GCE/C ₆₀ (OH) ₈ .2H ₂ O	No peak potential	No peak current
GCE/FA _{PBS} /C ₆₀ (OH) ₈ .2H ₂ O	0.84	26.7
GCE/FA _{PBS} in presence of FR α	0.84	51.5
GCE/FA _{PBS} /C ₆₀ (OH) ₈ .2H ₂ O in presence of FR α	0.82	24.7

In the presence of FR α for GCE/FA_{PBS}/C₆₀(OH)₈.2H₂O, the E_{pa} was shifted to 0.82 V with a corresponding I_{pa} of 24.7 μ A which was 7.5% less than the anodic peak current observed for GCE/FA_{PBS}/C₆₀(OH)₈.2H₂O in the absence of FR α . The shift in E_{pa} as well as the significant decrease in I_{pa} indicate that because of the molecular interaction between FR α and FA the E_{pa} was shifted from 0.84 V to 0.82 V but due to the presence of C₆₀(OH)₈.2H₂O I_{pa} continued to decrease further. Previous reports showed that the presence of FR α can display a decreasing trend in the peak current due to the formation of FR α -FA complex at the working electrode surface, however, an increasing trend in the peak current could be observed based on different combination of receptor-mediator to target FR α (He *et al.*, 2016; Castillo *et al.*, 2013). In the current study, the detection of FR α by FA in presence of C₆₀(OH)₈.2H₂O follows a decreasing trend in the I_{pa} and hence for the quantitative analysis the percentage of decrease in the anodic current should be considered to determine the detection limit.

The effect of C₆₀(OH)₈.2H₂O in the decreasing trend of I_{pa} was verified when FR α was detected by FA alone, where GCE/FA_{PBS} in the presence of FR α showed I_{pa} = 51.5 μ A at E_{pa} = 0.84 V depicting that in the absence of C₆₀(OH)₈.2H₂O the molecular interaction between FA and FR α may produce higher I_{pa} . This observation may suggest that only FA is also able to detect FR α , but the increase in I_{pa} was only 3% compared to I_{pa} (49.9 μ A) obtained for GCE/FA_{PBS} in the absence of FR α .

On the contrary, while $C_{60}(OH)_8 \cdot 2H_2O$ is present with FA it is limiting the anodic peak current of FA in a significant manner and showing a regular decreasing trend of anodic peak current at a significant percentage (7.5 %) which provides a clear direction for both the qualitative and the quantitative detection of $FR\alpha$ by GCE/ $FA_{PBS}/C_{60}(OH)_8 \cdot 2H_2O$. Hence, the synthesized $C_{60}(OH)_8 \cdot 2H_2O$ shows its potential effect on the voltammogram of FA which could be exploited in the detection of $FR\alpha$.

The slight increment for GCE/ FA_{PBS} in presence of $FR\alpha$ may also be derived from only the anodic oxidation of FA itself, hence not suitable for the quantitative purpose, as only 3% increase also may entail the uncertainties, e.g. noise associated to unavoidable IR drops. In such cases the homogeneous interaction of FA with $FR\alpha$ could be hindered and resulted in a slightly higher anodic oxidation current mostly coming from the anodic oxidation of folic acid only, which was controlled in the presence of $C_{60}(OH)_8 \cdot 2H_2O$ possibly due to the following reasons:

- presence of $C_{60}(OH)_8 \cdot 2H_2O$ reinforced the physisorption of folic acid onto GCE and thus a homogeneous interaction was possible between folic acid and $FR\alpha$.
- presence of $C_{60}(OH)_8 \cdot 2H_2O$ is able to limit the flow of electrons from the recognition site to the electrode in a descending-order-quantifiable manner possibly due to its both electrophilic and nucleophilic nature, and thus the role of $C_{60}(OH)_8 \cdot 2H_2O$ could be considered either as a negative-impact-electron mediator or as an electron-blocker.

However, the proposed application of the synthesized $C_{60}(OH)_8 \cdot 2H_2O$ still needs further investigation on several levels before applying it in the fabrication of a lab-on-chip or a point-of-care biosensor for the detection of $FR\alpha$. While three detections of $FR\alpha$ were conducted with GCE/ $FA_{PBS}/C_{60}(OH)_8 \cdot 2H_2O$ to check the repeatability of the detection of $FR\alpha$. The relative standard deviation (RSD) for three detections was calculated to be 22.3% which was higher than the usual acceptable range of RSD (10-15%). However, this also depends on the type of an electrochemical system. If the system is robust and reversible, then the RSD value should appear within the accepted range. In the current electrochemical set-up, where FA is being used in association with $C_{60}(OH)_8 \cdot 2H_2O$ to modify the bare GCE in detecting $FR\alpha$, the deviation due to the leaching out of FA into the solution should be taken into consideration, emphasizing that upon confirming more firm binding of FA onto GCE as well more stable

conjugation between FA to $C_{60}(OH)_8 \cdot 2H_2O$ may overcome the uncertainties and decrease the RSD.

Due to the uncertainty of FA voltammetric response, the RSD for the detection of FR α by GCE/FA(PBS)/ $C_{60}(OH)_8 \cdot 2H_2O$ was calculated to be 22%, whereas the general accepted value of RSD is considered as 10-15%, indicating that although the current finding has a scope in detecting FR α but for developing a real-time robust biosensor for FR α detection it needs several trials more, specially upon stabilizing the FA onto GCE with some potential binder. To investigate more the underlying possibility for the application the synthesized $C_{60}(OH)_8 \cdot 2H_2O$ in detecting FR α repeatability, reproducibility and stability of the detection was conducted, as well as attempted to calculate the LOD of the current method.

5.3.5 Detection of FR α : Stability

For the stability study, GCE/FA_{PBS}/ $C_{60}(OH)_8 \cdot 2H_2O$ was stored 7 days in a dark, cool place, avoiding any exposure to air and risk of heat. After 7 days, GCE/FA_{PBS}/ $C_{60}(OH)_8 \cdot 2H_2O$ was used to detect FR α under the same experimental conditions and the measured I_{pa} was 23 μA (Fig. 5.7), which was 93% of the initial I_{pa} (24.7 μA) implying that the proposed biosensor, although showing a higher RSD but possesses better stability similar to a robust biosensor where the stability should be valid within 90-100%.

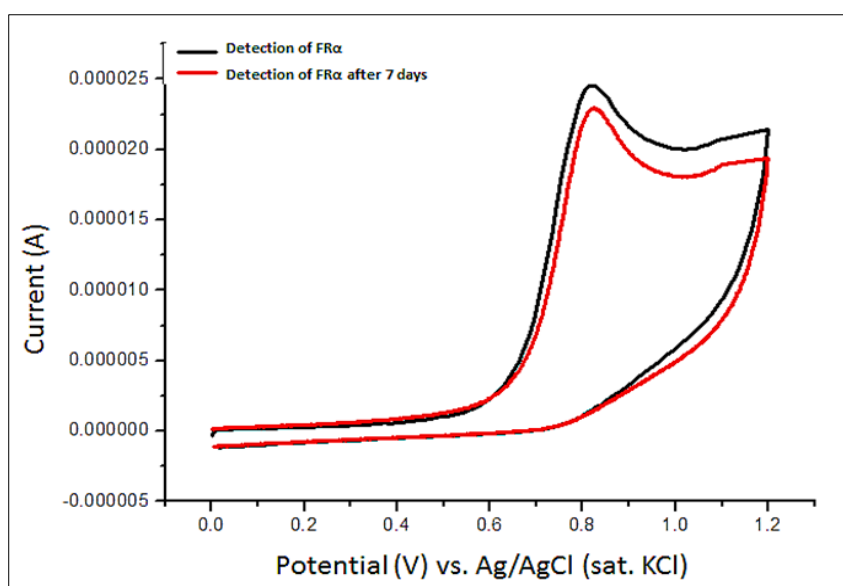


Figure 5.7 CV of GCE/FA_{PBS}/ $C_{60}(OH)_8 \cdot 2H_2O$ before and after 7 days in the presence of 1 nM FR α in 0.01 M PBS at a scan rate of 100 mV/s

5.3.6 Detection of FR α : Reproducibility

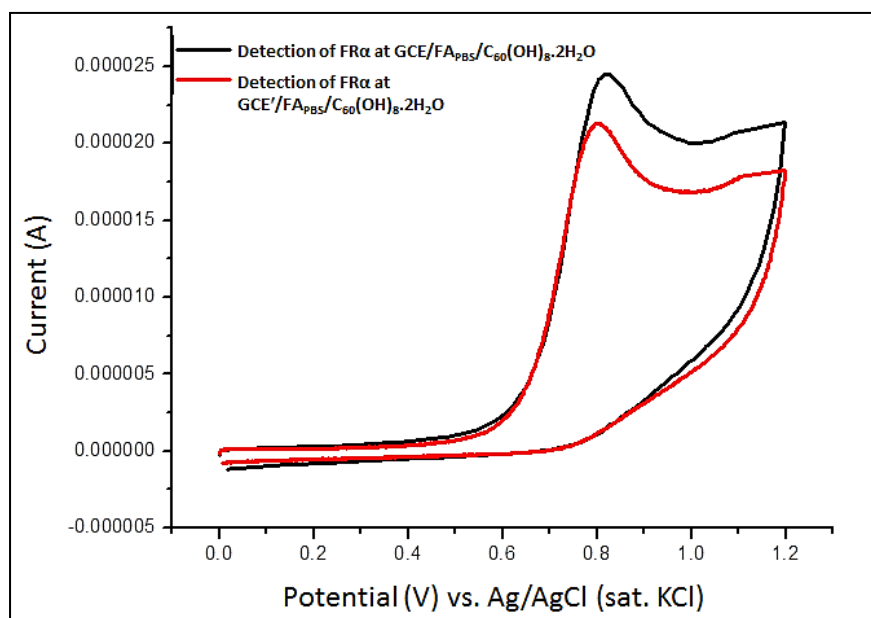


Figure 5.8 CV of GCE/FA_{PBS}/C₆₀(OH)₈.2H₂O and GCE'/FA_{PBS}/C₆₀(OH)₈.2H₂O in the presence of 1 nM FR α in 0.01 M PBS at a scan rate of 100 mV/s

The reproducibility of the proposed biosensor was verified by modifying a different glassy carbon electrode (GCE') with the same mixture of FA_{PBS} and C₆₀(OH)₈.2H₂O (GCE'/FA_{PBS}/C₆₀(OH)₈.2H₂O), where all procedures and experimental conditions were similar to that maintained for GCE/FA_{PBS}/C₆₀(OH)₈.2H₂O. The reproducibility to FR α detection on a different GCE electrode was calculated to be 86% (Fig. 5.8), implying that the detection of FR α at different glassy carbon electrodes needs careful measures in order to avoid any uncertainty related to different glassy carbon electrode. As shown in section 4.3.2 of chapter 4 that the active surface area of the GCE thoroughly used in this study was $\sim 5 \text{ mm}^2$, even made of the same material not all the GCE contain the same area of its active surface which varies based on the manufacturer's specification, hence it is quite difficult to obtain a true reproducibility value more than 90% in general cases while randomly different GCE to be used for the purpose of detection.

5.3.7 Detection of FR α : limit of detection (LOD) & selectivity

Under the current experimental condition, as discussed above, where the detection of FR α by the combination of FA and C₆₀(OH)₈.2H₂O follows a complex trend and mechanism, it is difficult to define the LOD precisely. A chronoamperometry was conducted to check whether the current electrochemical system can provide any potential information about the LOD for the detection of FR α (Fig. 5.9). In calculating the LOD, chronoamperometry was conducted at an applied voltage of 0.9 V, where FR α from 500 pM to 1400 pM was added at an interval of 60 s into PBS (Fig. 5.9).

It was difficult to find a regular decreasing trend in the amperometric response of FR α with the increase of concentration. A plot of amperometric current vs. concentration of FR α (Fig. 5.10) produced a linear regression equation of $R^2 = 0.4705$ indicating that the amperometric response was hindered by other factors, therefore deviating from a regular decreasing trend of FR α detection under the proposed design of experiments. The possible reason for this could be again due to the unstable binding of FA to the GCE surface. As a result, some FA could drop off from the GCE surface into the bulk electrolyte during electrochemical analysis so could not build the interaction with FR α on molecular level.

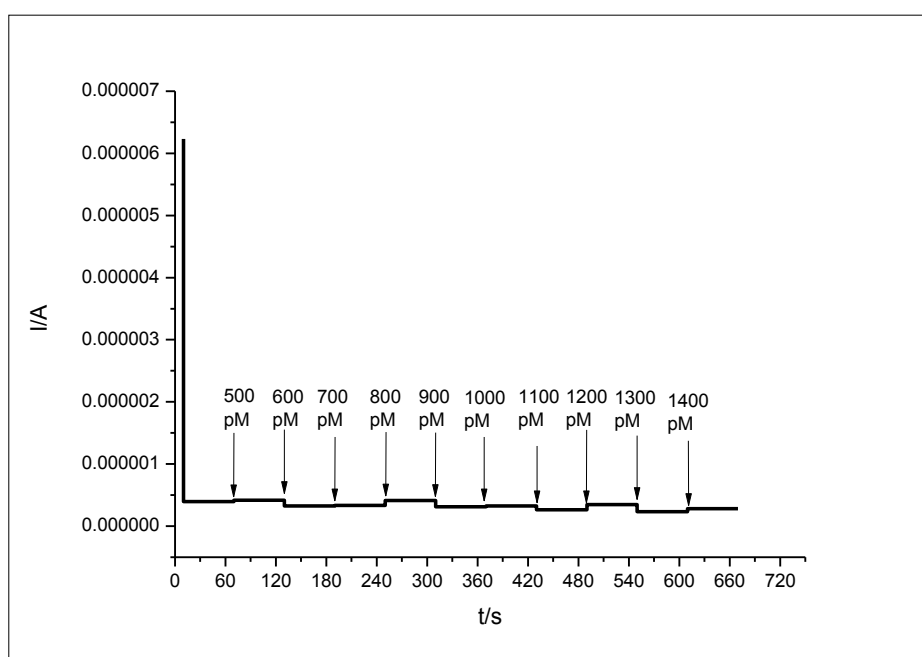


Figure 5.9 Chronoamperometry: current vs. time (I-t) for GCE/FA_{PBS}/C₆₀(OH)₈.2H₂O at an applied voltage of 0.9 V for the addition of 500-1400 pM FR α at a time interval of 60 s in 0.01 M PBS

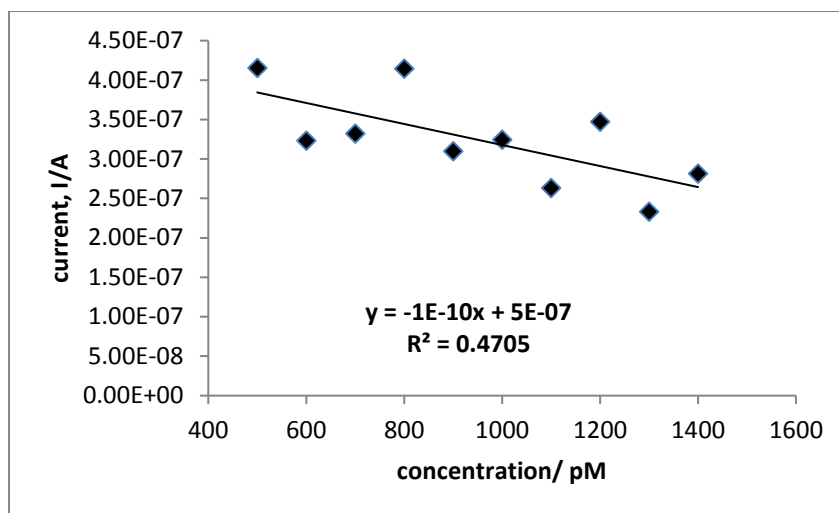


Figure 5.10 Plot of anodic peak current vs. concentration of FR α in a linear range

From the chronoamperometry study (Figs. 5.9 and 5.10), the LOD ($3\sigma/S$) was calculated to be 1.4 nM at a signal to noise ratio of 3.0. The LOD defines the lowest amount that could be detected in a solution, theoretically, which was close to the amount used for the detection (1 nM), however, deviated from precision due to the instability factor of FA as discussed above. However, the current value still provides useful information about the range of detection, where it is shown that the detection of FR α under the proposed method and experimental condition can detect nearly 1 nM FR α . The sensitivity (current density/concentration) of GCE/FA_{PBS}/C₆₀(OH)₈.2H₂O for the detection of FR α was calculated based on the current vs. concentration plot (Fig. 5.10) and the electrode area of GCE (0.049 cm² as calculated in section 4.3.2), where the calculated value of sensitivity was found to be 3 μ A/nM.cm² at the LOD of 1 nM for the detection of FR α at GCE/FA_{PBS}/C₆₀(OH)₈.2H₂O.

To further verify the LOD in the nM range as well as to check the selectivity of FR α detection another amperometric analysis was conducted with GCE/FA_{PBS}/C₆₀(OH)₈.2H₂O at an applied voltage of 0.9 V, where FR α from 2.5×10^{-5} mg/mL to 1.25×10^{-4} mg/mL (1 nM-5 nM) was added into the electrolyte solution of PBS over 310 s, then at 370 s HS (0.01 mg/mL) was added as an interfering species, then again at 430 s FR α of 1.25×10^{-4} mg/mL was added and finally at 490 s 5×10^{-3} mg/mL of BSA was added again as interfering species in the solution (Fig. 5.11). The addition of different species was at 60 s interval.

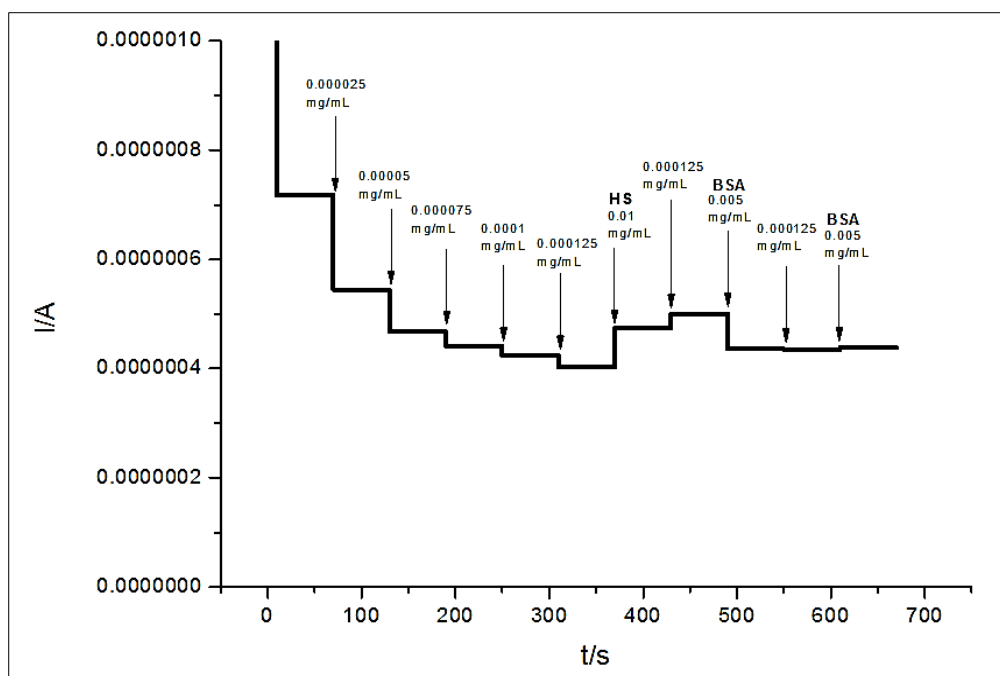


Figure 5.11 Chronoamperometry of GCE/FA_{PBS}/C₆₀(OH)₈.2H₂O at an applied voltage of 0.9 V for the addition of FR α , HS and BSA at varying concentrations* at a time interval of 60 s in 0.01 M PBS

*The unit of concentration was mg/mL as human serum (HS) was a collection of multiple protein molecules and so had no specific molecular weight, therefore could be expressed in the unit of molarity.

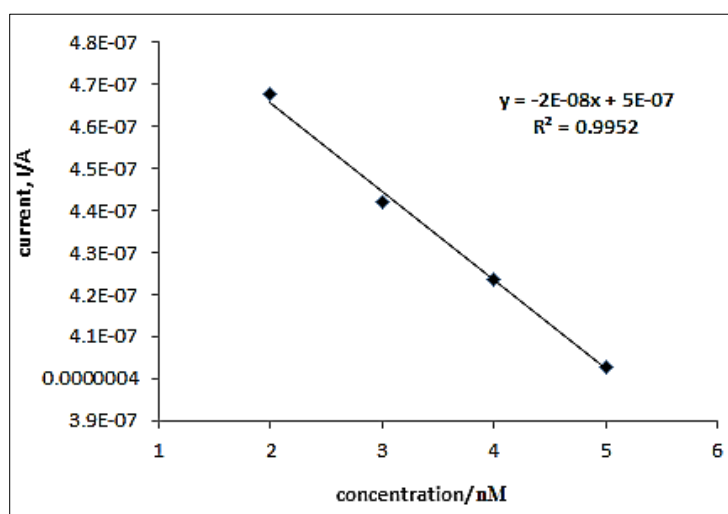


Figure 5.12 Linear range of current obtained from chronoamperometry for the addition of FR α in 0.01 M PBS before adding HS and BSA as interfering molecules

Table 5.5 Values of current vs. concentration for FR α while added with HS and BSA in 0.01 M PBS

Conc. of FRα (nM)	Current (μA)
2	0.468
3	0.442
4	0.424
5	0.403

A plot for the detection of FR α in the nM range was drawn on current vs. concentration of FR α added in the solution (Fig. 5.12 and Table 5.5). The linear regression equation obtained from this plot showed $R^2 = 0.9952$ indicating that the detection of FR α better performs in the nM range. As for the selectivity, since the detection of FR α follows a decreasing trend in the anodic peak current, hence during studying the % increase or decrease of current due to the presence of interfering molecules (HS and BSA) was calculated based on the current obtained for 2 nM FR α . The % increase in the current for HS was ~1% (whereas compared to the immediate previous concentration of FR α of 5 nM it was ~17.6%). An increase in the current for HS was complying as the trend for FR α is decreasing (also HS was added 3 times higher than the FR α added at 310 s). A slight increase was observed for the addition of FR α (5 nM) after human serum, further addition of FR α (5 nM) at 550 s following an addition of BSA (5×10^{-3} mg/mL) at 490 s decreased the amperometric response of current. The final addition of BSA as interfering molecule again showed an increase in the current. From this study, it was proven again that the detection of FR α shows a decreasing trend in the current, not much affected by the presence of interfering molecules but to avoid the slight interference as observed in the current study, in applying the synthesized C₆₀(OH)₈.2H₂O in association with FA for a prospective FR α biosensor it is quite essential to first enhance the stability of FA onto GCE surface which will help to overcome all the uncertainties and slight deviations as reported in the current study.

5.4 Overview of the Current Chapter and Direction to the Next Chapter

In this chapter the prospects of the synthesized fullereneol [C₆₀(OH)₈.2H₂O] in fabricating a folic acid based biosensor for the detection of a cancer biomarker folate receptor alpha was investigated in detail, which showed that fullereneol(s) produced by ultrasound-assisted technique could be taken into account in developing FR α biosensor, given the facts that further investigations are required to ensure the robustness of the biosensor and prior to develop a point-of-care biosensor device. Since the synthesized fullereneol was C₆₀(OH)₈.2H₂O, the current study also delivers a significant message that polyhydroxylated fullereneol with more hydroxy groups could also be considered as suitable candidates as an electron-mediator in developing an electrochemical biosensor for the detection of FR α . To exploring this possibility relevant other matters to be taken into consideration prior to designing the next generation electrochemical nanobiosensors for the detection of FR α . One of those matters to be developing a more facile technique of conjugation between potential fullereneol moieties and folic acid in order to obtain a stable molecular binding of receptor/ligand-mediator, which could be useful in enhancing the electrochemical signal and thus the sensitivity of the biosensor.

On this context, the next chapter of this thesis will draw a discussion supported by empirical data, toward some future directions pertinent to the abovementioned possibilities.

References

- Assaraf, Y.G., Leamon, C.P., & Reddy, J.A. (2014). The folate receptor as a rational therapeutic target for personalized cancer treatment. *Drug Resistance Updates*, 17(4–6), 89–95.
- Bueno, R., Appasani, K., Mercer, H., Lester, S., & Sugarbaker, D. (2001). The α folate receptor is highly activated in malignant pleural mesothelioma. *The Journal of Thoracic and Cardiovascular Surgery*, 121(2), 225-233.
- Cai, L., Michelakos, T., Ferrone, C.R., Zhang, L., Deshpande, V., Shen, Q., DeLeo, A., Yamada, T., Zhang, G., Ferrone, S., & Wang, X. (2017). Expression status of folate receptor alpha is a predictor of survival in pancreatic ductal adenocarcinoma. *Oncotarget*, 8(23), 37646.
- Castillo, J. J., Svendsen, W. E., Rozlosnik, N., Escobar, P., Martínez, F., & Castillo-León, J. (2013). Detection of cancer cells using a peptide nanotube–folic acid modified graphene electrode. *Analyst*, 138(4), 1026-1031.
- Cheung, A., Bax, H.J., Josephs, D.H., Ilieva, K.M., Pellizzari, G., Opzoomer, J., Bloomfield, J., Fittall, M., Grigoriadis, A., Figini, M., & Canevari, S. (2016). Targeting folate receptor alpha for cancer treatment. *Oncotarget*, 7(32), 52553.
- Dhawan, D., Ramos-Vara, J.A., Naughton, J.F., Cheng, L., Low, P.S., Rothenbuhler, R., Leamon, C.P., Parker, N., Klein, P.J., Vlahov, I.R., & Reddy, J.A. (2013). Targeting folate receptors to treat invasive urinary bladder cancer. *Cancer Research*, 73(2), 875-884.
- He, L., Wang, Q., Mandler, D., Li, M., Boukherroub, R., & Szunerits, S. (2016). Detection of folic acid protein in human serum using reduced graphene oxide electrodes modified by folic-acid. *Biosensors and Bioelectronics*, 75, 389-395.

Huang, P., Xu, C., Lin, J., Wang, C., Wang, X., Zhang, C., Zhou, X., Guo, S., & Cui, D., 2011. Folic acid-conjugated graphene oxide loaded with photosensitizers for targeting photodynamic therapy. *Theranostics*, 1, p.240.

Kalli, K. R., Oberg, A. L., Keeney, G. L., Christianson, T. J., Low, P. S., Knutson, K. L., & Hartmann, L. C. (2008). Folate receptor alpha as a tumor target in epithelial ovarian cancer. *Gynecologic Oncology*, 108(3), 619-626.

Kelemen, L.E. (2006). The role of folate receptor α in cancer development, progression and treatment: cause, consequence or innocent bystander?. *International Journal of Cancer*, 119(2), 243-250.

Ledermann, J. A., Canevari, S., & Thigpen, T. (2015). Targeting the folate receptor: diagnostic and therapeutic approaches to personalize cancer treatments. *Annals of Oncology*, 26(10), 2034-2043.

Lu, Y., Segal, E., Leamon, C. P., & Low, P. S. (2004). Folate receptor-targeted immunotherapy of cancer: mechanism and therapeutic potential. *Advanced Drug Delivery Reviews*, 56(8), 1161-1176.

Mignon, P., Loverix, S., Steyaert, J., & Geerlings, P. (2005). Influence of the π - π interaction on the hydrogen bonding capacity of stacked DNA/RNA bases. *Nucleic Acids Research*, 33(6), 1779-1789.

Nie, S., Xing, Y., Kim, G. J., & Simons, J. W. (2007). Nanotechnology applications in cancer. *Annual Review of Biomedical Engineering*, 9, 257-288.

O'Shannessy, D.J., Somers, E.B., Albone, E., Cheng, X., Park, Y.C., Tomkowicz, B.E., Hamuro, Y., Kohl, T.O., Forsyth, T.M., Smale, R., & Fu, Y.S. (2011). Characterization of the human folate receptor alpha via novel antibody-based probes. *Oncotarget*, 2(12), 1227.

O'Shannessy, D.J., Yu, G., Smale, R., Fu, Y.S., Singhal, S., Thiel, R.P., Somers, E.B., & Vachani, A. (2012). Folate receptor alpha expression in lung cancer: diagnostic and prognostic significance. *Oncotarget*, 3(4), 414.

O'Shannessy, D. J., Somers, E. B., Maltzman, J., Smale, R., & Fu, Y. S. (2012). Folate receptor alpha (FRA) expression in breast cancer: identification of a new molecular subtype and association with triple negative disease. *Springerplus*, 1(1), 22.

O'Shannessy, D. J., Somers, E. B., Palmer, L. M., Thiel, R. P., Oberoi, P., Heath, R., & Marcucci, L. (2013). Serum folate receptor alpha, mesothelin and megakaryocyte potentiating factor in ovarian cancer: association to disease stage and grade and comparison to CA125 and HE4. *Journal of Ovarian Research*, 6(1), 29.

Salazar, M.D.A., & Ratnam, M. (2007). The folate receptor: What does it promise in tissue-targeted therapeutics? *Cancer and Metastasis Reviews*, 26(1), 141–152.

Shakeri-Zadeh, A., Ghasemifard, M., & Mansoori, G. A. (2010). Structural and optical characterization of folate-conjugated gold-nanoparticles. *Physica E: Low-Dimensional Systems and Nanostructures*, 42(5), 1272-1280.

Topkaya, S. N., Azimzadeh, M., & Ozsoz, M. (2016). Electrochemical biosensors for cancer biomarkers detection: recent advances and challenges. *Electroanalysis*, 28(7), 1402-1419.

Zwicke, G. L., Ali Mansoori, G., & Jeffery, C. J. (2012). Utilizing the folate receptor for active targeting of cancer nanotherapeutics. *Nano Reviews*, 3(1), 18496.

Chapter 6

Fullerenol-Folic acid Bioconjugate: a potential scope for future study

6.1 Introduction

6.1.1 Further scopes toward bioconjugation

Current studies discussed in the previous chapters of this thesis have shown that $C_{60}(OH)_8 \cdot 2H_2O$ prepared by the ultrasound-assisted technique could be used in the detection of a cancer biomarker, $FR\alpha$. Further, a quantitative analysis has shown that a simple mixture of FA and $C_{60}(OH)_8 \cdot 2H_2O$ was able to detect $FR\alpha$ up to 1 nM indicating that the detection limit and the reproducibility of the proposed biosensor could further be elevated if a nanohybrid [FA- $C_{60}(OH)_8 \cdot 2H_2O$] could be prepared and used for the same purpose of detection. Nevertheless, most of the bioconjugation techniques in preparing nanohybrid biomolecules are involved with complex organic synthesis methods in making either a strong covalent or ionic bond between the molecules, in some cases making a polymeric chain connection between the ligand and the electron mediator by using an additional or intermediate molecule of another material (s). In that way, although it is possible to make a strongly bonded bioconjugate, but at the same time this strong covalent or ionic bond among the functional sites of the molecules may block the active sites specific for the analyte. As the host-receptor interaction between FA and $FR\alpha$ is much complex, it is important to maintain the original molecular structure of FA while designing a $FR\alpha$ biosensor so that a spontaneous molecular interaction between $FR\alpha$ and FA remains unaltered, which is also one of the main conditions to be maintained in an electrochemical biosensor. This is quite a challenge and a standing issue, especially for a non-enzymatic biosensor where often an electron mediator is used to intensify the sensitivity of the electrochemical signal generated owing to the chemical reaction between the ligand/receptor and analyte. In this case, it is also important to make sure that the mediator is able to make an electrochemical communication upon the chemical interaction between the ligand and analyte, which sometimes requires forming a Bioconjugate. Thus, it becomes very crucial a concern to make the electron mediator chemically and/or physically attached to the ligand at the same time without jeopardizing the active sites of the ligand for the docking of analyte

molecule. Hence, in the current study this issue is being addressed in view to investigating the possibilities to enhance the sensitivity and selectivity of the proposed biosensor based on FA and $C_{60}(OH)_8 \cdot 2H_2O$ for FR α .

A possible solution to the above discussed problem is to facilitate a noncovalent bond instead any strong chemical bond between the ligand and electron mediator molecules. Prospective scope is to investigate whether it is possible to form a stable pi-pi (π - π) interaction between FA and the synthesized fullereneol, in that way it could be possible to enhance the sensitivity and the selectivity of the biosensor in order to detect FR α . A more enhanced sensitivity and selectivity of a biosensor will help in the early detection of cancer as FR α which is one of the most pronounced cancer biomarkers for the epithelial-derived cancer progression. In doing so, it is first essential to understand whether a reaction mixture of FA and fullereneol in its simplest aqueous form at the room temperature over a prolonged period of continuous stirring can initiate any reaction between FA and fullereneol molecules.

In order to delineate the scopes of future studies on this context, a set of preliminary experiments were conducted focusing the possibility of the formation of π - π conjugation between folic acid and different fullereneols. Mainly two different fullereneols i.e. $C_{60}(OH)_{10} \cdot 5H_2O$ and $C_{60}(OH)_{36} \cdot 8H_2O$ were taken for a comparative study toward the possibility of forming π - π interaction in between folic acid and fullereneol moieties. Due to the low yield of synthesized fullereneol at this stage, $C_{60}(OH)_{10} \cdot 5H_2O$ was taken for the comparative studies, as $C_{60}(OH)_{10} \cdot 5H_2O$ is the neighboring fullereneol moiety of $C_{60}(OH)_8 \cdot 2H_2O$ and shows similar physicochemical properties of $C_{60}(OH)_8 \cdot 2H_2O$.

Results obtained from this additional study toward the future scopes will be useful in two ways:

- a) Will provide useful information about whether the synthesized fullereneol would be able to form any conjugation with FA in a facile way.
- b) Will help understand further application of the synthesized fullereneol and its prospects.

6.1.2 Background of study

Degradation of folic acid is inevitable but could be controlled as reported previously under different conditions of experimental setups. In general, folic acid is susceptible to heat and light. Not only thermal degradation, but also FA in its original amorphous form may also undergo degradation (Vora *et al.*, 2004) when exposed to light and heat. Despite its instability, FA is being used to a great extent nowadays in various food products and healthcare applications. For instances, to extenuate the metabolic folate deficiency nowadays many foods are fortified with folic acid (Refsum and Smith, 2017; Hertrampf *et al.*, 2003; Colman *et al.*, 1975). Most importantly due to its high affinity to FR α , folic acid has been markedly reported in many studies as a potential ligand in preparing biosensors for the early stage detection of cancer (Bellavinha *et al.*, 2014).

In the open structure of folic acid there are three building blocks - Pteridin, P-aminobenzolate and glutamate (Fig. 6.1). Being a photosensitive material, FA can degrade to various photoproducts when exposed to sunlight, UV radiation and visible light. The bond between C9 and N10 breaks down to degradation and may produce 2-amino-4-hydroxy-6-formylpteridine, 2-amino-4-hydroxypteridine, p-amino-benzoylglutamic acid and dihydro-2-amino-4-hydroxypteridine-6-carboxyaldehyde (Off *et al.* 2005; Jamil Akhtar *et al.* 2003; Akhter *et al.*, 1999). However, degradation of FA is also controlled by the pH of the solution. Akhter *et al.* (2003) showed that FA produces pterin-6-carboxylic acid and p-aminobenzoyl-L-glutamic acid under aerobic conditions. In a pH range of 2-10, subsequently it can produce 2-amino-4-hydroxy-6-formyl-pteridine, 2-amino-4-hydroxypteridine, p-amino-benzoylglutamic acid and dihydro-2-amino-4-hydroxypteridine-6-carboxyaldehyde. Due to this fact, prior to the experimentation of bioconjugation, it is important to first monitor the inter-day stability of FA in aqueous solution.

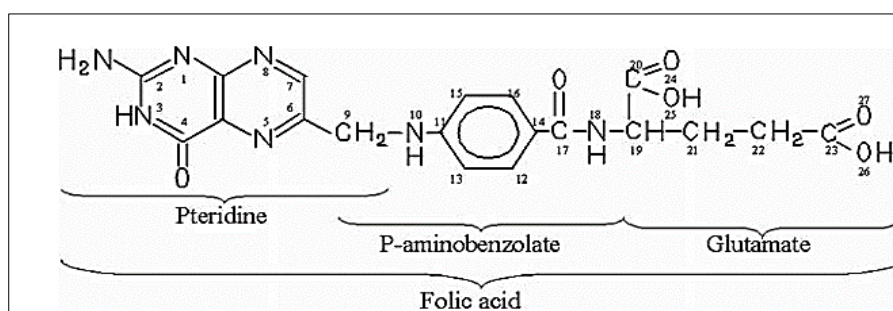


Figure 6.1 Molecular structure of folic acid (Off *et al.*, 2005)

Interestingly, while the main point of molecular cleavage takes place at C9 and N10, the functional sites of the molecule having –COOH groups are still active, which is on the glutamate part of FA. Due to the presence of multi-functional groups in the molecular structure of FA, conjugation of FA with various carbon nanomaterials including fullerene and fullerenols were achieved by organic linkers through both ionic and covalent bonding. While developing a biosensor based on FA and synthesized fullereneol, it is also important to ensure that any conjugation between FA and fullereneol does not block the active site(s) of FA which may take part in the detection of FR α . To overcome this situation, current study stresses the necessity to investigating the possibility of a facile technique of bioconjugation between FA and fullereneol based on π - π stacking. Since π - π stacking does not involve any permanent covalent or ionic bonds between the molecules rather joins the molecules via electrostatic attraction (alternatively postulated as dispersion forces) due to the presence of parallel aromatic rings in the molecules, hence molecules self-assembled or physically bonded in the their molecular level via π - π stacking are able to retain their individual molecular structure as well as contains unaltered functional groups, which make them suitable ligands or carriers in the application of biosensor and drug delivery. Therefore, without hampering the molecular structure or the active sites of FA molecule, the FA-fullereneol π - π stacked hybrid molecule could potentially be used in the detection of FR α . However, at this stage of study this is only a possibility standing on the theoretical ground of π - π stacking. It is to be noted that, although π - π stacking has been well-proven with the evidence of its significant role in the molecular intercalation into the structure of DNA and assembling various host-guest molecules, the origin as well as the various aspects of π - π stacking are still ambiguous and thus scarcely any report could be found with any explicit explanation on how to determine the π - π stacking in analytical chemistry. Due to this fact, although the concept of π - π stacking is very popular in theoretical chemistry but its application is still limited is analytical chemistry. Particularly, till to date, no study has been conducted to explore the possibility of π - π stacking between FA and fullereneol moieties. One possible reason behind this is that fullereneol itself is currently an emerging topic in the field of nanomaterial and science. Developing various organic/inorganic methods of fullereneol synthesis as well as attaching a different number of hydroxy groups in a different orientation onto C₆₀ molecule has currently been the main attention among scientists and researchers. On this scenario the application of fullereneol in forming bioconjugation with FA has little been studied by

others, hence the scope of conjugating FA and fullereneol via π - π stacking is yet to be regarded for future studies in relation to the current studies provided in this thesis.

In pursuit to understand how the proposed biosensor prepared by the synthesized $C_{60}(OH)_8 \cdot 2H_2O$ in this study could be designed to a robust biosensor, the above-discussed possibility of forming π - π stacking between FA and fullereneols has been taken into account as a potential area for future studies. To provide some directions toward a more elaborative research on this area, the current chapter will deliver some findings and explanations derived from the preliminary experiments on FA and fullereneol bioconjugation via π - π stacking.

6.2 Experimental

The current study on exploring future possibilities was conducted collaboratively in the University of Nottingham (UNMC), Malaysia and in Flinders University, Australia. Where the stability study of folic acid solution was conducted in UNMC, Malaysia, the conjugation study was conducted in Flinders University, Australia. Thus, all the experiments presented in this chapter only were designed based on the available materials and equipments which have been listed below.

6.2.1 Materials

6.2.1.1 Stability study of folic acid (FA) solution

Folic acid (FA) was purchased from Sigma Aldrich (China). Type II pure water (TOC <50 ppb) was used from a Milli-Q system (Merck Millipore Integral 5, France) for the preparation of all samples and cleaning of electrodes. Phosphate buffered saline (PBS) tablet [1 tablet in 200 mL DI water to prepare 0.01M PBS pH 7.4 which contains 0.0027 M potassium chloride (KCl) and 0.137 M sodium chloride (NaCl)] was purchased from Sigma Aldrich (Switzerland) and was used as the electrolyte.

6.2.1.2 Conjugation study

$C_{60}(OH)_{10}.5H_2O$ is a commercially available sample and was purchased as ‘nanom spectra D100’ from frontier Carbon Corporation (Japan). $C_{60}(OH)_{36}.8H_2O$ and $C_{60}(OH)_{44}.8H_2O$ were provided by Osaka University (Japan) which were prepared by the method of Kokubo *et al.* (2011). For the preparation of phosphate buffered saline (PBS), in this study, sodium chloride (NaCl) and potassium chloride (KCl) were purchased from Chem-Supply (Adelaide, Australia), disodium phosphate (Na_2HPO_4) and monopotassium phosphate (KH_2PO_4) were purchased from Sigma Aldrich (USA) and Merck (Germany) respectively. 1X PBS was prepared using the above-mentioned reagents and then was used to prepare FA solution for the conjugation study as well as a dialysis buffer for the reaction mixtures. For the dialysis of the reaction mixtures dialysis kit (Pur-A-Lyzer Mega 3500 having a MWCO of 3.5 kDa) was purchased from Sigma-Aldrich (Israel).

6.2.2 Equipment

6.2.2.1 Stability study of folic acid solution

To monitor the stability of the FA solution, UV-Vis spectroscopy was conducted in a PerkinElmer UV/Vis Spectrometer (Lambda 35, USA).

6.2.2.2 Conjugation study

To investigate the conjugation between FA and reference fullerenols UV-Vis spectroscopy was performed in Varian Cary 50 (Melbourne, Australia) spectrometer.

6.2.3 Methodology

6.2.3.1 Preparation of folic acid solution

1.5 mg of FA was dissolved into 1 L of DI water and was stirred continuously at room temperature for 5 days. The solution was analyzed every day in UV-Vis spectrometer in order to monitor the stability of the aqueous solution of FA.

6.2.3.2 Preparation of fulleranol-FA reaction mixtures

Considering the number of hydroxy groups commonly present in all the fullerenols which could possibly interact with FA, the solution of FA, $C_{60}(OH)_{10} \cdot 5H_2O$ (F10), $C_{60}(OH)_{36} \cdot 8H_2O$ (F36) and $C_{60}(OH)_{44} \cdot 8H_2O$ (F44) were prepared based on their molecular ratio and solubility in water. Accordingly, 0.5 g of FA was dissolved in 1 L of 1X PBS (8 g of NaCl, 0.2 g of KCl, 1.44 g of Na_2HPO_4 , 0.24 g of KH_2PO_4 in 1 L of MilliQ water). Fulleranol solutions of F10, F36 and F44 were prepared by dissolving 10 mg of each one in 40 mL of DI water. All the solutions containing vials and bottles were covered entirely and kept in a cool dark place overnight for allowing homogeneous distribution of all the particles in their solvents. After this, the reaction mixtures of fulleranol and FA were prepared as follows.

Reaction mixture, F10-FA: 20 mL of F10 solution was mixed into 188 mL of FA solution;

Reaction mixture, F36-FA: 20 mL of F36 solution was mixed into 122 mL of FA solution;

Reaction mixture, F44-FA: 20 mL of F44 solution was mixed into 112 mL of FA solution.

All the reaction mixtures were continuously subjected to prolonged stirring (~700 rpm) up to seven days. On day seven of the reaction, all the reaction mixtures were collected for dialysis. The reaction mixtures were dialyzed in 1X PBS for up to three days.

6.3 Results & Discussion

6.3.1 Stability and degradation of FA

For the stability study of FA, two sets of experiments were conducted. In the first set of experiments, FA solution without any stirring was observed for 5 days and every day was scanned by UV-Vis spectroscopy. In another set, FA solution was put on stirring continuously for 5 days and every day the sample was checked by UV-Vis spectroscopy. This was to compare whether in the absence of any other molecule, in an aqueous solution, FA may undergo any structural changes under stirring. This

information was important to understand the next experiments to investigating the possibility of any conjugation between FA and different fullerenols.

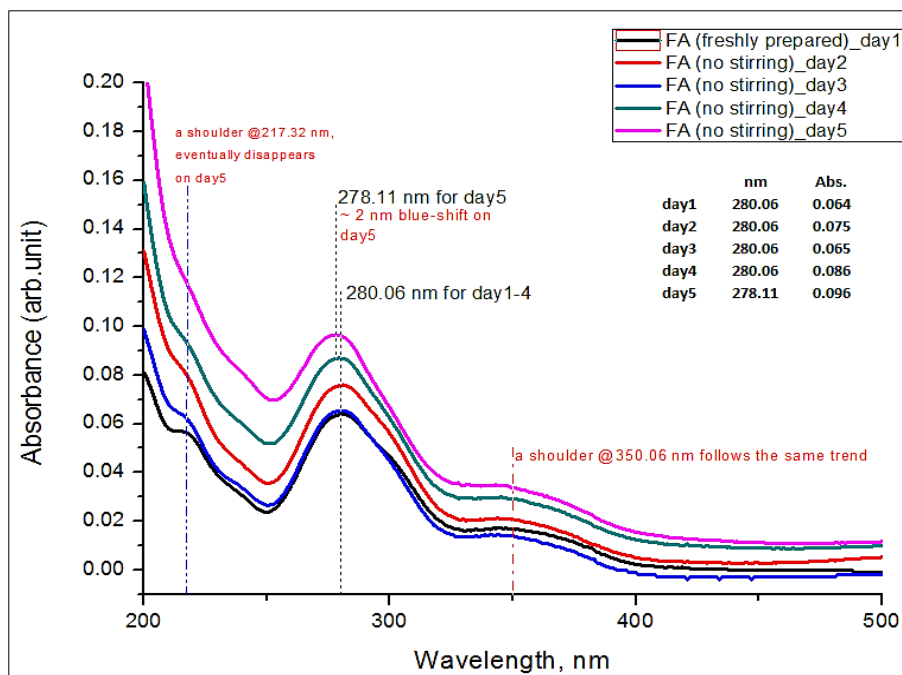


Figure 6.2 Absorption spectra of unstirred aqueous solution of FA recorded for five days

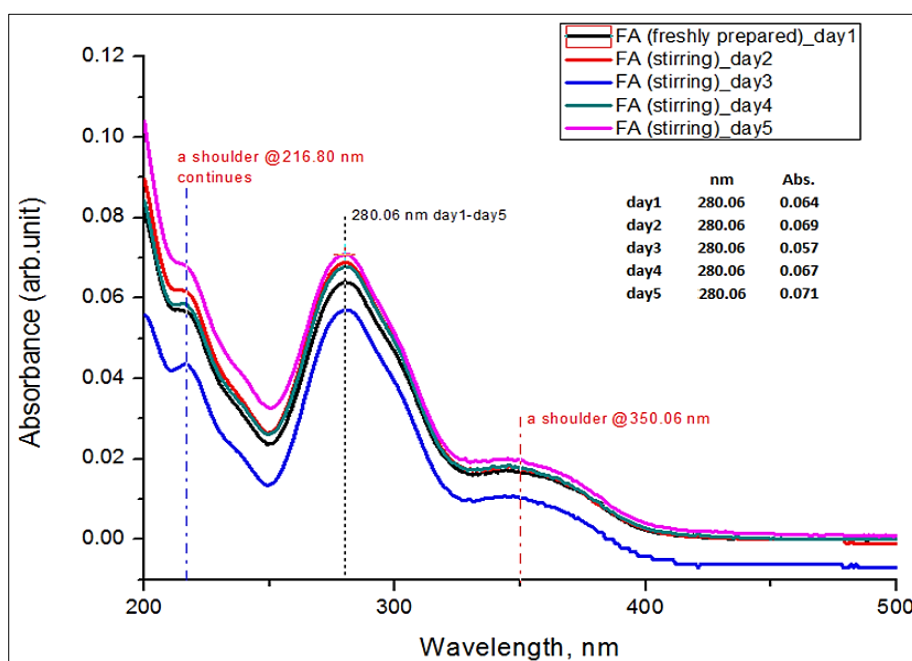


Figure 6.3 Absorption spectra of stirred aqueous solution of FA recorded for five days

In the first set of experiment, where FA solution was monitored by UV-Vis spectroscopy without any stirring showed that absorption value of FA was increasing from day 1 to day 5, however there is a decrease in the absorption value on day 3 (Fig. 6.2). The same trend was observed where FA solution was put on continuous stirring for five days and was monitored by UV-Vis spectroscopy (Fig. 6.3). The absorption maxima for the stirred FA solution was also appeared at 280.06 nm with an increase in the absorption intensity from day 1 to day 5, where on day 3 it was slightly decreased. An absorption shoulder at 217.32 nm and 216.80 nm in the UV region of spectra was observed both for the unstirred and stirred solution of FA; however, for the unstirred FA solution this shoulder was eventually disappeared on day 5, whereas for the stirred solution of FA it continued at the same wavelength till day 5. This small intensity absorption shoulder generally be considered as the effect of auxochrome and/or chromophore over the characteristic absorption spectra of FA. Since FA has a complex molecular structure where both σ and π bonds carrying orbital as well as n (non-bonding) orbital are distributed in the three counterparts (pteridine, p-aminobenzolate, glutamate) within the molecule, hence for FA molecule there are scopes for all the possibilities of electron, vibrational and rotational transitions. As a result of that besides the main characteristic absorption maximum of FA (280.06 nm) a small shoulder was observed not only in the UV region but also in the visible region of spectra (350.06 nm) in both the unstirred and stirred solution of FA over five days of observations. These shoulders are inconsistent due to the effect of solvent as well as the total energy gained by the molecule from the UV and visible light. The reason behind this feature could more precisely be described based on the concept of quantum chemistry, where in a complex molecule the energy levels, e.g. ground state or electronic level, vibrational level and rotational levels are more closely spaced, because of that photons both in the near ultraviolet and visible light play role in the transition, which is directly correlated to the absorption of the molecule. In fact, compared to the electronic energy state of a molecule the vibrational energy states are closer to each other in different parts of a molecule so even lower energy carrying photons can affect the transition in a molecule which has a structure similar to FA. The small shoulder both in the UV and visible range of spectra of FA (both in the unstirred and stirred solution) could be attributed to the transitions due to those vibrational states.

Interesting features were observed when compared to the UV-Vis spectra of the FA solution (without stirring) and FA solution (stirring). In the FA solution (without stirring) the characteristic peak of FA was observed at 280.06 nm which appeared possibly due to the change in the electronic state of FA which was consistent from day1 to day 4 (Fig. 6.2). On day 5 a slight hypsochromic shift at a value of 2 nm was observed for FA at 278.11 nm for the unstirred solution of FA (Fig. 6.2), whereas the stirred FA solution was still showing the absorption maxima at 280.06 nm similar to that of freshly prepared on day 1 (Fig. 6.3). However, the main characteristic absorption maxima (280.06 nm) of FA remained same for both unstirred and stirred FA solution up to day 4 (Fig. 6.4a - 6.4d).

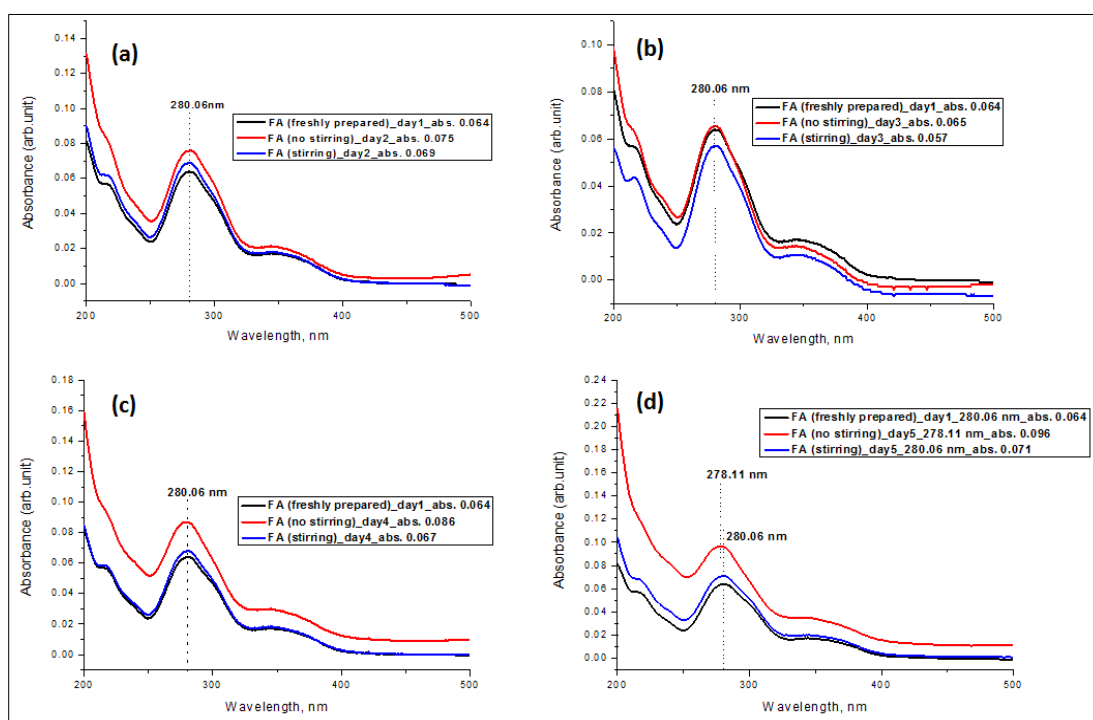


Figure 6.4 Comparative absorption spectra of unstirred and stirred aqueous solution of FA

Taking into consideration that the complex molecule FA may undergo various vibrational state in the UV and visible region of spectra, where concentration, selection of solvent, temperature may play vital role on the absorption spectra of FA, the current data evidence that a slight shift in the characteristic maximum absorption of FA may not necessarily indicate the degradation of FA, in the case of both unstirred and stirred solution of FA. Hence, for the conjugation study stirring of FA solution for 5 days,

under a controlled environment free of heat and light, showed consistent profile of both unstirred and stirred solution of FA. More importantly it indicated that stirring of FA solution for prolonged period may not result in any molecular change in FA, hence a change is to be observed in the UV-Vis spectra of reaction mixtures could possibly be attributed to the molecular interaction (covalent or noncovalent) between FA and fullerenols.

6.3.2 Comparative study: toward the possibility of F10-FA and F36-FA hybrid molecules

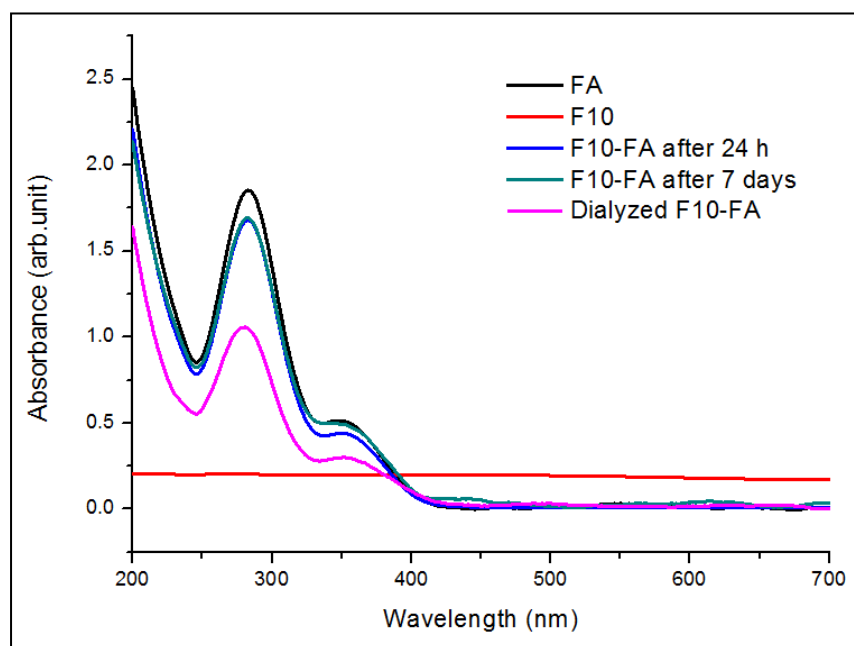


Figure 6.5 UV-Vis spectra of F10-FA reaction mixture

Both the reaction mixtures i.e. F10-FA and F36-FA were monitored after the first 24 h of reaction and then at the end of reaction on day 7. Fig. 6.5 shows the UV-Vis spectra monitored for the reaction mixture of F10-FA, where the absorption maxima of the reaction mixture after 24 h and on day 7 are almost similar with a slight decrease in the absorption intensity compared to that obtained for FA solution. No shift in the absorption spectra was observed for the reaction mixture, whereas the reaction mixture collected on day 7 when dialyzed for 3 days showed a significant decrease in the absorption intensity, indicating that the unreacted FA molecules were dialyzed, a very slight shift in the absorption maxima for the dialyzed reaction mixture F10-FA provides

an indication toward the presence of pi-pi interaction in between the F10 and FA molecule.

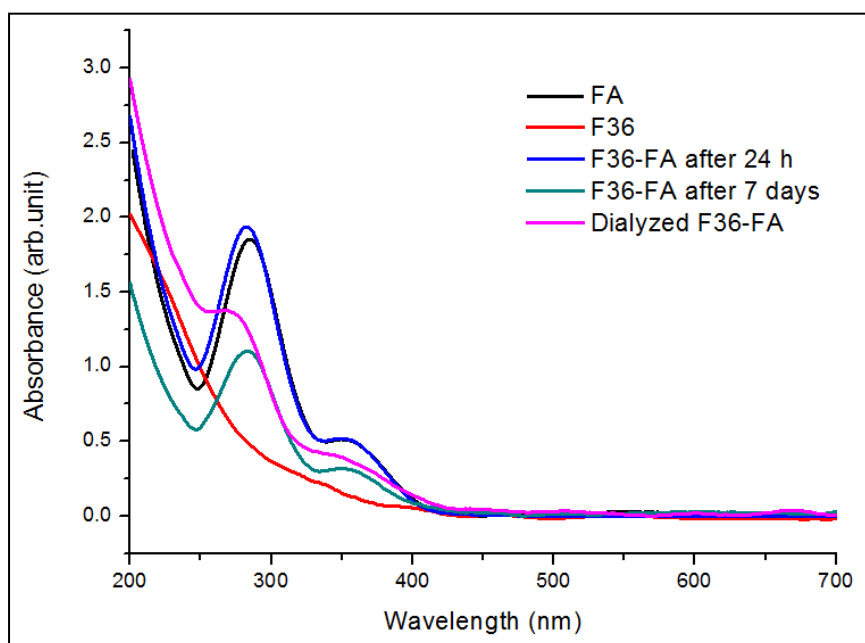


Figure 6.6 UV-Vis spectra of F36-FA reaction mixtures

A different phenomenon was observed while the same experiments were conducted for the reaction mixture of F36-FA (Fig. 6.6). F36 does not have any spectra in the UV-Vis region at the given concentration used in this experiment. The reaction mixture F36-FA was also kept on stirring for 7 days. The UV-Vis spectra of the F36-FA reaction mixture after 24 h and on day 7 showed a significant difference in the intensity of the absorption spectra, while the reaction mixture for 24 h showed almost similar absorption spectra like FA, but on day 7 the absorption intensity decreased up to 43 % compared to the reaction mixture F36-FA after 24 h reaction. This implies that the initial concentration of unconjugated FA in the mixture reduced to a significant level possibly due to the formation of π - π interaction between FA and F36 molecules. The UV-Vis spectra of the dialyzed reaction mixtures manifest this assumption too, where both the characteristic absorption maxima (~ 272 nm) as well as the shoulder at 350 nm were changed in intensity with a significant shift (~ 10 nm) in the wavelength in the absorption maximum compared to the absorption maxima (~ 282 nm) obtained for reaction mixture after 7 days of reaction. The absorption maxima of F36-FA dialyzed reaction mixture was increased to 24.5% compared to that obtained for F36-FA reaction mixture on day 7. These observations open up the possibility of molecular interaction

between FA and F36 where possibly π - π^* and n - π^* electronic transition of the conjugated molecule i.e. F36-FA in both UV and visible regime of spectrum results in a hypsochromic shift (or blue shift).

The above discussion implies that as compared to fullerenols having fewer –OH groups, those having more –OH groups may have higher potential to form a conjugated form with FA. To verify this assumption, fullereneol containing 44 hydroxy groups [$C_{60}(OH)_{44}.8H_2O$] was used for similar studies. The UV-Vis spectra (Fig. 6.7) of the reaction mixture [F44-FA] of $C_{60}(OH)_{44}.8H_2O$ and FA showed almost similar trend of F36-FA where the reaction mixture on day 7 showed a significant decrease in the absorption spectra both in the UV and visible regime, and for the dialyzed reaction mixture both the absorption maximum and the shoulder showed a hypsochromic shift (Fig. 6.7). The absorption maximum for F44-FA was reduced to 29 % after day 7 compared to that obtained for the reaction mixture after 24 h. Whereas, for the dialyzed reaction mixture of F44-FA the absorption maxima was changed to 29.0 % compared to that obtained for the reaction mixture on day 7.

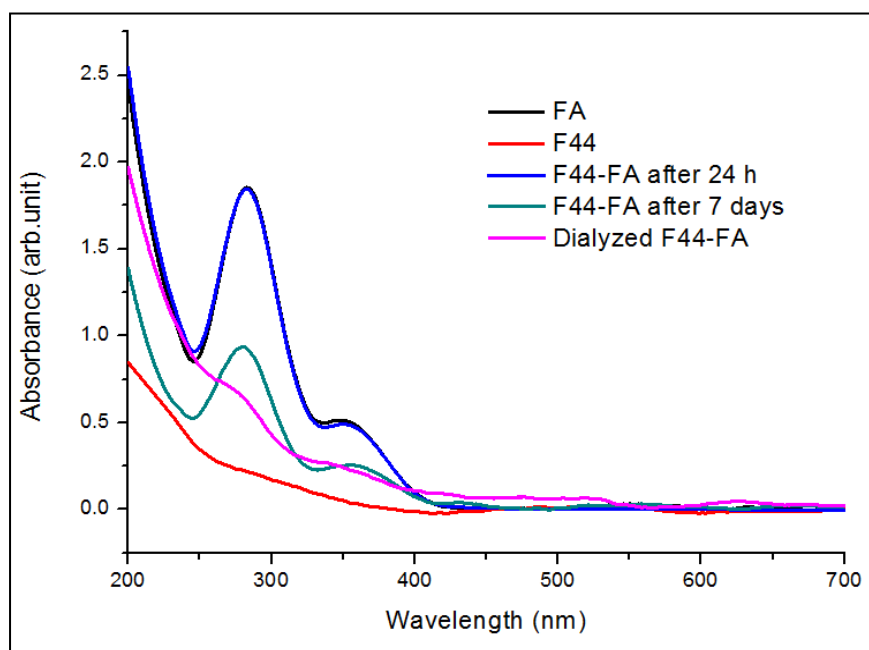


Figure 6.7 UV-Vis spectra of F44-FA reaction mixtures

The above discussion showing significant shifts and changes both in the absorption wavelength and absorption maxima for the reaction mixtures i.e. F10-FA, F36-FA and F44-FA which emphasizes that the possibility of the formation of any molecular interaction, specially π - π stacking between fullerenols and FA simply by prolonged

stirring cannot completely be ignored rather appear with certain possibilities, hence this should be taken into consideration as one of the further scopes on the current work. Specially, where the current discussion evidence that fullerenols having both few and more –OH groups have the potential to make intramolecular interaction with FA. The current observation in that way also evidence that the synthesized fulleranol prepared by the ultrasound-assisted technique should further be considered for similar studies. Moreover, fullerenols having more –OH groups at this stage could be considered for potential applications.

6.4 Summary of the Current Chapter and Direction to the Next Chapter

The current chapter showed a direction toward the future studies that should be carried out based on the reports supported by both theoretical concepts and experimental findings presented in this work. The future work to be focused on investigating the possibilities and means of π - π stacking between folic acid and potential fulleranol moieties, given that the primary data showed in this chapter already provide some grounds for the future works, where folic acid, $C_{60}(OH)_{10} \cdot 5H_2O$ (F10), $C_{60}(OH)_{36} \cdot 8H_2O$ (F36) and $C_{60}(OH)_{44} \cdot 8H_2O$ (F44) all showed some evidence of molecular interaction with folic acid. However, any possibility of molecular interaction under such conditions might not just be limited to π - π interaction rather there are scopes of potential arguments for other possibilities, e.g. covalent bonding between FA and fulleranol as well as simple H bonding. These arguments rather enclose further possibilities and hence should carefully be taken into consideration. Moreover, the number of hydroxy groups may also play differently on this scenario, so their spectroscopic analysis might provide further insights, bearing this potential fact it is suggested that in the future studies, a theoretical simulation on the molecular structure of FA and different fullerenols based on the density functional theory (DFT) could provide useful information to unfold the possibility.

Provided with these suggestion and guidance toward the future studies the current chapter will be moving onwards to the conclusion of this thesis in the next chapter.

References

- Akhtar, M. J., Khan, M. A., & Ahmad, I. (2003). Identification of photoproducts of folic acid and its degradation pathways in aqueous solution. *Journal of Pharmaceutical and Biomedical Analysis*, 31(3), 579-588.
- Colman, N., Green, R., & Metz, J. (1975). Prevention of folate deficiency by food fortification. II. Absorption of folic acid from fortified staple foods. *The American Journal of Clinical Nutrition*, 28(5), 459-464.
- Hertrampf, E., Cortés, F., Erickson, J. D., Cayazzo, M., Freire, W., Bailey, L. B., Howson, C., Kauwell, G.P., & Pfeiffer, C. (2003). Consumption of folic acid–fortified bread improves folate status in women of reproductive age in Chile. *The Journal of Nutrition*, 133(10), 3166-3169.
- Kokubo, K., Shirakawa, S., Kobayashi, N., Aoshima, H., & Oshima, T. (2011). Facile and scalable synthesis of a highly hydroxylated water-soluble fullereneol as a single nanoparticle. *Nano Research*, 4(2), 204-215.
- Off, M. K., Steindal, A. E., Porojnicu, A. C., Juzeniene, A., Vorobey, A., Johnsson, A., & Moan, J. (2005). Ultraviolet photodegradation of folic acid. *Journal of Photochemistry and Photobiology B: Biology*, 80(1), 47-55.
- Refsum, H., & Smith, A. D. (2017). Folic acid for the prevention of neural tube defects. *JAMA Pediatrics*, 171(7), 710-711.
- Sampogna-Mireles, D., Araya-Durán, I. D., Márquez-Miranda, V., Valencia-Gallegos, J. A., & González-Nilo, F. D. (2017). Structural analysis of binding functionality of folic acid-PEG dendrimers against folate receptor. *Journal of Molecular Graphics and Modelling*, 72, 201-208.
- Vora, A., Riga, A., Dollimore, D., & Alexander, K. (2004). Thermal stability of folic acid in the solid-state. *Journal of Thermal Analysis and Calorimetry*, 75(3), 709-717.

Chapter 7

Conclusions & Recommendations for Future Research

7.1 Findings and Implications

Throughout a series of correlated studies embedded with empirical data, this thesis finally comes up with two major claims, along with some potential directions toward further studies. The major findings achieved from the current works are leading to the following claims and novelty.

Claim 1: Ultrasonic dispersal of fullerene (C_{60}) leads to the formation of potential fulleranol moiety, where in this study first time the quantitative analysis revealed that $C_{60}(OH)_8 \cdot 2H_2O$ is the most possible fulleranol structure that could be obtained via the proposed method of ultrasonication. Thus, a potential method of attaching eight hydroxy groups onto C_{60} was established.

Claim 2: $C_{60}(OH)_8 \cdot 2H_2O$ could be considered as a potential nanomediator/electron-blocker in the fabrication of folic-acid based biosensor for the detection of $FR\alpha$, where the very first time in this work $C_{60}(OH)_8 \cdot 2H_2O$ synthesized via ultrasonication was applied in preparing an electrochemical biosensor for the detection of a cancer biomarker folate receptor alpha ($FR\alpha$) in association with folic acid.

As research studies propose new claims, consequently the new claims raise potential arguments, which as a result pioneers further possibilities. The current research investigation is also not beyond that scenario. In the closing chapter of thesis, few points to be noted regarding the overall prospects of the current research investigation and its findings. The current work is offering a potential synthesis technique of $C_{60}(OH)_8 \cdot 2H_2O$ via ultrasound-assisted technology simply in an aqueous medium. The proposed method of ultrasonication is not only providing a facile way of fulleranol synthesis but also very short time for the reaction. Since no phase transfer catalyst was required in the proposed method of synthesis, the purification and separation process of the synthesized $C_{60}(OH)_8 \cdot 2H_2O$ became much easier compared to the techniques used in the contemporary methods of fulleranol synthesis and purification. While generation of hydroxy groups in the aqueous medium during ultrasonication is an well-proven

phenomenon and the current study comes up with a novel scope of synthesizing $C_{60}(OH)_8 \cdot 2H_2O$ by exploiting the underlying phenomenon which occurs during ultrasonication in an aqueous medium, further scopes, e.g. synthesizing different fullerenols containing few or more hydroxy groups and preparing exohedral fullerene derivatives via ultrasonication technique are also in the queue of potential possibilities, thus needs further studies on diverse levels. At this stage of study, the yield obtained for $C_{60}(OH)_8 \cdot 2H_2O$ was 2% on an average and maximum was 4% which for the laboratory-oriented research purpose is quite promising, however this leaves with a question whether at this yield the current method will be applicable for bulk production, given that there are different ultrasonic systems available in the market hence by using different ultrasonic systems with varying the experimental parameters could possibly provide further development on this matter. Thus, it intrigues toward the study of designing its industrial process and investigating the possibility of bulk production. The current study not only provided a facile technique of fullereneol synthesis rather it was coupled with the application of the synthesized fullereneol as well, where a new application of the synthesized fullereneol [$C_{60}(OH)_8 \cdot 2H_2O$] along with the presence of folic acid was investigated in fabricating a biosensor for the detection of a cancer biomarker $FR\alpha$. This showed that the synthesized fullereneol, in another way fullerenols having fewer $-OH$ have potential effects on the electrochemical reaction between folic acid and folate receptor. The signal obtained from the biosensor under investigation showed that the synthesized fullereneol along with folic acid impacts on the current in a descending approach, which indicates that in developing a point-of-care biosensor the quantification of $FR\alpha$ should be related inversely with the intensity of current. This also implies that the effect of $C_{60}(OH)_8 \cdot 2H_2O$ could be considered as an electron-blocker rather an electron-accelerator. Till to date no study has been reported on using $C_{60}(OH)_8 \cdot 2H_2O$ in association with FA in detecting $FR\alpha$. Thus, the proposed biosensor provided new information on the behavior of the electrochemical biosensor prepared using FA and $C_{60}(OH)_8 \cdot 2H_2O$ mixture for the detection of $FR\alpha$. At the same time, some additional insights were obtained regarding the electrochemical behavior of folic acid which provided supporting information for those to be taking part in reproducing the current work and/or developing further based on the current reports. However, in the current study, where the main purpose of studying the electrochemical behavior of FA in aqueous solutions was to determine the most suitable method of folic acid preparation for the detection of folate receptor $FR\alpha$, it was beyond the scopes to investigate that

whether diffusion or adsorption played the vital role in the reaction kinetics due to less affinity of folic acid to the surface of glassy carbon. The current observations and findings leave with rooms for further studies in this zone. A binder might be useful in future studies to facilitate a stronger attachment of folic acid onto the surface of glassy carbon electrode where it is also important to understand that use of a binder for a folic acid should not be made on a random selection, as the strong attachment of folic acid on the electrode not only be regulated by the chemical structure and type of the binder but also on the type of working electrode as well as the electrolyte solution.

It has to be taken into account as well that a biosensor whether electrochemical or any other type, could be constructed based on different combination of receptor-mediator along with a diverse choice of electrolytes, electrodes, and other experimental conditions. Hence, the current study encourages more works in this avenue to exploring the potential of fullerenols, whether prepared via ultrasonication or conventional methods, in developing folic acid-based biosensors for the detection of FR α . As shown in the current study, that electrochemical response of folic acid is quite equivocal and hence future studies in this area should focus on enhancing the stability and retain time of folic acid onto working electrode, thus it could be useful not only for FR α detection rather for other biomolecules that may have molecular interaction with folic acid. In relation to that, it would also be quite interesting to investigate the possibility of a facile technique of bioconjugation between folic acid and fullereneol moieties which will render higher sensitivity in the FR α biosensor. Bioconjugation may also work differently, because during bioconjugation the active functional groups of folic acid will be engaged with the fullerenols, which might also block the functional groups used by FR α to interact with folic acid. Thus, further studies are highly recommended on this avenue that whether bioconjugation enhance the sensitivity of the proposed biosensor or hinders the molecular interaction between folic acid and FR α or even promotes any non-specific binding. Upon these further studies a more robust biosensor could be developed as a point-of-care diagnostic tool.

7.2 Recommendations for Future Studies

Having the findings from the current study and based on the given facts and possibilities as discussed in the earlier section of this chapter, the following prospects are to be noted for future studies:

7.2.1 Industrial scale-up of the proposed method of synthesis

With a view to establishing the industrial scale-up of the proposed method for synthesizing [8]hydroxy fullerenol, following investigations should be carried out in future studies:

- Feasibility of the ultrasound-assisted synthesis process in terms of the material and maintenance cost compared to other methods of preparing fullerenols.
- Increasing the yield of ultrasound-assisted synthesis at different frequencies of ultrasonication as well as with different concentrations of H₂O₂, however too higher concentration of H₂O₂ could make the process hazardous, hence concentration of 35% of H₂O₂ is recommended at the most. In that case different frequencies and power of ultrasonication could be alternative solutions to increase the yield of fullerenol.

7.2.2 Enhancing the sensitivity and selectivity of the fullerenol/folic acid-FR α biosensor

The ultimate target for developing a biosensor is to provide the scopes to fabricating lab-on-chip biosensor, which requires not only high sensitivity and selectivity but also high precision in its measurement. The proposed biosensor is the first one dealing with the detection of FR α where completely a new combination of ligand-mediator was introduced, where folic acid played the role of ligand for FR α and the synthesized fullerenol, C₆₀(OH)₈.2H₂O, was introduced to mediate the electrochemical process. Since current study showed that the presence of C₆₀(OH)₈.2H₂O is showing descending strategy for FR α , due to the formation of folic acid-FR α complex at the GCE which was also reported by others in similar studies with graphene, thus it is required to further understand whether the act of C₆₀(OH)₈.2H₂O in FR α biosensor could be attributed as a mediator effect or as a blocker effect. A few recommendations are suggested here for

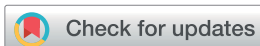
future studies to understand the synergetic mechanism of $C_{60}(OH)_8.2H_2O$, folic acid and $FR\alpha$ at the working electrode, the knowledge of which will guide us to enhance the sensitivity and selectivity of the proposed biosensor for the detection of $FR\alpha$ on a lab-on-chip biosensor. Further, selecting an appropriate binder to stabilize the coating of folic acid onto GCE as well as a facile bioconjugation to strengthen the molecular interaction between folic acid and $C_{60}(OH)_8.2H_2O$ could add more advantages to this effort. Thus, the following recommendations are suggested for the development of the proposed biosensor:

- Electrochemical impedance spectroscopy (EIS) of GCE/PBS and GCE/FAPBS/ $C_{60}(OH)_8.2H_2O$ both in absence and presence of $FR\alpha$ to be conducted to investigate the underlying effect of $C_{60}(OH)_8.2H_2O$ in enhancing the descending trend in the amperometry of $FR\alpha$, where the equivalent circuit that could be obtained from EIS study can delineate the electrochemical control mechanism for $FR\alpha$ biosensor in presence of $C_{60}(OH)_8.2H_2O$ and folic acid.
- Selection of a suitable binder to stabilize the coating of FA onto GCE, i.e. the electrochemical behavior of folic acid in presence of different binders, e.g. glucose acetate, Nafion, etc., should be studied because a binder that might work well with folic acid alone may not be favorable for the electrochemical interaction between folic acid and $FR\alpha$. Hence, extensive studies can provide an appropriate selection of binder for folic acid as well as for $C_{60}(OH)_8.2H_2O$.
- Developing a facile bioconjugation between fulleranol and folic acid could be an alternative as to the use of a binder. Where a bioconjugation should be in such a way that it can make a stable molecular bridge between folic acid and fulleranol moieties but do not block the active site of folic acid for $FR\alpha$. With that condition, it is recommended to investigate the possibility of forming pi-pi conjugation between folic acid and different fullerenols. As shown in chapter 6 of this thesis that there is a certain indication of the possibility of pi-pi stacking between folic acid and fullerenols having both few and more -OH groups. However, the observation gathered from the UV-Vis spectra of the fulleranol-folic acid reaction mixtures could further be investigated by several other analytical methods, e.g. mass spectroscopy, FTIR and fluorescence spectroscopy to quantify the degree of

conjugation as well as to understand the factors to be considered in favoring or limiting the pi-pi stacking between fullerlenols and folic acid. In doing that, not only the synthesized fullerlenol should be considered but a diverse range of fullerlenols should also be enlisted so a comparative study could be garnered.

Provided with the new findings and further possibilities toward future studies this thesis ends here leaving an impact in the two diverse and emerging fields of science and technology e.g. ultrasonication and biosensor.

PUBLICATIONS



Cite this: *RSC Adv.*, 2017, 7, 31930

Hydration or hydroxylation: direct synthesis of fulleranol from pristine fullerene [C₆₀] via acoustic cavitation in the presence of hydrogen peroxide

Sadia Afreen,^a Ken Kokubo,^b Kasturi Muthoosamy^a and Sivakumar Manickam ^{*a}

A green and clean approach that requires low energy and avoids the use of any toxic or corrosive reagents/solvents for the synthesis of potential fulleranol moieties [C₆₀(OH)_n·mH₂O] was proposed in this investigation, in which pristine fullerene (C₆₀) in dil. H₂O₂ (30%) aqueous media was ultrasonicated (20 kHz, 200 W) at 30% amplitude for 1 h. The attachment of hydroxyl groups (–OH) was investigated *via* FTIR and the quantification of –OH groups attached to the C₆₀ cage was conducted *via* elemental analysis. The number of secondary bound water molecules (mH₂O) with each fulleranol molecule [C₆₀(OH)_n] was measured *via* TGA, and the estimated average structure of fulleranol was calculated to be C₆₀(OH)₈·2H₂O. The synthesized fulleranol was moderately soluble in water and DMSO. Furthermore, the size of the synthesized C₆₀(OH)₈·2H₂O particles determined by both AFM and DLS analysis was found to be in the range of 135–155 nm. The proposed ultrasound-assisted acoustic cavitation technique encompasses a one-step facile reaction strategy, requires less time for the reaction, and reduces the number of solvents required for the separation and purification of C₆₀(OH)₈·2H₂O, which could be scalable for the commercial synthesis of fulleranol moieties in the future.

Received 3rd April 2017
Accepted 4th June 2017

DOI: 10.1039/c7ra03799f

rsc.li/rsc-advances

Introduction

The discovery of fullerene (C₆₀) by Sir Harold Kroto and his group in 1985^{1,2} pioneered the new chapter of fullerene chemistry in the domain of carbon allotropes and gradually this new area of chemistry has provided versatile fullerene (C₆₀) derivatives³ with potential features that could be exploited in numerous technological applications. Fullerene C₆₀, which is specifically known as Buckminster fullerene, is a carbon allotrope and has been incessantly reported as a useful potential carbon nanomaterial for various biological and metallurgical applications.^{4–6} However, owing to its insolubility in most organic and inorganic solvents,^{7,8} it is difficult to employ in many prospective studies. This tough to dissolve feature could be overcome by introducing various hydrophilic functional groups on the C₆₀ cage.^{9–14} Fulleranol, which is also known as fullerol, polyhydroxylated fullerene and hydroxylated fullerene, is one of the mostly pronounced and water-soluble fullerene derivatives¹⁵ that has been derived by the hydroxylation of the C₆₀ molecule in various ways (both solvent-associated and solvent-free methods) over the past few years. Ever since the first preparation of fulleranol, it has been a great challenge to increase the attachment of more hydroxyl groups

(–OH) onto the C₆₀ cage as well as to make the synthesis simpler and faster. The attachment of the largest number of –OH groups [C₆₀(OH)₄₄·8H₂O] has been reported by Kokubo *et al.*¹⁶ Zhang *et al.*¹⁷ reported the synthesis of C₆₀(OH)_{27.2} *via* mechanochemical means where potassium hydroxide was used as the hydroxylation reagent with C₆₀ and the two mixed vigorously in a ball mill. Wang *et al.*¹⁸ reported another solvent-free reaction path to obtain C₆₀(OH)₁₆ using a dil. H₂O₂ (30%) and sodium hydroxide mixture. The use of alkali was very common in almost all the reported successful methods for the preparation of fulleranol together with other chemicals, *e.g.*, sulfuric acid (H₂SO₄) and nitric acid (HNO₃), various solvents *e.g.*, toluene (C₇H₈), benzene (C₆H₆) and tetrahydrofuran (THF) and phase transfer catalysts (PTC) *e.g.*, tetrabutylammonium hydroxide (TBAH).^{19–21} The methods proposed by Zhang *et al.*,²² Alves *et al.*,²³ Kokubo *et al.*,²⁴ Lu *et al.*,²⁵ Zhang *et al.*²⁶ and Wang *et al.*²⁷ to prepare fullerenols with different numbers of –OH groups are also associated with the use of H₂O₂, NaOH and in some cases PTC. However, although the previous methods were proven to be successful for the synthesis of moderate to highly soluble fullerenols, it is difficult to remove the impurities obtained from NaOH and PTC which contaminate the synthesized fulleranol.^{27,28} In some cases the higher solubility of fulleranol was due to the presence of Na⁺ impurity introduced during the synthesis.²³

Also, the reaction time is much longer with these methods (from several hours to days) to generate and incorporate –OH groups onto the C₆₀ cage. In this context, the development of simpler and faster approaches for the synthesis fulleranol, which

^aDepartment of Chemical & Environmental Engineering, The University of Nottingham Malaysia Campus, Jalan Broga, Semenyih, Selangor D.E., 43500, Malaysia. E-mail: Sivakumar.Manickam@nottingham.edu.my

^bDivision of Applied Chemistry, Graduate School of Engineering, Osaka University, 2-1 Yamadaoka, Suita, Osaka 565-0871, Japan



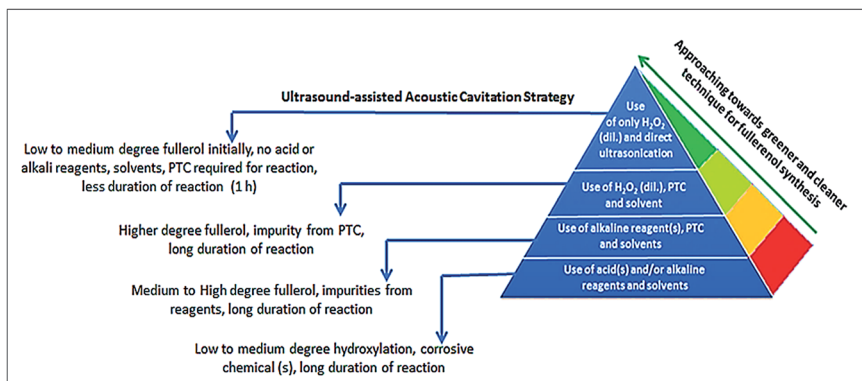


Fig. 1 Applying the greener and cleaner ultrasonic cavitation strategy to synthesize fullerene in a facile and faster way compared to other conventional methods.

are tailored by the use of minimal reagents and customized with easy purification and separation steps, is urgently required in fullerene chemistry. In this investigation, a facile method is demonstrated to overcome the above-mentioned barriers to a great extent *via* the direct ultrasonication of C_{60} in the presence of dil. H_2O_2 (30%).

Several studies^{29–31} evidence that ultrasonication in H_2O_2 associated aqueous media results in the formation of the hydroxyl radical ($\cdot OH$) which generates hydrated C_{60} as $C_{60}@ (H_2O)_n$.^{32–34} Alternatively, it will be advantageous if the formation of $\cdot OH$ radicals can be tuned to form potential fullerene moieties as well rather than just leaving it as hydrated C_{60} . Based on this, we explore an ultrasound induced acoustic cavitation strategy whereby with optimal ultrasonic variables (30% amplitude and 1 h sonication at pulse mode), pristine C_{60} is functionalized with $-OH$ groups in aqueous media in the presence of dil. H_2O_2 (30%). Following the synthesis, quantitative analysis is conducted with the functionalized C_{60} to determine the average structure of fullerene that could be potentially derived by this ultrasound assisted acoustic cavitation technique.

It is worth mentioning that the synthesis of fullerene using H_2O_2 as a hydroxylation reagent has been practiced before, but in association with other solvents and/or reagents and PTC as well.^{18,24} In this regard, herein, we propose a simpler technique which avoids the use of multiple reagents/solvents as well as PTC and thus produces fullerene more easily and efficiently in comparison to the methods reported thus far. Fig. 1 represents the chronological development of the methods proposed for the synthesis of fullerene over years and the salient features of the technique proposed in this study in comparison. Only dil. H_2O_2 (30%) is used as a hydroxylation reagent and no other supporting reagents and/or solvents or PTC are used for the synthesis. Besides, the reaction time is reduced to 1 h and unreacted C_{60} is only present as an impurity, the separation of which is easy after the reaction.

In the present method direct ultrasonication induces cavitation bubbles in the liquid H_2O_2 and C_{60} containing aqueous media. Continuous formation and then their collapse generate high energy transient hot spots inside the liquid media which dissociate water molecules into hydrogen and hydroxyl radicals.

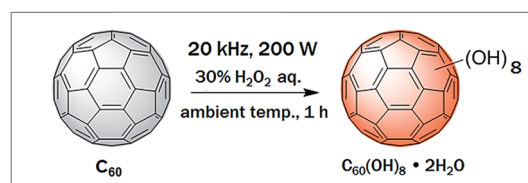


Fig. 2 Synthesis of water soluble fullerene *via* acoustic cavitation induced by ultrasound at ambient temperature, within 1 h reaction time and in the presence of dil. H_2O_2 (30%).

These hydroxyl radicals in turn combine and form H_2O_2 . Further disassociation of H_2O_2 due to the effect of acoustic cavitation generates $-OOH$ anions and/or $\cdot OH$ radicals which are exohedrally attached to the C_{60} cage by either nucleophilic attack or successive radical addition, respectively.^{35–39} Fig. 2 represents the experimental conditions for the synthesis of fullerene.

The attachment of $-OH$ groups onto the C_{60} cage was identified by Fourier transform infrared spectroscopy (FTIR) and the number of $-OH$ groups and bound water molecules were determined by elemental analysis and thermogravimetric analysis (TGA). The common formula of fullerene is $C_{60}(OH)_n$, where n is the number of $-OH$ groups attached to each C_{60} cage which could vary from 2 to 44.^{16,24,40} However, the presence of $-OH$ groups on the C_{60} cage also binds some water molecules, and the number of bound water molecules increases with an increase in the number of $-OH$ groups attached to each C_{60} moiety. Therefore, the most accurate formula of the fullerene molecule that could be obtained practically is $C_{60}(OH)_n \cdot mH_2O$,^{24,39} where m is the number of secondary bound water molecules associated with each fullerene moiety. Elemental analysis together with TGA clearly support that the average structure of the synthesized fullerene obtained by the present ultrasound-assisted technique is $C_{60}(OH)_8 \cdot 2H_2O$.

Experimental

Materials & equipment

Pristine C_{60} (98%) was purchased from Sigma Aldrich (USA) and used as the starting material to synthesize fullerene. Hydrogen peroxide (H_2O_2) aqueous solution (30% reagent grade) from



R&M chemicals (UK) was used as the hydroxylation reagent. Type II pure water (TOC < 50 ppb) was obtained from a Milli-Q system (Merck Millipore Integral 5, France). A Bandelin Sono-plus (UW 3200, 20 kHz, 200 W, Germany) with a titanium horn sonotrode (MS 73) was employed to introduce ultrasound. A graduated centrifuge tube (50 mL, angle 60° conical bottom) was used as the reactor or treatment vessel. A refrigerated circulator water bath (Julabo F34-ED, Germany) was used to maintain the reaction temperature close to ambient temperature during ultrasonication. Toluene (AR grade) was obtained from R&M Chemicals (Malaysia) for the separation and purification of unreacted C₆₀ from C₆₀(OH)₈·2H₂O. Dimethyl sulfoxide (DMSO) was obtained from Wako Pure Chemical Industries, Ltd (Japan) to check the solubility of synthesized fulleranol. After separation and purification, the C₆₀(OH)₈·2H₂O dispersion was dried in a freeze dryer (Christ Alpha 1-2 LDplus, Germany).

Characterization

The formation and attachment of -OH groups onto the C₆₀ cage was identified by Fourier transform infrared spectroscopy (FTIR) (JASCO FT/IR-4100). Quantification of the attached -OH groups was attained by elemental analysis using a Yanaco, CHN Corder MT-6. Thermogravimetric analysis (TGA) was performed on a Mettler Toledo instrument (TGA/DSC 1/LF/1100, Switzerland) to measure the amount of secondary bound water molecules with C₆₀(OH)₈. The particle size of C₆₀(OH)₈·2H₂O in solution was measured using a Photal, FPAR-1000HR. The thickness of the C₆₀(OH)₈·2H₂O particles was examined *via* a 5500 Agilent Technologies AFM (USA) using an ultra-sharp tip (non-contact high resonance frequency, nanosensor probe). The morphological study was carried out using a Quanta 400 (USA) field emission scanning electron microscope (FE-SEM).

Synthesis of C₆₀(OH)_n·mH₂O

Pure C₆₀ (200 mg) was added to 30% H₂O₂ (20 mL) and subjected to ultrasonication (30% amplitude, 200 W, pulse mode) for 1 h at ambient temperature. To avoid a rapid increase in the temperature owing to ultrasound dissipation through the liquid media, the reactor was fitted with a refrigerated circulator water bath which maintained the temperature inside the reactor close to ambient temperature. Initially, C₆₀ was immiscible in aqueous H₂O₂ and was a colorless heterogeneous mixture which turned light brown after 30 min of ultrasonication. Subsequently, in the next 30 min of ultrasonication it turned into a completely dark brown dispersion (Fig. 3a).

Separation and purification of C₆₀(OH)_n·mH₂O

Since pure C₆₀ was used as the starting material to synthesize fulleranol and no other reagents were used except 30% H₂O₂ for hydroxylation, after the reaction it was easier to separate the impurity, *i.e.* unreacted C₆₀, than the reported methods. After washing the dark brown dispersion with an equal volume of toluene 10 times, unreacted C₆₀ was separated from C₆₀(OH)_n·mH₂O. After adding toluene in the dispersion, two separated layers were formed immediately; the bottom layer was dark

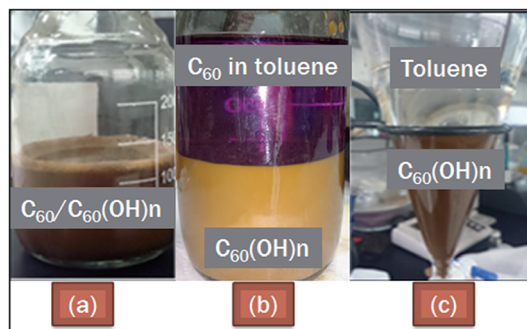


Fig. 3 (a) Dark brown dispersion immediately after ultrasonication. (b) Separation of unreacted C₆₀ from C₆₀(OH)_n·mH₂O using toluene. (c) Clear top layer of toluene after 10 times repeated washing. Here, *n* = 8 and *m* = 2 which were finally determined by elemental analysis and TGA.

brown and the upper layer was initially dark purple due to the dissolution of unreacted C₆₀ particles into the toluene layer (pristine C₆₀ is soluble in toluene and gives a purple colored solution) (Fig. 3b). Washing with toluene was repeated until the dark purple top toluene layer turned colorless, which indicated the complete removal of unreacted C₆₀ from the brown layer (Fig. 3c). The dark brown dispersion containing C₆₀(OH)_n·mH₂O was then separated from the toluene layer and dried in a freeze dryer for 30 h (-40 °C, 0.12 mbar).

Results and discussion

Identification of -OH groups

To identify the functional group(s), the dried C₆₀(OH)_n·mH₂O was analyzed *via* FTIR (Fig. 4a). The clear broad peak at 3395 cm⁻¹ within the range of 3600–3100 cm⁻¹ indicates the characteristic O–H stretching, which does not appear in the IR spectrum of pristine C₆₀ (Fig. 4b) but has been reported to be present also in the IR spectrum of pristine C₆₀(OH)₁₂ (Fig. 4c),²⁴ thus this initially confirms the attachment of -OH groups onto the C₆₀ cage after functionalization.

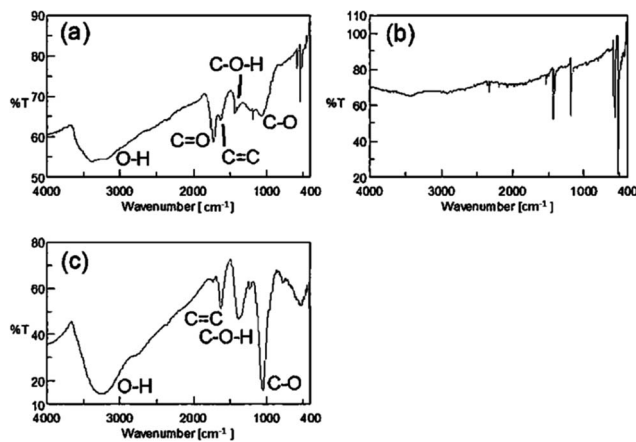


Fig. 4 FTIR spectra of (a) product C₆₀(OH)_n·mH₂O, (b) pristine C₆₀ and (c) pristine C₆₀(OH)₁₂.



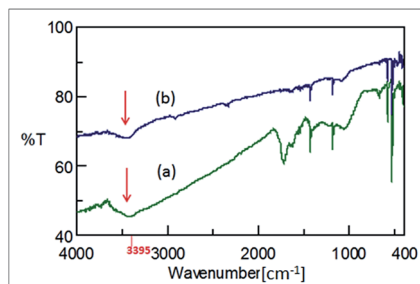


Fig. 5 IR spectra of $C_{60}(OH)_n \cdot mH_2O$ obtained via ultrasonication (a) in the presence of dil. H_2O_2 (30%) and (b) in type II pure H_2O without any H_2O_2 .

This peak was not intense when C_{60} was ultrasonicated in type II pure water (H_2O) under the same experimental conditions but in the absence of any H_2O_2 (Fig. 5b), which indicates that the use of H_2O_2 in aqueous media is a more efficient approach to introduce $-OH$ groups onto the C_{60} cage rather than only using H_2O for the synthesis of fulleranol in this ultrasound-assisted technique.

The peaks at 1625, 1427 and 1057 cm^{-1} (Fig. 4a and 5a) could possibly be attributed to the bond stretching of $C=C$, $C-O-H$ and $C-O$, respectively.^{41,42} Indeglia *et al.*⁴² emphasized that the presence of $C-O$ bond stretching is inevitable in all the fullerenols which perhaps indicates the formation of hemiketal groups prior to the hydroxylation of the C_{60} cage. In contrast, in the sample sonicated only with water, these significant peaks, which display the characteristic bond stretching of fulleranol, were absent in the IR spectrum (Fig. 5b), and thus also support that to synthesize fulleranol moieties *via* this ultrasound strategy the presence of H_2O_2 plays an important role in intensifying the hydroxylation. The additional peaks at 575 and 525 cm^{-1} in the finger print region ($<1000\text{ cm}^{-1}$) in the IR spectra of $C_{60}(OH)_n \cdot mH_2O$ (Fig. 4a and 5a) are the characteristic peaks of pure C_{60} , therefore these peaks are not attributed to any potential functional group(s). However, there could have been a trace amount of unreacted C_{60} remaining in $C_{60}(OH)_n \cdot mH_2O$ during separation and purification, which is possibly responsible for these peaks in the IR spectra of $C_{60}(OH)_n \cdot mH_2O$. We cannot rule out this possibility especially when we scale-up this method for the mass production of $C_{60}(OH)_n \cdot mH_2O$.

Estimation of the number of $-OH$ groups and the structure of fulleranol

IR spectra alone are not enough to determine and confirm the $-OH$ groups, their numbers and the structure of fulleranol. Therefore, elemental analysis was conducted to determine the composition and average structure of $C_{60}(OH)_n \cdot mH_2O$. The number of bound water molecules (m) within the $C_{60}(OH)_n$ structure was calculated *via* TGA. After the ultrasound-assisted functionalization of pure C_{60} , the average composition of C and O (C: 82.6 wt% and O: 17.2 wt%) in $C_{60}(OH)_n$ was first obtained from SEM-EDS analysis. In pure C_{60} , no trace of oxygen (C: 100%) was detected before the reaction which predicts the formation and presence of some oxygen containing functional

Table 1 Empirical formula of $C_{60}(OH)_n$ synthesized in the presence of dil. H_2O_2 (30%)

	% C	% H	H_2O^a (wt%)
Experimentally obtained	80.52	0.96	5.58
Estimated average structure calculated for-			
$C_{60}(OH)_2 \cdot 8H_2O$	80.18	2.02	16.0
$C_{60}(OH)_4 \cdot 6H_2O$	80.36	1.80	12.1
$C_{60}(OH)_6 \cdot 4H_2O$	80.54	1.58	8.1
$C_{60}(OH)_8 \cdot 2H_2O$	80.72	1.35	4.0
$C_{60}(OH)_{10} \cdot 1H_2O$	79.30	1.33	2.0
$C_{60}(OH)_{10} \cdot 0H_2O$	80.91	1.13	0

^a Measured by TGA, difference between exp. and calc. should be within $\pm 1\%$.

group(s) in the functionalized C_{60} . However, EDS cannot analyze the presence and composition of hydrogen present in a sample. The composition and structure of $C_{60}(OH)_n$ was finally deduced from elemental analysis (Table 1).

In the elemental analysis of fullerenols if the product is a pure single isomer and can be purified totally, the difference should be within 0.4%, but generally the product fulleranol is a mixture of many isomers and it is very difficult to separate the isomers from each other. Therefore, from our many synthetic experiences, even with reaction conditions completely the same as much possible, the difference in elemental analysis is somewhat large even though the chemical and physical properties of the fulleranol are essentially the same. Due to this fact, we always judge the average molecular formula of fulleranol within 1% error of elemental analysis [Tables 1 and 2]. From elemental analysis it became evident that the number of $-OH$ groups attached to each C_{60} cage is $n = 8$. The composition (C: 80.52%, H: 0.96%) obtained from elemental analysis is similar to that calculated theoretically for the structure of $C_{60}(OH)_8$, thus the structure of $C_{60}(OH)_n$ synthesized by the present ultrasound strategy was calculated as $C_{60}(OH)_8$ (Table 1). Similarly, elemental analysis was conducted to estimate the number of $-OH$ groups that could possibly be attached when pristine C_{60} was sonicated in only type II pure H_2O without the addition of H_2O_2 . By this method the number of $-OH$ groups that could be attached to the C_{60} cage is only 2 ($n = 2$) (Table 2), which again supports the role of H_2O_2 in intensifying the hydroxylation.

Table 2 Empirical formula of $C_{60}(OH)_n$ synthesized only in the presence of type II pure H_2O

	% C	% H	H_2O^a (wt%)
Experimentally obtained	92.41	0.57	1.4
Estimated average structure calculated for-			
$C_{60}(OH)_2 \cdot 2H_2O$	91.14	0.76	4.6
$C_{60}(OH)_2 \cdot 1H_2O$	93.27	0.52	2.3
$C_{60}(OH)_4 \cdot 0H_2O$	91.37	0.51	0

^a Measured by TGA, difference between exp. and calc. should be within $\pm 1\%$.



The formation and attachment of –OH groups were further confirmed by TGA (Fig. 6). The weight loss (wt%) of $C_{60}(OH)_8 \cdot 2H_2O$ was observed from room temperature to 900 °C at a rate of 10 °C min⁻¹ under N₂ flow at 20 mL min⁻¹.

An initial weight loss (5.58 wt%) was observed from room temperature to 100 °C which indicates the loss of bound water molecules. Since the number of –OH groups attached to the C₆₀ cage is less than 10, the weight loss (5.58 wt%) for secondary bound water in C₆₀(OH)₈ could be observed from room temperature to 100 °C.¹⁶ From this percentage of weight loss, the number of bound water molecules associated with each C₆₀(OH)₈ molecule was calculated to be 2 ($m = 2$) which is shown in Table 1 as well the estimated complete structure of the synthesized fullereneol.

After the decomposition of bound water the degradation continued to around 226 °C, which could be due to some of the intermediates such as epoxy or hemiketal oxygen and/or carbonyl oxygen generated during the ultrasound-assisted reaction.^{41–43} These intermediates may be present in C₆₀(OH)₈·2H₂O in trace amounts but possibly will not hinder the characteristic physical and chemical properties of C₆₀(OH)₈·2H₂O. However a detailed understanding of these intermediates present in fullereneol is not yet fully accomplished which encourages further studies. Dehydration of the –OH groups (16.85 wt%) attached to the C₆₀ molecular cage mostly occurred in the second step of TGA at around 396 °C, the value of which is very close to that theoretically calculated (15.2%) for the dehydration of 8 –OH groups. The degradation observed at around 714 °C is due to the sublimation of C₆₀ molecules. Together with the elemental analysis, the TGA result manifests that C₆₀ could actually be successfully functionalized to fullereneol *via* ultrasound-assisted hydroxylation in the presence of aq. H₂O₂ and the average structure of the fullereneol derived from these empirical studies is C₆₀(OH)₈·2H₂O.

In applying this technique for the production of fullereneol it is also necessary to explore the yield of the prepared C₆₀(OH)₈·2H₂O. In this work, the yield was verified by repeating the experiment three times. The yield of C₆₀(OH)₈·2H₂O was

investigated based on both the amount of C₆₀(OH)₈·2H₂O obtained after drying and the amount of unreacted C₆₀ separated after reaction. The yield was found to vary between 2.18 and 4.04%. There is always a possibility of material loss during the process of drying, especially directly from the liquid state to solid state, which should be considered in any future work when reproducing the proposed method to prepare C₆₀(OH)₈·2H₂O. The yield achieved is not high on the laboratory scale; however by optimizing the reaction conditions, selecting different solvents for separation and purification, improving the drying method to avoid any loss of the material, the yield of C₆₀(OH)₈·2H₂O could be increased using the proposed ultrasound method.

Particle size measurements

Usually the particles of fullereneols having a fewer number of –OH groups have been reported to be aggregative and the particle size may vary in the range of 50–300 nm.⁴¹ DLS analysis and AFM scanning were carried out to investigate the size and morphology of the C₆₀(OH)₈·2H₂O particles, respectively. For the particle size measurements, C₆₀(OH)₈·2H₂O was dissolved in DMSO (0.33 mg mL⁻¹). As a polar aprotic solvent, DMSO can dissolve both polar and nonpolar compounds. C₆₀(OH)₈·2H₂O in DMSO initially formed a suspension which was then centrifuged (TOMY, LC-200) for 5 min at 7500 rpm to obtain a clear solution of C₆₀(OH)₈·2H₂O in DMSO. Both the suspension and the solution (collected as supernatant after centrifugation) were analyzed for particle size measurements *via* the DLS method. The average particle size of C₆₀(OH)₈·2H₂O in the suspension was found to be larger (312 nm) (Fig. 7b) than that in the solution (120 nm) (Fig. 7a).

Also, larger sized particles of about 13.9 μm could be seen in the suspension (Fig. 7b) which could either be due to the highly aggregative nature of C₆₀(OH)₈·2H₂O along with some intermediates possibly present as described in the earlier section of this study or due to the presence of trace amounts of unreacted pristine C₆₀ which remained in the sample after the separation process. Hence, we infer that C₆₀(OH)₈·2H₂O when dispersed in DMSO contains particles of a wider size range and thus could be considered as a polydispersed suspension, which after centrifugation provides a clear solution of uniform sized particles of C₆₀(OH)₈·2H₂O of about 120 nm. The particle size was further verified using the topography *vs.* distance chart (Fig. 8b) obtained from the AFM analysis of C₆₀(OH)₈·2H₂O.

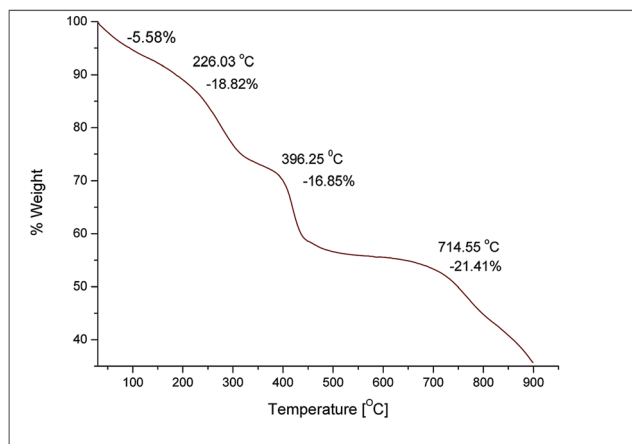


Fig. 6 TGA chart for measuring the weight loss (wt%) of C₆₀(OH)₈·2H₂O.

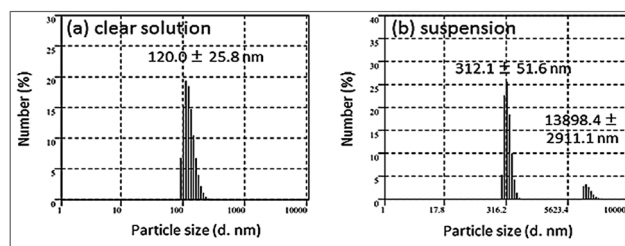


Fig. 7 Particle size measurements: (a) C₆₀(OH)₈·2H₂O/DMSO solution (collected as supernatant after centrifugation) and (b) C₆₀(OH)₈·2H₂O/DMSO suspension (0.33 mg mL⁻¹).



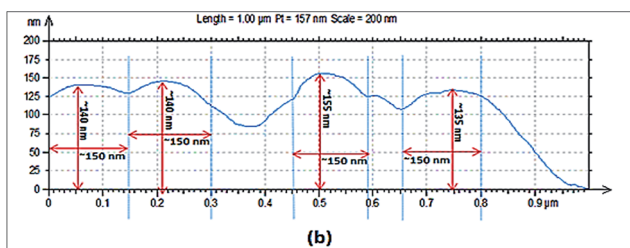
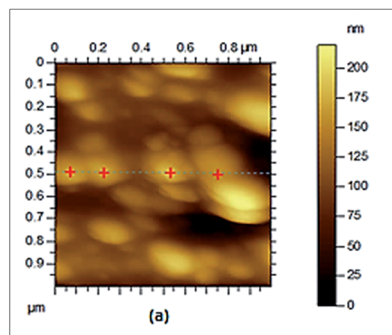


Fig. 8 (a) AFM image showing the topography of the $C_{60}(OH)_8 \cdot 2H_2O$ particles on mica substrate within a scan area of $1 \mu m \times 1 \mu m$; particles under the scanning line are marked with red crosses. (b) Topography vs. distance chart for thickness measurement, where the $C_{60}(OH)_8 \cdot 2H_2O$ particles show a consistent width of around 150 nm and the average height of the particles under scanning line is between 135 and 155 nm.

The cross section of the AFM image shows that the width of the particles is around 150 nm and their height varies from 135 to 155 nm (Fig. 8b), which indicates that the synthesized $C_{60}(OH)_8 \cdot 2H_2O$ particles could be considered spherical in shape with a diameter in the range of 135–155 nm. The average width and height of the particles obtained from the AFM analysis are congruent with the particle sizes (120 ± 25.8 nm and 312 ± 51.6 nm) obtained by DLS analysis for the saturated solution of $C_{60}(OH)_8 \cdot 2H_2O$ in DMSO (Fig. 7a) and suspension of $C_{60}(OH)_8 \cdot 2H_2O$ in DMSO (Fig. 7b), respectively. $C_{60}(OH)_8 \cdot 2H_2O$ is considered as the first member of the polyhydroxylated fullerene group to show solubility in water at a low concentration and at the same time forms aggregates when dispersed in water or DMSO. Therefore, some bigger particles are observed in the suspension of $C_{60}(OH)_8 \cdot 2H_2O$ /DMSO. This aggregation is observed in both the AFM and SEM images. The image (Fig. 8a) and height profile (Fig. 8b) obtained from the AFM analysis reveal that the individual particles of $C_{60}(OH)_8 \cdot 2H_2O$ are actually not finely separated from each other, rather they are assembled in the form of nearly spherical shaped aggregates with a range of sizes.

The SEM image (Fig. 9) provides further insight into the aggregation of the synthesized $C_{60}(OH)_8 \cdot 2H_2O$ particles when they are in the powder form. In the powder form, the $C_{60}(OH)_8 \cdot 2H_2O$ particles are much more aggregative and even display sizes bigger than 300 nm, but when they are dispersed in solvent(s), aggregation is less effective. Also, this aggregation nature decreases with an increase in the number of -OH groups attached to each C_{60} molecule.¹⁶ Even though $C_{60}(OH)_8 \cdot 2H_2O$

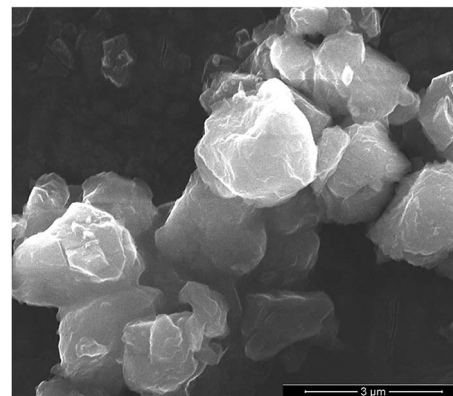


Fig. 9 SEM image of $C_{60}(OH)_8 \cdot 2H_2O$ (20 kV, magnification of 30 000 \times).

exhibits amphiphilic behavior, it is moderately polyhydroxylated; as a result the interaction potential between the particles becomes more effective than the intermolecular hydrogen bond potential which ultimately causes Brownian aggregation, and results in variable sizes of self-assembled $C_{60}(OH)_8 \cdot 2H_2O$ particles in the suspension.^{26,44}

Color and solubility

$C_{60}(OH)_8 \cdot 2H_2O$ obtained after separation, purification and drying was not completely black, rather it was nearly brown (Fig. 10a), and when dispersed in DMSO it gave a dark brown color suspension (Fig. 10b). Fullereneol having more than 10 -OH groups is observed to be dark brown in color, which gradually shifts from dark brown to yellow with an increase in the number of -OH groups (Fig. 10c), as previously reported.²⁴

The solubility of $C_{60}(OH)_8 \cdot 2H_2O$ was examined both in water and in organic solvents, *i.e.* DMSO, toluene and benzene (Table 3).

It is noteworthy to mention that $C_{60}(OH)_8 \cdot 2H_2O$ moderately dissolves in water at a lower concentration owing to its amphiphilic nature. It was found to be soluble in DMSO but did not show any solubility in toluene and benzene. On the other

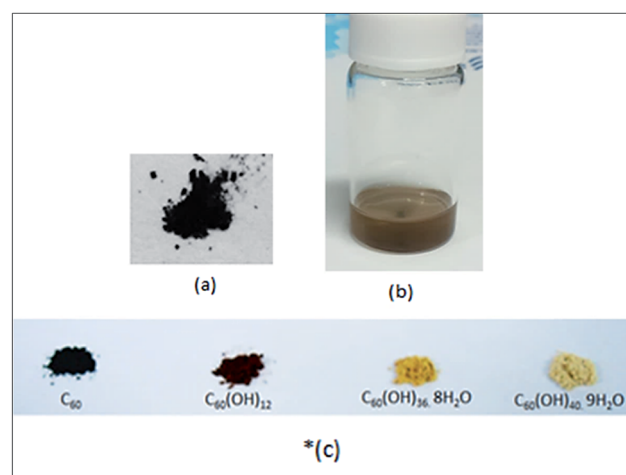


Fig. 10 (a) $C_{60}(OH)_8 \cdot 2H_2O$ after drying, (b) $C_{60}(OH)_8 \cdot 2H_2O$ in DMSO (0.33 mg mL^{-1}) and (c) colors of different fullereneols previously reported [*reprinted from Kokubo *et al.* (ref. 24)].



Table 3 Solubility of $C_{60}(OH)_8 \cdot 2H_2O$ in comparison to C_{60} in different solvents

	Water	DMSO	Toluene	Benzene
Fullerene (C_{60})	✗	✗	○	○
Fullerenol [$C_{60}(OH)_8 \cdot 2H_2O$]	○ ^a	○ ^a	✗	✗

✗ = not soluble, ○ = soluble. ^a Soluble at lower conc.

hand, pure C_{60} dissolves both in toluene and benzene but does not show any solubility in water and DMSO.

Reaction pathways

Acoustic cavitation generated from ultrasonication results in chemical reactions inside liquid media.⁴⁵ When acoustic cavitation is induced throughout liquid media (30% H_2O_2 in this case) it produces cavitation bubbles and upon continuous ultrasonication these bubbles form and collapse randomly. The collapse of these bubbles produces transient local hot spots with intense local heat and pressure inside the liquid media which assist in high-energy chemical reactions among the molecules either trapped inside the cavitation bubbles or present in the liquid media.^{46,47} In this investigation, due to ultrasound induced acoustic cavitation, radicals such as $\cdot OH$, $\cdot OOH$ and $\cdot H$ originate from H_2O and H_2O_2 molecules.^{31,48,49} Especially, the formation of $\cdot OH$ radicals due to the thermal decomposition of aqueous media has been found to be evident by electron spin resonance (ESR) and spin trapping^{29,30,50–52} studies. H_2O_2 is thermodynamically unstable and dissociates into H_2O and O_2 under thermal decomposition. During ultrasonic cavitation, H_2O and H_2O_2 molecules are trapped inside microbubbles, and when these bubbles collapse with the enormous amount of heat (several thousand degrees K) and pressure (hundreds of atmospheres)^{53,54} the molecules decompose to $\cdot OH$ and $\cdot OOH$ ^{55,56} radicals. The reaction may progress in two pathways simultaneously (Fig. 11). $\cdot OH$ radicals as reactive oxygen species (ROS) attach onto the C_{60} cage to give

fullerenol (Path I), and/or $\cdot OH$ and $\cdot OOH$ radicals attack the electron deficient C_{60} double bonds in a nucleophilic reaction and this leads to the formation of fullerene epoxide [$C_{60}O_n$] as an intermediate in the first stage (Path II) which is similar to the mechanism of the Bingel reaction.^{37,57} Further, the repeated attack of $\cdot OH$ (or $\cdot OOH$) on $C_{60}O$ *via* an S_N2 reaction results in polyhydroxylated fullerene or fullerenol.

Repeated epoxidation may take place which produces successive epoxide groups *e.g.*, $C_{60}O_2$ and $C_{60}O_3$. These epoxide groups could be possible candidates to generate other intermediates *e.g.* hydroxylated fullerene epoxide [$C_{60}(OH)_xO_y$]^{16,58} during sonolysis. Additionally, the subsequent ring opening of $C_{60}(OH)_xO_y$ with $\cdot OH$ can result in the formation of fullerenol.⁵⁹ The formation of these intermediates during the sonolysis of H_2O_2 or H_2O in the presence of C_{60} is inevitable, and their presence in the final fullerenol (although in a trace amount) cannot go unnoted. However, because they are only present in trace amounts in the fullerenol they are not expected to cause any significant impact.

Future prospects

To explore the potential applications of fullerenols, it is indeed essential to produce high quality fullerenol which means not only higher water solubility but also free of any impurities. The presence of impurities, which generally come from the preparation process, makes fullerenol undesirable for any specific biological and metallurgical applications. More importantly, the commercial value of fullerenol depends on the presence and percentage of impurities. Moreover, a faster approach is desirable to facilitate the commercial production of fullerenol. The proposed technique for the preparation of hydroxylated C_{60} by ultrasonication in the presence of H_2O_2 is free from the use of additional hydroxylating reagents, *i.e.* $NaOH$, H_2SO_4 , and PTC (causes impurities in fullerenol), which is a cleaner approach to produce fullerenol in an easier and a faster way. Previously, $C_{60}(OH)_{12}$ was used as a starting material to synthesize highly soluble fullerenols [$C_{60}(OH)_{36}$, $C_{60}(OH)_{40}$] by vigorously stirring

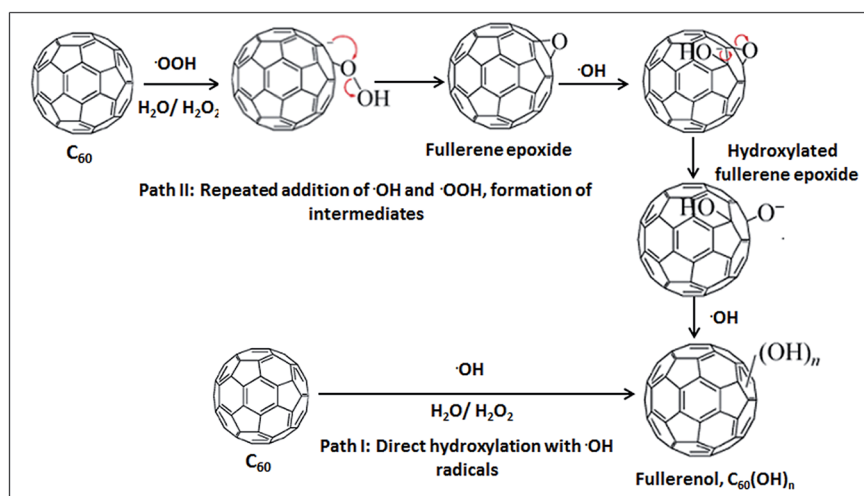


Fig. 11 Possible reaction paths in the ultrasound-assisted synthesis of fullerenol in the presence of dil. H_2O_2 (30%).



with dil. H_2O_2 for several days.²⁴ Similarly $\text{C}_{60}(\text{OH})_8 \cdot 2\text{H}_2\text{O}$ synthesized by this method could be used as a starting material to further produce fullerenols containing a greater number of hydroxyl groups, e.g. $\text{C}_{60}(\text{OH})_{24}$, $\text{C}_{60}(\text{OH})_{36}$ and $\text{C}_{60}(\text{OH})_{40}$. Moreover, compounds that express specific biochemical functions, which are required for diagnostics as well as drug therapy studies, can be derivatized from $\text{C}_{60}(\text{OH})_8 \cdot 2\text{H}_2\text{O}$ by conjugating it with other potential functional groups or biomolecules. The conjugation of folic acid with $\text{C}_{60}(\text{OH})_8 \cdot 2\text{H}_2\text{O}$ produced *via* this method is currently under investigation as an extended study of this work with the view to develop a highly sensitive biosensor for early stage cancer detection. Further potential applications for $\text{C}_{60}(\text{OH})_8 \cdot 2\text{H}_2\text{O}$ synthesized by the proposed method of ultrasonication include as an antioxidant since it offers higher antioxidant activities compared to the fullerenols that have more hydroxyl groups, i.e., $\text{C}_{60}(\text{OH})_{24}$, $\text{C}_{60}(\text{OH})_{26}$ and $\text{C}_{60}(\text{OH})_{36}$;³⁹ an electrochemically active nanomediator since based on density functional theory (DFT) it has also been found that fullerenols having less hydroxyl groups are thermodynamically more stable than those containing more hydroxyl groups due to the symmetric orientation of the $-\text{OH}$ groups around the C_{60} molecular cage;^{60,61} a light harvesting material in solar cell applications⁶² and the preparation of rich carbon structures of different shapes, sizes and isomeric orientations recently termed as Janus particles for various other applications.⁴⁴

It is anticipated that there must be a substantial difference between the levels of energy generated during continuous ultrasonication and pulse mode ultrasonication which should be also addressed in future investigations. In addition, the duration of ultrasonication may cause a remarkable difference in the structure of fullereneol. Besides the variables of ultrasonication (time and power input), it is equally important to optimize the other parameters in future studies, i.e. temperature, size and geometry of the treatment vessel, nature and concentration of any dissolved gas, concentration of H_2O_2 , solute to reagents ratio (C_{60} : 30% H_2O_2 , mg mL^{-1}) and height of the mixture in the treatment vessel, where all of them alone or together can play vital roles in producing fullerenols possessing different combinations of $-\text{OH}$ groups and bound H_2O molecules in addition to increasing the yield of $\text{C}_{60}(\text{OH})_8 \cdot 2\text{H}_2\text{O}$ while applying the proposed ultrasound technique for the synthesis of fullerenols.

Conclusion

Herein, we have proposed a facile and fast approach to prepare fullereneol *via* the ultrasound-assisted hydroxylation of C_{60} only in dil. H_2O_2 (30%) which acts as a hydroxylating reagent and we have quantified the possible structure of fullereneol that could be derived by this technique. It appears that during the ultrasonication of pure C_{60} in aqueous media, even only in the presence of H_2O_2 , not only leads to the hydration of C_{60} in the reaction media but also results in the generation of potential fullereneol candidate(s), which upon quantitative analysis has been identified as $\text{C}_{60}(\text{OH})_8 \cdot 2\text{H}_2\text{O}$. Since no alkali, acids or PTC have been used for the synthesis, the proposed method offers

a greener and cleaner approach towards the hydroxylation of the C_{60} cage compared to existing methods. Quantitative studies reveal that this hydroxylation technique assisted by ultrasonication in the presence of H_2O_2 can lead to the formation of fullereneol possessing an average structure of $\text{C}_{60}(\text{OH})_8 \cdot 2\text{H}_2\text{O}$ and with an average yield of 2%. $\text{C}_{60}(\text{OH})_8 \cdot 2\text{H}_2\text{O}$ was found to be amphiphilic and thus moderately soluble in water at a low concentration and it could further be exploited as a starting material to prepare highly water soluble fullereneol moieties. The presence of aq. H_2O_2 intensifies the hydroxylation and enhances the number of hydroxyl groups ($n = 8$) on the C_{60} cage in comparison to that obtained ($n = 2$) while applying the same ultrasonication but only in the presence of pure water. This indicates that H_2O_2 plays a vital role in the hydroxylation which could have potential to obtain fullereneol moieties, where the yield could be increased by varying the concentration of H_2O_2 . The proposed technique encompasses a one-step reaction strategy, requires a short time for the reaction, offers a green and clean approach with a low energy requirement, avoids the use of any toxic or corrosive reagents for the synthesis, and reduces the number of solvents required for the separation and purification of $\text{C}_{60}(\text{OH})_8 \cdot 2\text{H}_2\text{O}$. Hence, this potential approach should further be investigated to for the scale-up mass production of fullereneol moieties for a wider range of technological applications.

Author contributions

The manuscript was written through contributions of all authors.

Funding sources

Authors would like to thank Fundamental Research Grant Scheme (FRGS) for the funding support (FRGS/1/2013/SG05/UNIM/01/1).

Conflict of interest

The authors declare no competing financial interest.

Abbreviations

AFM	Atomic force microscopy
C_{60}	Fullerene
$\text{C}_{60}(\text{OH})_n \cdot m\text{H}_2\text{O}$	Fullereneol
DMSO	Dimethyl sulfoxide
DLS	Dynamic light scattering
FE-SEM	Field emission scanning electron microscopy
FTIR	Fourier transform infrared spectroscopy
$-\text{OH}$	Hydroxyl group
PTC	Phase transfer catalyst
SEM-EDS	Scanning electron microscopy with energy dispersive X-ray spectroscopy
TGA	Thermogravimetric analysis



Acknowledgements

KK thanks for the funding support by the Program for Creating Future Wisdom, Osaka University, selected in 2014. Authors would like to express their gratitude to Dr Huang Nay Ming, University of Malaya, Malaysia for carrying out AFM analysis.

References

- H. W. Kroto, J. R. Heath, S. C. O'Brien, R. F. Curl and R. E. Smalley, C₆₀: Buckminsterfullerene, *Nature*, 1985, **318**, 162–163.
- R. E. Smalley, Discovering the Fullerenes, *Rev. Mod. Phys.*, 1997, **69**(3), 723–730.
- S. Bosi, T. D. Ros, G. Spalluto and M. Prato, Fullerene Derivatives: an Attractive Tool for Biological Applications, *Eur. J. Med. Chem.*, 2003, **38**(11–12), 913–923.
- M. Prato, [60]Fullerene Chemistry for Materials Science Applications, *J. Mater. Chem.*, 1997, **7**(7), 1097–1109.
- T. D. Ros and M. Prato, Medicinal Chemistry with Fullerenes and Fullerene Derivatives, *Chem. Commun.*, 1999, 663–669.
- N. Tagmatarchis and H. Shinohara, Fullerenes in Medicinal Chemistry and their Biological Applications, *Mini-Rev. Med. Chem.*, 2001, **1**(4), 339–348.
- A. Hirsch, The Chemistry of the Fullerenes: An Overview, *Angew. Chem., Int. Ed. Engl.*, 1993, **32**(8), 1138–1141.
- N. Martin, New Challenges in Fullerene Chemistry, *Chem. Commun.*, 2006, **20**, 2093–2104.
- I. Lamparth and A. Hirsch, Water-Soluble Malonic Acid Derivatives of C₆₀ with a Defined Three-Dimensional Structure, *J. Chem. Soc., Chem. Commun.*, 1994, **14**, 1727–1728.
- I. C. Wang, L. A. Tai, D. D. Lee, P. P. Kanakamma, C. K.-F. Shen, T.-Y. Luh, C. H. Cheng and K. C. Hwang, C₆₀ and Water-Soluble Fullerene Derivatives as Antioxidants Against Radical-Initiated Lipid Peroxidation, *J. Med. Chem.*, 1999, **42**(22), 4614–4620.
- C. F. Richardson, D. I. Schuster and S. R. Wilson, Synthesis and Characterization of Water-Soluble Amino Fullerene Derivatives, *Org. Lett.*, 2000, **2**(8), 1011–1014.
- V. K. Periya, I. Koike, Y. Kitamura, S.-i. Iwamatsu and S. Murata, Hydrophilic [60]Fullerene Carboxylic Acid Derivatives Retaining the Original 60π Electronic System, *Tetrahedron Lett.*, 2004, **45**, 8311–8313.
- R. Partha and J. L. Conyers, Biomedical Applications of Functionalized Fullerene-Based Nanomaterials, *Int. J. Nanomed.*, 2009, **4**, 261–275.
- K. N. Semenov, N. A. Charykov and V. N. Keskinov, Fullereneol Synthesis and Identification. Properties of the Fullereneol Water Solutions, *J. Chem. Eng. Data*, 2011, **56**(2), 230–239.
- A. Dorđević and G. Bogdanović, Fullereneol – a New Nanopharmaceutic?, *Arch. Oncol.*, 2008, **16**(3–4), 42–45.
- K. Kokubo, S. Shirakawa, N. Kobayashi, H. Aoshima and T. Oshima, Facile and Scalable Synthesis of a Highly Hydroxylated Water-Soluble Fullereneol as a Single Nanoparticle, *Nano Res.*, 2011, **4**(2), 204–215.
- P. Zhang, H. Pan, D. Liu, Z.-X. Guo, F. Zhang and D. Zhu, Effective Mechanochemical Synthesis of [60]Fullerols, *Synth. Commun.*, 2003, **33**(14), 2469–2474.
- S. Wang, P. He, J.-M. Zhang, H. Jiang and S.-Z. Zhu, Novel and Efficient Synthesis of Water-Soluble [60]Fullereneol by Solvent-Free Reaction, *Synth. Commun.*, 2005, **35**(13), 1803–1808.
- J. Li, A. Takeuchi, M. Ozawa, X. Li, K. Saigo and K. Kitazawa, C₆₀ Fullerene Formation Catalysed by Quaternary Ammonium Hydroxides, *J. Chem. Soc., Chem. Commun.*, 1993, **23**, 1784–1785.
- L. Y. Chiang, L.-Y. Wang, J. W. Swirczewski, S. Soled and S. Cameron, Efficient Synthesis of Polyhydroxylated Fullerene Derivatives via Hydrolysis of Polycyclosulfated Precursors, *J. Org. Chem.*, 1994, **59**(14), 3960–3968.
- L. Y. Chiang, J. B. Bhonsle, L. Wang, S. F. Shu, T. M. Chang and J. R. Hwu, Efficient One-Flask Synthesis of Water-Soluble [60]Fullerenols, *Tetrahedron*, 1996, **52**(14), 4963–4972.
- J.-M. Zhang, W. Yang, P. He and S.-Z. Zhu, Efficient and Convenient Preparation of Water-Soluble Fullereneol, *Chin. J. Chem.*, 2004, **22**(9), 1008–1011.
- G. C. Alves, L. O. Ladeira, A. Righi, K. Krambrock, H. D. Calado, R. P. F. Gil and M. V. B. Pinheiro, Synthesis of C₆₀(OH)_{18–20} in Aqueous Alkaline Solution Under O₂-Atmosphere, *J. Braz. Chem. Soc.*, 2006, **17**(6), 1186–1190.
- K. Kokubo, K. Matsubayashi, H. Tategaki, H. Takada and T. Oshima, Facile Synthesis of Highly Water-Soluble Fullerenes More Than Half-Covered by Hydroxyl Groups, *ACS Nano*, 2008, **2**(2), 327–333.
- Y. Lu, K. Feng, P. Qiyun and Y. Xinlin, An Improved Method for Fullereneol Preparation Based on Dialysis, *Chin. J. Chem. Eng.*, 2010, **18**(5), 876–879.
- G. Zhang, Y. Liu, D. Liang, L. Gan and Y. Li, Facile Synthesis of Isomerically Pure Fullereneols and Formation of Spherical Aggregates from C₆₀(OH)₈, *Angew. Chem., Int. Ed.*, 2010, **49**(31), 5293–5295.
- F. F. Wang, N. Li, D. Tian, G. F. Xia and N. Xiao, Efficient Synthesis of Fullereneol in Anion Form for the Preparation of Electrodeposited Films, *ACS Nano*, 2010, **4**(10), 5565–5572.
- K. Matsubayashi, K. Kokubo, H. Tategaki, S. Kawahama and T. Oshima, One-step Synthesis of Water-soluble Fullereneols Bearing Nitrogen-containing Substituents, *Fullerenes, Nanotubes, Carbon Nanostruct.*, 2009, **17**(4), 440–456.
- K. Makino, M. M. Mossoba and P. Riesz, Chemical Effects of Ultrasound on Aqueous Solutions. Formation of Hydroxyl Radicals and Hydrogen Atoms, *J. Phys. Chem.*, 1983, **87**(8), 1369–1377.
- X. Fang, G. Mark and C. Sonntag, OH Radical Formation by Ultrasound in Aqueous Solutions Part I: the Chemistry Underlying the Terephthalate Dosimeter, *Ultrason. Sonochem.*, 1996, **3**(1), 57–63.
- Y. Hu, Z. Zhang and C. Yang, Measurement of Hydroxyl Radical Production in Ultrasonic Aqueous Solutions by a Novel Chemiluminescence Method, *Ultrason. Sonochem.*, 2008, **15**(5), 665–672.



- 32 W.-B. Ko, J.-Y. Heo, J.-H. Nam and K.-B. Lee, Synthesis of a Water-Soluble Fullerene [C₆₀] Under Ultrasonication, *Ultrasonics*, 2004, **41**(9), 727–730.
- 33 R. Rivelino, A. M. Maniero, F. V. Prudente and L. S. Costa, Theoretical Calculations of the Structure and UV-Vis Absorption Spectra of Hydrated C₆₀ Fullerene, *Carbon*, 2006, **44**(14), 2925–2930.
- 34 J. Labille, A. Masion, F. Ziarelli, J. Rose, J. Brant, F. Villieras, M. Palletier, D. Borschneck, M. R. Wiesner and J.-Y. Bottero, Hydration and Dispersion of C₆₀ in Aqueous Systems: The Nature of Water–Fullerene Interactions, *Langmuir*, 2009, **25**(19), 11232–11235.
- 35 W.-B. Ko and K.-N. Baek, The Oxidation of Fullerenes (C₆₀, C₇₀) with Various Oxidants under Ultrasonication, *Phys. Solid State*, 2002, **44**(3), 424–426.
- 36 T. H. Goswami, B. Nandan, S. Alam and G. N. Mathur, A Selective Reaction of Polyhydroxy Fullerene with Cycloaliphatic Epoxy Resin in Designing Ether Connected Epoxy Star Utilizing Fullerene as a Molecular Core, *Polymer*, 2003, **44**(11), 3209–3214.
- 37 W.-W. Chang, Z.-J. Li, W.-W. Yang and X. Gao, Reactions of Anionic Oxygen Nucleophiles with C₆₀ Revisited, *Org. Lett.*, 2012, **14**(9), 2386–2389.
- 38 S.-E. Zhu, F. Li and G.-W. Wang, Mechanochemistry of Fullerenes and Related Materials, *Chem. Soc. Rev.*, 2013, **42**, 7535–7570.
- 39 Z. Wang, S. Wang, Z. Lu and X. Gao, Syntheses, Structures and Antioxidant Activities of Fullerenols: Knowledge Learned at the Atomistic Level, *J. Cluster Sci.*, 2015, **26**(2), 375–388.
- 40 M. S. Meier and J. Kiegiel, Preparation and Characterization of the Fullerene Diols 1,2-C₆₀(OH)₂, 1,2-C₇₀(OH)₂, and 5,6-C₇₀(OH)₂, *Org. Lett.*, 2001, **3**(11), 1717–1719.
- 41 L. O. Husebo, B. Sitharaman, K. Furukawa, T. Kato and L. J. Wilson, Fullerenols Revisited as Stable Radical Anions, *J. Am. Chem. Soc.*, 2004, **126**(38), 12055–12064.
- 42 P. A. Indeglia, A. Georgieva, V. B. Krishna and J.-C. J. Bonzongo, Physicochemical Characterization of Fullereneol and Fullereneol Synthesis By-Products Prepared in Alkaline Media, *J. Nanopart. Res.*, 2014, **16**(2599), 1–15.
- 43 L. Y. Chiang, R. B. Upasani, J. W. Swirczewski and S. Soled, Evidence of Hemiketals Incorporated in the Structure of Fullerols Derived from Aqueous Acid Chemistry, *J. Am. Chem. Soc.*, 1993, **115**(13), 5453–5457.
- 44 Y. Liu, G. Zhang, L. Niu, L. Gan and D. Liang, Assembly of Janus Fullereneol: a Novel Approach to Prepare Rich Carbon Structures, *J. Mater. Chem.*, 2011, **21**, 14864–14868.
- 45 J. Raso, P. Mañas, R. Pagán and F. J. Sala, Influence of Different Factors on the Output Power Transferred into Medium by Ultrasound, *Ultrason. Sonochem.*, 1999, **5**(4), 157–162.
- 46 K. S. Suslick and G. J. Price, Applications of Ultrasound to Materials Chemistry, *Annu. Rev. Mater. Sci.*, 1999, **29**, 295–326.
- 47 J. Rooze, E. V. Rebrov, J. C. Schouten and J. T. F. Keurentjes, Dissolved Gas and Ultrasonic Cavitation – a Review, *Ultrason. Sonochem.*, 2013, **20**(1), 1–11.
- 48 L. Villeneuve, L. Alberti, J.-P. Steghens, J.-M. Lancelin and J.-L. Mestas, Assay of Hydroxyl Radicals Generated by Focused Ultrasound, *Ultrason. Sonochem.*, 2009, **16**(3), 339–344.
- 49 T. J. Mason, Some Neglected or Rejected Paths in Sonochemistry – a Very Personal View, *Ultrason. Sonochem.*, 2015, **25**, 89–93.
- 50 G. R. Buettner, Spin Trapping: ESR Parameters of Spin Adducts 1474 1528V, *Free Radical Biol. Med.*, 1987, **3**(4), 259–303.
- 51 C. L. Christman, A. J. Carmichael, M. M. Mossoba and P. Riesz, Evidence for Free Radicals Produced in Aqueous Solutions by Diagnostic Ultrasound, *Ultrasonics*, 1987, **25**(1), 31–34.
- 52 P. Riesz and T. Kondo, Free Radical Formation Induced by Ultrasound and its Biological Implications, *Free Radical Biol. Med.*, 1992, **13**(3), 247–270.
- 53 C. Leonelli and T. J. Mason, Microwave and Ultrasonic Processing: Now a Realistic Option for Industry, *Chem. Eng. Process.*, 2010, **49**(9), 885–900.
- 54 M. Kohnno, T. Mokudai, T. Ozawa and Y. Niwano, Free Radical Formation from Sonolysis of Water in the Presence of Different Gases, *J. Clin. Biochem. Nutr.*, 2011, **49**(2), 96–101.
- 55 C. Gong and D. P. Hart, Ultrasound Induced Cavitation and Sonochemical Yields, *J. Acoust. Soc. Am.*, 1998, **104**(5), 2675–2682.
- 56 G. Mark, A. Tauber, R. Laupert, H.-P. Schuchmann, D. Schulz, A. Mues and C. Sonntag, OH-Radical Formation by Ultrasound in Aqueous Solution – Part II: Terephthalate and Fricke Dosimetry and the Influence of Various Conditions on the Sonolytic Yield, *Ultrason. Sonochem.*, 1998, **5**(2), 41–52.
- 57 A. Hirsch, *Principles of Fullerene Reactivity. Fullerenes and Related Structures*, Springer, Berlin, Heidelberg, 1999, pp. 1–65.
- 58 T. H. Goswami, R. Singh, S. Alam and G. N. Mathur, Thermal analysis: a unique method to estimate the number of substituents in fullerene derivatives, *Thermochim. Acta*, 2004, **419**(1), 97–104.
- 59 L. Tianbao, L. Xinhai, H. Kexiong, J. Hanying and L. Jing, Synthesis and Characterization of Hydroxylated Fullerene Epoxide—an Intermediate for Forming Fullerol, *J. Cent. South Univ. Technol.*, 1999, **6**(1), 35–36.
- 60 X. J. Li, X. H. Yang, L. M. Song, H. J. Ren and T. Z. Tao, A DFT study on structure, stability, and optical property of fullereneols, *Struct. Chem.*, 2013, **24**(4), 1185–1192.
- 61 J. Zhuo, T. Wang, G. Zhang, L. Liu, L. Gan and M. Li, Salts of C₆₀(OH)₈ electrodeposited onto a glassy carbon electrode: surprising catalytic performance in the hydrogen evolution reaction, *Angew. Chem., Int. Ed.*, 2013, **52**(41), 10867–10870.
- 62 S. P. Singh, *Light Harvesting Nanomaterials*, Bentham Science Publishers, 2015.





ELSEVIER

Contents lists available at ScienceDirect

Biosensors and Bioelectronics

journal homepage: www.elsevier.com/locate/bios

Functionalized fullerene (C₆₀) as a potential nanomediator in the fabrication of highly sensitive biosensors

Sadia Afreen^a, Kasturi Muthoosamy^a, Sivakumar Manickam^{a,*}, Uda Hashim^b

^a Manufacturing and Industrial Processes Research Division, The University of Nottingham Malaysia Campus, Jalan Broga, Semenyih, Selangor D.E. 43500, Malaysia

^b Institute of Nano Electronic Engineering, Universiti Malaysia Perlis, Perlis 01000, Malaysia

ARTICLE INFO

Article history:

Received 25 April 2014

Received in revised form

14 July 2014

Accepted 14 July 2014

Available online 25 July 2014

Keywords:

Fullerene

Functionalization

Derivatives

Biosensor

Nano

Biomolecules

ABSTRACT

Designing a biosensor for versatile biomedical applications is a sophisticated task and how dedicatedly functionalized fullerene (C₆₀) can perform on this stage is a challenge for today and tomorrow's nanoscience and nanotechnology. Since the invention of biosensor, many ideas and methods have been invested to upgrade the functionality of biosensors. Due to special physicochemical characteristics, the novel carbon material "fullerene" adds a new dimension to the construction of highly sensitive biosensors. The prominent aspects of fullerene explain its outstanding performance in biosensing devices as a mediator, e.g. fullerene in organic solvents exhibits five stages of reversible oxidation/reduction, and hence fullerene can work either as an electrophile or nucleophile. Fullerene is stable and its spherical structure produces an angle strain which allows it to undergo characteristic reactions of addition to double bonds (hybridization which turns from sp² to sp³). Research activities are being conducted worldwide to invent a variety of methods of fullerene functionalization with a purpose of incorporating it effectively in biosensor devices. The different types of functionalization methods include modification of fullerene into water soluble derivatives and conjugation with enzymes and/or other biomolecules, e.g. urease, glucose oxidase, hemoglobin, myoglobin (Mb), conjugation with metals e.g. gold (Au), chitosan (CS), ferrocene (Fc), etc. to enhance the sensitivity of biosensors. The state-of-the-art research on fullerene functionalization and its application in sensor devices has proven that fullerene can be implemented successfully in preparing biosensors to detect glucose level in blood serum, urea level in urine solution, hemoglobin, immunoglobulin, glutathione in real sample for pathological purpose, to identify doping abuse, to analyze pharmaceutical preparation and even to detect cancer and tumor cells at an earlier stage. Employing fullerene-metal matrix for the detection of tumor and cancer cells is also possible by the inclusion of fullerene in single-walled carbon nanotubes (SWCNTs) known as peapods as well as in double-walled carbon nanotubes (DWCNTs), to augment the effectiveness of biosensors. This review discusses various approaches that have been reported for functionalizing fullerene (C₆₀) derivatives and their application in different types of biosensor fabrication.

© Elsevier B.V. All rights reserved.

Contents

1. Introduction	355
2. Biosensor and fullerene functionalization	356

Abbreviations: Au, gold; C₆₀[C(COOH)₂]₂, carboxyl-modified fullerene; C₆₀-NCNTs/CHIT, fullerene-nitrogen doped carbon nanotubes and chitosan; ChO, choline oxidase; CNO, carbon nano-onions; CNT, carbon nanotube; CS, chitosan; Cys, L-Cysteine; DWCNT, double walled carbon nanotube; ECL, electrochemiluminescence; *E. coli*, *Escherichia coli*; Fc, ferrocene; GCE, glassy carbon electrode; GOx, glucose oxidase; Hb, hemoglobin; H₂O₂, hydrogen peroxide; IgG, immunoglobulin G; IL, ionic liquid; ITO, Indium tin oxide; K_m, Michaelis–Menten Constant; Mb, myoglobin; MWCNT, multi-walled carbon nanotube; OMC, ordered mesoporous carbon; Pd, palladium; PDDA, poly (diallyldimethylammonium) chloride; PDGF-BB, platelet-derived growth factor B-chain; PdNCs, palladium nanocages; PGE, pyrolytic graphite electrode; Pt, platinum; PTC-NH₂, amino functionalized 3,4,9,10-perylenetetracarboxylic dianhydride; PZ, piezoelectric; QCM, quartz crystal microbalance; R.S.D, relative standard deviation; SAW, surface acoustic wave; s-BLM, self-assembled bilayer lipid membrane; SS2, *Streptococcus suis* Serotype 2; SWCNT, single walled carbon nanotube; SWNT, single walled nanotube; TMB, 3,3',5,5'-tetramethylbenzidine

* Corresponding author. Tel.: +60 3 8924 8156; fax: +60 3 8924 8017.

E-mail address: Sivakumar.Manickam@nottingham.edu.my (S. Manickam).

<http://dx.doi.org/10.1016/j.bios.2014.07.044>

0956-5663/© Elsevier B.V. All rights reserved.

3. Prospective biosensors based on functionalized fullerene.....	357
3.1. Glucose biosensors.....	357
3.2. Urea biosensors.....	359
3.3. Immunosensors.....	360
3.4. Analysis of drugs for clinical and pharmacological studies.....	362
3.5. Prospects of functionalized fullerene for the detection of tumor and cancer cells.....	362
4. Summary and conclusions.....	363
5. Future perspectives.....	364
Acknowledgments.....	364
References.....	364

1. Introduction

After the first successful presentation of biosensor by Leland C. Clark in 1962, numerous research studies have been executed by the scientific communities worldwide to advance the functionality of this device for the detection of different types of biomolecules. Nowadays we find a variety of biosensors based on distinctive physicochemical detectors, which are now being used in food analysis, environmental monitoring, drug delivery and diagnosis of health related issues, toxicity measurement, protein engineering, DNA sequencing, genetic analysis, cellular localization, cell identification and sorting, detection of pathogens, remote sensing of airborne bacteria and other biomedical applications (Perez, 2004; Jensen et al., 1996; Bosi et al., 2003). Some of the examples: carbon nanotube (CNT)/teflon matrix based glucose biosensor, glucose biosensor based on incorporation of laccase in CNT/chitosan matrix (Pumera et al., 2007), glucose nanobiosensor prepared with a bilayer of the poly(diallyldimethylammonium) chloride (PDDA) and poly(sodium-4-styrenesulfonate) (PSS) on 3-mercaptop-1-propanesulfonic acid-modified gold (Au) electrode (Pumera et al., 2007; Ahmed et al., 2010). Other types of biosensors are highly sensitive amperometric cholesterol biosensor using platinum (Pt) zinc oxide (ZnO) nanospheres (PtZONS) (Ahmed et al., 2010), multi-walled carbon nanotube (MWCNT) based biosensor [ChO/polyaniline/MWCNT] for choline detection (Pumera et al., 2007), insulated MWNT electrode biosensor and Pt-MWNT biosensor for ultra sensitive detection of DNA (Pumera et al., 2007;

Li et al., 2003; Zhu et al., 2005), CNT and MWNT based immunosensors (Pumera et al., 2007) and silver (Ag) nanoparticle based biosensor for the detection of squamous cell carcinoma antigen (SCCa) to diagnose cervical cancer (Zhao et al., 2014).

After the discovery of fullerene (C_{60}), a drastic change in the research of biosensors has taken place. The unique topological attribution and electrochemical properties of fullerene e.g. broad light absorption in the UV–vis region, photo-thermal effect, structural angle strain, the ability to accommodate multiple electrons and endohedral metal atoms, long-living triplet state, singlet oxygen production, as well as ability to act as an electron acceptor with a dual nature of electrophilic and nucleophilic characteristics have derived a sharp interest of researchers to investigate the possibilities of using this material as a mediator in biosensor devices (Biju, 2014; Baena et al., 2002). The outcome shows promising applications, whereby fullerene has been successfully used in developing biosensors for the detection of various biomolecules, such as glucose, urea, proteins as well as doping agents, such as dexamethasone, prednisolone, etc. in real samples. The application is not only limited in these areas, it frames in the high possibility to detect cancer cells at the earlier stage as well. It has been reported that fullerene derivatives can be used effectively in the photo-acoustic imaging of cancer and tumor cells (Chen et al., 2012).

Elemental fullerene individually is not an effective material to construct highly sensitive biosensors. The role of fullerene in biosensing devices is as a mediator. An effective mediator for

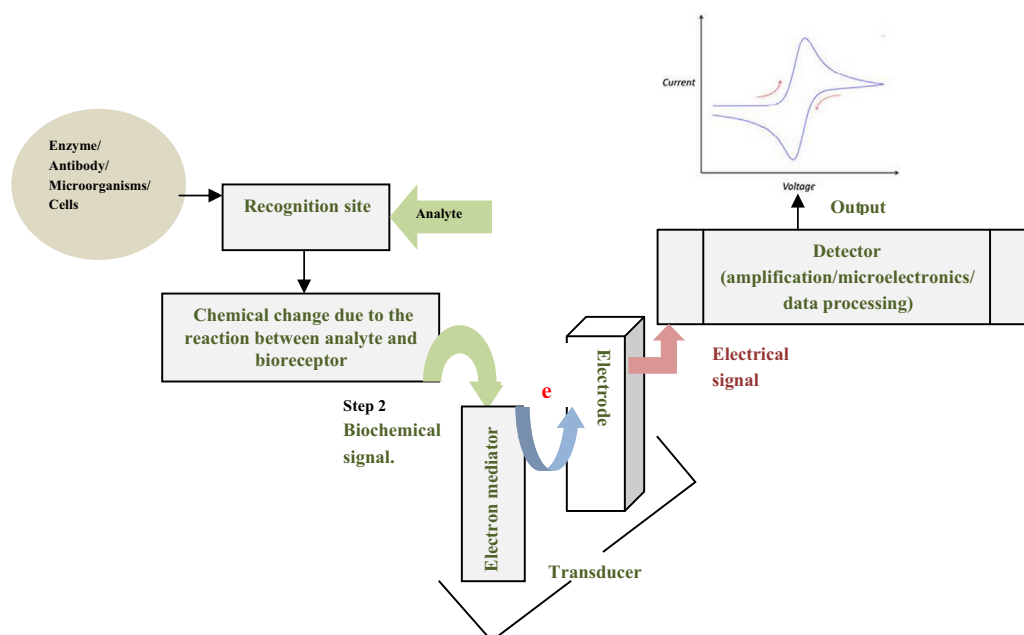


Fig. 1. Components and the involved mechanism of a conventional biosensor.

highly sensitive biosensor should possess two qualities, hydrophilic in nature and having some active functional groups so that it can conjugate with targeted biomolecules and make a liaison between the recognition site and the electrode surface to promote the transfer of electrons produced due to the biochemical reactions at recognition site. But elemental fullerene is hydrophobic in nature and also insoluble in polar solvents which make it difficult in bioconjugation with photosensitive and biologically active molecules such as ferrocenes, porphyrins, dendrimers, proteins, DNA, etc. (Biju, 2014). This difficulty can be overcome once it is functionalized with some suitable functional groups, e.g., carboxyl, hydroxyl, amine groups, etc. Once functionalized it becomes hydrophilic in nature and is characterized with active functional groups or radicals which helps conjugation of biomolecules on its cage. Therefore, prospective benefits could be achieved through novel modification of fullerene into potential derivatives. Functionalizing fullerene in a successful way for some of the specific purposes poses a big challenge for the researchers nowadays. Modern nanotechnology in coalition with other genre of science and technology has been engaged to do this since the discovery of fullerene. A bulk of research works and investigations implies that in order to incorporate fullerene derivatives or modified fullerene into biosensors, they need to possess a functional group that can be easily reacted with biomolecules (Perez, 2004; Baena et al., 2002). Two functional groups i.e. amine and carboxylic acid play very important role to create a liaison between fullerene and biomolecules. Also, fullerene molecules functionalized with hydroxyl groups can be effective mediators in biosensor applications (Chung et al., 2011). Depending on the area of application, the method of functionalization and the types of derivatives to be produced may vary. In fact, based on the type of biosensor (amperometric, potentiometric, optical, piezoelectric, etc.) and nature of analyte (protein, antigen, etc.) the target is to modify the elemental fullerene with necessary functional groups so that it is efficient in providing an amiable environment that will be allowing sufficient electron transfer between the analyte and the electrodes of biosensor. Numerous research efforts support that functionalized fullerene could be a suitable nanomaterial to enhance the sensitivity, selectivity and reproducibility of biosensors. The scope of this review is limited to those remarkable efforts of developing biosensors using functionalized fullerene (C₆₀) and its derivatives.

2. Biosensor and fullerene functionalization

A biosensor can be defined as an analytical device which can be used to detect and measure the presence and amount of an analyte by combining a biological component with a physicochemical detector (Chambers et al., 2008). Based on the area of application, biosensors can be of different types but generally they all maintain a common configuration. The following figure shows the common configuration of a biosensor (Fig. 1) which comprises five general steps for its functionality. Similar to other conventional sensors,

biosensors also possess a recognition site and a transducer. The recognition site responds to the presence of the analyte and the transducer converts this response into a different kind of energy that is amplified, processed and converted into the desired format of signal (Fig. 1).

In a biosensor, a biological component is used in the recognition site (enzymes, antibodies, organelles, microorganisms, tissues and cells). Fullerene is used as a mediator between the recognition site and electrode of a biosensor to amplify the rate of electron transfer produced due to the biocatalytic or biochemical reaction of analyte in contact with the biological component at the recognition site (Perez, 2004; Zhang et al., 2000; Davis et al., 1995; Perumal and Hashim, 2014). The function of fullerene at the interface of recognition site and electrode can be represented as shown in the following diagram (Fig. 2).

A robust biosensor must be reproducible along with the quality of having a remarkable degree of specificity to an analyte as well as a high sensitivity to detect the target analyte even in a very low concentration (Perez, 2004; Zhang et al., 2000; Perumal and Hashim, 2014). To achieve this target of robustness, number of methods has been brought by the researchers using distinct type of molecules to functionalize fullerene to increase its functionality in biosensor. From the view point of fullerene chemistry, functionalized fullerene can be categorized into two basic types: exohedral, where substituents are intercalated outside the cage; endohedral, where molecules are trapped inside the cage (Hirsch, 1993). It is found that exohedrally functionalized fullerenes bearing organic or organometallic functional groups attached to the exterior of the carbon cage are more diverse and accessible class of fullerene molecules than endohedral metallofullerenes. This type of functionalized fullerene has been considered very effective for biosensors and photoconductors (Britz et al., 2004; Loboda, 2013). Also, a comparative study towards the electrochemical properties of fullerene functionalized with palladium (C₆₀-Pd) and incorporated in different carbon nanostructures e.g. SWCNTs, MWCNTs, and oxidized carbon nano-onions (ox-CNOs) states that this type of composites can exhibit good electrochemical stability under multicyclic voltammetric conditions and give fast current responses upon potential changes (Gradzka et al., 2013).

Britz et al. (2004) synthesized modified fullerenes (C_n@SWNT), the cyclopropafullerene-C₆₀-dicarboxylic acid diethyl ester, C₆₁(COOEt)₂ and the cyclopropafullerene-C₆₀-dicarboxylic acid, C₆₁(COOH)₂ and then mixed with purified SWNTs in carbon-disulfide (CS₂). The fullerene-SWNT mixtures were then immersed in carbon dioxide (CO₂) under supercritical condition. From the analysis it has been found that fullerenes with ester groups can enter SWNTs much easily than fullerenes with hydrogen bonded carboxylic groups. This technique of filling nanotubes with functionalized fullerene at low temperature (50 °C) has offered a new structure of fullerene-CNTs which could be applied in biosensor fabrication. The nanotube-fullerene host-guest interaction also has proved that altering the functional groups of fullerene can enhance or inhibit encapsulation, as compared to elemental fullerene (Britz et al., 2004; Gradzka et al., 2013). Zhou et al. (2008)

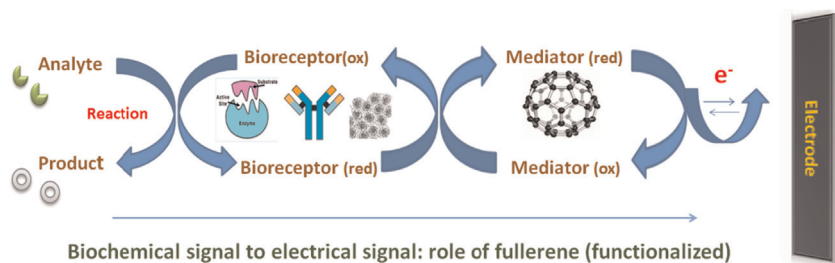


Fig. 2. Function of fullerene at the interface of recognition site and electrode.

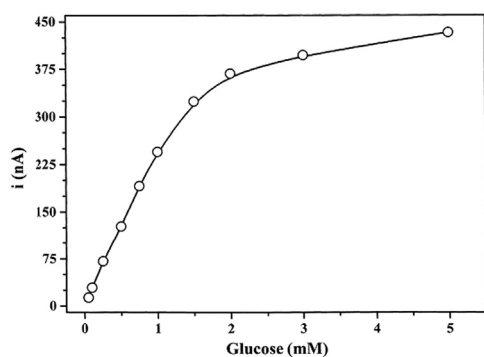


Fig. 3. Calibration curve of the glucose biosensor containing 1.7 μg C_{60} /mg of electrode material. Experimental conditions: 10 mM phosphate buffer, pH 7.5, under argon, at +350 mV vs. Ag/AgCl (Gavalas and Chaniotakis, 2000).

proposed a nanocomposite electrode system based on the synergistic effect of ordered mesoporous carbon (OMC) and fullerene. The OMC- C_{60} glassy carbon electrode (GCE) showed more favorable electron transfer kinetics in comparison to OMC/Glassy Carbon (GC) electrode. This investigation emphasized that modified fullerene or fullerene mediated electrode can offer an electrochemical sensing platform to detect biomolecules.

The function of fullerene has also been appreciated in the study of Tien et al. (1997) where they have investigated light-induced voltage and current generated by a self-assembled bilayer lipid membrane (s-BLM) doped with C_{60} . The C_{60} containing s-BLM acts as a molecular device which actuates the redox reaction across the substrate-hydrophobic lipid bilayer-aqueous solution junction. The cyclic voltammetry confirmed that fullerene embedded in the BLM can perform as an excellent electron carrier/mediator and hence are useful in developing electrochemical biosensors. Later on, Szyman'ska et al. (2001) developed an electrochemical sensor following Tien's method for the detection of neutral odorant. C_{60} saturated s-BLM formed on a freshly cleaved metallic surface was employed for the sensing of odorant molecules and again it proved that the presence of functionalized fullerene or fullerene modified electrodes can facilitate the charge transmission in an electrochemical sensor system. Recent investigation confirms that the modification of biosensor electrode by means of integration of gold nanoparticles and fullerenols can enhance the performance of biosensors (Lanzellotto et al., 2014). Also a recent review on nanodiagnosics for pathogens detection has underlined that fullerene modified immobilized C_{60} -enzymes/antibodies/proteins can be a good sensor material for the detection of various biological species (Shinde et al., 2012).

3. Prospective biosensors based on functionalized fullerene

3.1. Glucose biosensors

Generally glucose is determined by the conventional electrochemical method, but biological species such as ascorbic acid, uric acid, tyrosine, galactose and cysteine in the blood sample cause interference to the detection of glucose (Biju, 2014; Chuang and Shih, 2001). To overcome this limitation, fullerene has been assigned in the fabrication of different types of glucose biosensors, e.g. C_{60} coated piezoelectric sensors and fullerene based amperometric biosensors.

Fullerene (C_{60}) mediated biosensor for glucose detection was first claimed by Gavalas and Chaniotakis (2000), where varying amounts of fullerene were immobilized to develop an amperometric biosensor against glucose oxidase (GOx) enzyme. Trial was conducted with immobilized fullerene from 0.6 to 1.7 μg and GOx

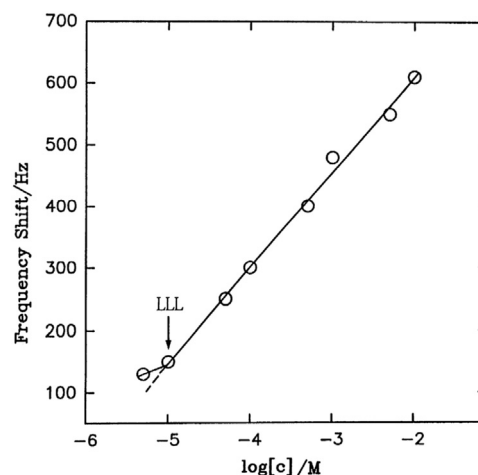


Fig. 4. Frequency response of the glucose biosensor against different concentration of glucose (Chang and Shih, 2000).

stabilized with diethylaminoethyl-dextran was used as the model enzyme. Their observation demonstrates that the sensitivity of biosensor increases with an increase in the amount of immobilized fullerene. The sensor has a linear range of response from 50 to 1000 μM glucose and the limit of detection based on signal-to-noise ratio was found to be 13 μM (Fig. 3). The response time was found to be in between 120 s and 300 s and was varying with the concentration of glucose in the solution (Gavalas and Chaniotakis, 2000). Chang and Shih (2000) proposed a piezoelectric glucose biosensor based on fullerene-cryptand-22. This biosensor was developed by coating fullerene-cryptand-22 on piezoelectric (PZ) quartz crystal with silver plated metal electrodes. The fullerene-cryptand-22-coated PZ quartz crystal was placed in the working cell containing a solution of glucose. The frequency of PZ crystal was measured in this glucose solution. After the injection of GOx enzyme into the cell containing glucose solution, the catalytic oxidation of glucose by GOx produces gluconic acid which is directly proportional to the glucose in solution and the oscillating frequency of the quartz crystal decreases due to the adsorption of gluconic acid on fullerene-cryptand-22.

A decrease in the frequency shift is a desired outcome since PZ crystals are very sensitive to the pressure difference that results from the adsorption of any foreign molecules onto their surface. The device showed a frequency change only when glucose was present in the aqueous solution. It also showed good reproducibility since the adsorption of gluconic acid molecules onto C_{60} -cryptand-22 was completely reversed after introducing pure water. The lower limit of linearity (LLL) was found to be approximately 1×10^{-5} M, which indicates the detection limit of a biosensor as shown in Fig. 4. On the other hand, the amount of glucose concentration in blood sample ranges from 10^{-2} to 10^{-3} M which implies that the proposed biosensor has high sensitivity to glucose molecules and can be employed to detect glucose in biological samples.

Analytical results demonstrate that the proposed biosensor is very selective to the glucose molecules and shows no interference in its performance that generally occurs due to the presence of other biological species found in the blood or urine samples. Also the device showed nearly no response to other inorganic species such as Na^+ , NH_4^+ and Cu^{2+} . An optimum frequency shift was observed at around pH 6 and at a temperature of 30 $^\circ\text{C}$. These findings resulted into a first attempt of developing a sensitive glucose biosensor using fullerene and PZ crystal detector (Chang and Shih, 2000). A similar attempt was also reported by Chen et al. (2007) to detect L-amino

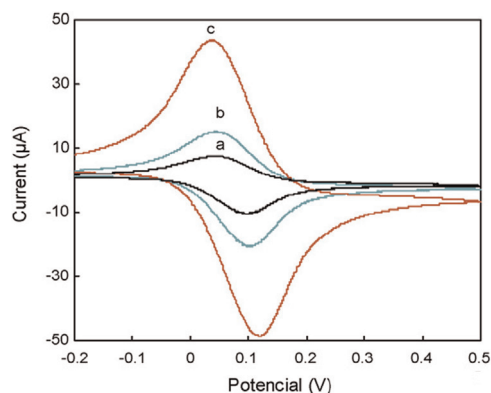


Fig. 5. Cyclic voltammogram of GOx/C₆₀-Fc-CS-IL-GCE in the absence of glucose (a), presence of 1.0 M glucose (b) and 5.0 M glucose (c) at pH 7.0 PBS and at 100 mV/s (Zhilei et al., 2010).

acid esters in aqueous solution by functionalizing fullerene with cryptand-22.

Chuang and Shih (2001) developed another glucose biosensor using C₆₀-glucose oxidase immobilized enzyme which was coated on porous silica plates to create an active platform for the enzymatic reaction of glucose molecules and C₆₀-coated piezoelectric quartz crystal was used for the sensing of biochemical changes occurring due to the enzymatic reaction. The oxidation of glucose under the catalytic activity of immobilized GOx enzyme produces gluconic acid, which was detected by a C₆₀-coated PZ quartz crystal sensor. Analytical results have shown that the more C₆₀-glucose oxidase is present, the more oxidation of glucose takes place in the solution. To determine the reproducibility and stability of the C₆₀-enzyme coated porous silica plates, the experimental trials were repeated seven times and the consumption of oxygen was found to be almost the same in all the measurements. Also, the C₆₀/PZ biosensor showed a high reproducibility with a relative standard deviation (R.S.D) of 2.12%. This reproducibility was checked with a series of 10 repetitive injections of 5×10^{-3} M glucose. The optimum frequency shift of glucose oxidation was observed at pH 7.0 which is the desirable range of pH for the physiological activity of the enzyme. The device showed its best performance at a temperature of 30 °C, which is similar to the optimum temperature desired for solvated glucose oxidase enzyme. To prevent the thermal denaturation of enzyme, this optimum temperature is an important factor. The shelf-life of this biosensor was found to be 93 days, with an activity of 88% in its initial performance. The proposed PZ crystal biosensor with immobilized enzyme, C₆₀-glucose oxidase has shown a good selectivity to glucose and can overcome the interference raised due to the presence of various biological species in the sample, e.g., Na⁺ and K⁺ ions, galactose, cysteine, tyrosine, ascorbic acid, urea and creatine. Analytical results also showed that this PZ

Table 1
Comparison of K_m among different types of glucose biosensor (Zhilei et al., 2010).

Type of glucose biosensor	Analytical value of K_m (mM)
GOx/C ₆₀ -Fc-CS-IL-GCE	0.03
Sol-gel organic-inorganic hybrid material	20
Pt nanoparticles/mesoporous carbon matrix	10.8
GO _x immobilized at chitosan and Au nanoparticles	10.5
Boron doped carbon nanotube modified electrode	15.19
Single-walled carbon nanotube modified electrode	8.5
Ferrocene-modified multi walled carbon nanotube nanocomposites	3.12
Immobilization of osmium complex and glucose oxidase onto carbon nanotubes modified electrode	0.91

Table 2
Comparative study of glucose limit in the blood serum samples (Zhilei et al., 2010).

Samples	Glucose found by the proposed method (mM)	Glucose found by the hexokinase method (mM)
Serum 1	8.41 ± 0.12	8.37 ± 0.11
Serum 2	3.23 ± 0.09	3.25 ± 0.13
Serum 3	3.66 ± 0.06	3.70 ± 0.09
Serum 4	4.53 ± 0.10	4.51 ± 0.15
Serum 5	5.11 ± 0.11	5.05 ± 0.12

crystal biosensor with two pieces of immobilized enzyme-coated silica plates can detect the presence of glucose nearly up to 3.9×10^{-5} M in an aqueous solution of glucose, where the concentration limit of glucose in the blood is found to be within 10^{-2} – 10^{-3} M. The frequency response of C₆₀-coated PZ quartz crystal glucose biosensor against the coating load of C₆₀ was examined and the result showed that excessive coating is not necessary for the sensitive response of biosensor; in fact excessive loading of C₆₀ can make unstable oscillation or even oscillation failure to the glucose biosensor. It is visualized that the proposed biosensor can show good sensitivity using a moderate amount of C₆₀ coating on PZ crystals (Chuang and Shih, 2001).

An excellent approach was accomplished by Zhilei et al. (2010) to fabricate glucose biosensor using fullerene along with ferrocene (Fc), chitosan (CS) and ionic liquid (IL). In this, GOx has been used as a catalyst for the oxidation of glucose which was detected by the electrodes. For the successful immobilization of enzyme, it is essential to nurture a biocompatible environment to allow the electron transfer between the GOx and the electrodes. Fullerenes in conjugation with Fc, CS and IL have been employed to fulfill this requirement. The modified GCE i.e. GOx/C₆₀-Fc-CS-IL-GCE has shown a precise voltammogram both in the presence (at different concentrations) and absence of glucose as shown in Fig. 5 (Zhilei et al., 2010).

The analytical results showed a very fast response time which was less than 0.752 s to reach 95% of the maximum steady state current. The Michaelis–Menten Constant (K_m) of GOx was found to be 0.03 mM for this biosensor which indicates a higher biocatalytic activity of immobilized GOx towards glucose oxidation. Their observation implies that this is a satisfactory value of K_m , better than the K_m values derived from other glucose biosensors during that time. Table 1 represents the performance of this fullerene based glucose biosensor in comparison to others developed for the same purpose.

The smallest value of K_m for GOx/C₆₀-Fc-CS-IL-GCE (Table 1) represents the synergistic performance of C₆₀, Fc, CS and IL that were used to build this biosensor. In this combination, fullerene in particular plays an important role as a mediator. Due to its electrocatalytic properties, fullerene helps to activate the oxidation of glucose molecules in the presence of GOx and stimulates the electrochemical reaction, which is a must for getting a successful output from any amperometric biosensors. Observations confirmed that the sensor can detect glucose in the human blood serum more easily, selectively and precisely, and the performance is equivalent to the conventional hexokinase method (Zhilei et al., 2010) as shown in Table 2.

C₆₀ functionalized with L-Cysteine (Cys) and Pd by *in situ* spontaneous reduction forms Pd@Cys-C₆₀ nanoparticles which can be employed in glucose detection (Zhong et al., 2012). Proposed biosensor has shown a fast response to glucose molecules both in glucose solution and human serum. It was found from the analytical results that the sensor can reach 95% of the steady state current within 9 s by changing the concentration of

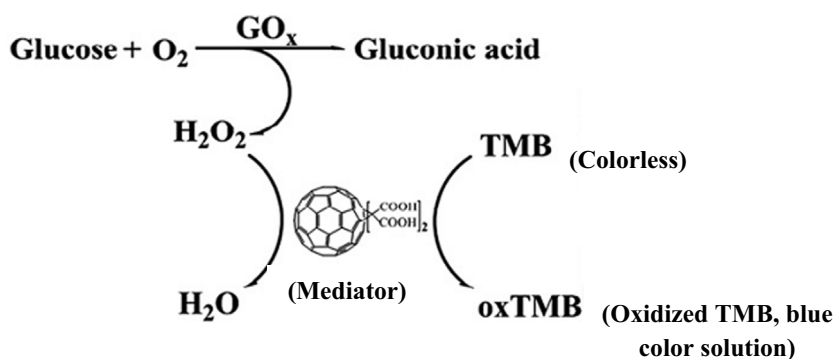


Fig. 6. Mechanism of reaction: role of fullerene derivative $C_{60}[C(COOH)_2]_2$ as a mediator in catalysing the reaction of TMB in presence of H_2O_2 (Li et al., 2013).

glucose. The study of amperometric signal of this biosensor has shown that it has a linear range from $2.5 \mu M$ to 1 mM with a lower detection limit of $1 \mu M$ at a signal to noise ratio of 3. Reproducibility and repeatability study have shown that in the presence of 0.5 mM glucose solution, this sensor has the R.S.D of 4.1% against six assayed electrodes and five successive tests of single sensor have shown that the R.S.D value is 3.9%. Also the sensor has a good anti-interfering ability towards other biomolecules commonly present in human serum and the sensitivity decreases to 7.6% of its initial response towards glucose molecules after 30 days.

Recently, Li et al. (2013a, 2013b) have reported that carboxyl-modified fullerene, ($C_{60}[C(COOH)_2]_2$) has peroxidase-like catalytic activity which can be employed to produce a highly selective, sensitive and comparatively cheaper, simpler and more convenient colorimetric biosensor to detect glucose in human serum. $C_{60}[C(COOH)_2]_2$ in the presence of peroxidase substrate 3,3',5,5'-tetramethylbenzidine (TMB) displays peroxidase-like activity that can catalyse the reaction of TMB in the presence of hydrogen peroxide (H_2O_2) which produces a deep blue color in the colorimetric analysis of glucose molecules. The following mechanism of reaction (Fig. 6) describes the role of fullerene derivative, $C_{60}[C(COOH)_2]_2$ in identifying glucose molecules. TMB gets absorbed on the surface of fullerene cage by dint of π - π stacking interaction and donates lone-pair of electrons from the amino groups to fullerene cage. These electrons transfer from fullerene cage to H_2O_2 are accelerated via the interface of hydrophilic moiety of fullerene cage. H_2O_2 is produced due to the catalytic reaction of glucose molecules with GO_x in the presence of oxygen (O_2). This sensor has been reported to be able to detect glucose in human serum from different persons with a linear range varying between 3.76 mM and 12.7 mM .

The vital role of C_{60} derivatives as electron transfer mediators has already been reported and well discussed. Recent studies (Ye et al., 2014; Gao et al., 2014) reconfirm that C_{60} molecules when derivatized properly with appropriate functional groups can act as

a promising mediator in detecting glucose molecules. This ultimately proves that the excellent electron accepting and transferring ability of fullerene derivatives can easily be employed in detecting other types of biomolecules as well. Further discussions on this perspective are presented in the following sections of this review.

3.2. Urea biosensors

The first piezoelectric-fullerene biosensor for urea detection was reported by Wei and Shih (2001), where they have suggested that fullerene-cryptand-22 can be used as a coating material on the surface of PZ quartz crystal to detect the presence of urea in an aqueous solution. They proved that similar to glucose biosensor, it can also be applicable for the detection of urea in the blood sample since the device showed a good sensitivity to urea in an aqueous solution with a detection limit of $\leq 10^{-4} \text{ M}$. The main purpose of using fullerene with cryptand-22 is to make an insoluble compound for coating on the PZ crystal and also to enhance the absorption of NH_4^+ that results from the catalytic hydrolysis of urea by solvated urease or immobilized C_{60} -urease enzyme used. To test the comparative efficiency of this sensor, both the solvated urease and immobilized C_{60} -urease were used separately to crack the urea in an aqueous solution and the frequency response was observed under both of these conditions. Similar performance was observed under both of these conditions proving that C_{60} -urease can be an alternative to the solvated urease in biosensing of urea molecules. The immobilized C_{60} -urease membrane showed a similar performance as it was found when solvated urease was used in the biosensor. The performance of this urea biosensor based on C_{60} -cryptand coated PZ crystal detector and immobilized C_{60} -urease membrane does not get blocked due to the presence of other biological species, organic and inorganic molecules e.g. creatinine, glucose, glycine, serum, ascorbic acid, acetic acid, Na^+ , K^+ , etc. Optimal frequency

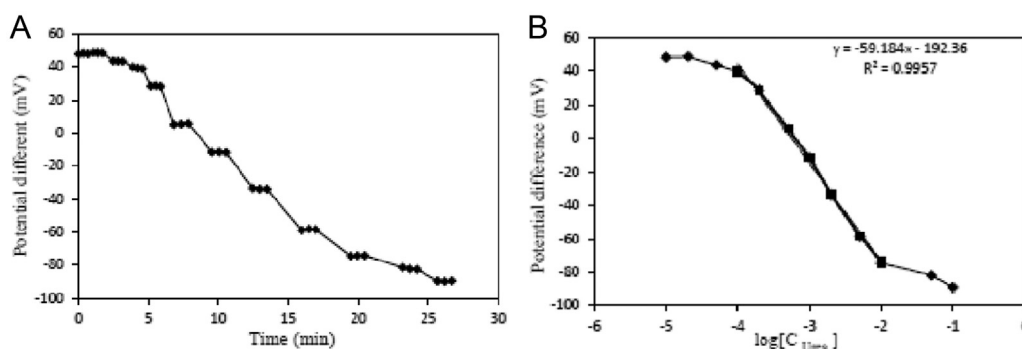


Fig. 7. Response time with relation to potential difference when the concentration of urea was changed step by step from 10^{-5} to 10^{-1} M (A), observed potential vs. urea concentration ranges from 10^{-5} to 10^{-1} M (B) (Saeedfar et al., 2013).

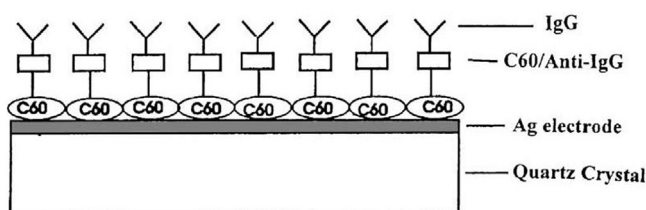


Fig. 8. C₆₀-anti-human IgG coated quartz crystal electrode for IgG (Pan and Shih, 2004).

response was observed at pH 8 and at a temperature of 30 °C. The immobilized C₆₀-urease membrane was reusable 20 times and the signal of the biosensor was found to be 96% after repeated application in one day (Wei and Shih, 2001).

A potentiometric urea biosensor was fabricated by Saedfar et al. (2013) to measure the amount of urea in the urine sample. The sensor used in this investigation was a fullerene-urease bio-conjugate on an acrylic based hydrogen ion sensitive membrane, which has shown its stability for up to 140 days. Fullerene was functionalized with carboxyl (–COOH) groups by sonication, heat, and ultraviolet (UV) radiation. Urease enzyme was then immobilized onto the fullerene–COOH derivative to devise the potentiometric biosensor for the quantitative identification of urea. Analysis with real samples of diluted urine solution has shown promising results, comparable to that of UV-Vis standard method. The difference between the fullerene-urease bio-conjugate sensor and standard UV-Vis method was found to be less than 5%, which confers a degree of reliability to the fullerene that it can be used as an effective nanomaterial in the construction of such biosensors. This fullerene based electrode showed good sensitivity and response time which was found to be 2 min for each determination and the responses were constant within the dynamic range area as shown in Fig. 7 (Saedfar et al., 2013).

Analytical results revealed that after 140 days the sensitivity of biosensor was decreased by 5%. Storage condition affected the performance of this type of sensors. The activity of the enzyme decreased with time ensuing a diminution in the sensitivity at a rate of $2.18 \times 10^{-2} \Delta mV/\text{decade}$ per day. However, this eventually highlights that fullerene can be a key component in the fabrication of biosensors to detect urea and possibly other biomolecules generated due to the metabolism in our body.

3.3. Immunosensors

Copious research works reported on developing C₆₀ based immunosensors can help in the diagnosis of different types of biological disorders caused due to any malfunction in the metabolism of our body (Chou et al., 2008; Pan and Shih, 2004; Liao and Shih, 2013; Carano et al., 2002; Chang and Shih, 2007, 2008; Sheng et al., 2013; Zhang et al., 2006). Besides, some of them showed the potential of C₆₀ based immunosensors in the detection

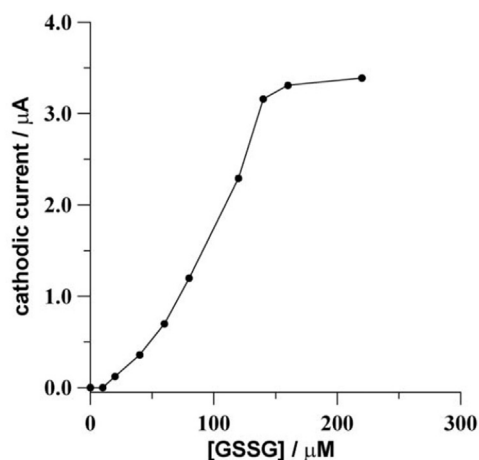


Fig. 9. Calibration curve corresponding to the chronoamperometric responses of the proposed biosensor at different concentrations of glutathione (Carano et al., 2002).

of microorganisms such as *Escherichia coli* (*E. coli*) in the real samples (Guo et al., 2012; Li et al., 2013a, 2013b).

Pan and Shih (2004) used antibody immobilized fullerene to detect immunoglobulin G (IgG) and hemoglobin (Hb) in an aqueous solution. Both these bio-species have vital roles in human immune system, therefore their approach is useful in diagnosing any disorder in immunity. In this study, C₆₀-antibody coated-quartz crystals were prepared to detect IgG and hemoglobin in aqueous solution. The C₆₀-antibody coated-quartz crystals were obtained by firstly coating C₆₀ on quartz crystals combined with silver (Ag)-plated metal electrodes, followed by adsorption of antibodies, e.g., anti-human IgG and anti-hemoglobin in aqueous solution (Fig. 8).

The analytical results obtained by using the immobilized C₆₀-anti-IgG coated PZ crystal sensor have been depicted in Table 3. Moreover, the immobilized C₆₀-anti-hemoglobin coated piezoelectric biosensor showed a good linear response frequency to the concentration of Hb with a sensitivity and detection limit of $1.56 \times 10^4 \text{ Hz}/(\text{mg}/\text{ml})$ and $< 10^{-4} \text{ mg}/\text{ml}$ respectively. The most successful feature of this PZ crystal immunosensor based on immobilized fullerene antibodies is that various common organic and inorganic bio-species in the blood, e.g., cysteine, ascorbic acid, uric acid, tyrosine, urea, Na⁺, K⁺ and Ca²⁺ have shown very minimal interference to the sensitivity of this biosensor (Pan and Shih, 2004).

A similar type of observation was reported by Liao and Shih (2013) with C₆₀-myoglobin (C₆₀-Mb), C₆₀-Hb and C₆₀-gliadin coated piezoelectric (PZ) quartz crystal immunosensors. The optimum frequency response for these anti-protein PZ-immunosensors was observed at pH 7.0 and at a temperature around 30 °C. Sensitivity of C₆₀-Mb, C₆₀-Hb and C₆₀-gliadin PZ-immunosensors were 1.43×10^3 , 2.59×10^3 and $8.05 \times 10^3 \text{ Hz}/(\text{mg}/\text{mL})$ respectively and their detection limits were 4.36×10^{-3} , 3.23×10^{-3} and

Table 3
Analytical results of the C₆₀-anti-human IgG coated quartz crystal electrode (Pan and Shih, 2004).

Controlling factors	Analytical results
Effect of concentration of IgG	$\leq 10^{-4} \text{ mg}/\text{ml}$ (in aqueous solution).
Effect of temperature	Adsorption of IgG on the biosensor increases at lower temperature (e.g. $< 30 \text{ }^\circ\text{C}$); similar effect was observed in the activity of some of the bio-species.
Effect of pH	Operates well at 6.7 which is close to the optimum pH for the physiological activity of most of the bio-species, e.g. enzymes, proteins and antibodies (7.0).
Reproducibility	High reproducibility with a R.S.D of 3.6%.
Lifetime	85% after 7 days.
Selectivity	Small interfering factors (ca. 10^{-2} – 10^{-3}) for various interfering bio-species and a quite high selectivity (ca. 0.96–0.99) of IgG solution.

1.98×10^{-3} mg/mL respectively. The interference due to other biological species found in the human blood e.g. cysteine, tyrosine, urea, glucose, ascorbic acid and metal ions was negligible (Liao and Shih, 2013).

Glutathione is an enzyme which is considered as a powerful scavenger of free radicals. It plays an important role in our immune system by making proteins and chemicals required for body metabolism and helps in tissue building and repairing. Carano et al. (2002) fabricated an amperometric biosensor to detect glutathione. Fullerene was functionalized to dipyrrolofullerene in line with glutathione reductase to act as a redox mediator for the detection of glutathione. The biosensor has shown a fast and reproducible response to glutathione. A characteristic change in the cathodic current with successive addition of glutathione was observed (Fig. 9).

Numerous approaches have been looked into the development of immunosensors based on fullerene derivatives or immobilized fullerene since they can strongly adsorb proteins e.g. Hb, Mb, gliadin, etc. One of these approaches focused on the development of surface acoustic wave immunosensor (SAW) based on the immobilized C₆₀-protein (Chang and Shih, 2007). Both C₆₀-Hb and C₆₀-Mb were used to study the response of this biosensor against the presence of anti-Hb and anti-Mb in solution. Anti-Hb is a biomarker of megaloblastic anemia cells and anti-Mb is found in the blood of polymyositis patients. Instead of quartz crystal microbalance (QCM) transducer, SAW transducer has been employed as it can offer a better operation frequency which is up to 1 GHz whereas QCM can perform up to 30 MHz. Three strategies were followed to detect anti-Hb and anti-Mb using SAW transducer: first, C₆₀-Hb-coated SAW immunosensor was applied to detect anti-Hb antibody in solution; then immobilized C₆₀-Mb SAW immunosensor was employed to detect anti-Mb antibody in solution; finally a dual channel immunosensor with both C₆₀-Hb and C₆₀-Mb was employed to detect and monitor the amount of anti-Hb and anti-Mb antibodies in the solution, simultaneously. The first one showed sensitivity of 140 Hz/(μg/mL); detection limit of 0.32 μg/mL and good reproducibility with a standard deviation of about 2.1%. The activity of immobilized C₆₀-Hb SAW crystals was found to be 80% after 10 days. This biosensor was found to be very selective to the anti-Hb antibody (ca. 0.94–1.03) and minimal response was observed for other interfering agents such as glucose, tyrosine, Na⁺, K⁺, Ca²⁺, etc. (ca. 0.02–0.06). The optimum performance was observed at a temperature of 27 °C and at a pH of 7.3. The immobilized C₆₀-Mb-coated SAW biosensor also showed a good sensitivity of 1.27 kHz/(μg/mL) with a detection limit of 0.035 μg/mL. The dual channel SAW immunosensor showed its capability to detect both anti-Hb and anti-Mb antibodies simultaneously with good sensitivity (Chang and Shih, 2007).

To detect insulin present in aqueous solution, Chang and Shih (2008) developed a shear horizontal surface acoustic wave (SH-SAW) immunosensor based on C₆₀/anti-insulin antibody which showed a similar level of performance. The sensitivity of this immunosensor was found to be 130 Hz/pM with the detection limits of 0.58 pM for insulin within the normal human insulin concentration range. The interference that generally occurs due to the presence of common inorganic and organic bio-species in blood sample was also investigated and was found to be very negligible in this immunosensor. Also it has shown excellent reproducibility with a R.S.D of 2.24%.

Sheng et al. (2013) proposed a modified approach where functionalized fullerene was used with Hb. To understand the electrochemistry of Hb, they have introduced fullerene-nitrogen doped carbon nanotubes and chitosan (C₆₀-NCNTs/CHIT) composite matrix. Hb was immobilized on this composite matrix to develop Hb/C₆₀-NCNT/CHIT/GC electrode. Their ultimate target

was to study how such a configuration based on redox protein in conjugation with C₆₀-NCNTs/CHIT could contribute in the performance of an immunosensor. This proved that immobilized Hb/C₆₀-NCNT/CHIT/GC can perform a faster electron transfer process which can be applied to determine hydrogen peroxide (H₂O₂) in biological and pharmaceutical samples. The synergistic effect of fullerene and NCNT plays a vital role behind this electron transfer between the protein and electrode, besides CS and C₆₀-NCNT together elevate the protein stability in this device. The above biosensor has shown nearly 95% of initial activity even after 2 months of storage (Sheng et al., 2013).

The results obtained from the work of Zhang et al. (2006) also support this i.e. fullerene can facilitate electron transfer between the redox proteins and the electrode. They developed C₆₀-MWCNT on GC electrode and used that electrode to detect Hb. For a comparative study, cyclic voltammograms of both bare MWCNT film on GC electrode and C₆₀-MWCNT film on GC electrode was obtained. The peak current was much higher in case of C₆₀-MWCNT film on GC electrode which indicates that due to the presence of C₆₀ in MWCNT, Hb receives a favorable environment for its redox reaction. Also the adsorption behavior for both MWCNT film and C₆₀-MWCNT film was studied to understand the effect of fullerene in this type of biosensor. The cyclic voltammogram as a function of time showed that the cathodic peak current increased in parallel with the scan time and reached saturation implying that there is a gradual and more stable adsorption of Hb on the electrode surface. Whereas, MWCNT film electrode initially showed a higher cathodic current but it decreased rapidly over time which indicates an unstable adsorption of Hb on the electrode surface. This confirms that C₆₀ can ensure a facile electrochemical deal between the electrode and the redox site of proteins, e.g., Hb, Mb, gliadin, etc. (Zhang et al., 2006). Another interesting finding by Guo et al. (2012) states that polyhydroxylated fullerene derivatives can reduce the oxidant damage caused due to the attack by H₂O₂ in Hb electrochemical biosensors. This adds a great advantage in the functionality of biosensor and it ensures a favorable microenvironment for the direct electrochemistry and electrocatalysis of Hb.

A very recent attempt on the development of an electrochemical immunosensor for sensitive detection of *E. coli* 0157:H7 using C₆₀ based biocompatible platform has been reported by Li et al. (2013a, 2013b). Previously Shiraishi et al. (2007) reported that fullerene impregnated screen printed electrode (FISPE) can be used to detect 16S rDNA extracted from *E. coli* (JCM1649). In these days, the detection of *E. coli* is very important in clinical diagnostics, food safety testing and environmental monitoring. In this connection, analysis of 16S rDNA from *E. coli* which has a significant role in phylogenetic research and electrochemical DNA sensor fields. Shiraishi et al. (2007) used the approach of mixing carbon ink with C₆₀ benzene solution to generate fullerene ink which was then impregnated onto the electrode surface and the resultant sensor was employed to detect 16S rDNA. It has been reported as a novel method of electrochemically detecting 16S rDNA by using C₆₀-ink. Li et al. (2013a, 2013b) assembled a sandwich type electrode by immobilizing C₆₀, Fc, thiolated chitosan (CHI-SH), Au nanoparticles coated SiO₂ nanocomposites (Au-SiO₂), avidin (SA) and biotinylated capture antibodies of *E. coli* 0157: H7 (bio-Ab₁) onto the surface of GCE to make a modified electrode bio-Ab₁/SA/Au-SiO₂/CHI-SH/Fc/C₆₀ to detect *E. coli* 0157:H7. The sensitivity of this immunosensor was found to have a detection limit of 15 CFU/mL which is below the commonly accepted threshold concentration in clinical diagnosis. It means that this type of biosensor can offer a subtle measurement in the detection of *E. coli* in real samples.

Recent investigation also shows that fullerene functionalized with L-Cysteine (C₆₀-L-Cys) has better biocompatibility, conductivity

and hydrophilicity in comparison to pristine fullerene which can be used in fabricating electrochemiluminescence (ECL) immunosensor for the detection of *Streptococcus suis* Serotype 2 (SS2) (Wang et al., 2014). SS2 is known as a pathogen which is responsible for many diseases, e.g., meningitis, arthritis, pneumonia, etc. C_{60} -L-Cysteine when absorbed around palladium nanocages (PdNCs) forms an integrated nanostructure of C_{60} -L-Cys functionalized PdNCs (C_{60} -L-Cys-PdNCs) which acts as an immobilizing platform and enhances the ECL signal due to its high surface area, superior electron transport capacity and efficient photocatalytic activity obtained via functionalization of C_{60} . A wide linear detection range of 0.1 pg mL^{-1} – 100 ng mL^{-1} with a relatively lower detection limit of 33.3 fg mL^{-1} has been reported in this biosensor.

The effect of fullerene in developing highly sensitive deoxy-nivalenol (DON) immunosensor was visualized by Zhilei et al. (2011). For the detection of DON in food samples, they made a sensitive electrochemical immunosensor using GCE and a composite prepared from fullerene (C_{60}), Fc and IL. This biosensor showed high sensitivity, selectivity and shelf-life of about 180 days. To investigate the effect of fullerene as well as IL in this type of biosensor, they have also examined the device without using fullerene and IL. The results showed that when fullerene and IL were used, the sensitivity of biosensor increases substantially which is twice than that of a biosensor without fullerene and IL. Due to its unique electrochemical properties, fullerene promotes electron transfer on the surface of modified electrodes and helps to increase the sensitivity of biosensor (Zhilei et al., 2011).

3.4. Analysis of drugs for clinical and pharmacological studies

The advantages of fullerene's electrochemical properties have also been utilized to determine the amount of drugs in various clinical and pharmacological studies. Fullerene modified gold electrode (C_{60}/Au) has been proved to detect prednisolone in human urine or whole blood sample, a potential application during the investigation of doping cases by athletes (Goyal et al., 2009a). Better results were obtained by using SWNTs instead of C_{60} in the detection of triamcinolone, which is also considered as a doping agent (Goyal et al., 2009b). Nevertheless, fullerene exhibited significant performance in the detection of dexamethasone (Goyal et al., 2009c). In the determination of prednisolone in human blood and urine samples, C_{60}/Au modified indium tin oxide (ITO) electrode showed a quite impressive voltammogram. The anodic peak current gave a sharp and a significant peak rise in the voltammogram when C_{60}/Au electrode was used rather than bare ITO electrode. Although the stability of Au modified ITO (Au/ITO) electrode was found to be better than that of C_{60}/Au electrode (4.78% after 10 days for C_{60}/Au electrode and 3.35% after 15 days for Au/ITO electrode), it was also observed that the sensitivity of C_{60}/Au was much better than that of Au/ITO electrode. It again demonstrates the advantage of using fullerene in biosensing as the electrocatalytic activity of fullerene as well as Au promotes the oxidation of prednisolone and increases the rate of electron transfer (Goyal et al., 2009a).

Dexamethasone is a glucocorticoid class of steroid and is immensely used in the pharmaceutical formulations. It is used, for the treatment of cancer to reduce the side effects of antitumor therapy; to alleviate high altitude illness; for viral infections, respiratory diseases, gastrointestinal diseases; to cure skin disorders and nervous system abnormalities, etc. Due to the strong efficacy of dexamethasone to these diseases, it is very much required to determine its dosage to ensure the safety limit of its use for any treatment. Moreover, dexamethasone is also considered to be a doping agent among the athletes. Goyal et al. (2009c) developed a biosensor to determine this dexamethasone in human plasma which is a simple and rapid methodology in comparison to

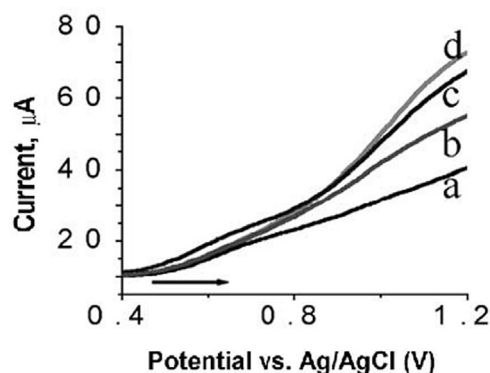


Fig. 10. Effect of dosage of C_{60} cast onto a GC electrode: (a) 5 μl ; (b) 10 μl ; (c) 15 μl ; and (d) 20 μl (Tan et al., 2003).

other available methods. They introduced fullerene modified edge plane pyrolytic graphite electrode (PGE) to form a reproducible and stable biosensor. Due to the presence of fullerene, this biosensor showed acceleration in the electrocatalytic reduction of dexamethasone, which brought a significant peak current indicating a higher sensitivity towards dexamethasone. This study was carried out with both commercial and real samples and ascertained that C_{60} -PGE can offer better quantitative results for dexamethasone in the pharmaceutical preparations and doping investigations (Goyal et al., 2009c).

Many investigations reiterate that functionalized fullerene mediated electrode surface can enhance the electrical signal towards the voltammetric outputs. The voltammetric study carried out by Tan et al. (2003) to detect L-Cysteine using GCE modified by fullerene strongly supports this postulate. L-Cysteine, commercially known as E920 is widely used in food industries as an antioxidant and in pharmaceutical industries as a biomarker which can assist to investigate the biomolecular structure and dynamics. The modified electrode was prepared by casting C_{60} containing dichloromethane (CH_2Cl_2) solution onto the surface of clean GC electrode which was then applied to detect and measure the presence of L-Cysteine in two types of samples, alcovite (100 mg L-Cysteine per pill) and casamino acid (90% L-Cysteine and 10% lactose). Both these samples contained a known amount of cysteine which was provided by the manufacturer. Other samples of root beer syrup and soya bean milk were spiked with L-Cysteine to do a comparative study. Voltammetric study showed that the obtained current from the oxidation of cysteine is a function of C_{60} dosage and higher current was observed with an increase in the C_{60} coating. The observed results have been shown in Fig. 10.

The presence of C_{60} microcrystals on the surface of GC improved the oxidation current of L-Cysteine. This biosensor also has good reproducibility and selectivity to the determination of L-Cysteine and presents a distinctive scenario where fullerene mediated electrode is used in mediating the irreversible oxidation of a species in an aqueous media (Tan et al., 2003).

3.5. Prospects of functionalized fullerene for the detection of tumor and cancer cells

Usage of fullerene (C_{60}) is increasing gradually due to its potential physicochemical features, for example, in the detection and treatment of chronic conditions such as cancer and tumor (Chen et al., 2012; Rasooly and Jacobson, 2006; Orlova et al., 2013), to detect and target DNA strain in real samples (Xu et al., 2009) and to investigate the nature of HIV (Friedman, 1993; Ros and Prato, 1999). It has been suggested that C_{60} derivatives can be used effectively as inhibitors of HIV-1 protease (HIVP) since fullerene possesses steric and chemical reciprocity with the active site of

HIVP (Friedman, 1993;). The most recent research on the application of fullerene is focused on its use as a biosensor material for the detection of cancer in their early stages (Chen et al., 2012; Han et al., 2013). The objective is to fabricate the easiest and the simplest electrochemical system which enables to detect the presence of cancer and its extent inside the human body. The challenge is that it should be selective and specific to the biomarkers of various types of cancer and tumor cells along with a good reproducibility and user-friendly configuration, so that it can stand as an effective tool for the early detection and measurement of cancer in comparison to other available methods.

Han et al. (2013) established a biosensor which composed of multi-labeled C_{60} nanohybrid molecules derived from the supra-molecular interaction between fullerene and amino functionalized 3,4,9,10-perylenetetracarboxylic dianhydride (PTC-NH₂) and was employed for the early diagnosis, treatment and prognosis of cancer by detecting cancer related protein known as platelet-derived growth factor B-chain (PDGF-BB). In this investigation PTC-NH₂ was dispersed in the nano- C_{60} suspension to obtain amino functionalized nano- C_{60} (PTC-NH₂- C_{60}). The resultant product was functionalized C_{60} nanoparticles with amino and thiol groups (FC₆₀-NPs). This biosensor was found to be highly sensitive and selective towards PDGF-BB with satisfactory reproducibility at a R.S.D of 4.79%, and the interfering biological species have almost negligible influence to this detection. The stability of this biosensor was found to be 95.2% of its initial performance after one week and 86.7% of its initial performance after four weeks (Han et al., 2013).

Recently, it has been proved that the fullerene derivatives i.e. polyhydroxy fullerenes (PHF; $C_{60}(OH)_xO_yNa_z$) and carboxy fullerenes (CF; $C_{60}(C(COOH)_2)_3$) can be used in photo-acoustic imaging of tumor and cancer cells (Chen et al., 2012). A mechanical scanning photo-acoustic system has been developed by the researchers. A higher photo-acoustic image of the functionalized fullerene was obtained after laser irradiation and a notable result was found when the study was conducted on tumor-bearing mice. Distinctive images were observed between tumor and non-tumor regions after the injection of polyhydroxy fullerene. This observation adds a new dimension to the application of functionalized fullerene that it can act as an *in vivo* biosensor material to detect cancer and tumor cell lines. Due to the excellent response of fullerene and its derivatives to photo-acoustic imaging, it is now conceived that fullerene can be used as a diagnostic and therapeutic agent to these diseases in the near future.

4. Summary and conclusions

Overall, we have discussed the key aspects of various biosensors based on fullerene derivatives and the prospects of functionalized fullerene as an effective nanomaterial to ramp up the sensitivity and

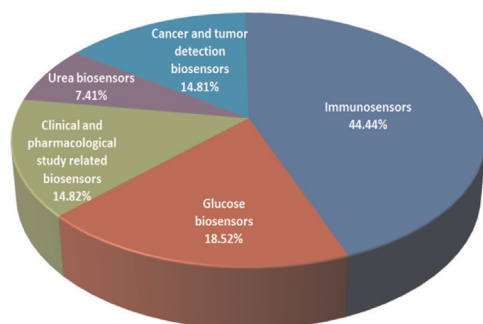


Fig. 11. Usage of functionalized fullerene in different types of biosensors [1999–2013].

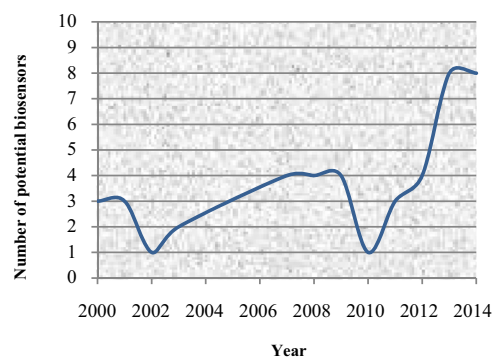


Fig. 12. Trend of using functionalized fullerene for biosensor devices over the last decade.

functionality of biosensor devices. It is visualized that due to its excellent electron accepting capacity and its ability to accelerate charge separation in any electrochemical process, fullerene can be used in various types of biosensors, e.g., potentiometric, amperometric, piezoelectric, etc. The novel characteristics of fullerene have already been appreciated (Sotiropoulou et al., 2003; Forró and Mihály, 2001; Martin, 2006; Umeyama et al., 2008). The gist is, fullerene performs as a ‘nano negotiator’ between the recognition site and the electrodes to complete the deal of electron transfer which ultimately produces an electric signal that appears as a final output after being amplified by the detector. When fullerene is functionalized by any selective molecules or radicals, it becomes more active to bind and pass the electrons. However, the function of fullerene is still under investigation and it is essential to know that what might be the other promising advantages of using fullerene in biosensor devices other than facilitating the rate of electron transfer.

From this review it is also visualized that most of the investigations (~44.4%) are focused in developing the immunosensors, to the best of our knowledge (Fig. 11). Following this much of the work concentrates in developing glucose biosensors. In fact glucose and urea biosensors were the initial type of biosensors based on functionalized fullerene. Later on, it has been expanded to the field of clinical and pharmacological studies and to the field of cancer and tumor cells detection. At present, functionalized fullerene has received attention in detecting cancer and tumor cells. A comparative scenario has been shown in Fig. 11.

However, considering the intensity of research that focusses on the development of novel and potential biosensors over the last decade, it is realised that biosensors using functionalized fullerene is on the rise in between 2002 and 2009 (Fig. 12). This may be due to that before 2002 the potential aspects of fullerene in biosensing applications were not completely familiar to the researchers. Since 2002 a gradual surge in the investigations and approaches were directed on the development of biosensors using fullerene derivatives. More importantly, the number of fullerene based biosensors developed has a decrease after 2009 (Fig. 12) which might be due to the rapid fashion of using various types of other nanomaterials such as SWCNT, MWCNT, graphene, Au nanoparticles, Pt nanoparticles, etc. for similar purpose. Nevertheless, this is a temporary scenario and the statistical results clearly show that after 2010, the utilization of functionalized fullerenes in developing biosensors has got a sharp increase till to date and this trend ultimately asserts that fullerene could be a promising nanomaterial in the field of biosensors and a good proportion of research investigations are still under progress to exploit its potentiality to the fullest.

5. Future perspectives

Scientific community is engaged to upgrade the biosensor technology using fullerene (C₆₀) derivatives with a view to implementing it commercially in the diagnosis of various diseases more conveniently. It is appreciable that the outstanding features of fullerene have brought many prospects in clinical diagnosis and pharmaceutical applications, but further research is required for its overall development as a biosensor. There are tons of examples of developing biosensors using distinct combination of nanomaterials besides fullerene and almost every sensor has some good attributes. The competition is mainly between fullerene and other nano moieties, e.g. SWCNT, MWCNT, Au nanoparticles, silver nanoparticles, platinum nanoparticles, etc. However, behind the success scenario, above biosensors may also have some limitations which are either not felt or unconsidered by the researchers unless they are involved in the diagnosis for practical cases. This is because any new technology not only brings bright scopes but also bears some tentative obstructions that may cause both pros and cons to its application in real life cases. Numerous investigations and trials are yet to exploit the unique properties of fullerene in the field of biosensing. Surely, this is not a challenge anymore seeing that all the experimental findings and discussions reveal that fullerene is able to perform as an active material in various types of biosensor devices for the detection and measurement of different types of biomolecules. The major issue that should be examined immediately is that how conveniently it can be incorporated in a biosensor and how robustly it can deliver its performance under different experimental conditions, to detect and measure different types of biomolecules, in comparison to other potential nanoparticles based biosensors that have been proposed so far for similar purposes. Certainly, fullerene based biosensors can offer high sensitivity, selectivity and good reproducibility in biosensing and bioimaging but that does not comprehend all the features of a biosensor those are required particularly for point-of-care diagnosis. It must be cost-effective besides possessing an easy-to-handle configuration. Proper chemical modification and bio-conjugation of fullerene molecules will be able to bring more development in biosensing and bioimaging, but at the same time it involves high cost. This is mainly due to that fullerene itself is an expensive nanomaterial, along with this for its functionalization and then finally for the fabrication of all the materials and components into a biosensor system, different types of agents and tools are required which are too expensive. From all these perspectives, fullerene biosensors can be successfully employed in the diagnosis of real samples only when they will be robust and convenient as well. The rapid development and attention in the research of functionalizing fullerene and cutting-edge biosensor technology over the past few years emphasize the possibility that in the near future fullerene based biosensors can appear as effective devices in biosensing and bioimaging of various diseases. Numerous research investigations are still in progress on this issue to achieving comprehensive fullerene based biosensors which will be commercially worthy for point-of-care diagnosis of various diseases in their early stages.

Acknowledgments

Authors would like to thank Fundamental Research Grant Scheme (FRGS) for the funding support (FRGS/1/2013/SG05/UNIM/01/1).

References

Ahmed, M., Pan, C., Gan, L., Nawaz, Z., Zhu, J., 2010. *J. Phys. Chem. C* 114, 243–250.
Baena, J.R., Gallego, M., Valcarcel, M., 2002. *Trends Anal. Chem.* 21 (3), 187–198.

- Biju, V., 2014. *Chem. Soc. Rev.* 43, 744–764.
Bosí, S., Ros, T.D., Spalluto, G., Prato, M., 2003. *Eur. J. Med. Chem.* 38, 913–923.
Britz, D.A., Khloubostov, A.N., Wang, J., O'Neil, A.S., Poliakov, M., Ardavan, A., Briggs, G.A.D., 2004. *Chem. Commun.* 2, 176–177.
Carano, M., Cosnier, S., Kordatos, K., Marccaccio, M., Margotti, M., Paolucci, F., Prato, M., Roffia, S., 2002. *J. Mater. Chem.* 12, 1996–2000.
Chambers, J.P., Arulanandam, B.P., Matta, L.L., Weis, A., Valdes, J.J., 2008. *Curr. Issues Mol. Biol.* 10 (1–2), 1–12.
Chang, M.S., Shih, J., 2000. *Sens. Actuators B* 67, 275–281.
Chang, H., Shih, J., 2007. *Sens. Actuators B* 121, 522–529.
Chang, H., Shih, J., 2008. *J. Chin. Chem. Soc.* 55 (2), 318–325.
Chen, C.H., Chang, H.W., Shih, J., 2007. *Sens. Actuators B* 123, 1025–1033.
Chen, Z., Ma, L., Liu, Y., Chen, C., 2012. *Theranostics* 2 (3), 238–250.
Chou, F.-F., Chang, H.-W., Li, T.-L., Shih, J.-S., 2008. *J. Iran. Chem. Soc.* 5 (1), 1–15.
Chuang, C.W., Shih, J., 2001. *Sens. Actuators B* 81, 1–8.
Chung, D.-J., Seong, M.-K., Choi, S.-H., 2011. *J. Appl. Polym. Sci.* 122, 1785–1791.
Davis, J., Vaughan, H., Cardosi, M.F., 1995. *Enzyme Microb. Technol.* 17, 1030–1035.
Forró, L., Mihály, L., 2001. *Rep. Prog. Phys.* 64, 649–699.
Friedman, S.H., Decamp, D.L., Sijbesma, R.P., Srdanov, G., Wudl, F., Kenyon, G.L., 1993. *J. Am. Chem. Soc.* 115, 6506–6509.
Gao, Y., Yang, T., Yang, X., Zhang, Y., Xiao, B., Hong, J., Sheibani, N., Ghourchian, H., Hong, T., Moosavi-Movahedi, A., 2014. *Biosens. Bioelectron.* 60, 30–34.
Gavalas, V.G., Chaniotakis, N.A., 2000. *Anal. Chim. Acta.* 409, 131–135.
Goyal, R.N., Oyama, M., Bachheti, N., Singh, S.P., 2009a. *Bioelectrochem.* 74, 272–277.
Goyal, R.N., Gupta, V.K., Chatterjee, S., 2009b. *Biosens. Bioelectron.* 24, 3562–3568.
Goyal, R.N., Gupta, V.K., Chatterjee, S., 2009c. *Biosens. Bioelectron.* 24, 1649–1654.
Guo, X., Yang, S., Cui, R., Hao, J., Zhang, H., Dong, J., Sun, B., 2012. *Electrochem. Commun.* 20, 44–47.
Gradzka, E., Winkler, K., Borowska, M., Plonska-Brzezinska, M.E., Echegoyen, L., 2013. *Electrochim. Acta* 96, 274–284.
Han, J., Zhuo, Y., Chai, Y., Yuan, R., Xiang, Y., Zhu, Q., Liao, N., 2013. *Biosens. Bioelectron.* 46, 74–79.
Hirsch, A., 1993. *Angew. Chem. Int. Ed. Engl.* 32 (8), 1138–1141.
Jensen, A.W., Wilson, S.R., Schuster, D.I., 1996. *Bioorg. Med. Chem.* 4 (6), 767–779.
Lanzellotto, C., Favero, G., Antonelli, M.L., Tortolini, C., Canistraro, S., Coppari, E., Mazzei, F., 2014. *Biosens. Bioelectron.* 55, 430–437.
Li, J., Ng, H.T., Cassell, A., Fan, W., Chen, H., Ye, Q., Koehne, J., Han, J., 2003. *Nano Lett.* 3 (5), 597–602.
Li, R., Zhen, M., Guan, M., Chen, D., Zhang, G., Ge, J., Gong, P., Wang, C., Shu, C., 2013a. *Biosens. Bioelectron.* 47, 502–507.
Li, Y., Fang, L., Cheng, P., Deng, J., Jiang, L., 2013b. *Biosens. Bioelectron.* 49, 485–491.
Liao, Y., Shih, J., 2013. *J. Chin. Chem. Soc.* 60 (11), 1387–1395.
Loboda, O., 2013. *Quantum-Chemical Studies on Porphyrins, Fullerenes and Carbon Nanostructures.* Springer, Berlin Heidelberg.
Martin, N., 2006. *Chem. Commun.*, 2093–2104.
Orlova, M.A., Trofimova, T.P., Orlov, A.P., Shatalov, O.A., 2013. *Br. J. Med. Med. Res.* 3 (4), 1731–1756.
Pan, N., Shih, J., 2004. *Sens. Actuators B* 98, 180–187.
Perez, V.V., 2004. *Synthesis of Highly Quenching Fullerene Derivatives for Biosensor Applications.* Department of Chemistry, Massachusetts Institute of Technology, pp. 5–17 (Master thesis).
Perumal, V., Hashim, U., 2014. *J. Appl. Biomed.* 12, 1–15.
Pumera, M., Sánchez, S., Ichinose, I., Tang, J., 2007. *Sens. Actuators B* 123, 1195–1205.
Rasooly, A., Jacobson, J., 2006. *Biosens. Bioelectron.* 21, 1851–1858.
Ros, T., Prato, M., 1999. *Chem. Commun.*, 663–669.
Saeedfar, K., Heng, L.Y., Ling, T.L., Rezayi, M., 2013. *Sensors* 13, 16851–16866.
Sheng, Q., Liu, R., Zheng, J., 2013. *Bioelectrochem.* 94, 39–46.
Shinde, S.B., Fernandes, C.B., Patravale, V.B., 2012. *J. Control. Release* 159, 164–180.
Shiraishi, H., Itoh, T., Hayashi, H., Takagi, K., Sakane, M., Mori, T., Wang, J., 2007. *Bioelectrochem.* 70, 481–487.
Sotiropoulou, S., Gavalas, V., Vamvakaki, V., Chaniotakis, N.A., 2003. *Biosens. Bioelectron.* 18, 211–215.
Szymanska, I., Radecka, H., Radecki, J., Kikut-Ligaj, D., 2001. *Biosens. Bioelectron.* 16, 911–915.
Tan, W.T., Bond, A.M., Ngooi, S.W., Lim, E.B., Goh, J.K., 2003. *Anal. Chim. Acta* 491, 181–191.
Tien, H.T., Wang, L.-G., Wang, X., Ottova, A.L., 1997. *Bioelectrochem. Bioener.* 42, 161–167.
Umeyama, T., Tezuka, N., Fujita, M., Hayashi, S., Kadota, N., Matano, Y., Imahori, H., 2008. *Chemistry* 14 (16), 4875–4885.
Wang, H., Bai, L., Chai, Y., Yuan, R., 2014. *Small* 10 (9), 1857–1865.
Wei, L.F., Shih, J., 2001. *Anal. Chim. Acta* 437, 77–85.
Xu, K., Huang, J., Ye, Z., Ying, Y., Li, Y., 2009. *Sensors* 9, 5534–5557.
Ye, C., Zhong, X., Yuan, R., Chai, Y., 2014. *Sens. Actuators B* 199, 101–107.
Zhang, S., Wright, G., Yang, Y., 2000. *Biosens. Bioelectron.* 15, 273–282.
Zhang, H., Fan, L., Yang, S., 2006. *Chem. Eur. J.* 12, 7161–7166.
Zhao, Q., Duan, R., Yuan, J., Quan, Y., Yang, H., Xi, M., 2014. *Int. J. Nanomed.* 9, 1097–1104.
Zhilei, W., Zaijun, L., Xiulan, S., Yinjun, F., Junkang, L., 2010. *Biosens. Bioelectron.* 25, 1434–1438.
Zhilei, W., Xiulan, S., Zaijun, L., Yinjun, F., Guoxiao, R., Yaru, H., Junkang, L., 2011. *Microchim. Acta.* 172, 365–371.
Zhong, X., Yuan, R., Chai, Y., 2012. *Chem. Commun.* 48, 597–599.
Zhou, M., Guo, J., Guo, L.P., Bai, J., 2008. *Anal. Chem.* 80 (12), 4642–4650.
Zhu, N., Chang, Z., He, P., 2005. *Anal. Chim. Acta.* 545, 21–26.